IN VIVO INDENTER EXPERIMENTS ON SOFT BIOLOGICAL TISSUES FOR IDENTIFICATION OF MATERIAL MODELS AND CORRESPONDING PARAMETERS

A THESIS SUBMITTED TO
THE GRADUATE SCHOOL OF NATURAL AND APPLIED SCIENCES
OF
MIDDLE EAST TECHNICAL UNIVERSITY

BY

ALİ TOLGA PETEKKAYA

IN PARTIAL FULFILLMENT OF THE REQUIREMENTS
FOR
THE DEGREE OF MASTER OF SCIENCE
IN
MECHANICAL ENGINEERING

SEPTEMBER 2008

Approval of the thesis:

IN VIVO INDENTER EXPERIMENTS ON SOFT BIOLOGICAL TISSUES FOR IDENTIFICATION OF MATERIAL MODELS AND CORRESPONDING PARAMETERS

submitted by **ALİ TOLGA PETEKKAYA** in partial fulfillment of the requirements for the degree of **Master of Science in Mechanical Engineering Department, Middle East Technical University** by**,**

Prof. Dr. Canan Özgen _____
Dean, Graduate School of **Natural and Applied Sciences**

Prof. Dr. Kemal İder _____
Head of Department, **Mechanical Engineering**

Assist. Prof Dr. Ergin Tönük _____
Supervisor, **Mechanical Engineering**

Examining Committee Members:

Assist. Prof. Dr. Cüneyt Sert _____
Mechanical Engineering Dept., METU

Assist. Prof Dr. Ergin Tönük _____
Mechanical Engineering Dept., METU

Assist. Prof. Dr. Buğra Koku _____
Mechanical Engineering Dept., METU

Assist. Prof. Dr. Yiğit Yazıcıoğlu _____
Mechanical Engineering Dept., METU

Assist. Prof. Dr. Serdar Arıtan _____
School of Sports Science and Technology, Hacettepe Unv.

Date: 05.09.2008

I hereby declare that all information in this document has been obtained and presented in accordance with academic rules and ethical conduct. I also declare that, as required by these rules and conduct, I have fully cited and referenced all material and results that are not original to this work.

Name, Last name : Ali Tolga Petekkaya

Signature :

ABSTRACT

IN VIVO INDENTER EXPERIMENTS ON SOFT BIOLOGICAL TISSUES FOR IDENTIFICATION OF MECHANICAL MATERIAL MODEL AND CORRESPONDING PARAMETERS

Petekkaya, Ali Tolga

M.Sc., Mechanical Engineering Department

Supervisor: Assist. Prof. Dr. Ergin Tönük

September 2008, 347 Pages

Soft biological tissues, being live and due to their physiological structures, display considerably complex mechanical behaviors. For a better understanding and use in various applications, first study to be carried out is the tests made particularly as in vivo. An indenter test device developed for this purpose in the METU, Department of Mechanical Engineering, Biomechanics Laboratory is operational.

In this study, in order to carry out precise and dependable tests, initially, various tests and improvements were conducted on the device and the software controlling the device. At the end of this study, displacement and load measurement accuracies and precisions were improved. Better algorithms for filtering the noisy data were prepared. Some test protocols within the software were improved and new protocols were annexed. To be able to conduct more dependable tests a new connection system was attached to the device. In order to study the anisotropic behavior of soft tissues ellipsoid tips were designed and produced.

In the second phase of the study, tests on medial forearm were carried out. In these tests, hysteresis, relaxation and creep behaviors displaying the viscoelastic

properties of the soft biological tissues were observed. In addition to viscoelastic behaviors, preconditioning (Mullin's) effect and anisotropic response were examined. By using the results of the relaxation and creep tests, parameters of the Prony series capable of modelling these data were determined.

With this study, some important conclusions regarding the soft biological tissues were drawn and thus the behaviors of the soft biological tissues were better understood. Besides, the difficulties inherent to in-vivo tests were recognized and actions to reduce these difficulties were explained. Finally, clean experimental data, to be used in the computer simulations, were obtained.

Keywords: Soft Biological Tissues, Indenter Test Device, Viscoelasticity, Anisotropy, In-vivo Experiments

ÖZ

MEKANİK MALZEME MODELİ VE İLGİLİ PARAMETRELERİN KESTİRİLMESİ İÇİN YUMUŞAK BİYOLOJİK DOKULAR ÜSTÜNDE YAPILAN YERİNDE İNDENTÖR DENEYLERİ

Petekkaya, Ali Tolga

Yüksek Lisans, Makina Mühendisliği Bölümü

Tez Yöneticisi: Y. Doç. Dr. Ergin Tönük

Eylül 2008, 347 Sayfa

Yumuşak biyolojik dokular canlı olmaları ve fizyolojik yapıları sebebiyle karmaşık bir mekanik davranış sergilerler. Bu mekanik davranışın iyi anlaşılması ve çeşitli uygulamalarda kullanılması için yapılacak ilk çalışma özellikle yerinde (in-vivo) olarak gerçekleştirilecek deneylerdir. ODTÜ Makina Mühendisliği Bölümü Biyomekanik Laboratuarında bu amaç doğrultusunda geliştirilen bir indentör deney sistemi mevcuttur.

Çalışmada ilk olarak hassas ve güvenilir deneylerin yapılabilmesi için indentör ve sistemi kontrol eden yazılım üzerinde çeşitli çalışmalar yapılmıştır. Çalışma sonucunda yerdeğiştirme ve yük ölçüm hassasiyetleri geliştirilmiştir. Alınan gürültülü verinin filtre edilmesi için daha iyi yöntemler önerilmiştir. Yazılımdaki bazı deney protokolleri geliştirilerek yeni protokoller eklenmiştir. Yine daha güvenilir deneylerin yapılabilmesi için cihaza yeni bir bağlantı sistemi eklenmiştir. Dokuların göstermiş olduğu anizotropik davranışı inceleyebilmek için elipsoid uçlar tasarlanıp üretilmiştir.

Çalışmanın ikinci aşamasında önkol iç yüzeyinde (medyalinde) deneyler yapılmıştır. Bu deneylerde yumuşak biyolojik dokuların viskoelastik özelliklerini gösteren histeresiz, gevşeme ve sünme davranışları gözlenmiştir. Viskoelastik

davranışlarına ek olarak alışma (Mullin) etkisi ve anizotropik yanıtlar incelenmiştir. Yine gevşeme ve sünme deney sonuçları kullanılarak bu verileri modelleyebilecek Prony serilerine ait parametrelerin değerleri tespit edilmiştir.

Çalışma ile birlikte yumuşak biyolojik doku davranışlarına dair önemli sonuçlara ulaşılmış ve bu sayede yumuşak biyolojik doku mekanik davranışı daha iyi anlaşılmıştır. Ayrıca yerinde (in-vivo) deneylerin zorlukları gözlenmiş ve bu zorlukları en alt düzeye indirebilecek hususlar açıklanmıştır. Son olarak bilgisayar andırımlarında kullanılmak üzere temiz deneysel veriler elde edilmiştir.

Anahtar Kelimeler: Yumuşak Biyolojik Dokular, İndentör Deney Cihazı, Viskoelastisite, Anizotropi, In-vivo Deneyler

To My Parents

ACKNOWLEDGMENTS

First of all, I would like to express my deepest gratitude to my supervisor Asst. Prof. Dr. Ergin Tönük for his closeness from the first day, for his supports; also for his understanding and patience.

I would like to thank Mr. Emir Birant owner of the Birant Makina for his great support to produce apparatus which we need

I would like to thank TÜBİTAK for the generous financial and moral support, provided through the graduate scholarship given for this study.

At last, I thank my beloved Mother and Father who both were always with me and who has raised my spirits when I fell into despair and who had not waivered in rendering the support I need.

TABLE OF CONTENTS

APPENDICES

LIST OF TABLES

TABLES

LIST OF FIGURES

FIGURES

CHAPTER 1

IMPORTANCE OF THE STUDY, AIM AND FIELDS OF USE

The study we have carried out was a group project. Project consisted of two parts. This study was the first part and included such matters as conducting indenter tests on the soft biological tissues, collecting and interpreting the test data and observing the behaviors of soft biological tissues under different conditions.

In order to simulate the mechanical behavior of soft biological tissues on computer, various tests must be carried out on the tissues to understand how it behaves in detail. When one thinks independently from this study, basic source for determination of the soft tissue constitutive equation is the experiments. Furthermore, understanding the tissue behaviors and observation of the responses against different stimuli can be achieved by systematic experimentation.

It is possible to carry out soft biological tissue tests by employing different devices (See Chapter 2.6). Yet, these methods have certain advantages and disadvantages. The point which must be noted here is that, the soft biological tissues are alive. Therefore, losing liveliness influences the tissue mechanical response greatly (Ottensmeyer et al., 2004). Also Fung, (1984), states that physiological stresses are an important factor affecting the soft tissue behavior. It is therefore extremely important to make observations while the tissue is in its physiological environment and while it is still alive. While working on the soft biological tissues, best method making such possible, is indenter tests (Zheng et al., 1999).

We have therefore carried out tests by the help of an indenter device in our studies. In order to obtain relevant, clear and correct data, we have achieved

improvements on the indenter device and its software. We have developed test protocols with due regard to needs, design and used components additional to the test system, solved the problems encountered and brought solutions (Chapter 3).

With this study, way to dependable tests was opened and also studies were carried out to be used in the simulations and also for the observation of the soft biological tissue behaviors.

Unexpected situations observed in the test data were examined and clarified. Furthermore, problems encountered during in-vivo indenter tests and the matters to be attended were also clarified in great extent. This will be an important guide for the new researches who plan to conduct in-vivo indenter tests.

In the study, many soft biological tissue behaviors were observed. Among these, preconditioning (Mullin's) effect, viscoelasticity and anisotropy were the ones worth to mention. Furthermore, test data are in such quality that, they can be used by the researches for different evaluations. Such difficulties as in-vivo observations of the influence of varying speed loading on the soft biological tissues, were eliminated through various modifications (Chapter 4). Thus, soft biological tissue behavior was understood better and clean and dependable data was collected.

In other part of the study comprised of the scrutinization of the constitutive models existing in the literature, diagnosing and simulating in computer media those, capable of modelling the tissue behaviors in the best way. In this study where the inverse finite element method is used, initially, a suitable constitutive model is determined. This model determined, is an improved quasi-linear viscoelastic model (Üsü, 2008, Bischoff, 2004) and can simulate great many number of behaviors observed in the soft biological tissues. These behaviors may listed as the nonlinear behavior, preconditioning (Mullin's) effect, viscoelasticity, and anisotropy.

The reason for using inverse finite element method was due to not knowing the coefficients of the constitutive law (i.e. material model). In this method, initially, a finite element model was formed on computer, boundary conditions within the test region were approximated and the finite element model was operated by entering the assumed constants as the initial guess. By comparing the results obtained in computer and the test results, the relevancy of the assumed constants were then inquired. This process was continued until the response of finite element model was within the desired closed vicinity of the experimental data where these coefficients for the constitutive law is assumed to model the material behavior.

With the other portion of the project and with its further improvement, a very detailed and realistic simulation of the soft biological tissue behaviors on computer will be feasible (Üsü, 2008). Thus, great many number of objects require for the health and comfort of human kind will be designed in a better way and in much less durations. One can give examples to these objects like prothesis and orthesis designs, bed designs for the bedridden patients, product designs for the diabetic patients, especially for the products contacting to the diseased parts of the body. Again, in further stages, contribution of such studies will be considerable for the development of surgical simulation systems which will be used in such matters as training of sergeants. It is also possible to use the experimental data in early diagnosis of the illnesses (Korhonen et al., 2003). Yet, to this end, it is still necessary to carry out further studies.

CHAPTER 2

LITERATURE SURVEY

2.1 What is Soft Biological Tissue?

Our body is composed largely of soft biological tissues. Almost all our organs, except our skeleton are soft tissues. Brain, lungs, liver, kidneys, skin and cartilages bearing very important functions to sustain our liveliness are all soft biological tissues.

Soft biological tissues are live organisms with substantially complicated physiology. They are composite structures serving a certain aim through a combination of elements with different functions. For instance, our heart pumping the clean blood to every point of our body and dirty blood to our lungs is a soft biological tissue and is composed of heart muscles, ventricles, veins feeding it and the nerve cells (Fox, 1992). Not limited to these, heart muscles are formed by three different layers, and each layer is, in turn formed of different cell structures. Therefore, soft biological tissues, as organs, are extremely complex structures built by combining elements capable of different mechanical responses when they are observed one by one (Fung, 1984).

Thus, the mechanical behaviors and responses of the soft biological tissues displaying extremely different functions are also complicated and complex. Even on the cellular basis, for these structures which are more complicated and incomprehensible than all devices and explorations found by the human kind up to date, this conclusion is understandable. Beyond all, soft biological tissues are live.

Well, how are we perceiving the behaviors of the soft biological tissues? How are we observing their responses under different circumstances and how are we obtaining the various information pertinent to them. No doubt, as in all

investigations, we are conducting tests to collect information and we are observing and interpreting the test results obtained. And in consequence, we are striving to find mathematical formulas which can explain the information gathered. Thus, formulas called constitutive equations are derived by observing and interpreting the various test data for the soft biological tissues.

Our motivation target of our efforts were also to explore such an equation. To this end, as discussed in Chapter 4, great many number of observations were carried out, and the behaviors of soft biological tissues were tried to be understood. As these efforts were progressed, in addition to the observations conducted, different test protocols also were practiced as requires by the constitutive models determined, and a dynamic procedure was followed by improving the test system (Chapter 3). Already in the existing literature, many constitutive models are in existence. Displaying some general information on these models will be beneficial for this study.

2.2 Some Constitutive Models Used in the Modelling of Soft Biological Tissues

As mentioned before, there exist numerous models in the literature. Yet, due to the complex structures of the soft biological tissues and due to their ever varying features in relation to several factors (See Chapter 2.3), a widely acceptable constitutive model has not yet been laid down. Most of the existing models hardly simulate all experimentally observed features of the soft biological tissues. Some models are deficient in modelling even only certain limited number of selected features (Zheng et al., 1999).

Yet, depending on the purpose, such models are also being used. As mentioned by Zheng et al. (1999), certain models are more suitable for the observation and comparison of the effects of various factors, such as aging, rather than the explanation of the behaviors of the soft biological tissues. Furthermore, another important point is the determination of the parameters under which the test results will be evaluated. For instance, soft biological tissues display the

preconditioning (Mullin's) effect under cyclic loading. This behavior which will be discussed in the following chapters, explains the retrieval of the repeatable data displayed with the progress of successive loadings. Thus, some of these models are set up on the basis of these repeatable data. Yet, in real life, tissue is not always subjected to such loading situation and this is a matter to be contemplated. In other words, for certain cases, studying the data where the initial loading takes place, may render to be important (Gefen and Margulies, 2003, Provenzano et al., 2001). Yet these data are disregarded and eliminated in certain models (Fung, 1984). Similarly, behavior showing the interactions of a bedridden patient with his bed or of a man sitting, with his chair is the behavior of creep.

The lack of the necessary constitutive equation for which can be used various designs like beds for bedridden patients, researching prothesis - orthesis relation under constant loads is a major obstacle to make computer aided design used in many industry fields.

Under the light of the above explanations, let us discuss the major constitutive models in short. These models classified under three basic headings may be listed as the phenomenological modelling, structural modelling and multi dimensional modelling (Maurel et al., 1998).

2.2.1 Phenomenological Models

These are the models constituted by direct consideration of the test data. In these models, a mathematical model capable of simulating the test data is derived (Maurel et al., 1998).

Pseudo-elastic and quasi-linear viscoelastic models may be mentioned as the examples of this type of models. These models developed by Fung have an extremely wide range of usage, and they also constitute the basic building stones of certain models (Bischoff, 2004).

Data obtained through cyclic loading is used in the pseudo-elastic modelling**.** Soft biological tissues display preconditioning effect under cyclic loading. Thus, following a certain number of cycles, repeatable loading – unloading curves can be obtained. Fung, utilizing this feature, forms the pseudo-elastic theory. Soft biological tissues, display viscoelastic behavior. This is realized from the cycle taking place during the loading and unloading process. That is, curve obtained during loading can not follow the same route with the curve obtained during unloading. Yet, by obtaining repeatable curves following a certain number of cycles, Fung has examined the loading and unloading curves and in order to explain the mechanical features of both cases, has used the method of elasticity theory. Modelling of the soft biological tissues which are normally non-elastic, is therefore described as pseudo elastic modelling (Fung, 1984).

The most noteworthy deficiency of this model, which in fact is a considerably major step in modelling of the soft biological tissue behaviors, is its inability of modelling time dependent relaxation and creep behaviors of the soft biological tissues. Nevertheless, Fung taking a further big step, has developed the quasi-linear viscoelastic model. With this model, modelling of the relaxation and creep behaviors of the soft biological tissues was made possible (Fung, 1993) and door to many advanced studies were opened (Üsü, 2008, Bischoff, 2004, Holt et al., 2008).

The foundation of this model was described by Üsü and Tönük (2008) as “taking the integral of the multiplication of reduced relaxation function with the time related derivative of the elastic stress function, throughout the test duration”. Equation corresponding to this conclusion is given as follows;

$$\sigma(t) = \int_{\tau=0}^{t} G(t-\tau) \frac{\partial \sigma^{(e)}(\varepsilon)}{\partial \varepsilon} \frac{\partial \varepsilon}{\partial \tau} d\tau \quad \text{.....(2.1)}$$

where,

$\sigma(t)$ = stress

G (t) = reduced relaxation function

$\sigma^{(e)}(\varepsilon)$= Instantaneous stress function related to strain

ε = strain

it is possible to use the reduced relaxation functions in different forms, (Fung, 1993). Most frequently used of these form is,

$$G(t) = \frac{1 + c\left[E(t/\tau_2) - E(t/\tau_1)\right]}{1 + c\ln(\tau_2/\tau_1)} \quad \text{.....(2.2)}$$

where $E_1(x)$ first exponential integral function and is expressed as,

$$E_1(x) = \int_{y_1}^{\infty} \frac{e^{-y}}{y} dy \qquad \begin{cases} y = \dfrac{1}{\tau} \\ y_1 = \dfrac{1}{\tau_1} \end{cases} \quad \text{.....(2.3)}$$

τ_1 and τ_2 represent the short and long term relaxation behaviors. Like in the first exponential integral function, it is possible to select $\sigma^{(e)}(\varepsilon)$ in different forms. These selected forms vary depending on the tested tissue. In one modelling study, the following form is preferred (Üsü and Tönük, 2008).

$$\sigma^{e}(\varepsilon) = A\left(e^{B\varepsilon} - 1\right) \quad \text{.....(2.4)}$$

where, A and B are parameters pertinent to the material in concern.

2.2.2 Structural Models

Structural models are the models formed with due regard to the structure and elements of the tissue. In the basic approach, behaviors of the collagen fibers are tried to be modeled (Maurel et al., 1998). Viscoelasticity is also strived to be modeled by adding the viscoelastic features to these types of models.

Two damper generalized linear Kelvin-Voigt material where the soft biological tissues is modeled as an example (Tönük and Silver-Thorn, 2004). Here, relaxation and creep behaviors of the soft biological tissues are modeled by a structure, in the form shown in Figure 2.1. This model also, is described by the help of the Prony series (Equation 2.5 and 2.6).

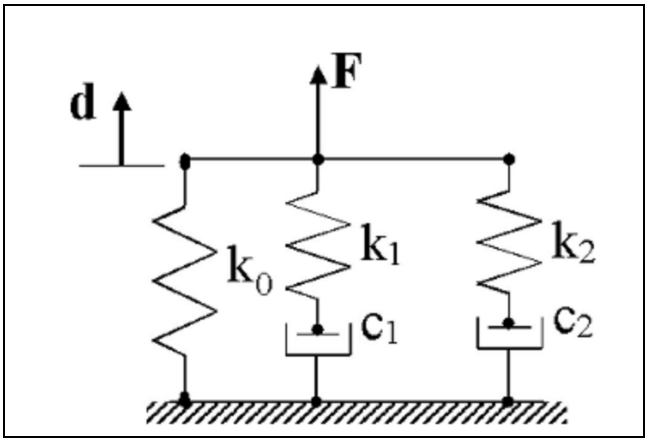

Figure 2.1 Kelvin-Voigt linear viscoelastic material model (Tönük and Silver-Thorn, 2004)

$$F(t) = F_0\left[1 - \delta_1\left(1 - e^{-t/\tau_1}\right) - \delta_2\left(1 - e^{-t/\tau_2}\right)\right] \quad \text{.....(2.5)}$$

$$d(t) = d_0\left[1 + \delta_1\left(1 - e^{-t/\tau_1}\right) + \delta_2\left(1 - e^{-t/\tau_2}\right)\right] \quad \text{.....(2.6)}$$

Equation 2.5 and 2.6 are used for the relaxation and creep behavior respectively. Where, τ_1, τ_2 are short and long-term time constants δ_1, δ_2 are short and long term relaxation and creep magnitudes.

F_0 and d_0 are the force and displacement at the start of relaxation and creep.

In present study also, constants of the Prony series in different forms were determined by using the relaxation and creep test data obtained. Forms were

compared with regard to each other and the anisotropic behavior in relation to the constants were observed (See Chapter 4).

2.2.3 Multi - Dimensional Models

These are the models where the stress- strain relation is established by the help of an element called strain energy function (strain potential) (Fung, 1993). Fung presents the determination of stress components in relation to the strain energy function as follows,

"Let W be the strain energy per unit mass of the tissue, and ρ_0 be the density (mass per unit volume) in the zero-stress state, then $\rho_0 W$ is the strain energy per unit volume of the tissue in the zero stress state. Let W be expressed in terms of the nine strain components E_{11}, E_{22}, E_{33}, E_{12}, E_{21}, E_{23}, E_{32}, E_{31}, E_{13}, and be written in a form that is symmetric in the symmetric components E_{12} and E_{21}, E_{23} and E_{32}, E_{31} and E_{13}.the nine strain components are treated as independent variables when partial derivatives of $\rho_0 W$ are formed. Then when such a strain – energy function exists, the stress components S_{ij} can be obtained as derivatives of $\rho_0 W$:

$$S_{ij} = \frac{\partial(\rho_0 W)}{\partial E_{ij}} \text{„}$$

where i and j represent the principal directions. Normally, soft biological tissues do not posses stress-strain function. In other words they are not hyperelastic materials (Fung, 1993) because soft biological tissues are not elastic materials. Yet, their pseudo – elastic behaviors, discussed in Chapter 2.2.1, makes it possible to identify such a function for the soft biological tissues (Fung, 1993). In the literature, great many number of strain – energy functions pertinent to soft biological tissues exist. Various strain energy functions are determined and used for arteries, skin, veins, lung parenchyma and similar bodies (Maurel et al., 1998).

2.3 Factors Influencing the Mechanical Properties of the Soft Biological Tissues

Mechanical properties of the soft biological tissues may show variations depending on various factors. Some of those factors are age, illnesses, physiological structures of the tissues and the livelihood. Also, a result of injuries the physiological structure of the tissue deteriorates and its mechanical properties are influenced. The effect livelihood among these factors will be discussed when the test methods are described.

2.3.1 Age

One of the important factors influencing the behavior of the soft biological tissue is age. Borniger (1905) in a study he carried out at the start of the 20^{th} century, has revealed that, elastic stress in childhood is lower compared to elastic stress in adults and that it shows another decrease with old age.

In creep tests carried out by Kirk and Kvorning (1949), with 50 gram loads on the lower aspect of the tibia, have determined that, with the instantaneous application of the load in youngsters a 3.4 mm impression and in elderly a 2.7 mm impression has taken place. Creep test has been continued for 2 minutes and at the end of this duration, it was observed that in both of these groups total creep came out to be equal (Figure 2.2). Yet 3 minutes after the release of load, tissue has recovered by 76% among young individuals. Among the elderly this recovery ratio has remained at 43%. Same tests are carried out at the upper aspect of the tibia and similar results are observed.

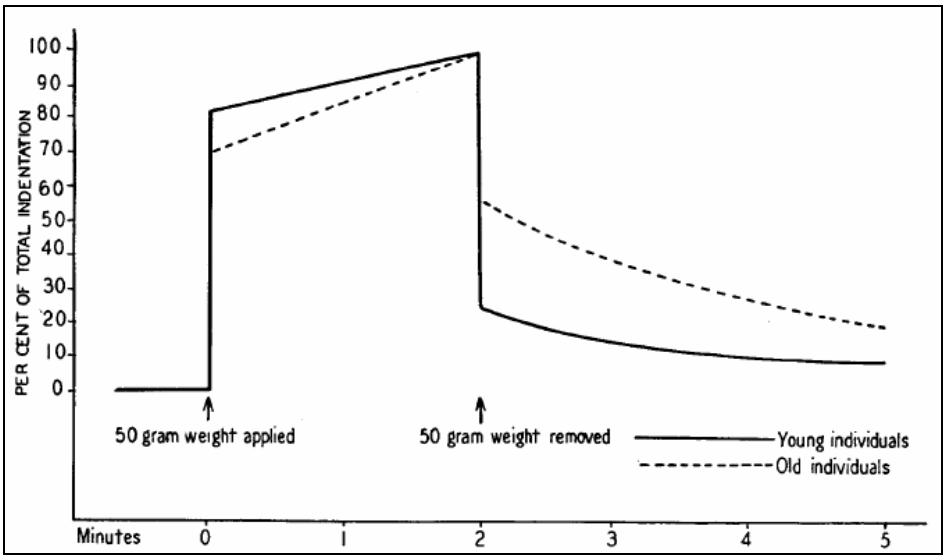

Figure 2.2 Creep test carried out Kirk and Kvorning (1949), on young and old individuals. 50 gram load is applied on the young and old individuals and their reactions are observed. Later load is released and 3 minutes later their conditions are observed. Dashed and continuous lines are related to young and old individuals respectively.

In another study carried out on the rib cartilage, similar results supporting the Kirk and Kvorning's (1949) study and the creep in young individuals were found to be higher than the creep in old individuals (Skolof, 1966).

Effective elasticity modulus obtained from the indenter tests conducted on healthy 6 young and amputated 3 old individuals, have been on higher side for young individuals (Zhang et al., 1999). Reason for this is recorded as the aging and not the amputation.

2.3.2 Illnesses

Different illnesses cause alteration in the tissue physiology. These alterations influence also the mechanical behavior of the tissue. Doctors from past to date, try to diagnose the illnesses by observing these mechanical changes (Manduca et al., 2001). Examples of complications influencing the tissue physiology may be mentioned as cancer, various vein illnesses and diabetes.

Cancer is one of the frequently encountered illnesses influencing the mechanical behaviors of biological tissues. Types of cancers such as breast cancer can be diagnosed, not always perhaps, by the use of hands (palpation) thanks to the hardened tissues at the cancerous region.

Manduca et al. (2001), in his study, has determined that, the region with tumor is 5 to 20 times harder than the region without tumor. A similar observation is made by Lawrance et al. (1999) and the shear modulus being approximately 5 times higher than that of the adipose and glandular tissues (Figure 2.3).

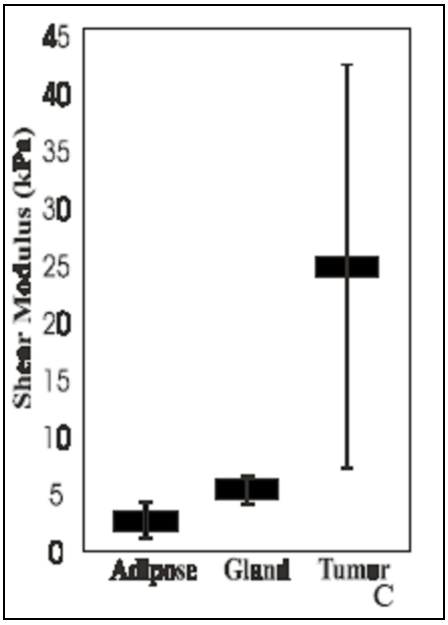

Figure 2.3 "Average shear modulus values of normal adipose and glandular tissues compared with tumor tissues."(Lawrance et al, 1999, p.1)

Venous complications are also illnesses deteriorating the soft tissue physiology and their pertinent mechanical properties. In almost all of these complications, fibrotic soft biological tissue alterations are observed. Geyer et al. (2004) states the changes in tissue as "This change is observed as an ever-increasing skin and sub tissue hardening and it is called as lipodermotosclerosis (LDS)" (p.131).

Geyer et al. (2004) in his study on the tissues with LDS and without LDS, calculates elasticity modulus giving the relative hardness of the tissue. Average elasticity moduli of the tissues are observed to be within the range of 5.63 to 16.62 kPa. This value is calculated as 22.36±8.61 kPa for the objects with LDS. Here, tissues assume modulus of elasticity within the range of 8.62-34.28 kPa. Finally, a modulus of elasticity value for the objects with LDS comes out to be almost twice of those of the objects without LDS.

In the studies carried out on the soles of the feet of the normal persons and individuals with diabetes, effective shear and elasticity modulus of the tissue with diabetes comes out to be higher than those of the normal tissue (Gefen et al., 2001).

2.3.3 Physiological Structures of the Tissues

Organs serving different purposes display also different physiological structures. Internal organs like brain, lung and liver are not suitable to carry the intensive external mechanical forces and are protected inside their natural media. Such organs are called as the very soft biological tissues. The strain levels coped by the very soft biological tissues do not exceed 30% and above this limit, tissue assumes permanent deformation as stated by Miller (2000).

Soft biological tissues such as skin and cartilage are subject to external forces and they posses structures capable of coping with these forces. Therefore strain levels which are endured by these soft biological tissues are higher.

Although their physiological structures are same, mechanical properties of the organs in different parts of the body may show variations from each other. A good example of this is cartilage. This phenomena is clearly observed in the articular and rib cartilages (Skolof, 1966). In the tests, creep measurements are carried out for 60 minutes and following the test, tissue is left to recover for 60 minutes. It is observed that, rib cartilage is more resistant against pressure deformation as compared to the articular cartilage. Indentation following the

instantaneous loading is 0.75 mm and 0.2 mm for articular and rib cartilages respectively (Figure 2.4).

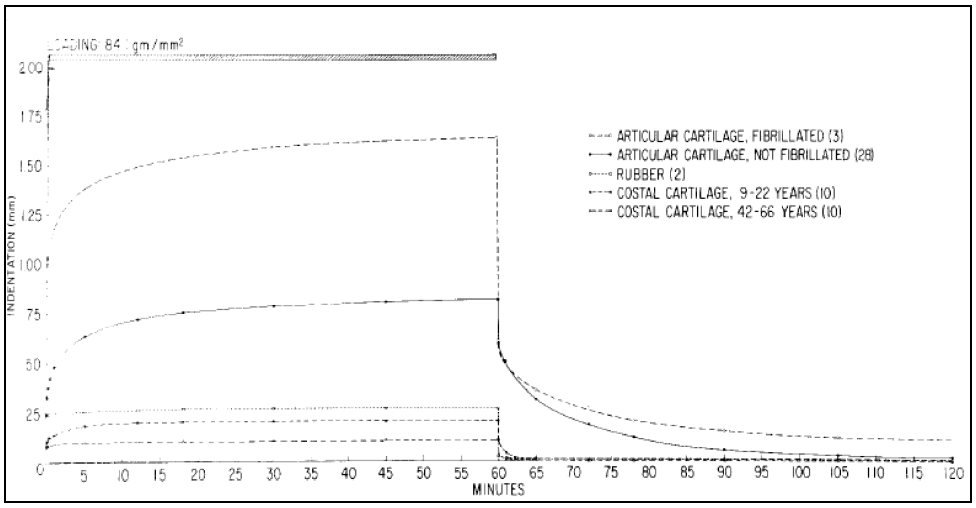

Figure 2.4 Results of indenter tests on articular and rib cartilages

2.4 Test Methods

It is possible to conduct tests on soft biological tissues in many different methods. These methods have advantages and disadvantages compared to each other. These tests may be categorized as ex-vivo, in-vitro, in-situ and in-vivo tests.

2.4.1 Ex-Vivo Tests

In the ex-vivo tests, organ is taken out of the organism and by the help of various systems, their living conditions are tried to be duplicated. Thus, obtaining more dependable and convenient data is aimed.

Ottenmeyer et al, (2004), have carried out ex-vivo tests on liver and observed the effects of test conditions on the data. This system, is a good example with regard to ex-vivo test arrangements, and its operation is explained as follows,

"To accurately measure the mechanical properties of the liver, it is crucial that we maintain cellular integrity while keeping the organ in as natural a state as possible *ex vivo.* Thus we have built an apparatus similar in concept to normothermic extracoporeal perfusion systems using heparinzed Lactated Ringer's solution as the perfusate (see Fig. 1(Figure 2.5)). The system stores this solution in reservoirs suspended at specified heights to obtain the appropriate physiologic pressures into the hepatic artery (100-120 mmHg) and portal vein (15-20 mmHg). Both pressures and flow rates can be easily adjusted by altering the height of the reservoirs and by partially closing tubing clamps respectively. The perfusate is then allowed to drain via the intrahepatic vena cava into a bath where it is heated to a physiologic temperature (39° C for pigs) and circulated to the reservoirs via a pump. The solution also flows over the organ to maintain hydration without having to submerge the organ. To ensure consistency in our measurements, the organ rests on a sturdy plate covered with fine grit sand paper to localize and stabilize the area of tissue under study, and the perfusion pressure is held constant rather than mimicking physiologic pulsatile pressure." (p.3)

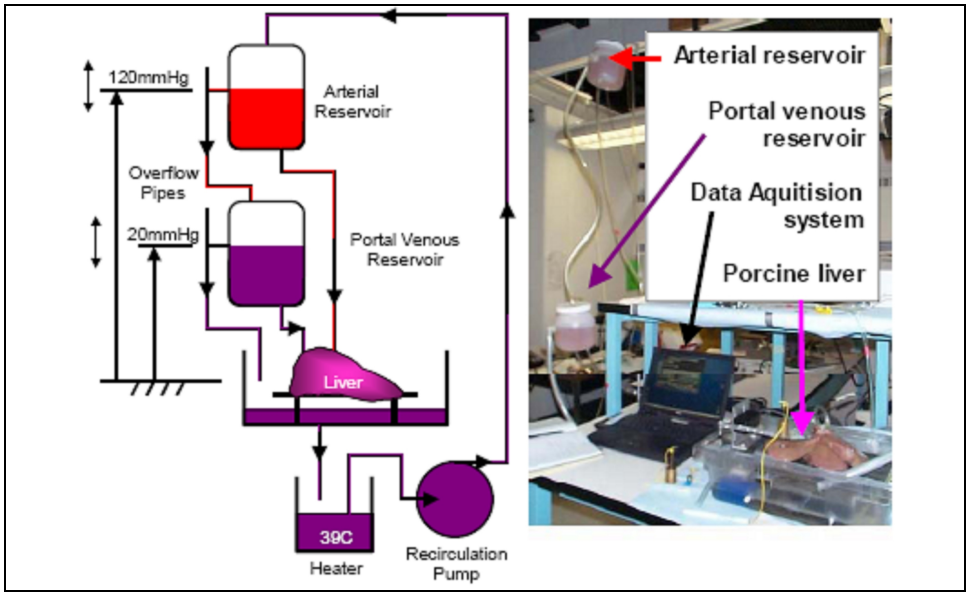

Figure 2.5 "(left) Our Normothermic Extracorporeal Liver Perfusion system schematic. (Right) NELP system in use". (p.3)

2.4.2 In-Vitro Tests

In the in-vitro tests organ is taken out of its place in the organism, as in the ex-vitro tests. Tests are carried out as the tissues are dead. In the in-vitro tests, duplication of the natural environment of the tissues is not a concern, and the tissue is studied is its raw form. In these tests, tissue may be studied as a whole or as divided to parts (Gefen and Margulies, 2003, Tanaka et al., 2002).

2.4.3 In-Vivo Tests

In the in-vivo tests, organ is studied at its original place and while it is alive. In-vivo tests can be conducted by two different methods. These are the invasive and non-invasive methods.

2.4.3.1 Non-Invasive Method

In the imaging based non-invasive method, basically the strain area within the tissue is studied. Ottensmeyer (2002) describes the non-invasive method as follows:

“Essentially, some known displacement, which may include static or dynamic compression or shear displacement, is applied to the exterior of the tissue under consideration. Since the tissue is continuous, the surface displacement produces a strain field within the tissue, which is a function of the surface displacement, the elastic properties of the tissue and other boundary conditions. The strain field is measured through the use of some non-invasive imaging technique, including, but not limited to, magnetic resonance imaging (MRI) and ultrasound. In the static case, “before” and “after” scans are made, and the strain can be calculated based on the local displacements measured between them. For dynamic testing, vibration amplitude or velocity can be used instead of static strain” (p.328).

2.4.3.1.1 Disadvantages of the Non-Invasive Method

Non-invasive method allowing in-vivo studies in the internal organs on one hand carries some deficiencies on the other. Ottensmeyer (2002) mentions some handicaps as he states “Tissues are known to exhibit non-linearity in their stress-strain relationships, and the majority of the non-invasive techniques can only examine the small strain, linear portion of the response. Further, the static techniques cannot examine the visco-elastic behavior of tissues, while the dynamic techniques require excitation frequencies large enough so that the wavelength of sound is small enough compared with the structures under consideration.” (p.329). Another important shortcoming is that, in great many number of systems operating under non-invasive method, non-linear behavior of the soft biological tissue can not be observed and that a small strain can be applied for linear response.

2.4.3.2 Invasive Method

In the invasive method, stress-strain magnitudes are measured locally. In other words, force is applied on the external surface of the tissue and the displacement of tissue in relation to the force, is observed. Thus, this displacement and the force magnitudes are recorded for the analysis to be carried out.

In the invasive methods, it is possible to conduct many tests by using different techniques. Methods such as indenter tests, stress and torsion application are the examples of these methods, which will be discussed in the following sections.

2.4.4 In-Situ Tests

In the in-situ tests, organ is studied at its original medium. Differing from the in-vivo tests, the donor and therefore the tissue is not alive.

2.5 Advantages and Disadvantages of the Test Methods

These test method which were described in general terms, relative to each other, possess various advantages and disadvantages. We shall try to explain these, by studies carried out also to compare these methods.

Ideal approach is conducting tests in-vivo conditions if one is seeking the material law of the tissue or organism when it is alive. Yet, it is not always possible to secure the in-vivo test conditions. In such case, the solution is strived for by using methods giving nearest outcomes to the in-vivo test results. Starting from the most ideal rating of the methods may be in order of in-vivo, ex-vivo, in-situ and in-vitro.

These are two basic reasons for in-vivo to be the ideal method. First of these is that, the tissue is alive and the second is that, the tissue is studied in its original medium. Tissue is in interaction with its encasing medium. Tissue is surrounded with various supporting structures such as muscles, bones and other different organs. In a study carried out by Fung (1984) on different blood vessels, he described this fact in a very comprehensive way,

“The peripheral capillaries in the mesentery are embedded in a gel. A gel behaves as a solid; and, as a consequence, a capillary blood vessel embedded in it behaves as a tunnel in solid earth. That is why the capillary is so rigid with respect to blood pressure, and so stable with respect to compression(Fung et al., 1966). On the other hand, a pulmonary capillary is exposed to alveolar gas which provides little resistance to deformation; and as a consequence the pulmonary capillaries are distensible and collapsible.

If we compare a pulmonary artery with a peripheral artery, we see that latter is an isolated vessel, whereas the pulmonary vessel is embedded in the lung parenchyma. The lung tissue (alveolar walls) pulls on the pulmonary blood vessel wall, and keeps it patent when the alveolar gas pressure exceeds the blood pressure; and the tissue stress influences the vessel deformation so much that

nearly linear pressure-diameter relationship is obtained. If the pulmonary artery were isolated, it would most likely behave the same way as the peripheral vessels" (p.512).

As can be understood from Fung's studies, medium surrounding the tissue, has great influence on the mechanical behavior of the tissue. Even blood vessels with same physiologies may display different mechanical behaviors due to the media they are encased in. Therefore, this also influences the mechanical test results. In the comparative studies, results obtained through the in-vivo tests are never duplicable by other methods and that they show certain deviations.

In a study carried out on pig brain, in-vivo, in-situ and in-vitro tests are conducted and the results are compared (Gefen and Margulies, 2003). In this study, the influence of perfusion is also desired to be seen. In the study following conclusions pertinent to the subject matter were drawn;

- Long term time constant pertinent to relaxation comes out to be on the low side for in-situ tests.

- Mechanical response of the live brain against preconditioning is different than that of the dead tissues. Decrease in the shear modulus as a result of the preconditioning effect is higher in the in-situ and in-vitro tests.

- It is revealed that, many mechanical properties for the in-vivo and in-situ tests are identical.

- In the comparison made between in-situ and in-vitro to observe the effect of skull, while the transition properties remains to be uninfluenced, short and long-term shear modulus of in-vitro measurements come out to be lower than in-situ values.

In another study carried out on pig liver, in-vivo, ex-vivo and in-vitro test results are compared (Ottensmeyer, 2004). Ex-vivo tests are carried in two different ways and the effect of perfusion on the test results are also observed. In the tests,

two types of test device are used, and in the first of these tests, small strain magnitudes are applied and observations in the linear region are made. With the second test device, on the other hand, applying higher magnitudes of strain is made possible. In the measurements taken by the first test device, lowest hardness was observed in the in-vivo tests, with perfused tissues displaying more solid and with unperfused tissues displaying most solid behavior.

With the second test device, tests are conducted and strains are calculated for the in-vivo, perfused ex-vivo, unperfused ex-vivo and in-vitro cases. At the end of the tests, it is observed that, organ which is measured in in-vivo is softer than the perfused one. Perfused organ, on the other hand, comes out to be softer than the unperfused one. The organ subjected to in-vitro test, organ shows a softer behavior compared to the results of the all other tests. Besides, a stable strain value for this case is not available.

The nearest result to in-vivo test obtained in the ex-vivo perfused test and for stable cases, it shows a deviation of 17%. This deviation is above 50% for unperfused ex-vivo test (Figure 2.6).

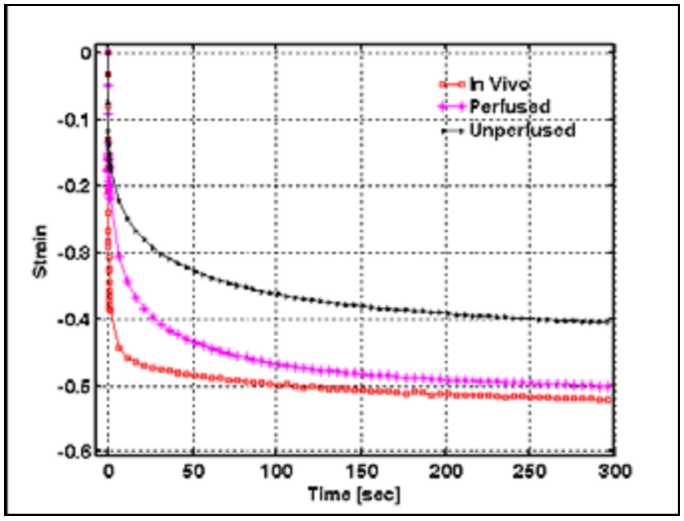

Figure 2.6 Strain graphs obtained under different conditions (Ottensmeyer, 2004, p.7).

Again as an important conclusion, it is observed that, repeatable tests in–vivo and perfused ex-vivo tests can be carried out. For the unperfused test such is not encountered (Figure 2.7).

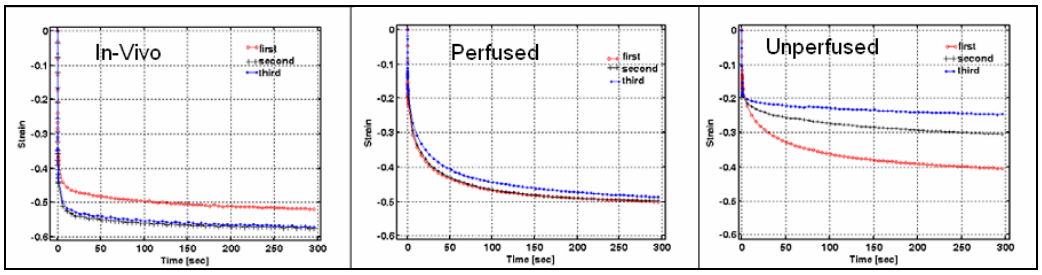

Figure 2.7 Observation of the repeatability for the in-vivo, ex-vivo perfused and unperfused cases (Ottensmeyer, 2004, p.7).

After making these explanations, advantages and disadvantages of the test methods are item by item as follows:

For the in-vivo measurements,

Advantages of the in – vivo tests,

– For the tissue keeping its vividity, and for it is being studied in its original medium, most appropriate results are obtained in the in-vivo tests.

Disadvantages of the in – vivo tests,

– Yet, in the studies carried out on human beings, necessity of testing live tissue, brings great importance not to harm the tested individuals, measurements are carried out only on external organs such as skin. Although studies on the internal organs by employing non-invasive methods are possible, the properties of the tissue would not be properly characterized and only a linear stress-strain relation would be observed.

- Due to the tissue not possessing a regular geometry, stress-strain (-time) relations cannot be obtained by simple calculations and more advanced techniques (like inverse finite element method) are required.

- For the studied tissue not to be damaged, observations can be carried out by restricting only certain test devices.

For the ex-vivo measurements,

Advantages of the ex – vivo tests,

- With the ex-vivo tests closest results to the in-vivo tests are obtainable.

- Due to working on the dead tissues, tests can be carried out much more easily, behavior of internal organs which are normally unobservable in the in-vivo tests, can be investigated in a much closer way.

Disadvantages of the ex – vivo tests,

- In the ex-vivo tests, complicated and expensive systems must be arranged and such systems must also be preserved in appropriate environmental conditions.

- Due to the necessity of examining the organs as a whole, the test devices which can cope with the task may render to present limitations.

- Determination of the boundary conditions may not be possible like in the in-vivo tests.

For the in-situ measurements,

Advantages of the in-situ tests,

- In the in-situ tests, dead tissue can be examined in its original position. Thus, the interaction of the tissue with the neighboring tissues are preserved and the presence of such interactions makes the obtaining of

more realistic results possible. Naturally, such is not valid when solely the organ behavior is desired to be observed.

Disadvantages of the in-situ tests,

- In-situ examination of the tissue in its original position as a whole, also limits the test devices to be utilized in these tests.

- As stated in in-vivo and ex-vivo tests disadvantages, also in in-situ tests, examined tissue may not possess a regular geometry. Consequently, stress-strain (-time) relations can not be obtained by simple calculations.

For the in-vitro measurements,

Advantages of the in-vitro tests,

- In the in-vitro tests, tissue can be examined in every way desired.

- Test specimens can be prepared in the desired manner and the tests can be carried out by the help of various materials test devices.

- Test specimens being in regular geometries allow for the determination of the boundary conditions.

- Another important advantage is that there exists lots of works in the literature about the in vitro tests. Consequently it is possible to benefit from these works while searching soft tissues behaviors as in-vitro.

Disadvantages of the in-vitro tests,

- Yet, due to tissue being dead, its examination outside its original position and necessity of examination as a whole cause the data obtained to be questionable and in the presently carried out test also, maximum deviations from the in-vivo test results are observed to be in the in-vitro tests.

Also, the following table was prepared for easy comparison;

Table 2.1 The table showing soft tissue test methods comparison[1]

	in-vivo	ex-vivo	in-situ	in-vitro
Observability of the real behavior of the tissue	⊕⊕⊕⊕	⊕⊕⊕	⊕⊕	⊕
Liveliness of the tissue	⊕⊕⊕⊕	⊕	⊕	⊕
Observability in neutral environment	⊕⊕⊕⊕	⊕	⊕⊕⊕	⊕
Workability on the internal organs	⊕⊕	⊕⊕⊕⊕	⊕⊕⊕	⊕⊕⊕⊕
Workability on the external organs	⊕⊕⊕	⊕⊕⊕	⊕⊕⊕	⊕⊕⊕⊕
Easiness of the calculation stress-strain relation	⊕⊕	⊕⊕	⊕⊕	⊕⊕⊕⊕
Variability on the test devices which can be used tests	⊕	⊕⊕	⊕⊕	⊕⊕⊕⊕
Simplicity of the test system	⊕⊕⊕	⊕	⊕⊕	⊕⊕⊕⊕
Cost of the test device set-up	⊕⊕⊕	⊕	⊕⊕	⊕⊕⊕⊕
Works amount in the literature	⊕⊕⊕	⊕	⊕⊕	⊕⊕⊕⊕

2.6 Devices Used in the Soft Biological Tissue Tests

It is possible to carry out tests on soft biological tissues by substantially different devices. Use of these devices depends on the method. It is possible to employ such tests as tension, traction, compression, indentation on the soft biological tissues.

[1] ⊕⊕⊕⊕ very good ⊕⊕⊕ good ⊕⊕ not bad ⊕ bad

2.6.1 Tensile Tests

Devices used in the tensile tests are the devices frequently used in tests where different material properties are investigated. Therefore, they exist in most mechanical materials laboratories. Yet, since the soft biological tissues are not capable of enduring large loads, such devices are needed to be suitable for precise measurements. Therefore, commercial test systems custom made for the soft biological tissue tests are available (Planar-Biaxial Soft Tissue Test System, 2004). Tests being easily conductible and presence of the test devices readily in almost all laboratories makes these tests frequently used tests.

Tensile tests are normally very suitable tests for the in-vitro method. With the help of some special systems in-vivo tests can also be conducted. In-vitro tests can be employed by uniaxial and bi-axial loading. In the in-vitro tests, on the other hand, devices and methods such extensometer and suction cub may be used (Payne, 1991).

2.6.1.1 Uniaxial Tensile Tests

Several in-vitro studies are carried out by engaging uniaxial tensile tests devices (Tanaka et al., 2002, Prete et al., 2004). In these tests, rectangular specimens are prepared. These specimens are marked at two points along their longitudinal axis. The distance between these points gives the reference length. Later these specimens are fixed to the tension device from any point outside the reference points by the help of jaws. One of the jaws is stationary while the other is mobile. Movement of the jaw is achieved by a motor in the system. Stationary jaw is equipped with a load cell and thus, the load applied during the test specimen is recorded together with the stretch which is measured by the displacement of the reference points which is recorded by cameras (Figure 2.8). Using the data collected, graphs yielding the results such as strain-time, force-displacement is obtained.

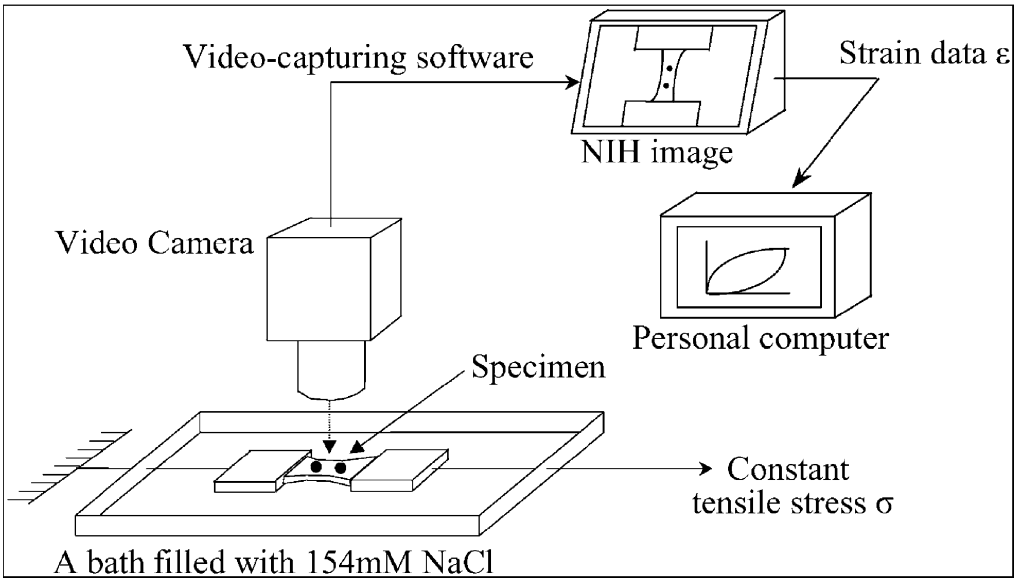

Figure 2.8 Extension test system arranged by Tanaka et al (2002)

2.6.1.2 Bi-Axial Tensile Tests

In these tests rectangular specimens are used. In the system used by Fung (1993, p.295-296) clips at four sides of the specimen are fixed and the connection between the moving platforms and the specimen is secured by silk strings. Specimen must be connected to the device in a very neat way. Local deformations at the connection points must be minimized. For attaining homogenous lateral deformations in bi-axis, lateral deformations must be free. In addition, strain measurements must not damage the tissue, must not cause strain accumulations and must calculate strains in all loading directions.

During the test, sample is pulled from its four edges. For the center of the specimen not to offset various mechanisms are employed. As an example of such a mechanism, a commercial system namely the mechanism of the product developed by Instron Company may be given (Figure 2.9). In this system, there exists four movers, each mounted on a common table allowing their location at different distances at 90º angle to each other. One of each two movers in X and Y directions, can move in relation to either one of the position, force or strain

parameters. At the same time, corresponding mover resumes the centralization. In this system, centralization can be secured even under dynamic loading conditions (Planar-Biaxial Soft Tissue Test System, 2004).

Figure 2.9 Bi-axial extension test system (Planar-Biaxial Soft Tissue Test System, 2004).

In this system, force is determined by the load cell mounted on one of the x and y axis in contrast to the uniaxial test, and the differences accruing during the test are recorded by the help of the cameras. Strain magnitudes are calculated through these records.

Subject to the adequacy of the device, it is possible to conduct uniaxial tests by using the bi-axial test systems.

There exist several difficulties that must be avoided which may be encountered during the course of the bi-axial tests. Fung (1993, p. 298) draws the attention to some of these difficulties. Controlling the boundary conditions by the bi-axial extension test devices is more complicated compared to the uniaxial extension

test device. For the analysis to be easily made, stress and strain situations at the target area must be organized. In order to avoid the deterioration effects of the loading device, target area must be kept small and at an appropriate distance from the exterior edges.

2.6.1.3 Suction Cup Tests

To realize the tension tests in in-vivo is very difficult. Since the live tissue can not be connected to uniaxial and bi-axial test devices, these tests can not be conducted under in-vivo conditions.

One of the methods allowing in-vivo tension tests is the suction cub method. These are the tests, conducted by putting a casing on the surface of the tissue to be examined, by evacuating the air in the casing and by observing the change in the tissue. Test arrangement is more suitable to be worked on the skin. A good example of the test devices is laid down by Alexander and Cook (1977). Their developed device comprise of two systems. These systems are strain metered pre-stressing device and the vacuum device (Figure 2.10).

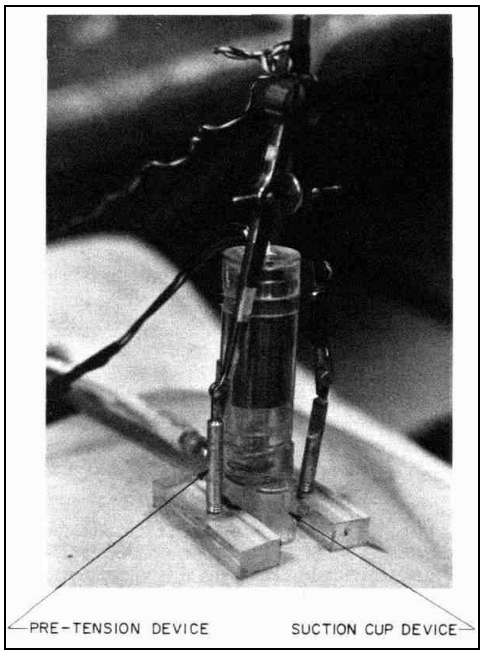

Figure 2.10 Pre-stressed suction cup device (Alexander and Cook, 1977, p.312) The reason of the preference of a pre-stress metering device in the system is the loading of the skin in double axis when the skin is in its natural form in the early examinations. In the studies carried out only with the absorption dish, obtaining the data only to certain the values related to the natural status of the skin, makes the evaluation of the results difficult.

Combined system works as follows (Alexander & Cook (1977)**)**:

"The pretension device was first used to determine the natural skin tension directions. After each of these determinations, the suction cup device was applied to the relaxed skin area yielding a pressure versus center deflection characteristic in each direction. Using the data of all four tests, the skin tension versus extension ratio characteristic in both directions was computed. Since the test was performed on a relaxed skin area, the effect of natural tension on the characteristic curve was effectively eliminated. The resultant skin tension versus extension ratio curves were representative of the skin, regardless of its natural tension state" (p.311).

This device, although important from the viewpoint of achieving the in-vivo elongation, carries inherent deficiencies. To observe the anisotropic behavior of

the tissue is difficult with this method. Viscoelastic behaviors creep and relaxation properties of the soft biological tissues also, can not be observed by this method.

2.6.2 Traction Tests

Traction tests, by method, are similar to the uniaxial tensile tests. Yet, in this case, specimen is not planar. Specimen subjected to extension tests possess very small thickness compared to the dimension in the direction of extension. Thickness of the sample specimen in the traction tests on the other hand, is not small when compared to its other dimensions, and the test is carried out in this direction. In other words, when we anticipate the specimen in x-y-z space, in the traction test is conducted in z direction in contrast to extension tests here pulling is done in x and y directions. Traction tests are more suitable to in-vitro tests (Miller and Chinzei, 2002) and can be applied in-vivo only by special devices.

In-vitro traction tests are conducted as follows. Samples are cemented to tables connected to the upper and lower jaws of the device for pulling. One of the jaws is stationary and the other is mobile. Surface areas of the jaws are larger than the surface area of the test specimen. With the commencement of the test, mobile jaw begins to move causing deformation of the specimen and at the same time, applied force in the direction of pulling and the displacement are recorded (Figure 2.11). In these tests, due to the realization of pulling only in one direction, anisotropic behaviors of the soft biological tissues are not observable.

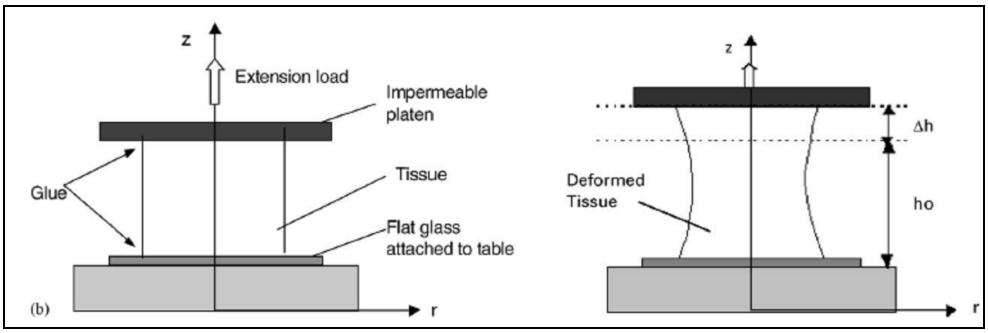

Figure 2.11 Traction test system and its application (Miller, K., Chinzei, K., 2002, p.485)

Device facilitating the in-vivo test on skin can be seen in the Figure 2.12.

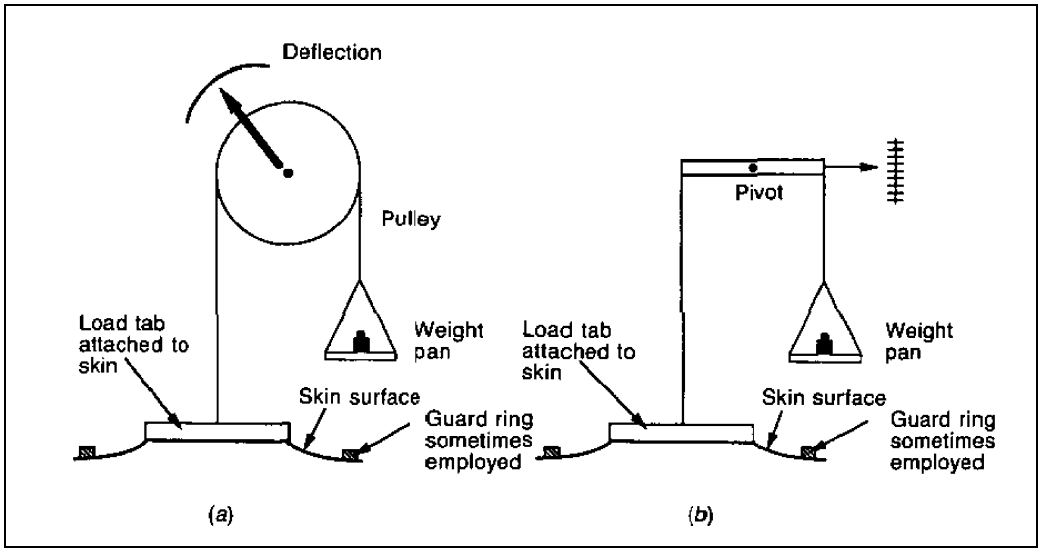

Figure 2.12 "Simple traction measurements of load against deflection for skin. (a) Pulley system. (b) Pivoted support system." (Payne, 1991, p.111).

In this test arrangement, the skin portion to be examined is cemented on the surface of the plate which will apply the pulling force. Since the test is done on the live tissues, not to damage the skin while it is separated from the plate at the end of the test, a suitable cement must be used and also such cement must be strong enough to cope with the force applied during the test. In these tests, tissue

is flexed by applying load on the plate in the direction of extension. Test is completed by recording the applied load and the magnitude of extension (Payne, 1991).

Problems pertinent to the measurements taken, are summarized in the article where the device is described, “However, analysis shows that the stresses and strains in the test area are inhomogeneous and again the anisotropy of skin is not measured.” (Payne, 1991, p.110)

2.6.3 Compression Tests

Same system used for the traction tests is used in the compression tests. Mobile jaw realizes loading in such a way that mobile jaw applies pressure on the sample. During the test force-displacement data is collected.

Compression test may be conducted by using two methods. These are the confined and unconfined compression tests (DiSilvestro and Suh, 2001).

Unconfined compression tests are carried out as described above. Load is applied on the specimen placed in between the two jaws, by the upper jaw. Specimen can flex freely in lateral directions (Miller – Young et al., 2002).

In the confined compression tests, the lateral faces of the specimens are harnessed not to move outwards. Surface of the lower jaw is porous and allows flow of liquids. With the application of load by the upper jaw, specimen can not flex in lateral direction. Yet, the tissue liquids, flow through the porous lower jaw and thus the specimen is squeezed. Simultaneously, data such as the applied load and displacement is collected (Figure 2.13).

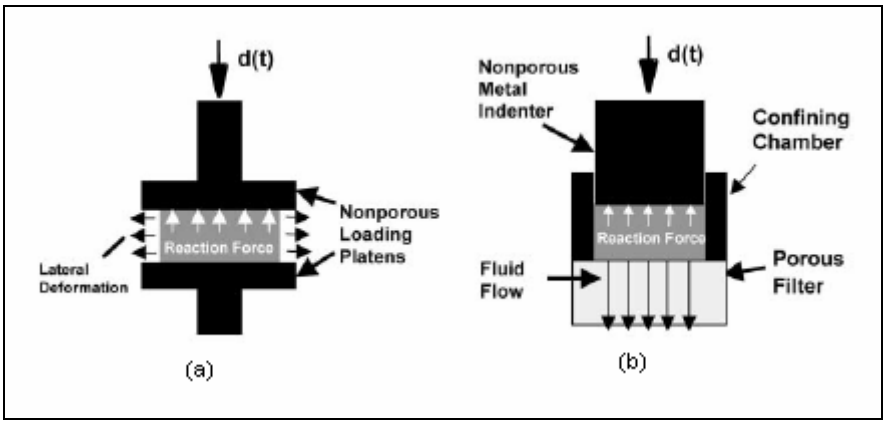

Figure 2.13 Unconfined compression test (a), Confined compression Test (b) (DiSilvestro and Suh, 2001, p.521)

Cyclic loading, relaxation and creep tests can be carried out by using compression test devices.

Compression tests described above and known in classic terms, can only be conducted in in-vitro. In the other test methods, on the other hand, studies can be made by using the indenter tests, which are in fact, special for of the compression tests.

2.6.4 Torsion Tests

In these tests, torsion operation is applied on the tissue by a cylindrical rod. Rod can be moved by motor or electromagnetic drivers (Figure 2.14). Connection of bar on the tissue without slip, can be achieved by different ways. For connection, various glues may be used or connection may be achieved by applying vacuum. It is important that the rod should not slip on the skin. Shear modulus are calculated by using the data obtained through measurements and these are utilized for further studies (Valtorta and Mozza, 2005). With the method, the anisotropic behavior of the tissue can not be observed.

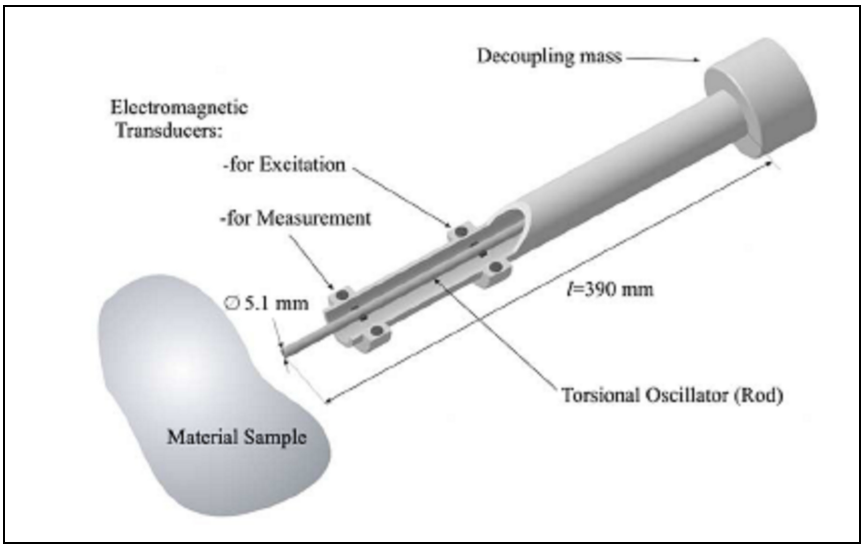

Figure 2.14 Torsional resonator device (Valtorta, 2005, p.483)

2.6.5 Indenter Tests

Methods which are frequently used in the investigation of the mechanical properties of soft biological tissues are the indenter tests (Yin et al., 2004, Korhonen et al., 2003, Choi et al., 2005). Indenter tests possess many advantages and some of these merits are as follows:

1. Can be used in all tests methods. Thus comparative studies are feasible.
2. It is the most suitable method to be applied in in-vivo testes
3. Viscoelasticity, relaxation and creep behaviors as well as anisotropy in one plane (Bischoff, 2004), which are the important features of the soft biological tissues, can be examined by the tests where the indenter device is engaged.

These tests are made by the forward movement of the indenter tip towards the tissue and the simultaneous recording of the time, force and displacement data (Figure 2.15).

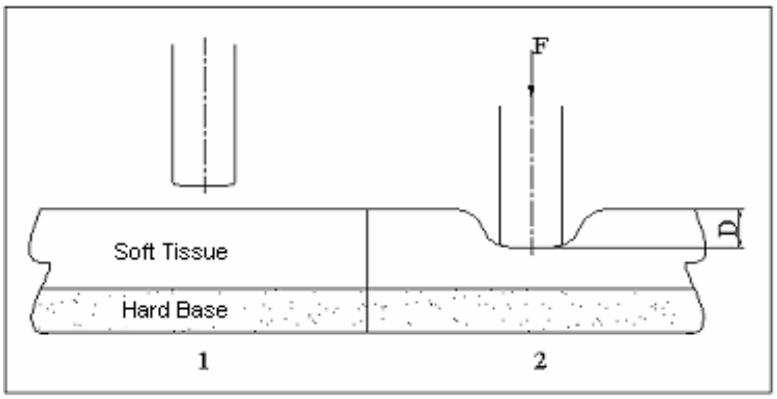

Figure 2.15 Before loading the soft tissue by the indenter device (1) After loading the soft tissue by the indenter device (2) Here, F is force and D is the distance traveled in the tissue.

As mentioned before, one of the important features of the soft biological tissues is that, they are anisotropic (Kroon and Holzapfel, 2008, Peña et al., 2008). It is not possible to realize these features when the circular indenter tips are used. This problem can be solved by using tips with different geometries. One of the geometry used is ellipsoid indenter tips (Bischoff, 2004). Yet, ellipsoid tip is used in a finite element simulation and is not used for experiments up to now.

Another necessity is the determination of the tissue thickness at tested point, which is to be used in the computer simulations. This determination may be done by different imaging devices such as the ultrasonographic devices either after or during the course of the test. In such measurements, previously described as the non-invasive method, an ultrasound device is attached to the indenter device and with the help of this device difference in the tissue thickness is collected simultaneously with other data (Figure 2.16) (Suha et al., 2006).

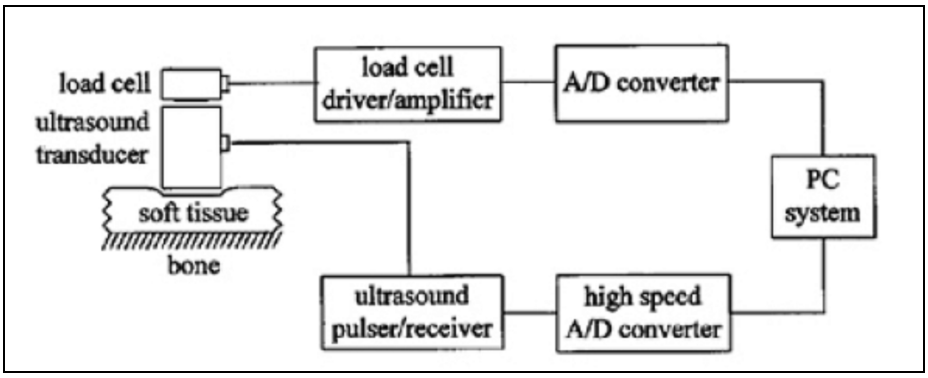

Figure 2.16 Ultrasound attached indenter device schematics arranged by Zheng et al. (1999)

Other than determining the tissue thicknesses, simultaneous observations of the area subjected to the measurements, is achieved by devices operating with methods called magnetic resonance imaging techniques (Gefen et al., 2001). By the help of magnetic resonance elastrography which is one of these techniques, strain distribution intensities developing in the tissue as a result of applying external effect on the tissue are observed.

CHAPTER 3

IMPROVEMENTS IN THE INDENTER DEVICE

Carrying out dependable tests is possible only by correct and sensitive measurements. Exhaustive investigations on the indenter device were carried out, and on the basis of the results of these investigations, improvements were carried out. The investigations carried out were,

- the study of the indenter movement sensitivity and,
- the study of the reaction force data sensitivity.

Before the explanations about the studies, it is necessary to give some information about the indenter test device and important parts of the software, controlling the indenter test device.

3.1 Indenter Test Device

Existing indenter test device was developed by the funding through TUBITAK MİSAG-183 project and can implement the cyclic loading, relaxation and creep test protocols. Device, designed for the persons who have undergone trans-tibial amputation operations, but may also be used in-vivo tests on all soft tissues which are externally accessible.

The initial design criteria were (Tönük**,** 2004):

- System to be computer controlled and the data to be collected through the computer
- Loading to be carried out as soft tissue location and speed controlled
- Soft tissue to be loaded by different indenter tips

- Designed to facilitate ease of use in clinical environment.
- To incorporate the capability of altering the test protocols or to be flexible enough to include new test protocols.
- To ensure the safety of the persons volunteered to participate in the tests.

The designed indenter device is composed of three fundamental units. These are; portable computer, control box and the test unit (Figure 3.1).

Figure 3.1 Indenter test device. Control box (1) test unit (2) portable computer (3)

Within the context of this study, an indenter device fixing apparatus was designed and implemented to improve the tissue-device connection and experiment results.

Before describing the test device parts, let us explain the operation of the indenter test system for better understanding.

3.1.1 Operation of the Indenter Test System

First of all, the necessary parameters for the indenter test are entered by the user interface (Figure 4.2). These parameters are, distance to be traveled by the indenter tip for the cyclic loading test, motor speed, number of cycles, distance to be traveled by the indenter tip for the relaxation test, motor speed, relaxation time, for the creep test on the other hand, distance, motor speed, target force, creep duration and gain are the parameters (See Section 4.1). Following the input of the parameters and commencement of the related protocol, data collection card receiving the direction and motor speed values from the USB terminal, transmits these information to the motor driver card (Figure 3.2). Motor speed is determined by the voltage channel, receiving varying voltage at 0-5 V range. This voltage being transformed in to 0.1-1000 Hz frequency square wave through the voltage to frequency (V/F) converter is further transmitted to step motor deriver card. Since the step motor produces a 0.048768 mm translation at each step, indenter tip can move within the range of 0.049-49 mm/s speeds. Other voltage channel, on the other hand, activates a movement by falling to 0 V from 5 V for each step of the motor.

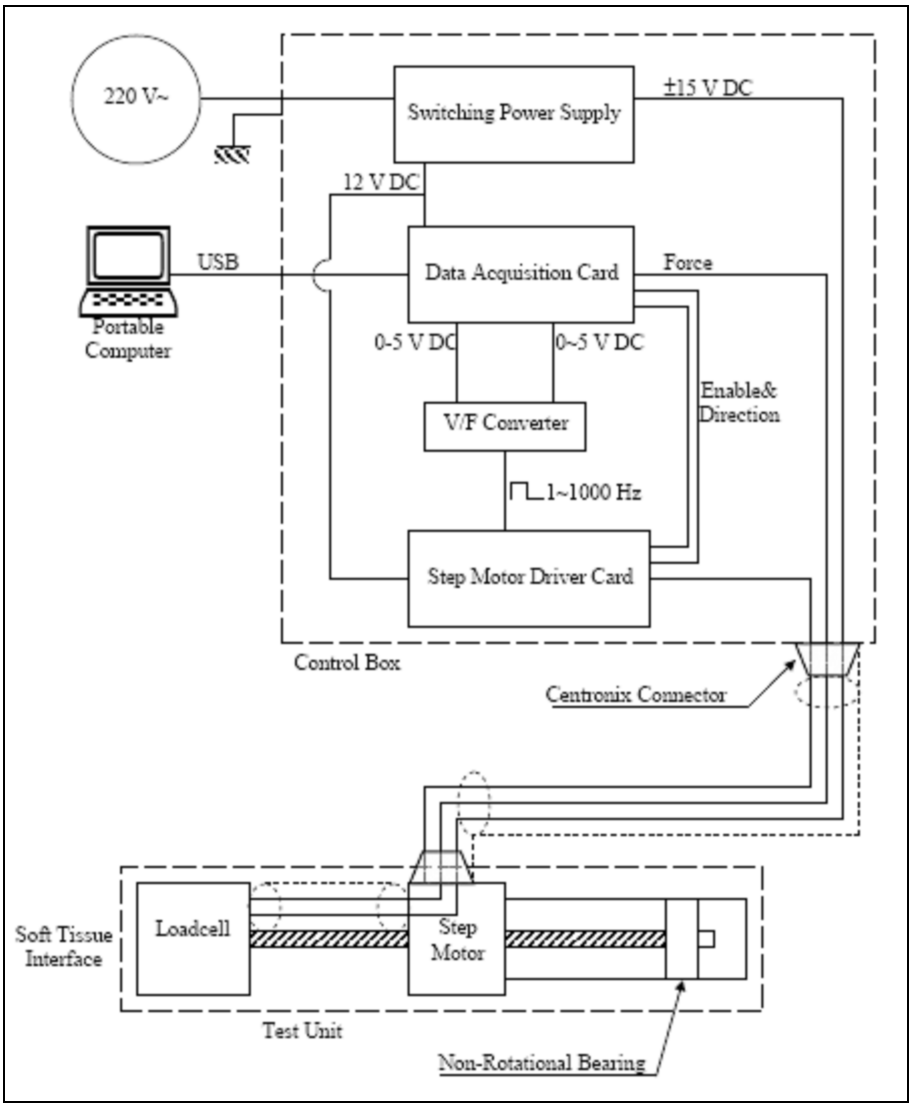

Figure 3.2 Block diagram of the indenter test system (Tönük, 2004, p.8).

Motor driver card is fed by the 12 VDC power supply. Movement of the step motor is determined in relation to the command coming from the motor driver card. Motor driver card forms this command according to the data coming from the data collection card and V/F converter. Data entered in accordance with the test protocol selected in the data collection card, is transmitted. Frequency data denoting the motor speed is taken from the V/F converter. Under the light of these data, soft biological tissue is tested under the applied protocol.

Parallel to this, with the start of the test, data collected from the load cell, is initially transferred to the data collection card where it is digitized to be transmitted to the computer.

3.1.2 Portable Computer

It is a Pentium III 900 MHz processor, 30 GB hard disk capacity, 256 MB RAM, CD writer Hawlett Pacard Omnibook XE3 lap-top computer. With its built in battery, it can run over 3 hours under the test conditions. The operating system is METU licensed Microsoft Windows XP®. Computer's task in the system, may be summarized as the control of the indenter device, collection and processing of the experimental data which is achieved by the software prepared in Matlab® 6.1. Computer communicates with the control box via one of the two USB ports, transmitting the commands to the control box and collecting the incoming data. Using a lap-top computer in the test system facilitates for easy transportation of the system and utilization in a clinical environment.

3.1.3 Control Box

A National Instruments NI 6020E data acquisition card, a step motor card driving the step motor in accordance with the command coming from data collection card, a sensitive voltage-frequency (V/F) converter, 12 and 15 VDC power sources were all incorporated within the control box.

A data collection card communicating with the computer via a USB port was used. The cables for communication of the data collection card with the motor driving card and force measurement units were kept in the control box, free of the exterior electromagnetic interferences as well as mechanical strains. Cables being kept in the box also make the use of the device easier in the clinical environment. Data collection card posses 16 common or 8 differential measurements (insulated from each other) 12 bit analog input, 2 analog output and 16 digital input-output ports.

12 VDC power source powers the step motor and data acquisition card while ±15 VDC symmetric power source powers the load cell. These power sources are powered by 220 V AC mains and they filter the electrical noise which may be present in the mains.

Analogue output of the data acquisition card can produce pulse at a maximum of 25 Hz. This frequency, limits the speed of step motor at 1.2 mm/s therefore an LM-331 sensitive voltage-frequency (V/F) converter was used between the data collection card and motor driving card and converts the 0-5 V analog output of the data acquisition card into 0.1-1000 Hz square function therefore, the step motor speed can be controlled in a range of 0.049-49 mm/s.

3.1.4 Test Unit

It fundamentally consists of a Haydon Switch Instrument 43000 series linear movement step motor and Entran ELW-50N load cell. Load cell is positioned at the tip of the indenter and can measure compressive loads up to 50 N. Step motor has a resolution of 0.048768 mm/step. The rotating motion of the rotor of the step motor is transformed into a linear motion by the screwed shaft secured against rotation at the back of the test unit. It is possible to attach various form and diameter test tips on the front part of the load cell (Figure 3.3). Communication between the test unit and the control unit is realized by a shielded cable equipped with centronix connectors at each end.

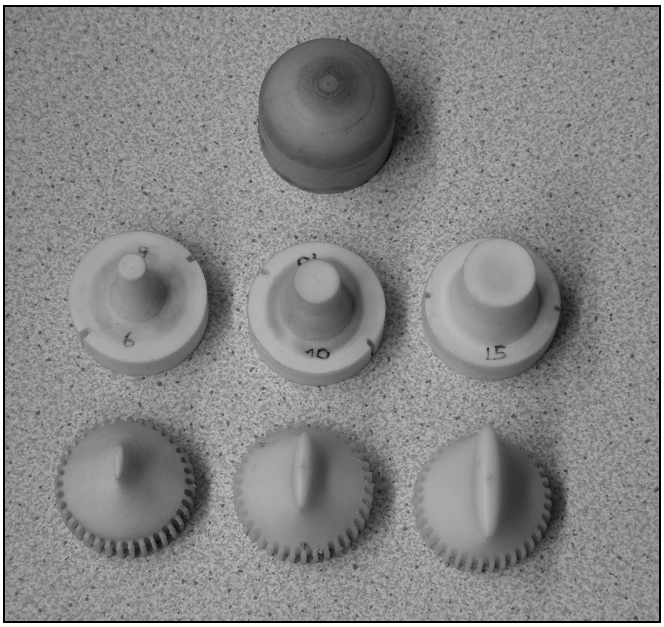

Figure 3.3 Different type of indenter tips

3.1.5 Indenter Device Fixing Apparatus

In the tests carried out, it was observed that, in the existing test arrangement, method of connecting the device to the tissue to be measured, created many problems. In this arrangement, device was connected to the tissue by the help of a belt (Figure 3.4).

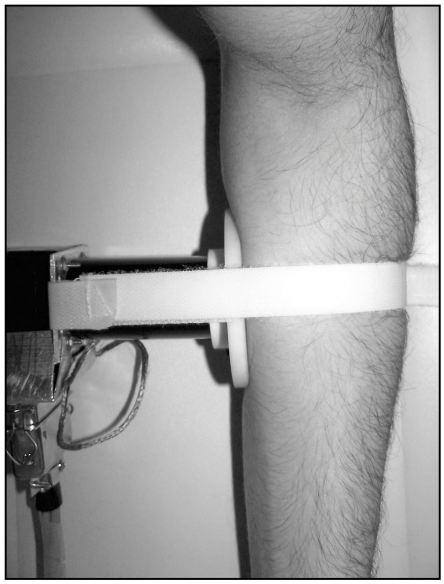

Figure 3.4 Device connection to the tissue by the help of a belt

This way of connection caused many problems as given item by item below.

1. The thickness of the tissue at the measurements changed depending on the tightness of the belt. In all measurements, it was not possible to tighten the belt at same level and the position of belt was hard to be preserved. This caused the change in a very important parameter normally the thickness of the tissue, which was to be kept necessarily constant for the computer simulations to be processed after measurements.

2. Act of connection influenced the tissue physiology of the area where the measurements were done. Depending on the tightness of the connection and the position of the indenter device, tissues within the area in concern, were either squeezed or tensioned. Therefore, the measured values for the same point would vary and the tissue might have been observed as either less stiff or more stiff.

3. In order to measure the reactions under varying conditions, capability of repeatable measurements were extremely important. These varying

conditions were set by using different indenter speeds and different indenter tips. Conditions other than these were desired to be kept same, but as stated in the above paragraphs this was not possible. Besides this, with this way of connection, it was difficult to perform the test always at the same point. Indenter device may slip away and consequently the tested point may have changed. Dismantling and reconnection of device again to same point was also very difficult to achieve.

4. With the existing connection way, to fix the indenter tip to the tissue in concern, always at the same position was not achievable and every connection this position was altered. Therefore for the same displacement values entered, indenter tip acted on the tissue in different magnitudes.

5. With this connection way, conducting measurements after the removal of the base (Figure 3.5) of the indenter device as necessitated was not feasible.

Figure 3.5 Base part of the indenter test device

Due to these reasons, a new connection arrangement was needed to be developed. Therefore, in the new arrangement to be developed, it was aimed to get rid of all these problems mentioned. The improved system was designed in accordance with the following parameters:

1. The area to be measured must not be subject to any external effect due to the connection made
2. Thickness of the tissue must not change due to connection
3. It must be possible to fix the indenter at different positions and angles so that, tissue can be measured at different points
4. When the anisotropic behaviors of the soft biological tissues are studied, as the angles of the ellipsoidal tips used are changed the position of the test point must be preserved. Such is necessary also for the successive tests where the edges with different dimensions are replaced.
5. It must be easy to use and carry
6. It must allow to conduct repeatable tests at the same test point

Under consideration of these parameters, system shown in Figure 3.6 was arranged. Since the tests were to be carried out on the forearm, design was made with the connection of the forearm in mind.

Indenter device fixing apparatus comprised of three basic elements. These were the table, arm rests and the indenter device positioner.

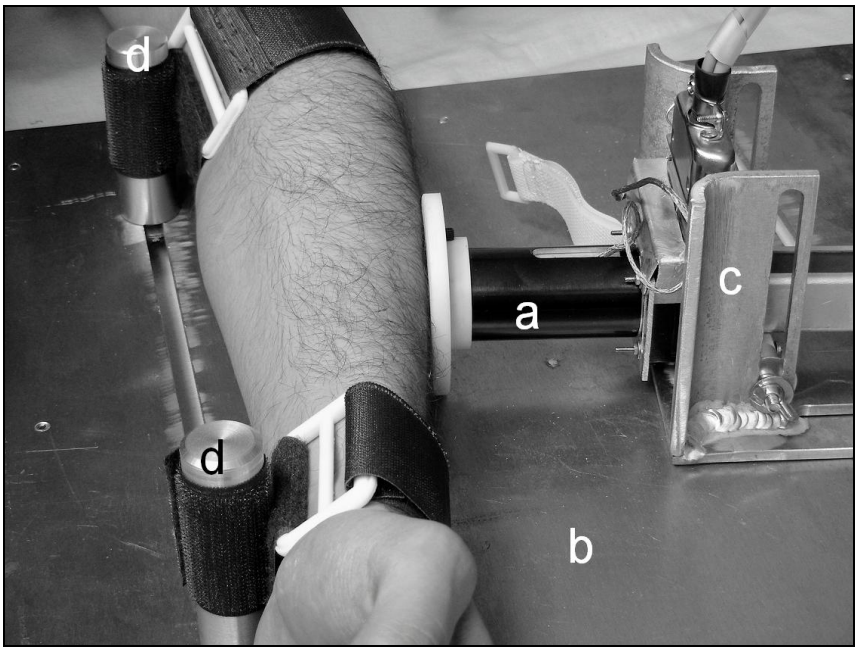

Figure 3.6 Indenter test device (a) table (b) indenter device positioner (c) arm rests (d)

3.1.5.1 Table

This is the element on which all the other components are fixed and where two guide routes take place. Arm rests are fixed on one of the guide routes and the indenter device positioner is fixed to the other. Arms rests and indenter device positioner can be moved in right-left directions on these routes and thus can be fixed at the desired points (Figure 3.7).

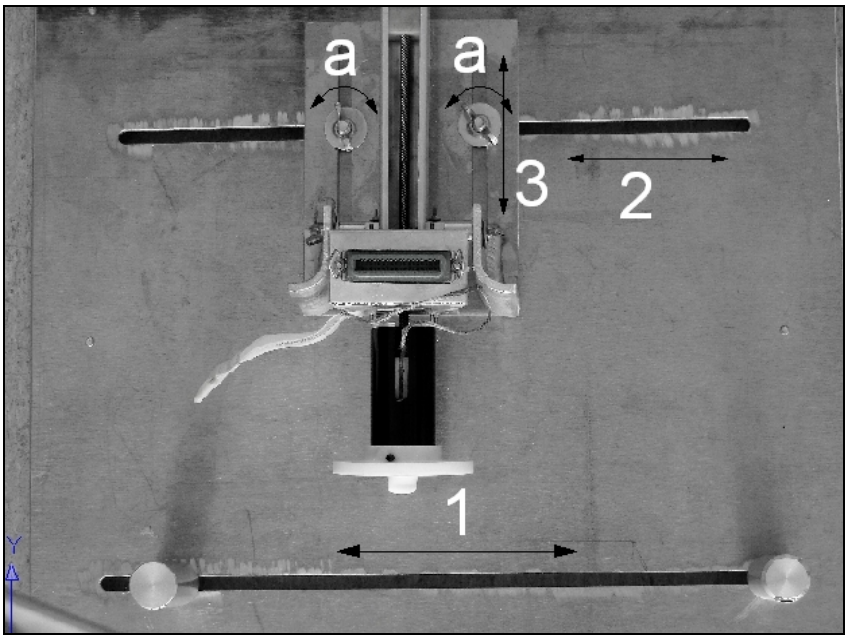

Figure 3.7 Table and operation directions (1, 2 and 3) and angle (a)

3.1.5.2 Arm Rests

These rests fix the forearm to its position. Arm rests are set so that they rest against the wrist and elbow bones. Thus, flexing of forearm backwards due to the compression of the indenter tip on the test point is minimized.

3.1.5.3 Indenter Device Positioner

Indenter device is positioned along x, y and z axis with the help of this positioner (Figure 3.8). Positioner can move on the table in forward – backward and lateral directions. It is also possible to fix the positioner on the table at different angles. Indenter device is connected on lateral routes of the positioner. Indenter device can be connected and fixed at any point along this route. This fixing process needs to be parallel to the table plane and the device may be placed at any angle desired.

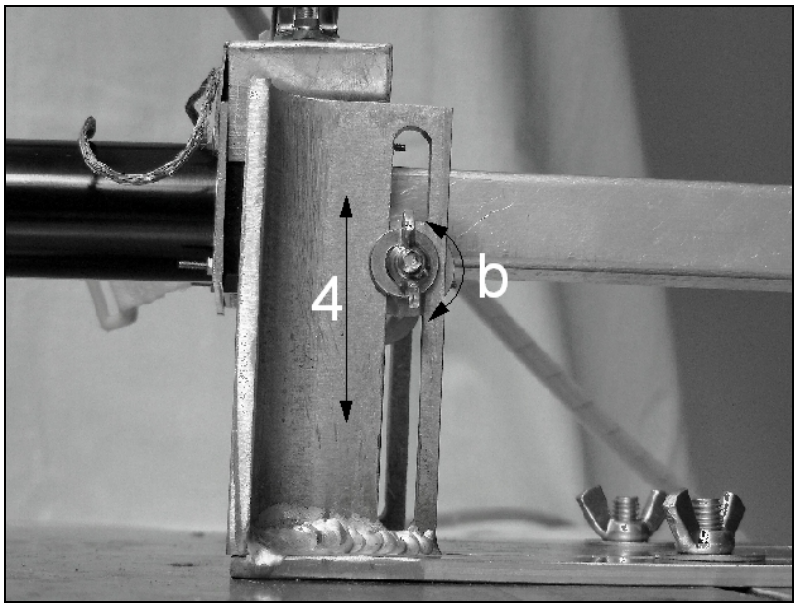

Figure 3.8 Indenter device positioner and direction (4) and angle (b)

3.1.5.4 Indenter Device Fixing Apparatus, Indenter Device and Arm Positioning Measures

The length of routes facilitating the forward – backward movement of the positioner on the table, is 100 mm. Length of the lateral routes are 82 mm. Indenter device, therefore, can be fixed at these distances depending on the arm's dimension and position. Length of route at the positioner side of the table is 350 mm, and lateral movements of the positioner are realized along this route. Arm rests can be kept constant at any point on the 370 mm long table route. Therefore, measurements can be made on individuals with wrist – elbow distance up to 370 mm. yet, in individuals with longer wrist – elbow distance, conducting comfortable and dependable tests are also possible. The clearance between two routes on the table is 255 mm.

3.2 Major Equations of the Software Achieving the Movement of the Indenter Device

Software, controlling the indenter device has initially developed for the TÜBİTAK MİSAG-183 project, by using Data Acquisition Toolbox (DAQ)

which is one of numerous toolboxes in Matlab® 6.1. Data Acquisition Toolbox (DAQ) is a Matlab Toolbox containing numerous matlab functions and MEX-file dynamic link libraries. Via this toolbox, control of various systems and the collection of pertinent data are possible. DAQ supports the analogue input, analog output, digital input/output sub systems and allows simultaneous analogue input output conversions. It can be used harmoniously with great many number of hardware.

Sections pertaining to different test protocols exist in the software and these are forward movement, backward movement, forward-backward movement, cyclic loading, relaxation 1 (target displacement), relaxation 2 (target force) and creep. Software used for these protocols, showing differences from each other, also incorporates common portions and formulas.

Some of these formulas play relatively important role in the control of the device. In the studies which will be discussed later (Chapter 3.3), these formulas will be amply discussed and revisions on them will be conducted.

First and perhaps most important of those formulas is the formula determining the indenter speed that is the motor speed.

Voltage = A*(motorspeed-B) or Voltage = A*motorspeed-C ..... (3.1)

where,

Voltage determines the first of the two analogue voltage outputs of the data acquisition card. It can be any value within the 0 and 5 V range. This voltage value is converted to frequency within 1-1000 Hz range via a Voltage / Frequency converter. Therefore the indenter tip can move within the 0.049-49 mm/s speed range. Motorspeed is the indenter speed value in mm/s entered by the user by utilizing the test interface. Indenter tip is desired to move with this speed. A, B and C are constants: which were obtained from a series of

measurements, to assure the voltage value towards attaining the desired motor speed.

Other important formula in the software is the formula determining the number of data to be collected each second (Equation 3.2).

$$Rate = A \times (20.50524934) \times motorspeed \quad (3.2)$$

where,

Rate is the number of force data collected per second, A is a constant determining the number of data collected in terms of one motor step. Selection of this constant is very important for the proper performance of the indenter device and the cleanness of the data collected. Keeping the constant on the low side, may influence the control and proper performance of the device. At some situations, device may even not function at all. Keeping the constant on the high side, on the other hand, causes increase in the noise. Yet, this problem may be alleviated by the use of a suitable filter (See Section 3.5). In this study therefore, constant was kept high at 200. The number 20.50524934 is derived from 1/step, motorspeed is the speed value entered by user through the test interface.

3.3 Study of the Indenter Movement Sensitivity

Whether the indenter tip has traveled up to the desired distance or not, was observed in this study. For this study, the set up shown in Figure 3.9 was used.

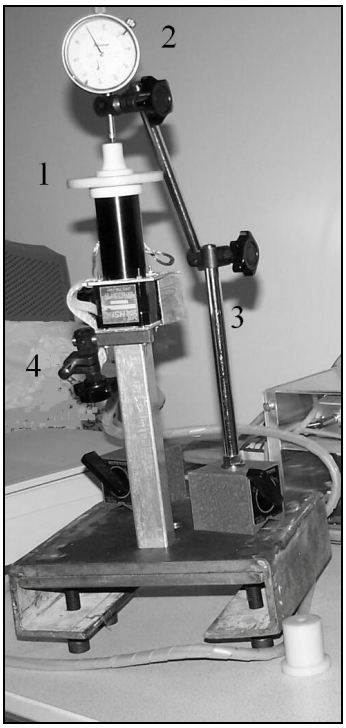

Figure 3.9 Mechanism to observe the precision of the displacement of the indenter tip during the tests. Indenter (1) 1/100 mm sensitivity Mitutoya displacement gauge (2) Mitutoya magnetic footings (3) (4).

This system consists of two Mitutoyo magnetic footings and a dial gauge. Displacement measurements with 1/100 mm sensitivity are possible via this dial gauge. Indenter's response sensitivity to the displacement orders varying within the 0.2 to 10 mm/s speed and 0.1 to 5 mm displacement ranges was observed with this system. Test for each displacement was repeated five times in both forward and backward travel directions, the results showing large deviations are eliminated and the averages of the remaining values were considered. Measurement results are presented in the Appendix A. Later, input distance-measured distance graphs (Figure 3.10) were obtained by using these average values and the regressions of these graphs were obtained.

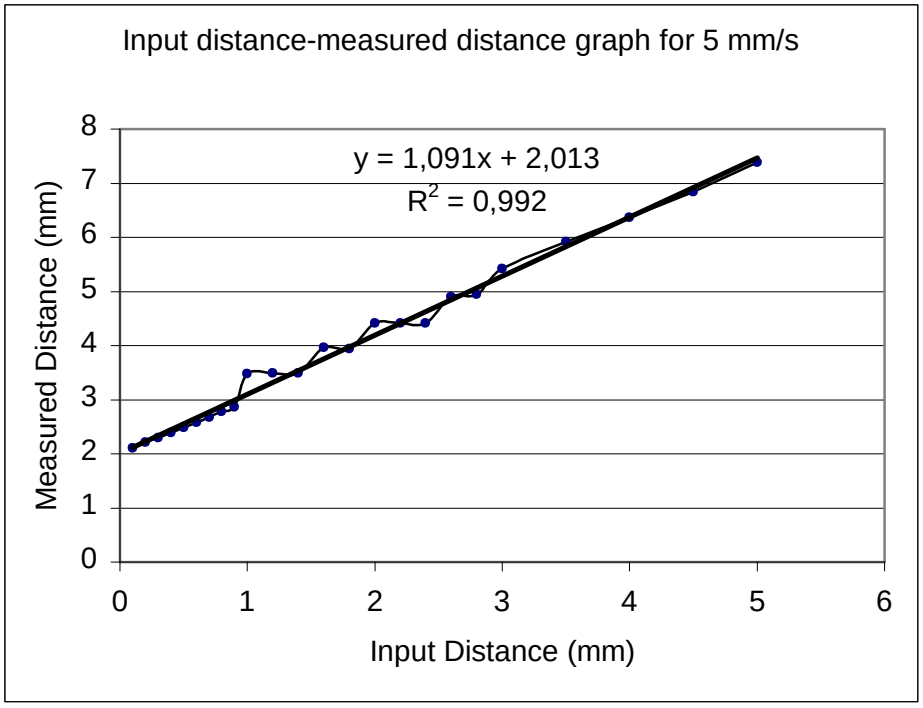

Figure 3.10 Graph obtained for the measurements carried out at 5 mm/s speed. As a result of measurements, it was observed that there exists a linear relation between the input distance value and the measured distance value.

Slope and y-intercept pertinent to this graph were used to obtain their variation versus the test speeds and thus, the equations of these graphs were also obtained (Figure 3.11 and Figure 3.12).

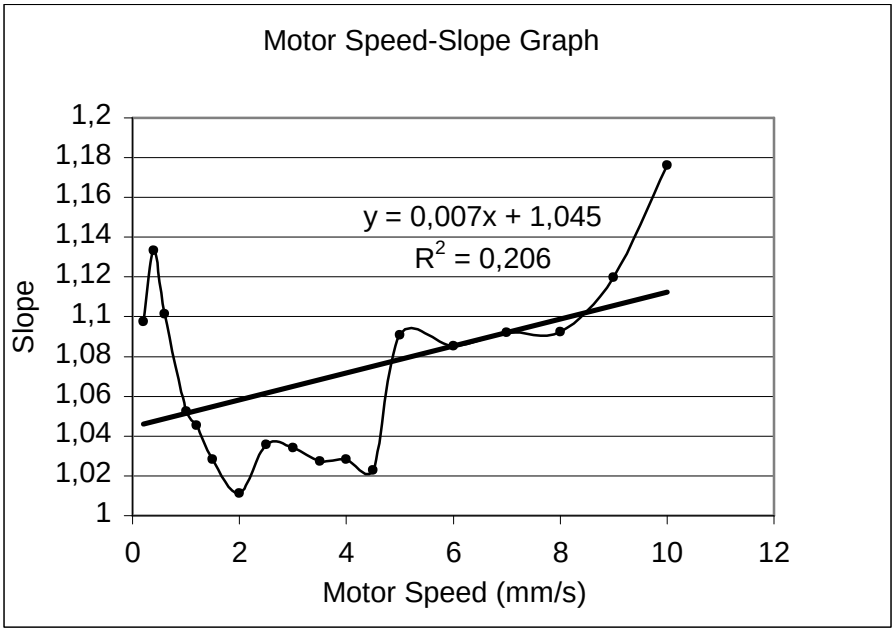

Figure 3.11 Graph drawn for the slope of the equations for graphs shown in Figure 3.10 and Appendix A as constant versus speed. In this graph, it is observed that, the constant does not show a regular variation in relation to speed and that; it sharply increases after 7 mm/s speed.

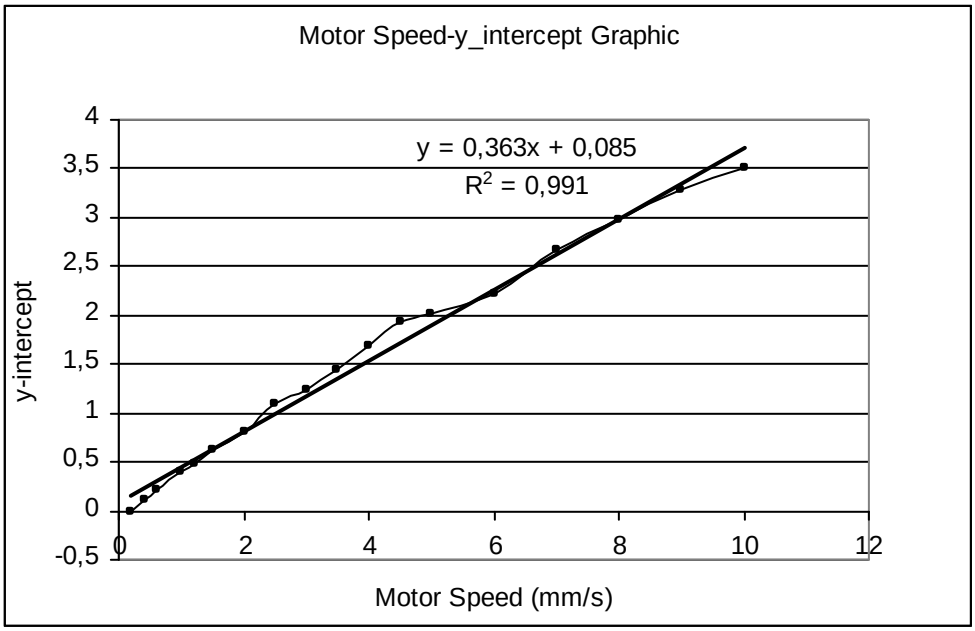

Figure 3.12 With this graph drawn, it was revealed that, a linear relation between the motor speed and the y-intercept existed.

Following these analyses by using the equations derived from Figure 3.10 and Figure 3.11 and Figure 3.12, equation 3.3 is obtained.

$$x = \frac{y - Em - F}{Cm + D} \quad \text{.....(3.3)}$$

where,

x = Displacement input value

y = Measured displacement value

m = Motor speed

C = 0.007, D = 1.045, E = 0.363, F = 0.085

In this equation, x values to be designated for the desired movement distance by given y and m values, are obtained. In fact, indenter moved as desired but the data obtained is found to be faulty**,** for the duration of indenter movement was less than expected due to the lower distance taken by the input x value. At this point, it is decided to measure the voltage output from the data collection card.

3.3.1 Study of the Data Collection Card Voltage Values

As a consequence of the previous study, it is revealed that, the correctness of the indenter movement is not realizable through derivation of a simple formula, and it is decided to investigate whether the source of problem is related to the voltage values laid on the data collection card or not. These measurements are carried out by HP, 34401A precise digital laboratory multimeter (Figure 3.13).

Figure 3.13 HP 34401A precise digital multimeter

In order to carry out the measurements easily, small modifications on the software used in the operation of the indenter device are made and a simplified interface is used (Figure 3.14).

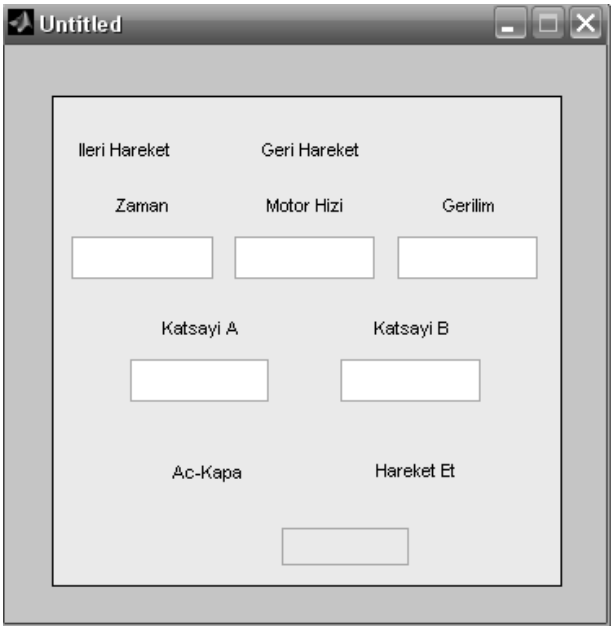

Figure 3.14 Simplified interface

With the help of the simplified software and interface three different observations were possible. In the first of these, only voltage value is entered

(motor speed was deleted by taking it either as zero or lower than zero) and the voltage at the card terminals were read by the help of the multimeter. Then the read and entered values are compared (Table 3.1). In the second observation, indenter tip movement is observed under different A and B constant while the motor speed and time parameters are kept constant. In the third observation, number of pulses occurring in the measurements are read from the text window located at the bottom of steps encountered by device are determined (Table 3.4). Voltage values were input by using this interface and the voltage values were measured through the data acquisition card terminals. As a result, data given Table 3.1 were obtained.

Table 3.1 Table showing the measured volt values versus the entered volt value

Input Voltage (V)	Output Voltage (V)	Input Voltage (V)	Output Voltage (V)
0	0.000157	4	3.9942
0.1	0.093	5	4.9951
0.2	0.195	5.1	5.0932
0.3	0.293	5.5	5.4937
0.4	0.395	6	5.9964
0.5	0.493	7	6.9923
0.75	0.747	8	7.9937
1	0.996	9	8.9944
2	1.9969	10	9.9955
3	2.9934		

As can be observed from Table 3.1, the input and measured values came out to be almost equal and thus, it was understood that, this is not the source of problem. At the end of this attempt, voltage of the second channel of the card was computed more accurately, and when it was fed as 5.004 it is observed that the measured value is 4.9993 which was very close to the required value, 5 V. In this study, voltage supplied to voltage –to-frequency converter was also

measured by the HP multimeter. Indenter tip speed was then calculated through these measured frequencies (Table 3.2).

Table 3.2 Measured frequencies versus entered voltages and the motor speeds derived from these frequencies by the help of Equation 3.4.

V	F [Hz]	mm/s
2,5	293,6	14,3183
2	234,8	11,4507
1,8	211,3	10,3047
1,6	188	9,16838
1,4	164,9	8,04184
1,2	141,7	6,91043

This computation was carried out as follows. As described in detail previously, a single step of the step motor causes a 0.048768 mm movement of the indenter tip. Output frequency, on the other hand, controls number of steps per second of the motor. Thus, speed of the indenter tip was calculated by the following formula,

Indenter Tip Speed [mm/s] = Output Frequency [Step/s] × Distance taken in one step [1/ 0.048768 mm/step] ..... (3.4)

As a result, voltage – motor speed (Figure 3.15) graph was plotted and the equation given in Equation 3.1 is derived from this graph.

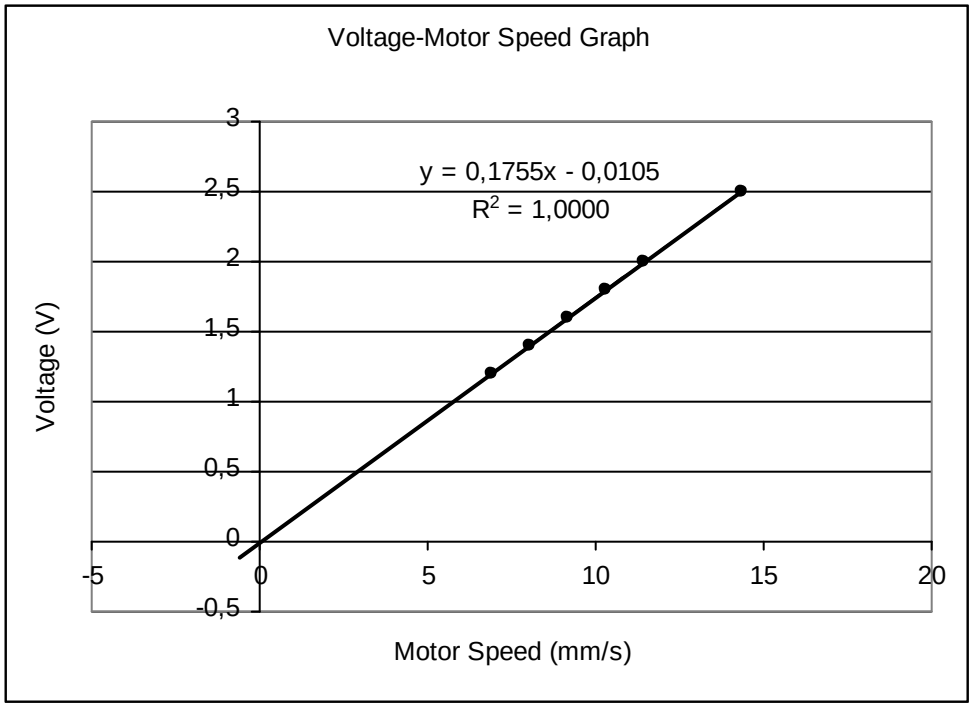

Figure 3.15 Graph drawn by the help of the values in Table 3 and giving the relation between voltage – motor speed. With the help of this graph, constants of equation 1 were derived.

In conclusion based on this investigation, no problem related to the output and input voltage data of the data acquisition card was detected. In addition, fine adjustment of the second voltage output was achieved and voltage-motor speed relation was improved. Discovering that the problem was not arising from output voltage errors, it was decided to compare indenter tip displacement versus motor step.

3.3.2 Carrying out the Step-Position Comparison

Purpose of this comparison is to observe if the motor in fact, takes steps as much as required by the indenter tip movement. To achieve this, an algorithm sensing the electrical pulses fed to the motor control card is monitored by the software using one of the free input channels of the data acquisition card (Appendix B). For each step, 5 V value of the second channel falls down to 0 V (Figure 3.16).

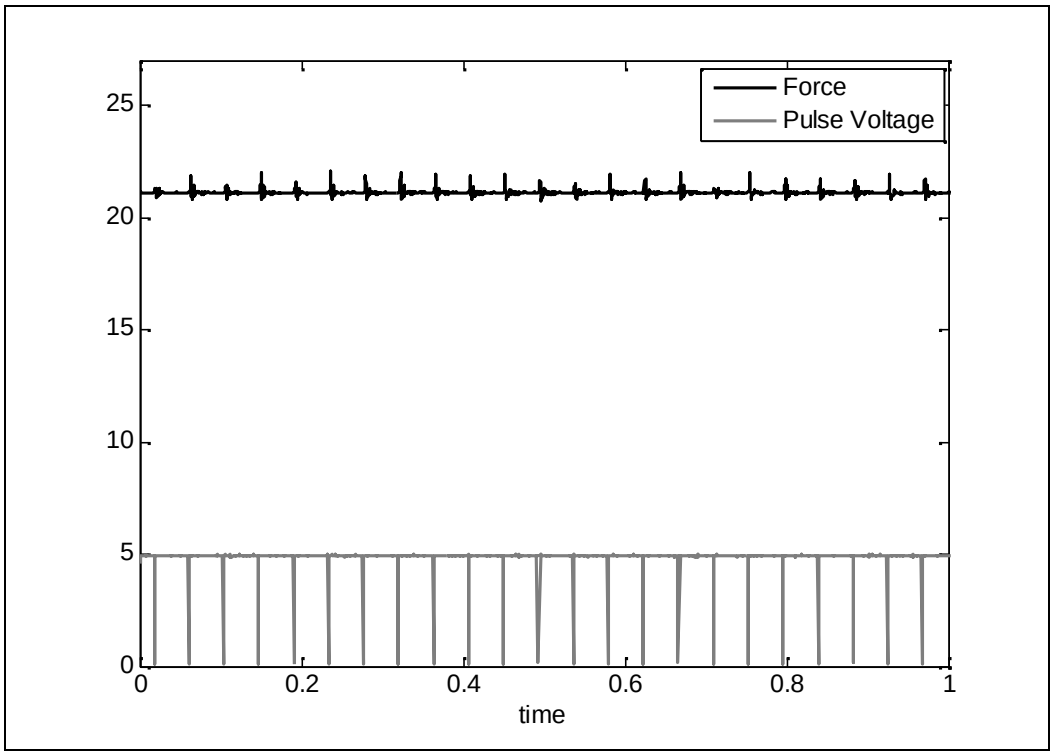

Figure 3.16 At each step of the motor, voltage value of the second channel of data collection card voltage channels instantaneously drops to 0 V from 5 V. Therefore, the total number of these voltage drops of 5 V to 0 V, gives us the number of steps taken. In the graph, such points were observed.

Therefore, an algorithm counting these downfalls from 5 V to 0 V was added to the software. It was observed that, setting the sample rate lower than a critical value, results with non readability of the produced pulses. Code generating the data collection the sample rate (sample rate to be taken per second) was as follows:

$$\text{Rate} = x \times 20.50524934 \times \text{mothiz}$$

Meaning of this is, collect x samples per motor step. Yet, it resulted missing pulses at low motor speeds (up to 5 mm/s). This problem was solved by setting the variable mothiz 10 as constant. The same way, problem can also be alleviated by altering the coefficient x. Following termination of this problem, tests were commenced. Results of the tests can be observed in Table 3.3.

Table 3.3 Table where the number of steps necessary for the entered distance is compared with the number of steps calculated by voltage drops (Figure 3.16) at different speeds.

0,04877	Step should be taken	Steps taken with input speeds				
Distance (mm)		1 mm/s	2 mm/s	4 mm/s	5 mm/s	10 mm/s
1	21	23	21	21	20	20
2	41	45	41	40	40	39
3	62	67	62	60	59	59
4	82	89	82	79	78	78
5	103	110	101	95	98	97
6	123	132	121	118	117	116
7	144	154	142	137	136	135
8	164	176	162	157	156	154
9	185	198	182	176	175	173
10	205	220	202	196	194	193

As can be observed from Table 3.3, as speed increases, number of steps realized by the electric motor deviated from the value it should be and for low speeds closer values are encountered. For the sake of more detailed observation, step inquiry for 1 mm/s motor speed is made. During the course of the step inquiry, coefficients, found for voltage-motor speed equation derived by engaging sensitive voltmeter, were used. Due to incorrectness of results obtained by using these coefficients, appropriate results were attained through modifications on these coefficients. Additionally, movement of the indenter was measured by dial gauge and this movement distance was harmonized with the distance obtained by measured step. Test data can be observed in Table 3.4.

Table 3.4 Comparison of the distance values calculated from steps with the measured – entered distance values found by changing the first and second constants of Equation 3.1 describing the voltage – motorspeed relation. With distance calculated from steps in mind, most suitable constants for 1 mm/s speed were determined at the third trial.

A=0.175479 B=0.0104714	time(s)	Motor Speed (mm/s)	measured distance(mm)	number of steps	wanted distance(mm)	Distance calculated from step(mm)
	1	1	1.82	24	1	1.170
	2	1	2.95	47	2	2.292
	3	1	4.02	70	3	3.414
	4	1	5.13	93	4	4.535
	5	1	6.24	115	5	5.608
	6	1	7.37	138	6	6.730
	7	1	8.49	161	7	7.852
	8	1	9.60	185	8	9.022
A=0.098 B=0.0104714	time(s)	Motor Speed (mm/s)	measured distance(mm)	number of steps	wanted distance(mm)	Distance calculated from step(mm)
	1	1	1.03	15	1	0.732
	2	1	1.81	29	2	1.414
	3	1	2.49	43	3	2.097
	4	1	3.18	57	4	2.780
	5	1	3.93	71	5	3.463
A=0.153651 B=0.0104714	time(s)	Motor Speed (mm/s)	measured distance(mm)	number of steps	wanted distance(mm)	Distance calculated from step(mm)
	1	1	1.57	22	1	1.073
	2	1	2.6	42	2	2.048
	3	1	3.64	62	3	3.024
	4	1	4.61	83	4	4.048
	5	1	5.55	103	5	5.023

At the end of these operations, together with the iterations made, proper coefficients were derived at the 3rd measurement, and the travel amount originating from step, come out to be very close to the travel amount expected from the indenter. Yet, values measured by dial gauge deviated 0.6 mm on the average, from the values found by normal step calculations. In addition to that, it

was observed that, in the measurements made by using the same A and B coefficients for 2 mm/s speed, amount of step came out to be differing from the expected values.

At the end of this stage, it was decided to reconsider these first test results by carrying out more detailed investigations.

3.3.3 Reconsideration of the Test Results

Studies up to this stage, have revealed that, indenter's correct movement is not achievable by formula based solely on motor speed- voltage parameters and that, there exists no problem with regard to the data collection and output voltage values. Step-position investigation has been carried out and from thereon, a conclusion towards the solution is not achieved. At this point it was decided to proceed with a more detailed insight of the first test results. Target is to calculate the indenter travel distance and motor speed to the different input parameters, by the help of this test results. Also, by this approach, it was expected that, problem of obtaining measurements at lower time intervals arising from the desired distance value, a problem observed also in the first formulation, will be alleviated.

Our previous studies were carried out with the consideration that source of the problem was the equation pertinent to the relation between voltage and motor speed.

This relation was achieved by the formula,

$$\text{Voltage} = A \times \text{MotorSpeed} - B \quad (3.5)$$

Here, A and B are two constants and are determined prior to study, as A = 0.1686 and B = 0.017422. Before the studies were commenced, it was anticipated that, indenter tip would move in desired distance by changing these constants and measurements were carried out by using the system shown in Figure 3.8. Measurements were taken in 0.2-10 mm/s speed range and 0.1 – 5

mm displacement range. As a result, for each speed, characteristic curves shown in Figure 3.9 were obtained (Appendix A). Yet, these results indicated that the solution of the problem was not possible only by altering the A and B constants. The reason was that, each of these constants was also dependent on different inherent variables. That is, obtaining correct results were possible only by formulizing the A and B constants in relation to the parameters such as motor speed and time. The studies were therefore progressed in this direction. In fact, this phenomenon was observed in the equation given in Section 3.3 and Equation 3.3, but then, a clear conclusion was not yet drawn. Distance desired for the indenter tip to travel was calculated by Equation 3.3 and the entrance distance was calculated via motor speed, yet, the calculated distance was smaller and although the indenter tip had traveled the desired distance, measurements were obtained in a smaller time interval. It was then anticipated that, the problem would be tackled by applying the same logic to variables other than the position parameter.

Considering that, time is calculated through travel path/motor speed formulation, playing around with path does not effect the time parameter, and, calculation of time directly through the travel distance to be taken, results with a longer travel path of the indenter. It is therefore understood that, it is not possible to derive a practical formula by using the distance as an output parameter. At this stage, it is contemplated on the attainment of a usable formula by utilizing the data already collected, and, it is decided to form a formula by which the motor input speed can be derived in relation with the desired path and time parameters.

To this end, motor speed values were calculated by utilizing the indenter travel path and time obtained as test data, and the motor speed time graphs were drown. A sample of this graph is Figure 3.17 for 8 mm/s.

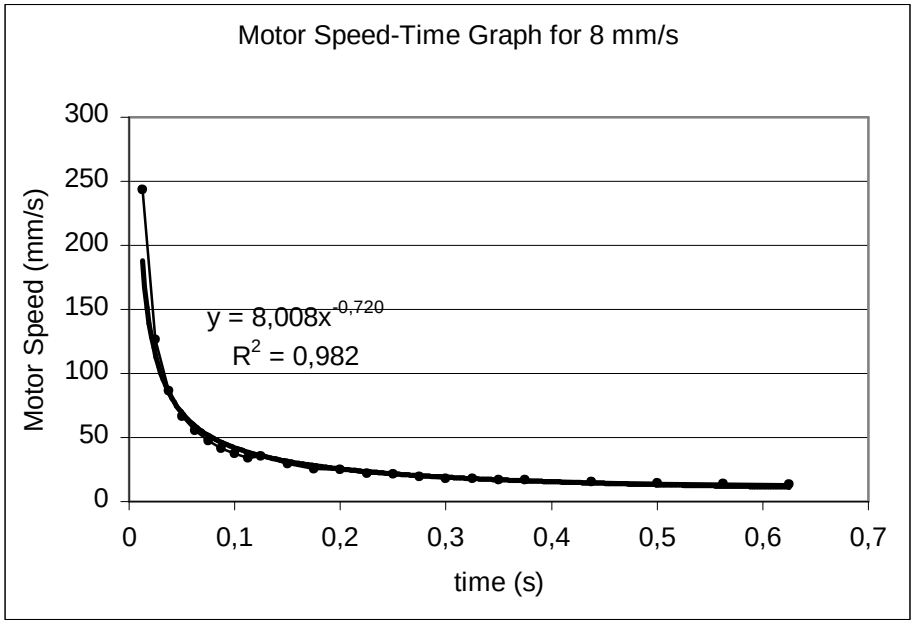

Figure 3.17 Graph and equation of speeds versus time, calculated by using the displacement values as read from the dial gage during measurements and the time elapsed during the indenter's movement.

Later the equations of these graphs were derived and the graphs of first and second coefficients in relation the input motor speed are laid down (Figure 3.18 and 19).

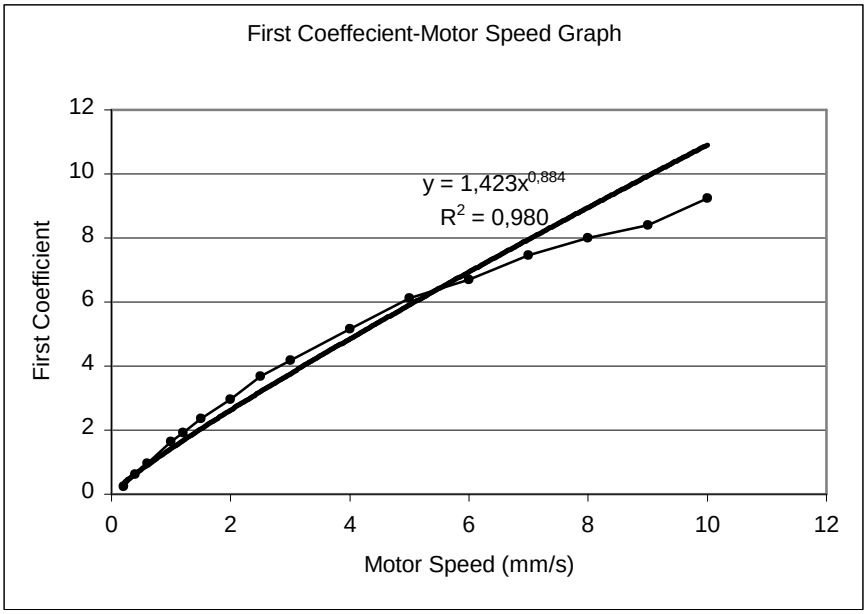

Figure 3.18 Variation of first coefficient determined, in relation to the variation of the motor speed

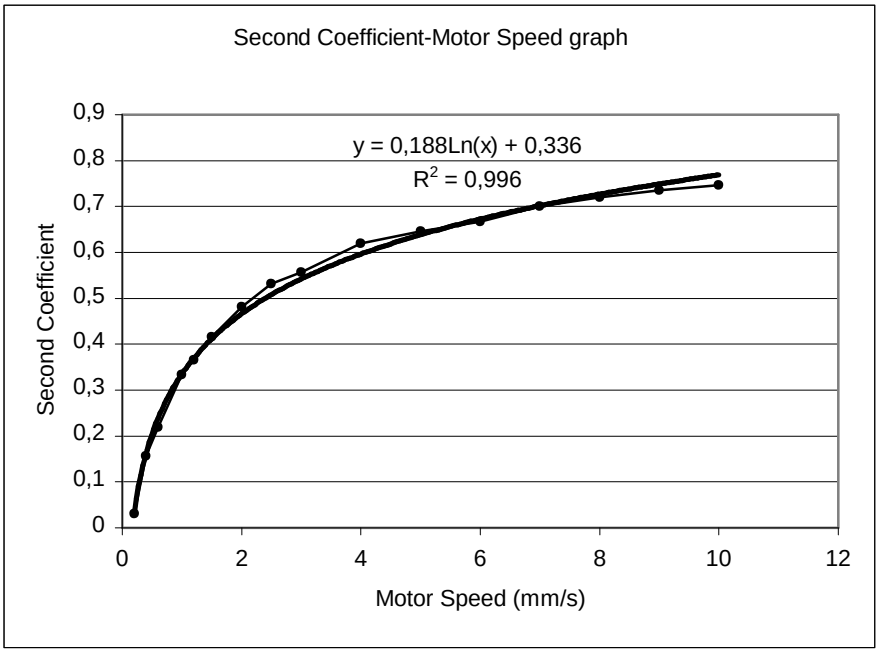

Figure 3.19 Variation of second coefficient determined, in relation to the variation of the motor speed

The approximate equations of these graphs were also determined by Microsoft Excel® Trend. Thus obtained equations are as follows;

$$y = A \times t^{-B} \quad \text{.....(3.6)}$$

$$A = C \times m^{D} \text{.....(3.7)}$$

$$B = E \ln(m) + F \text{.....(3.8)}$$

where;

y = motor speed (computed from data)

t = time

m = motor speed (input)

C = 1.423, D = 0.884, E = 0.188, F = 0.336

Equation (3.7) and (3.8) have been inserted in their respective places in Equation (3.6) and by drawing m out, it is calculated as a function of time and motor speed at which the indenter tip is desired to move. This way, indenter's movement as required by the desired path [y (motor speed) ×time] and time, is obtained. Yet, at this case and at the end of the tests carried out, it is clearly observed that, for different position value inputs different motor speeds prevail. For instance, speed originating from motor movement of y = 1 mm/s and t = 1 s differs from the speed originating from motor movement of y = 1 mm/s and t = 5 s. In fact, the incompatibility of such a conclusion can also be observed from the graphs in Figure 3.16. Although no variation was encountered in the motor speed in the tests carried out, in the data obtained motor speed seems to decrease as the motor speed position amount increases.

The same procedure was applied between the entered time and the time calculated from measurements as well as between the calculated time and entered distance. In the first case, indenter's measured travel distance and time

values were calculated by using the test data and motor speeds respectively, and the calculated –entered time curves were drawn (Figure 3.20, Appendix A). Later by determining the graphs equations, motor speed related graphs of the first and second constants were drawn (Appendix A). Finally, equations given below were derived.

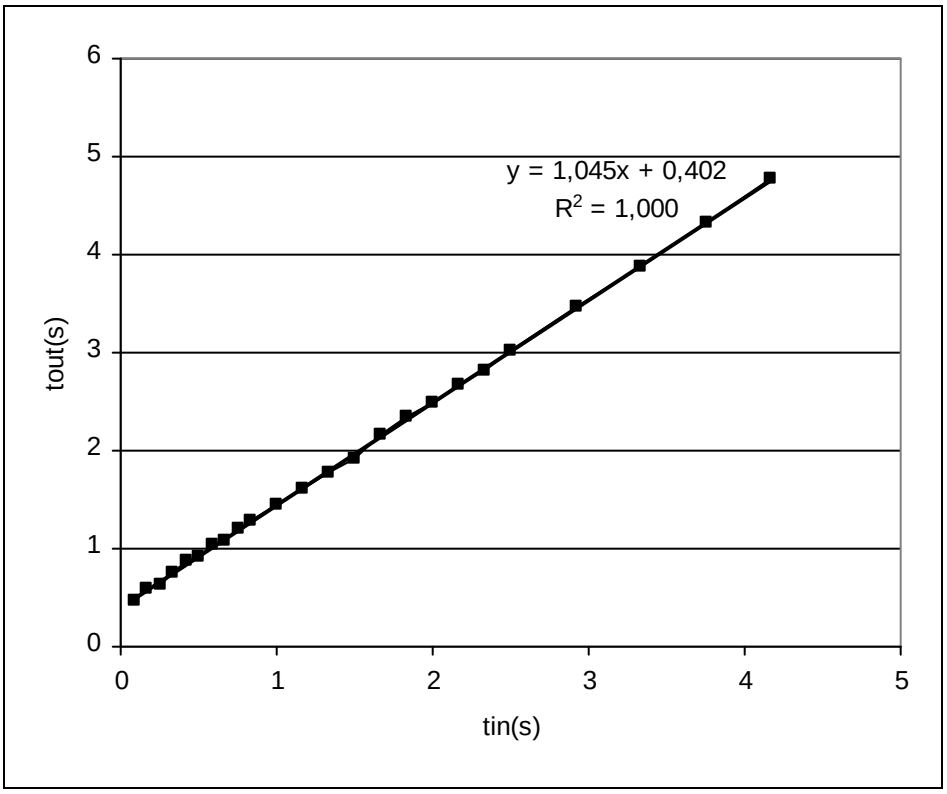

Figure 3.20 Graph of input time versus calculated output time

$$t_c = At_g + B \quad \text{..... (3.99)}$$

$$A = C_1x^4 - D_1x^3 + E_1x^2 - F_1x + G_1 \quad \text{..... (3.10-a)}$$

$$A = C_2x^6 - D_2x^5 + E_2x^4 - F_2x^3 + G_2x^2 - Hx + J \quad \text{..... (3.10-b)}$$

$$B = K\ln(m) + L \quad \text{..... (3.11)}$$

where,

t_c = Calculated time

t_g = Entered time

$C_1 = 0.0005$

$D_1 = 0.011$

$E_1 = 0.076$

$F_1 = 0.189$

$G_1 = 1.173$

$C_2 = 0.00003$

$D_2 = 0.0009$

$E_2 = 0.008$

$F_2 = 0.04$

$G_2 = 0.11$

$H = 0.18$

$J = 1.159$

m = motor speed

K= 0.0533

L= 0.315

Inserting equations 10-a, b and 11 into 9,

$$t_g = \frac{t_ç - K\ln(m) - L}{C_1x^4 - D_1x^3 + E_1x^2 - F_1x + G_1} \quad \text{..... (3.12-a)}$$

or

$$t_g = \frac{t_ç - K\ln(m) - L}{C_2x^6 - D_2x^5 + E_2x^4 - F_2x^3 + G_2x^2 - Hx + J} \quad \text{..... (3.12-b)}$$

With the help of this equation, although the desired movement of the indenter tip was achieved, suitable output times were not obtainable.

For the second case, graphs of the output time, and entered distance together with the motor speed related graphs of the slope and y-intercept were drawn (Figure 3.21, Appendix A). In conclusion following equations were obtained.

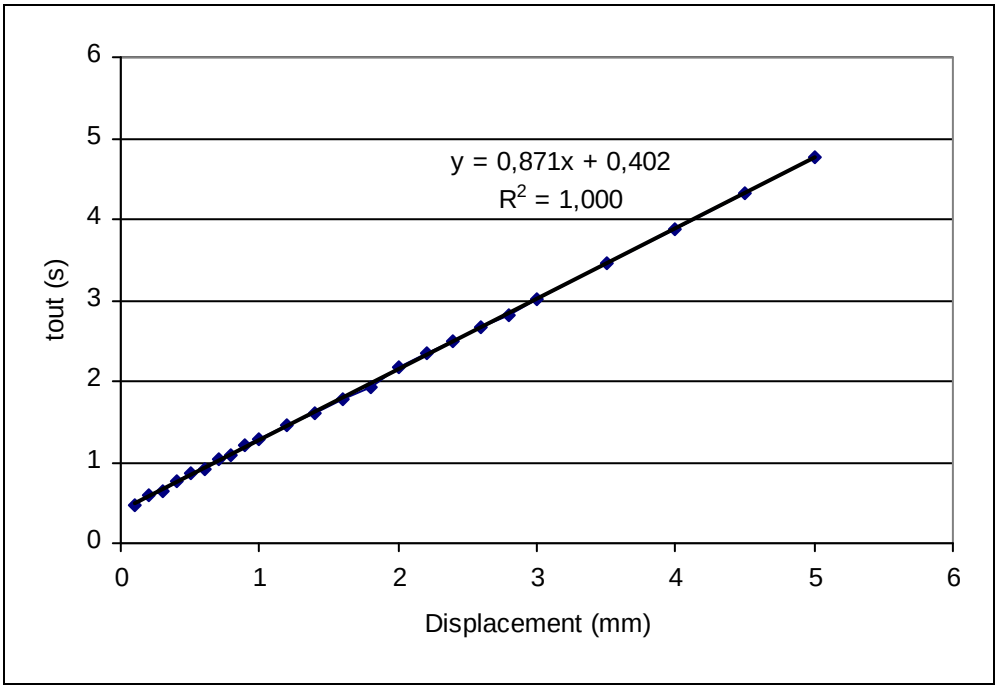

Figure 3.21 Graph of displacement versus calculated output time

$$t_c = Ax + B \quad \text{..... (3.13)}$$

$$A = Cm^{-D} \quad \text{..... (3.14)}$$

$$B = E\ln(m) + F \quad \text{..... (3.15)}$$

where,

t_c = calculated time

x = entered distance

C = 1.072

D = 0.995

E = 0.053

F = 0.315

m = motor speed

Inserting equations 3.14 and 3.15 to equation 3.13

$$x = \frac{t_ç - E\ln(m) - F}{Cm^{-D}} \quad \text{..... (3.16)}$$

Again, although motor speed for the entered position values was determined by this equation, time parameter was still incompatible.

It was understood that, the problem does not arise from the voltage motor speed interrelation, but that, the source of movement parameters overrun is the software controlling the indenter.

3.3.4 Diagnosing the Problem and Solution

At the end of the previously carried out studies, problem was diagnosed as the movement of indenter more than the desired duration. In the software, indenter's travel duration is represented by analogue input object. Normally, in the software, time at which analogue input stays open is determined, and this time interval is closed with analogue input and analogue output objects just after the motor data collection, again under normal circumstances, it is thought that,

analogue output, that is, the object determining the indenter movement runs for the desired duration due to the simultaneous opening and closing of two objects. Yet, the investigations revealed that the indenter continues to move longer than designated duration. It is therefore realized that, problem can be solved by attaching a timing code within the analogue output controlling the indenter movement. This code was inserted to the existing software, and at the end of the measurements, it was observed that the indenter's movement take place at the desired levels (Table 3.5).

Table 3.5 Measured results obtained by the addition of timing code for the Analogue Output object.

1 mm/s	1 mm	2 mm	4 mm	6 mm	10 mm
M1*	1,25	2,2	4,2	6,47	10,46
M2	1,13	2,21	4,28	6,29	10,46
M3	1,12	2,17	4,2	6,29	
M4	1,12	2,19	4,28	6,29	
2 mm/s	1 mm	2 mm	4 mm	6 mm	10 mm
M1	1,1	2,04	4,07	5,99	10
M2	1,17	2,15	4,12	5,99	9,94
M3	1,18	2,14	4,06	5,99	
M4	1,16	2,15	4,13	5,99	
4 mm/s	1 mm	2 mm	4 mm	6 mm	10 mm
M1	1,2	2,2	4,09	6,03	9,93
M2	1,32	2,29	4,19	6,03	9,93
M3	1,33	2,29	4,09	6,03	9,93
M4	1,31	2,29	4,18	6,03	9,93
6 mm/s	1 mm	2 mm	4 mm	6 mm	10 mm
M1	1,05	1,89	4,02	6	9,86
M2	1,18	2,05	4,04	6	9,75
M3	1,17	2,04	3,95	6	9,75
M4	1,17	2,06	3,99	6	
10 mm/s	1 mm	2 mm	4 mm	6 mm	10 mm
M1	1,16	2,04	3,95	5,89	9,74
M2	1,17	2,15	4,03	5,89	9,76
M3	1,18	2,13	3,94	5,89	9,76
M4	1,17	2,15	4,03	5,89	

Still, despite the movement of indenter at desired distances, it is realized that the collected force data does not start simultaneously with the indenter movement (Figure 3.22).

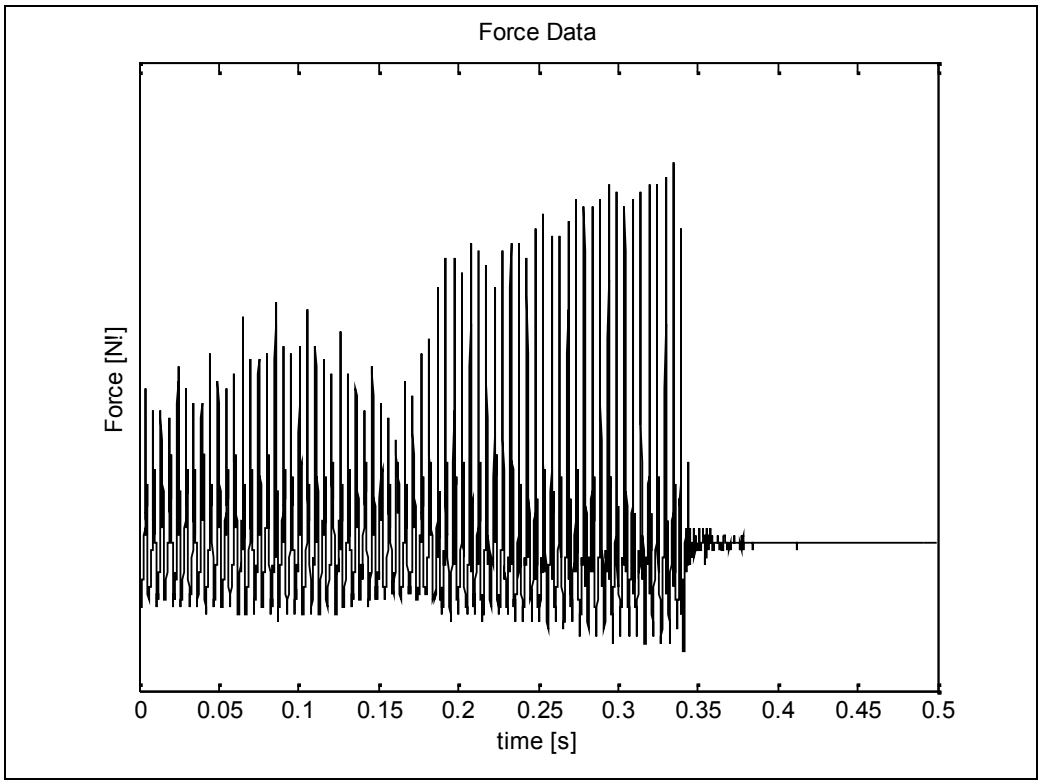

Figure 3.22 Force-time graph obtained for 10 mm/s motor speed and 5 mm displacement

As can be seen from Figure 3.22, force data collection commences after the start of indenter movement and is completed only a certain time after the stop of indenter movement. This is revealed through observing the last portion of the graph of pulses generated by step motor. In order to overcome this problem, simultaneousness issue between the analogue input and output objects was analyzed and it was concluded that with the following code it is possible to solve the problem,

```
set ( [AI,ao] , ‘ManualTriggerType’, ’Manuel’)

set ( AI , ‘ManualTriggerHwOw’, ’Trigger’)
```

where, first line starts the AI (analog input) and ao (analog output) objects with trigger command and second line increases the sensitivity of the both object’s simultaneousness. Additionally, in order to observe the actual simultaneousness of the objects following code showing the trigger times.

```
AItime = AI.InitialTriggerTime

aotime = ao.InitialTriggerTime

t = fix(AItime);

sprintf(’%d:%d:%d’, t(4),t(5),t(6))

t = fix(aotime);

sprintf(’%d:%d:%d’, t(4),t(5),t(6))

delta = abs(aotime - AItime);

sprintf(’%d’,delta(6))
```

In the tests carried out after the corrections made, simultaneous commencement of the AI and ao objects has been actually assured (Table 3.6).

Table 3.6 Trigger times and differences obtained by adding the analogue input and the code determining the trigger times of the output objects, to the software.

First Observation	Analog Input	Analog Output	Difference
Start	11:09:40	11:09:39	$\approx 3.1\times10^{-5}$
Trigger	11:09:40	11:09:39	
Stop	11:09:41	11:09:40	
Second Observation			
Start	11:28:37	11:28:37	$\approx 3.1\times10^{-5}$
Trigger	11:28:38	11:28:38	
Stop	11:28:39	11:28:39	

As can be seen on the tables, in the simultaneous commencement of the objects, average commencement lag between ao and AI is in the vicinity of 3×10^{-5} seconds. This lag was 0.1 seconds levels in the previous software and this would result with a delayed AI, that is, force data collection would start at certain duration after the start up of the indenter, and even after the stop of the indenter, force data collection would continue (Figure 3.19). This problem thus eliminated through the simultaneous commencement of the objects, has revealed a different problem to be observed. A graph derived for 1 mm/s speed and 1 mm path of simultaneously commenced object can be seen in Figure 3.23.

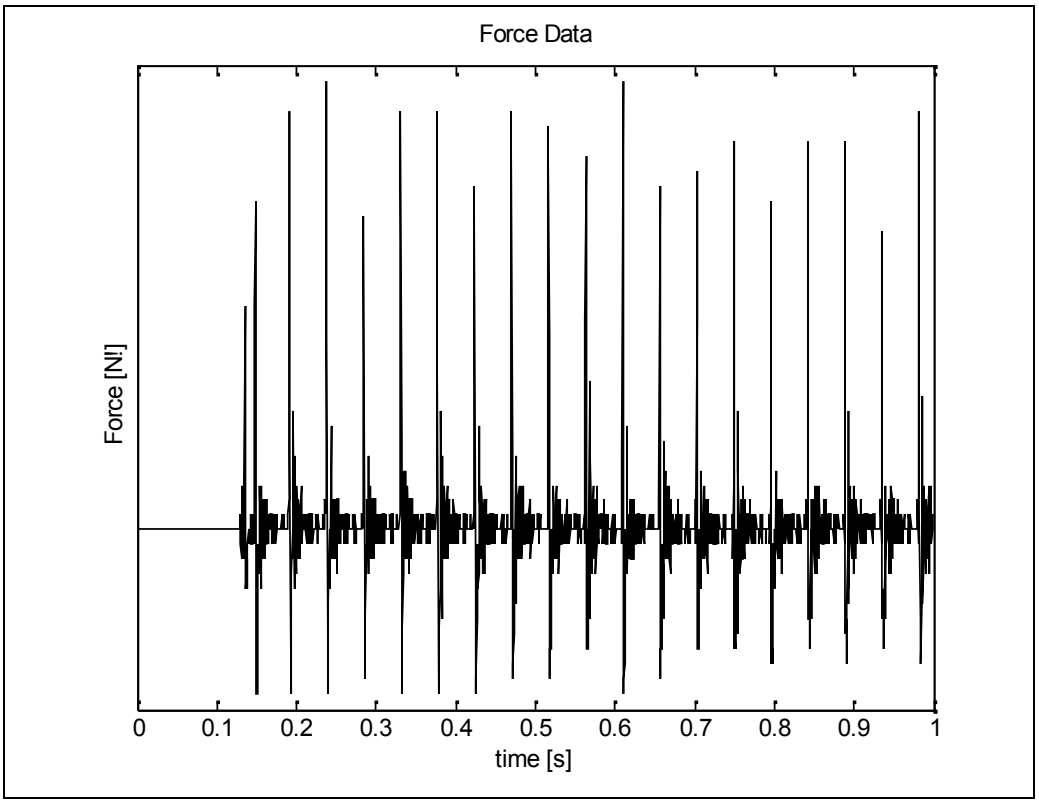

Figure 3.23 Force-time graph obtained for 10 mm/s motor speed and 1 mm displacement in the case of collection of force data simultaneously with the starting of indenter's movement.

As can be noted on the figure, analogue input object, that is the entity providing the force data starts to operate before the indenter's start up. This is valid for a time interval of approximately 0.1 second and especially in high speeds it results with a considerable data loss. For instance, for 10 mm/s and 1 mm path values, measurements indicate the indenter device as completely static (Figure 3.24).

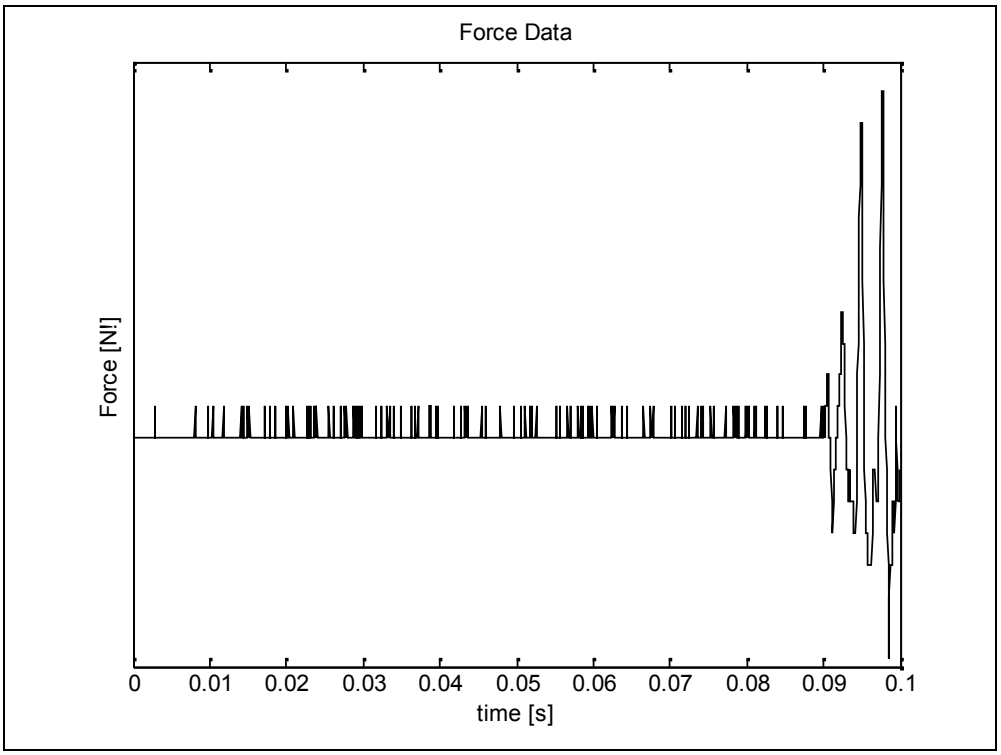

Figure 3.24 Considerable data loss is encountered when the force data is collected simultaneously with the starting of the indenter's movement. In this graph data collected for 10 mm/s speed and 1 mm displacement is seen

In the time tests conducted, it is observed that the objects start simultaneously. Yet, a certain lag period following the signal for the step motor start up, is required. Therefore, AI object starts to collect data before the motor starts to operate, and the motor starts on the average 0.1 seconds later. Thus, force data collection needs to be commenced with the start up of the motor.

As was noted before and as can be observed from Figure 3.16, when motor takes a step, voltage value of the second channel falls down to approximately 0 V. Thus, it was contemplated that, by using this case, this last problem may be solved. To start the analogue input object by voltage drop and thus to collect the force data simultaneously with the indenter's start to move are targeted here. For this purpose following code was inserted in the software.

```
set(AI,'TriggerChannel',Chans2)
set(AI,'TriggerType','Software')
set(AI,'TriggerCondition','Falling')
set(AI,'TriggerConditionValue',4)
set(ao,'TriggerType','Manual')
```

With this code, impact data in the third channel is obtained and as soon as the drop of this data to 4 V, collection of the force data commences. After the application of this, it was observed that, this correction worked rather well (Figure 3.25).

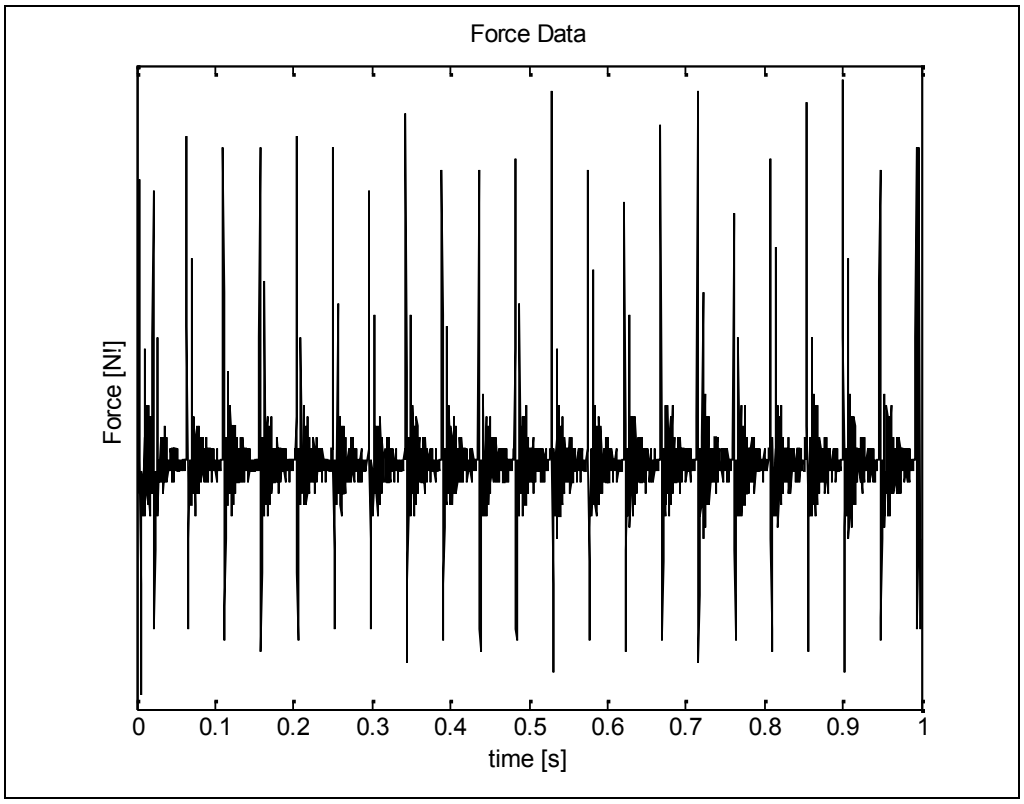

Figure 3.25 Graph obtained for 1 mm/s motor speed and 1 mm displacement, in that case where the force data collection takes place simultaneously with the step motor's initial start.

Yet, two important risks, deserving attention are still valid. First of these risks is that, in case the sample rate is kept low, pulses could not be detected. This, in turn, might cause the delayed perception of the pulse and consequentially results with delayed collection of the force data. When the sample rate was set as 200 times the motor speed, on the other hand, such a problem was not encountered. Second point is the problem arising when the reference voltage facilitating the force data collection is taken at low levels. Voltage actuating the motor does not always drop to 0 V and this value sometimes becomes much higher. This is a situation observed in the derived graphs. This possibly arises from the collection of pulse data not so correctly, that is, from the low level of sample rate at certain situations. Therefore, reference voltage is taken as 4 V and the force data is commenced to be collected with the first voltage drop to below 4 V. With this measure, no problem has been encountered.

Realizing that the modifications worked well, these modifications were also applied to the other test protocols, that is, to the software prepared for cyclic loading, relaxation and creep tests.

3.3.5 Quantization Error

As can be seen from Figure 3.9, errors observed in the measurements are related to precision. For certain displacement inputs it was observed that, values read were same. For instance, in Figure 3.9, in measurements of 1.1 and 1.4 mm such observation is encountered. For 5 mm/s speed, points where the same results observed were 1.6-1.8 mm, 2-2.2-2.4 mm and 2.6-2.8 mm (Appendix A). This was due, insufficiency of the minimum voltage increase (Figure 3.26).

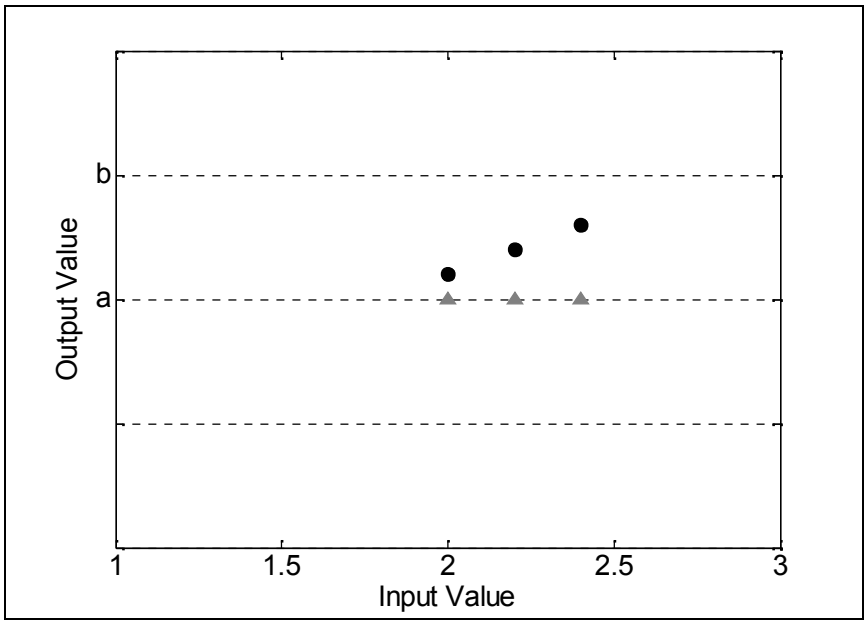

Figure 3.26 Quantization Error

As it can be seen from the Figure 3.26, voltage produced for the entered values 2, 2.2 and 2.4 mm lie within the interval a-b. Therefore, all these three values are evaluated with voltage a. Origin of this problem is related to the bit resolution of the data acquisition card. Data acquisition card used by us were a 12 bit and it was not possible to upgrade this. With a 16 bit card, it will be possible to obtain more precise measurements.

Graphs with same characteristics were obtained at certain speeds (Appendix A). No problem is encountered at speeds up to 2 mm/s. At 2.5-4 mm/s, 5-9 mm/s speed intervals and at 10 mm/s, graphs with 3 different characteristics were obtained.

3.3.6 Determination of the Correct Voltage-Motor Speed Equation Constants for the Selected Speed Values in the Cyclic Loading Tests

Improvements made on the software written for the cyclic loading test protocol were already discussed before (See Chapter 3.3). Results of these improvements were also presented in Table 3.5. As could be noted on Table 3.5, indenter tip

moved nearly as much as the entered distance, in different speed values. Yet, in different speeds, movement distance of indenter tip varied. As the indenter tip speeded up, the distance taken got smaller marginally. For instance, when it was desired that indenter tip moved 9 mm and 1 mm/s speed, tip moved approximately 9.5 mm and at 8 mm/s speed it moved 8.60 mm. This situation was thought to affect the test data and therefore was decided to be corrected.

Cyclic loading tests would be carried out at 1, 2, 4 and 8 mm/s speeds. It was therefore decided to use different voltage constant values for these speeds. In other words, first constant of the equation 1 determining the speed were determined separately for each individual test speed.

For instance, at 1 mm/s speed, indenter tip has taken 9.51 mm distance for a constant of 0.1686 and 9 mm track. By employing direct proportioning, constant was determined to be 0.15922. Constants determined for each speed and the results of measurements made by these constants are listed in Table 3.7.

Table 3.7 The determined first constants and the measurement results for the speeds 1, 2, 4 and 8 mm/s at which the cyclic loading test were carried out

Motor Speed (mm/s)	Constant A	Mesurement Nr.	Distance (mm)			
			7	8	9	10
1	0.15922	1	7.02	7.99	9	9.98
		2	7.03	8	9	9.99
2	0.1686	1	7.07	8.09	9.06	10.08
		2	7.07	-	9.06	10.08
4	0.1686	1	7.12	8.08	9.05	10.02
		2	7.11	8.08	9.05	10.02
8	0.17174	1	6.9	8.05	8.83	10
		2	6.89	8.06	8.83	10

Note: In determining the constants, measurements carried out for 10 mm distance which is measurable limit by dial gauge, were taken into consideration.

3.4 Force Data

Force data was measured by ENTRAN ELW-01-50N load cell. For the determination of possible errors in the force data a series of calibration measurements within 2-50 N range were carried out. Graph in Figure 3.27 and calibration equality were obtained at the end of these measurements.

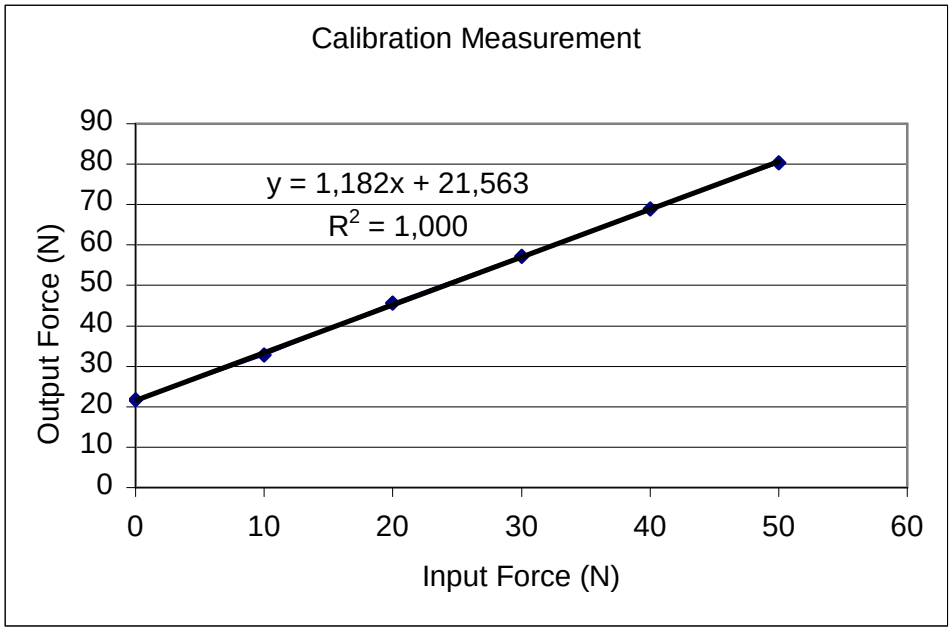

Figure 3.27 Force graph measured against the applied load and calibration equation.

Slope in the equation indicates that calibration constant provided by the manufacturer is slightly altered. y-intercept originates from the fact that, load cell has an offset when there is no load on it. It is clear that, force data correctness can be attained by equaling the slope to one and by subtracting the y-intercept from existing value.

In order to convert the slope to one, an inverse proportion with sensor range is established and the new value of the sensor range is determined as 0.34543. This value provided by the manufacturer before calculation of it, was 0.29218.

Following the corrections, measurements were repeated and the graph in Figure 3.28 was obtained.

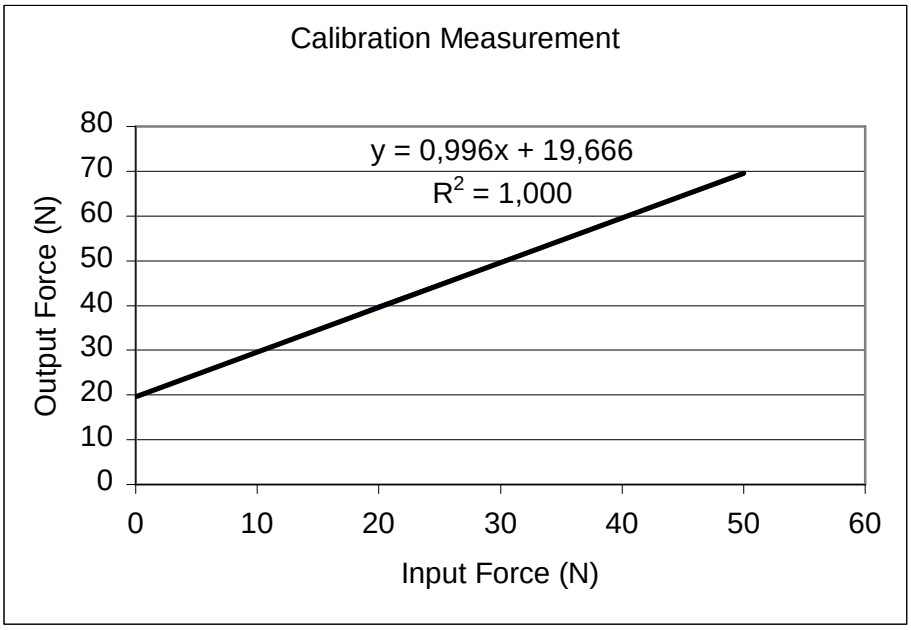

Figure 3.28 Applied load versus force graph and equation obtained after the alteration of the load cell calibration equation.

As can be observed from the graph, slope comes out to be very close to one. y-intercept, on the other hand, comes out to be lower than its previous value. For the derivation of y-intercept from the data, prior to measurements when the indenter is unloaded force data is determined and this value is subtracted from the values obtained throughout the measurements, during the tests. In the measurements conducted after the corrections, it is observed that the force data deviates between -0.25 N and +0.43 N and the average deviation is 0.19 N.

3.4.1 Correction of the Input Range Interval for the Calibration Process

In the start of the studies, the real target was to make measurements for deriving a calibration equation. To this end, a series of measurements within 0-50 N range were conducted. At the end of the measurements, it was noted that, after 19 N, output voltage was saturated at 0.5 V (Figure 3.29).

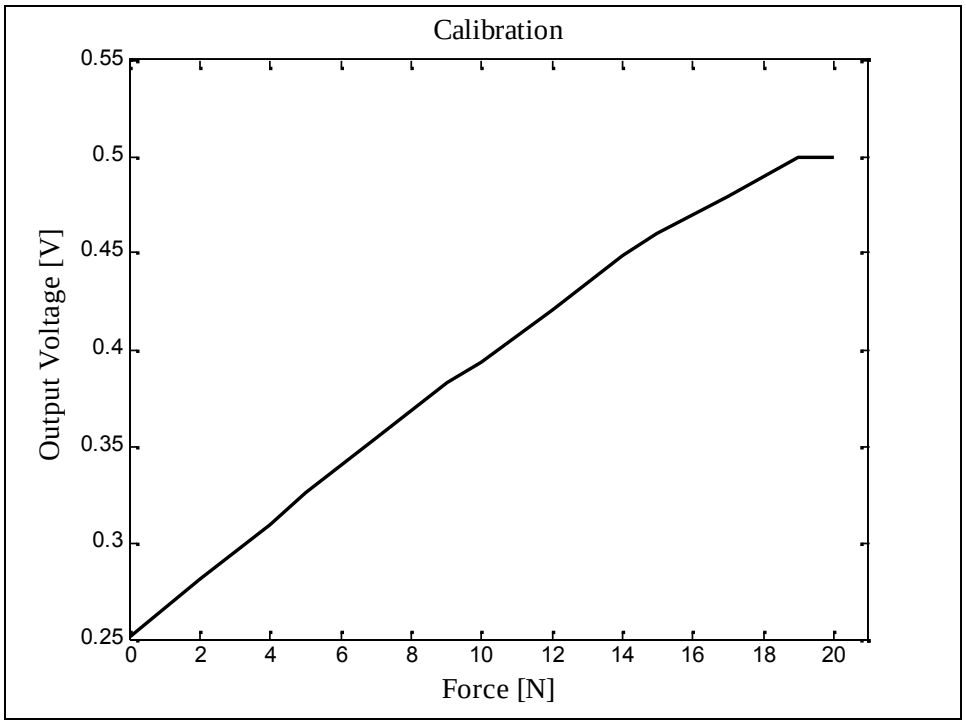

Figure 3.29 During the calibration measurements, it was observed that, it was observed that the output voltage stays constant at 0.5 V for forces above 19 N.

At this point, it was realized that the input range remains deficient and that it should be altered. In the software, previously ± 0.5 V has been used as input range, and realizing that this range supported 20 N load at the maximum, input range was revised as 0 – 1 V interval. Following alterations, measurements were repeated and was seen that the problem is alleviated (Figure 3.30).

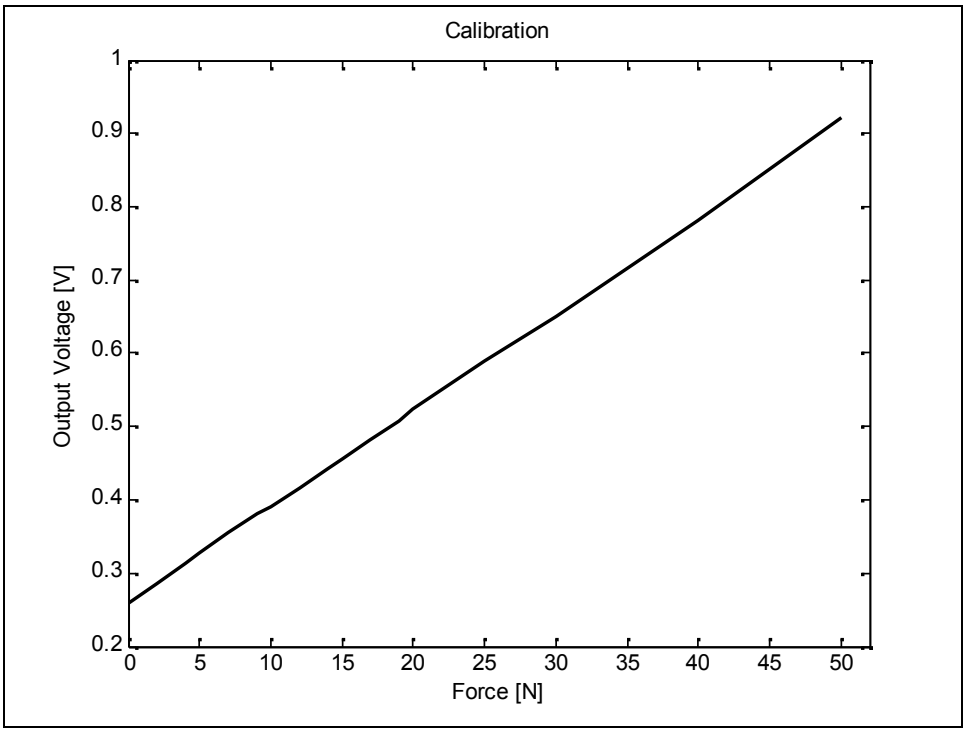

Figure 3.30 Force – output voltage graph obtained when the input range is varied within the interval of 0-1 V.

Another observation of this study was that, the force data would be measured more correctly when input range was taken as [-1 1]. Measured force load graph obtained when input range was taken as [0 1] can be seen in Figure 3.31.

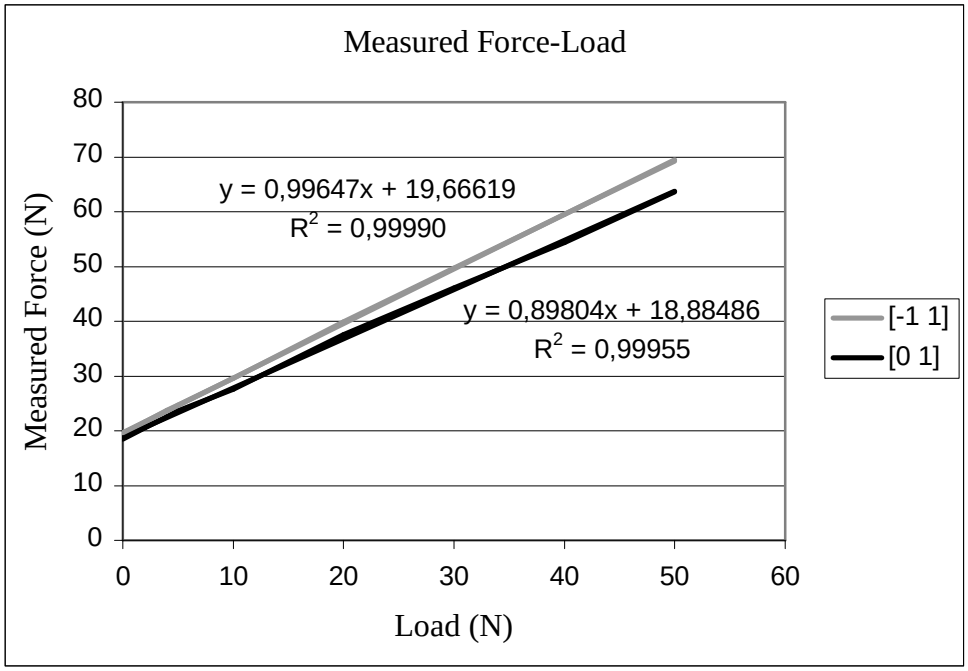

Figure 3.31 Calibration graphs and equations obtained when the ranges are taken within 0-1 V and -1, 1 V intervals.

In fact under normal conditions, better results are expected to be obtained when the input range becomes [0 1]. Because the precision obtained for the [0 1] interval is twice better than the precision obtained for the [-1 1] interval. Yet, in the help page of Matlab, it is stated that, signal polarity is a fixed character of the sensor and that, input range must necessarily be in conformity with this character (The MathWorks, 2008). Therefore, although very explicit, obtaining better results when worked in the [-1 1] range might have been attributed to this.

3.5 Filtering the Test Data

Test data may contain noise attributable to the environmental factors and due to causes originating from the character of the test system. In our test system data contain noises arising from the pulses created by the step motor. Number of these impacts either increased or decreased, depending on the sample rate value input in the software, controlling the indenter device. Sample rate value was kept

high within the software, in order to collect the force data and to assure synchronization of the indenter movement. Consequently, this has required with the accumulation of noise data.

For the clearing from noise process, sgolayfilt function in the Matlab® 6.1 was used (Appendix B). Results obtained can be seen in Figure 3.32 and Figure 3.33.

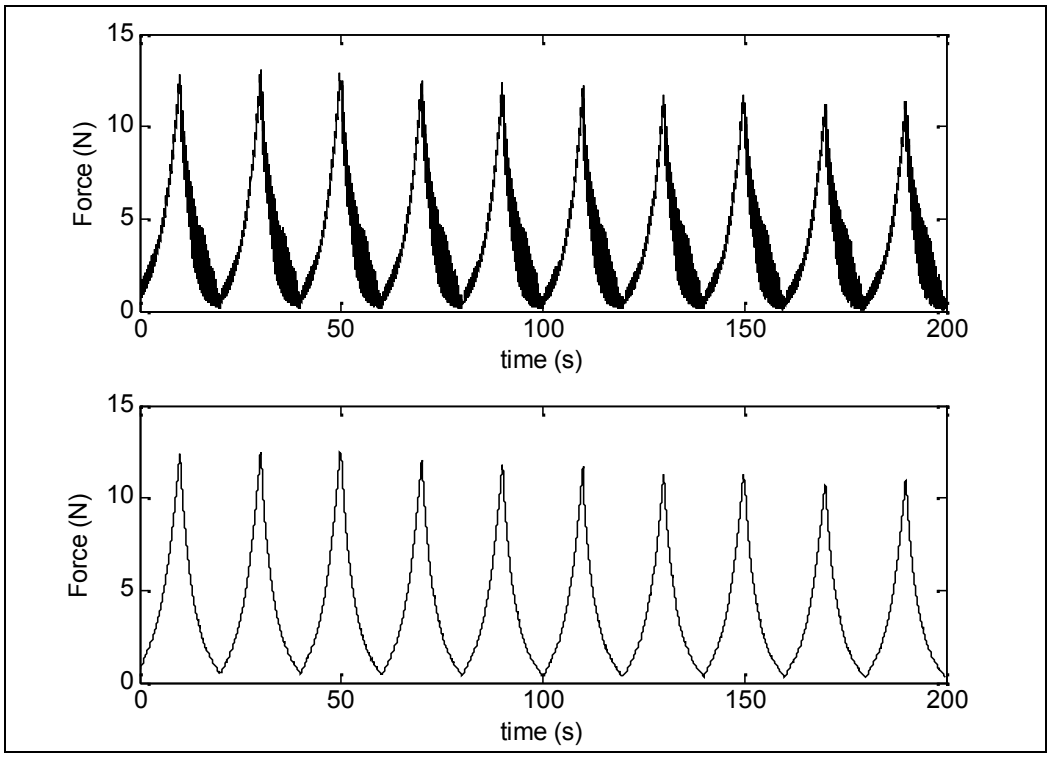

Figure 3.32 Measurement result for 1 mm/s indenter tip speed, 10 mm displacement and 10 cycles is seen at the first graph. Filtered results can be seen under the first graph.

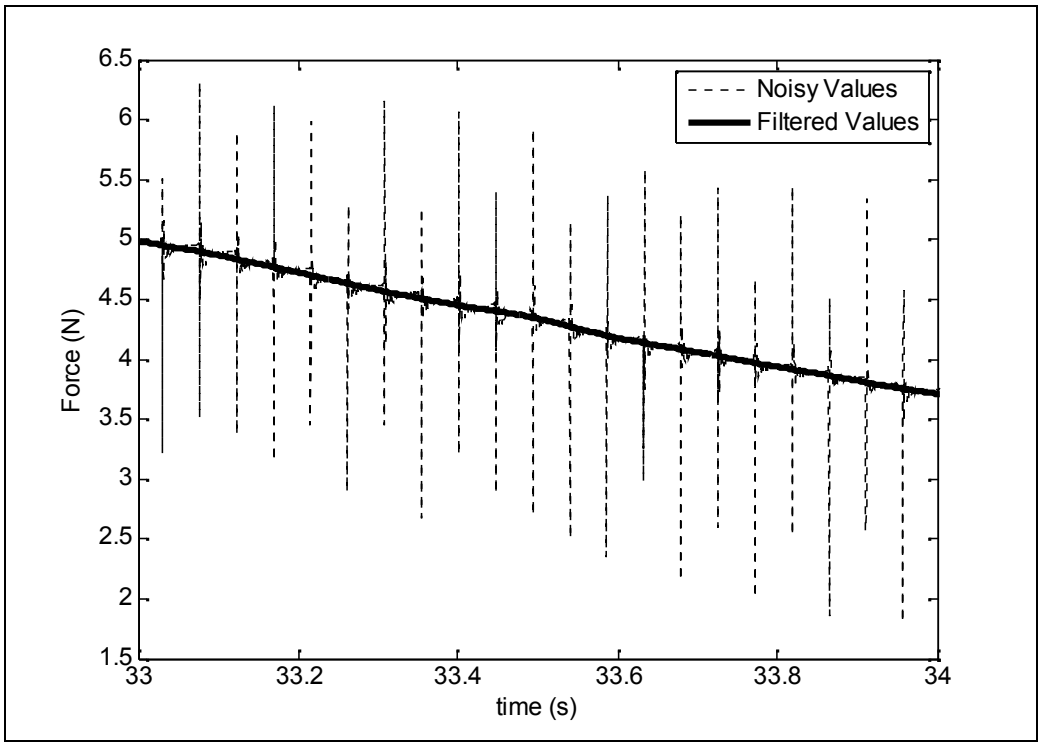

Figure 3.33 Detailed view for the Figure 3.32

3.6 Improvement Made on the Creep Test Protocol Software

Creep test consists basically of two stages. Indenter tip continues to move until a certain force value is reached after its tip touches the tissue. This constitutes the first stage of the creep test. At the second stage, indenter tip's movement is secured to continue as to keep the force constant after this desired force value reached (Figure 3.34). At the end of the creep test, two important data groups are filed. These are force-time and displacement time data.

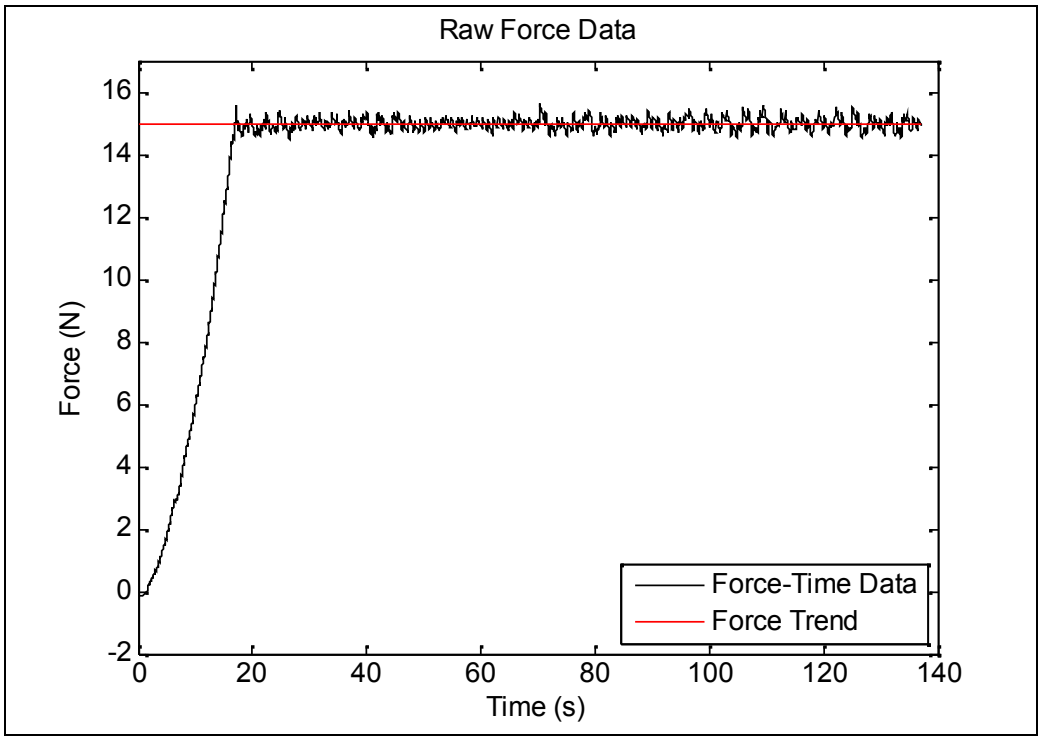

Figure 3.34 Creep test for 1 mm/s indenter speed, 1.5 N target force and 120 second creep duration. In the Graph, loading up to 15 N and the fixation phases at this load are seen.

Therefore, software used for the creep test protocol must fulfill the above conditions. Once the target force and creep time are loaded as input parameters, force-time and displacement-time data must be obtained through the software.

In the available software, creep protocol was substantially completed, yet, the creep duration was not started with the achievement of the target force but was initiated with the first movement of the indenter tip. Therefore, depending on the duration required to reach the target force, creep duration decreases.

This problem was eliminated by adding into the software the codes which assure the start of creep duration at the verge of reaching the target force and by making the necessary arrangements to this end (Appendix F). Furthermore, another problem faced during the creep test was deficiency of the capacity of the computer, with regard to obtaining the displacement information. This problem

was also eliminated by making some changes in the software (Appendix F). Thus the problems other than the movement precision of the indenter tip were substantially solved.

3.6.1 Adjustment of the Movement Sensitivity in Creep Test

With the changes mentioned above, creep test are commenced. Following a great many number of measurements, it was realized that, distance taken by the indenter tip until the target force was reached, was different than the data obtained. This result was more clearly exposed when the measurements were carried out with indenter device connected to the setup in Figure 3.9.

Measurements were carried out as follows. Indenter test device was connected to the test assembly. Target force was entered at low value such as 4 N and creep time at 5 – 10 second interval. In the test, the important data was the amount of displacement when the target force is reached and at the end of the creep time. Determination of these values clearly, by the help of dial gauge was another preference reason. Thus, the test was started and the movement of the indenter tip was observed. When the indenter tip took a distance of about 8 mm, a force exceeding target force 4 N was applied on the tip. Following this, movement of tip was achieved by applying force on the tip during the creep time and at the end of the test dial gauge was read where the indenter tip halted. After this process, a graph as shown in Figure 3.35 was obtained.

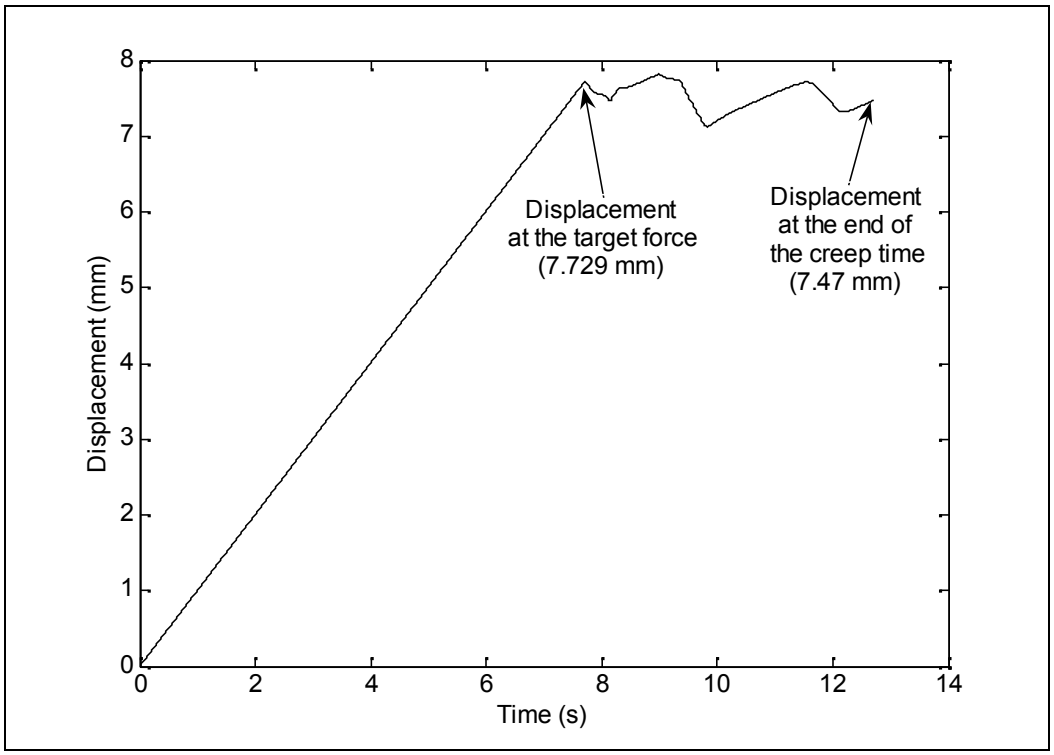

Figure 3.35 In the creep graph, two points important for the study are seen.

Two points on this graph were important. These were the distance taken by the indenter tip until the target force was reached and the position of the indenter tip at the end of the test. These values were observed on the graph and were compared to those measured by dial gauge. In the measurements pertinent to Figure 3.35, distance taken to reach the target force was 8.44 mm and the position as the indenter tip stopped was 8.5 mm as read from the dial gauge. Yet on the graph, these values were 7.47 mm and 7.729 mm respectively. In the software a section prepared for the indenter tip to return to its first position, following the completion of test was present. Therefore, within the test, indenter tip returned to its original position. Another point observed at this stage was, failure of the indenter tip to return to position where it started to move. Talking about the above test, 0.07 mm prior to the indenter tip started to move and with the completion of test when the indenter tip assumed its movement to its original

position, 1.45 mm were read on the dial gauge. In other words, indenter has moved about 1.4 mm less than it should.

In order to get rid of this problem, great many numbers of modifications were made on the existing software and new methods were practiced. Yet, these efforts ended with,

- indenter tip to stay unmoved
- obtaining error as the indenter tip has reached the target force
- creep time to extend much more than the entered time

At this level, although rather unwillingly, the desired result was sought to be achieved by changing the equation constants identifying the speed in software.

As was discussed in detail, in Section 3.2, indenter tip speed was identified by the equation,

gerilim = 0.1686 * (mothiz -31 / 300) ..... (3.17)

where,

gerilim = input voltage

mothiz = step motor speed determined by the user

This equation is used in the form of,

hizbilgi (i) / 0.1686 + 31/300..... (3.18)

when the displacement in creep software is calculated.

Here, it was thought that by changing the constant 0.1686 the desired result would be sought and measurements were carried out by entering different constants. Observations were made by entering equal and also varying constants for Equation 3.18 and 3.19.

Results of these measurements can be seen in Table 3.8.

Table 3.8 Measurement results for different first and second constants in the Equation 3.17 and Equation 3.18.

Constant in Eq.1	Constant in Eq.2	Disp. at the target force-Reading from dual gage (mm)	Disp. at the end of the creep time-Reading from dual gage (mm)	Disp. at the target force-Reading from graph (mm)	Displacement at the end of the creep time-Reading from graph (mm)	Start point reading from the dual gage (mm)	Original position reading from the dual gage (mm)
0.175479	0.175479	8.63	8.46	7.33	6.975	0.06	1.61
0.175479	0.1686	8.42	8.43	7.394	7.059	0.09	1.29
0.1686	0.175479	8.48	8.38	7.113	6.714	0.11	1.86
0.1686	0.1686	8.62	8.51	7.572	7.295	0.06	1.27
0.1686	0.162	8.44	8.5	7.729	7.47	-	1.45
0.1686	0.145	8.45	9.08	8.553	7.847	0.17	0.26
0.159	0.153	8.8	9.03	8.534	8.317	-	0.67
0.159	0.153	8.62	8.49	8.409	7.956	-	0.64
0.159	0.153	8.45	9.03	8.137	8.274	-	0.79
0.153	0.153	9.22	9.15	8.74	8.538	-	0.6
0.145	0.175479	8.59	8.52	7.239	6.944	0.06	1.96
0.145	0.1686	8.43	8.01	7.332	7.211	0.11	1.08
0.145	0.145	8.42	8.13	8.484	8.072	0.05	0.17
0.145	0.145	8.6	8.2	8.577	8.411	0.11	0.06
0.145	0.145	5.56	5.13	5.454	4.841	0.06	0.36
0.145	0.145	9.78	9.44	9.734	9.377	0.07	0.4
0.14	0.153	8.8	8.75	8.415	7.949	-	0.93
0.14	0.153	8.4	7.76	7.979	7.857	-	0.02
0.14	0.153	8.71	8.61	8.34	7.838	-	0.79

At the end of the measurements, it was observed that best results were obtained when both constants were entered as 0.145 (Figure 3.36). For this constant, deviations when the indenter tip has reached the target force and when the indenter tip completed its movement have been within -0.048, +0.087 and +0.011, 0.337 ranges respectively.

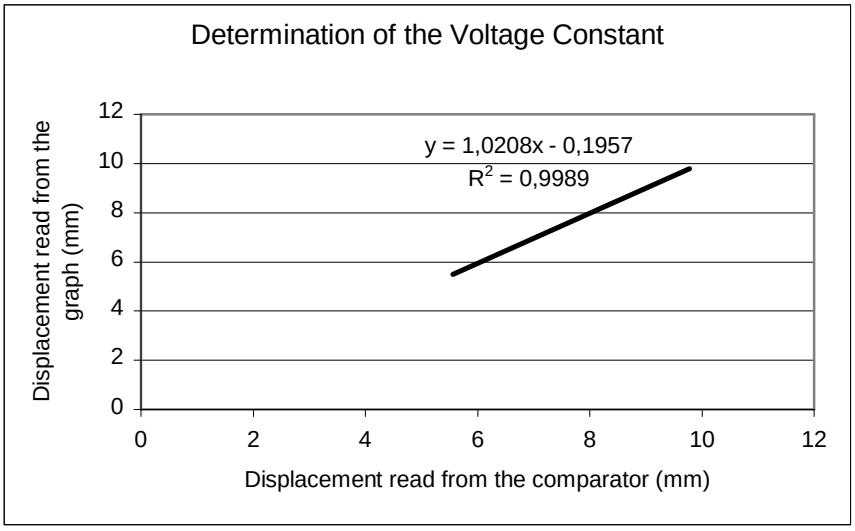

Figure 3.36 Graph and equation for values obtained from the dial gage when the constants are determined as 0.145 versus values read from the graph.

3.7 Determining the Contact Point of Indenter's Tip with the Tissue

Indenter's tip in contact with the tissue at the commencement of the test result with data to start with a force value other than zero. Following the connection of indenter device to the tissue, if calibration works are carried out, data is observed if it starts with zero, yet, in fact, it starts with a positive force value. This causes the obtained data graphs to be incomplete (Figure 3.37) and also, tissue's behavior can not be fully apprehended.

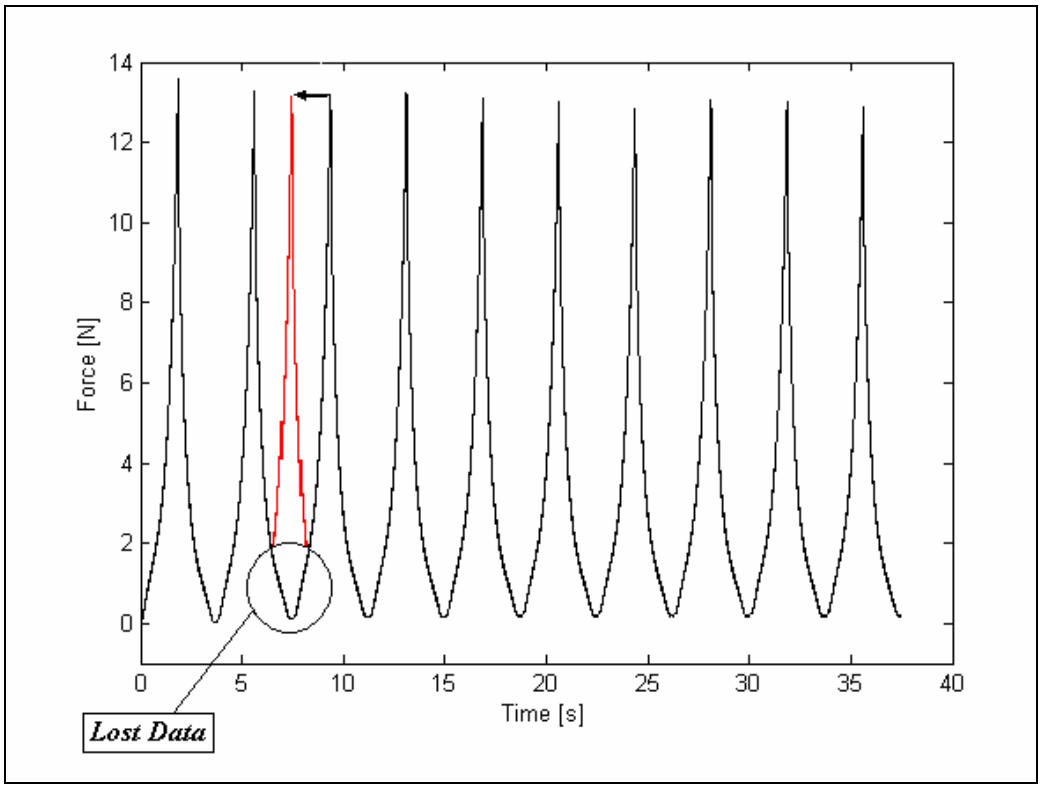

Figure 3.37 When the indenter tip is in contact with the point tested, data starts with a certain force value and this causes data loss.

Therefore, indenter device is connected in such a way that the indenter tip does not touch the tissue. Since contact is not attained, force affecting the indenter's tip becomes zero. A zone where zero force prevails is thus encountered contact with the tissue and force-displacement behavior of the tissue is observed (Figure 3.39).

Data obtained after the indenter touches the tissue, is the data necessary for the studies to be carried out. It is therefore essential to determine the point when the indenter comes into contact with the tissue and to obtain the data prior to this point. Under ideal conditions, this is a relatively easy deed. Point where the force data transforms into a force other than zero is the point sought (Figure 3.38). This point can be determined by a rather simple algorithm.

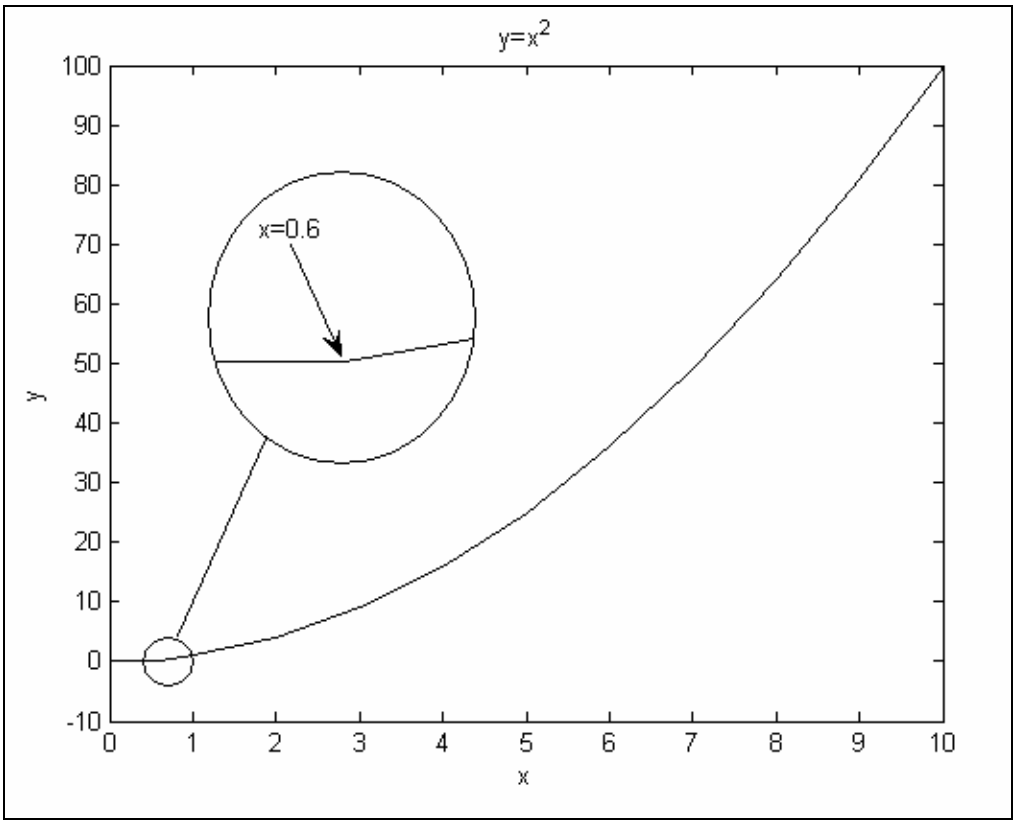

Figure 3.38 To final the transition point in clean data where no outside intrusions exist, is relatively easy. In the $y = x^2$ graph, up to $x = 0.6$, zero values are designated. Therefore, up to that point, graph is shown as a flat line. Yet, in the noised data, such an observation may not be possible.

Yet, data obtained by the indenter are not that clear. Most important problem is the prevalent noise encountered in data, in spite of the substantial filtration effort (Figure 39-A). When the data are closely scrutinized, they show a fluctuating appearance and therefore, contact point is not clearly pinned down. A second important problem is that, the force data obtained after calibration do not start exactly from zero (Figure 39-B). Although small, it still shows deviation from zero, either in positive or negative direction.

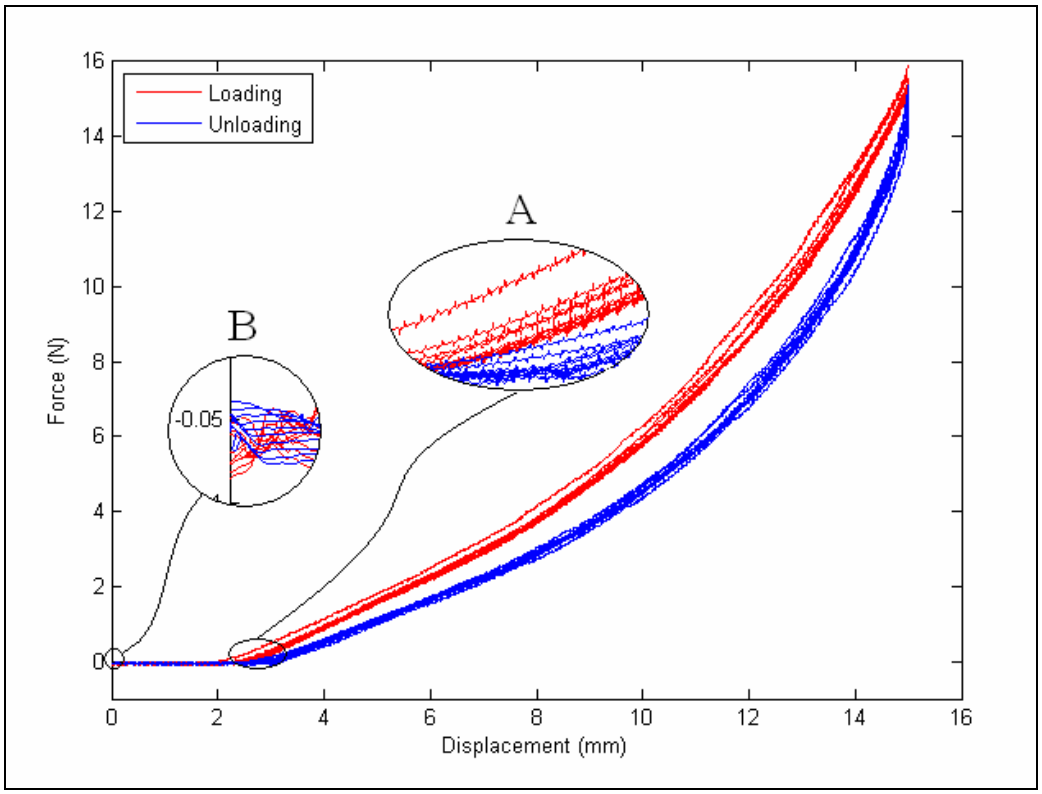

Figure 3.39 In spite of the filter, data contains a certain level of noise. This, consequently makes the location of contact point unclear (3.39-A). Data after this force calibration would not start at zero point and some small deviations would be inevitable (3.39-B).

Consequentially, deviation of the pre-contact force from zero and the noise in data make the determination of the contact point by a simple algorithm impossible and make the observations more difficult. When the test data are scrutinized singly, contact point is barely recognizable. Yet, since great many numbers of tests is to be processed and due to the fact that, any one test incorporates 20 curves as loading and unloading curves, development of an algorithm for the automatic determination of the contact point was necessitated. Thus, a considerable time saving would be feasible.

3.7.1 The Contact Algorithm

In Figure 3.40 loading curve and detail of a cycle of data pertinent to cyclic loading test are shown. As mentioned before, determining the contact point at this stage is rather difficult. In the first portion of the graph there exists an unsloped part. This portion is that portion where the indenter tip has not yet touched the tissue. Following this portion, it is noted that, slope of the graph increases with the increasing displacement. If we suppose that, the data is free of noise, the difference between two consecutive points therefore, increases as the displacement increases.

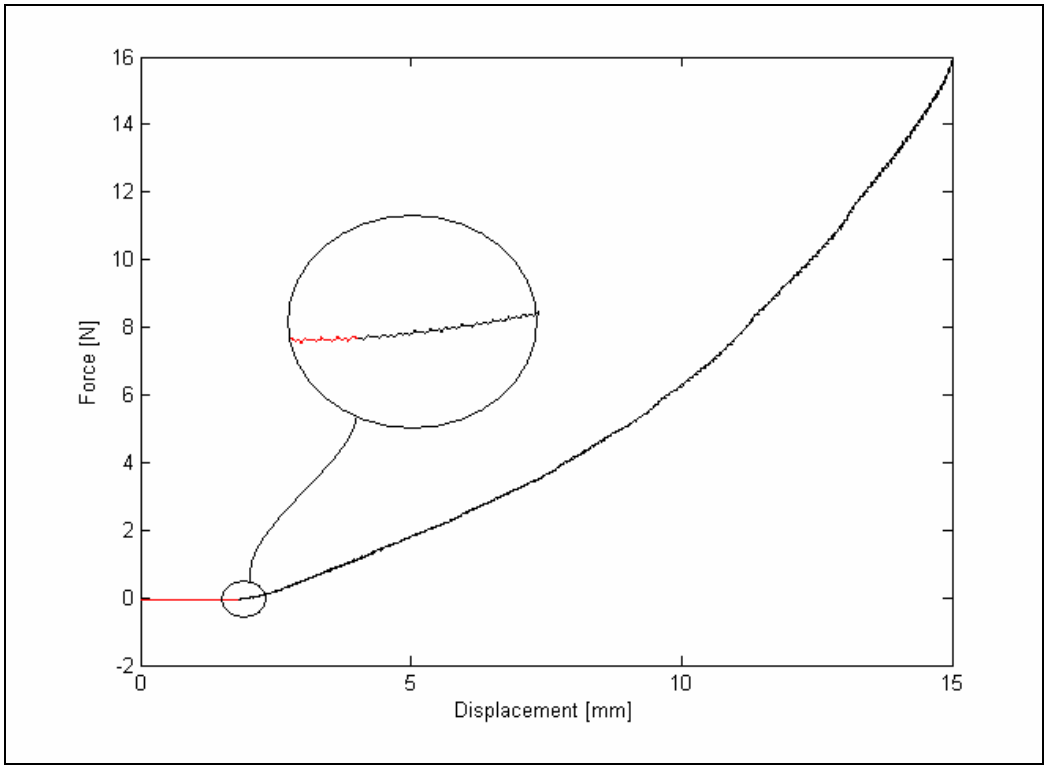

Figure 3.40 Red portion within the graph corresponds to the data where the indenter tip has not yet made contact with the tissue. Black portion, on the other hand, gives the data after the contact. As would be observed from the graphs, just at this transition, a slight slope is formed and with the increasing distance this slop gets steeper.

This phenomenon can be more clearly followed through the graph in Figure 3.38. In Figure 3.38, a graph related to $y = x^2$ function is laid down. When we compare the differences between the consecutive points of x = 21, 22 and x = 96, 97 we reach to following conclusion.

y (21) = 441
y (22) = 484
y (96) = 9216
y (97) = 9406
y (97) – y (96) = 190 > y (22) – y (21) = 43

Therefore, as the slope increases, the difference between the consecutive points also increases. Although the same behavior prevailed in the test data, this could not have been clearly observed, due to noise. Still, with this point in mind, it is possible to approximately locate the contact point.

In case the points are selected not consecutively but with certain intervals, it is observed that the difference increases with the increasing displacement (Figure 3.41). In the portion following the contact portion also, this difference is in minimum level.

Thus explaining the essential points, we can now describe the algorithms more explicitly.

Firstly, N number points with N+ 1 interval on the test data were selected (Figure 3.41). First of these points was the first data on the graph. Later the differences between these points were assessed (b2 - b1, b3 - b2 …). These differences were compared with a constant value determined by the user. In case the difference was larger than was assumed as the interval containing the contact point.

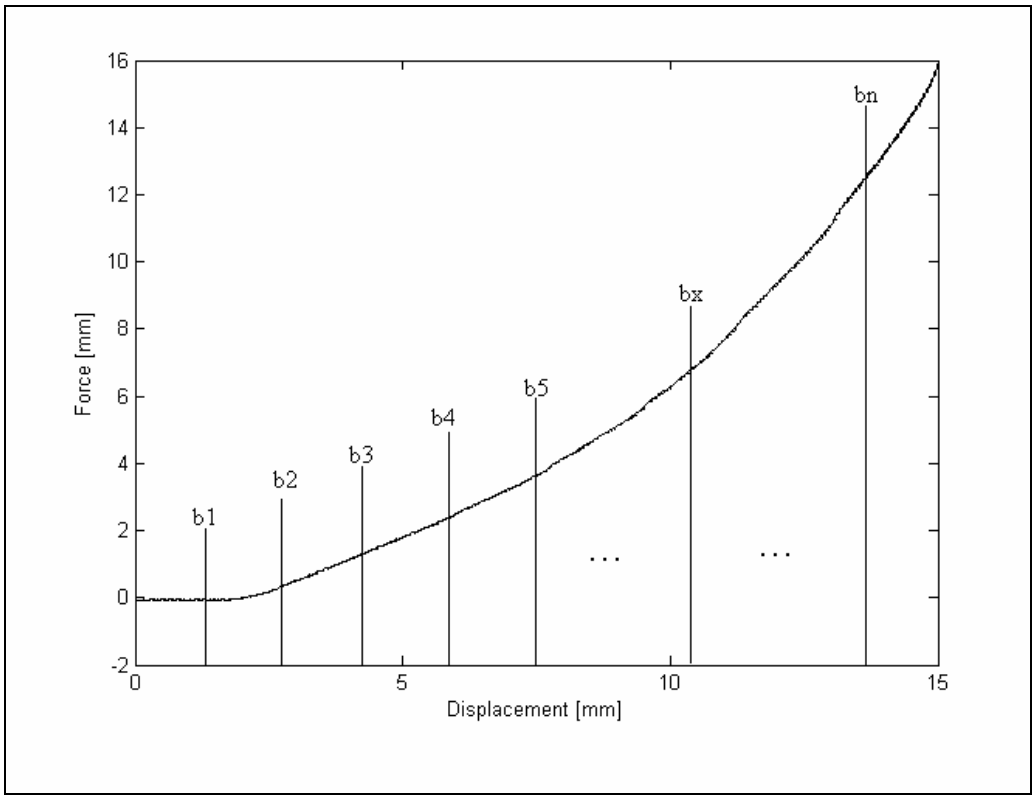

Figure 3.41 n number points are designated in equal intervals on the test data. Differences of these successive points are then calculated and the constants determined by the user are compared.

The same way, within a selected interval N2 points were determined and a second constant was taken. Number of points and the magnitude of constant were kept lower than those of the previous ones, and above procedure was repeated. Thus, a closer point to the actual contact point was detected (Figure 3.42).

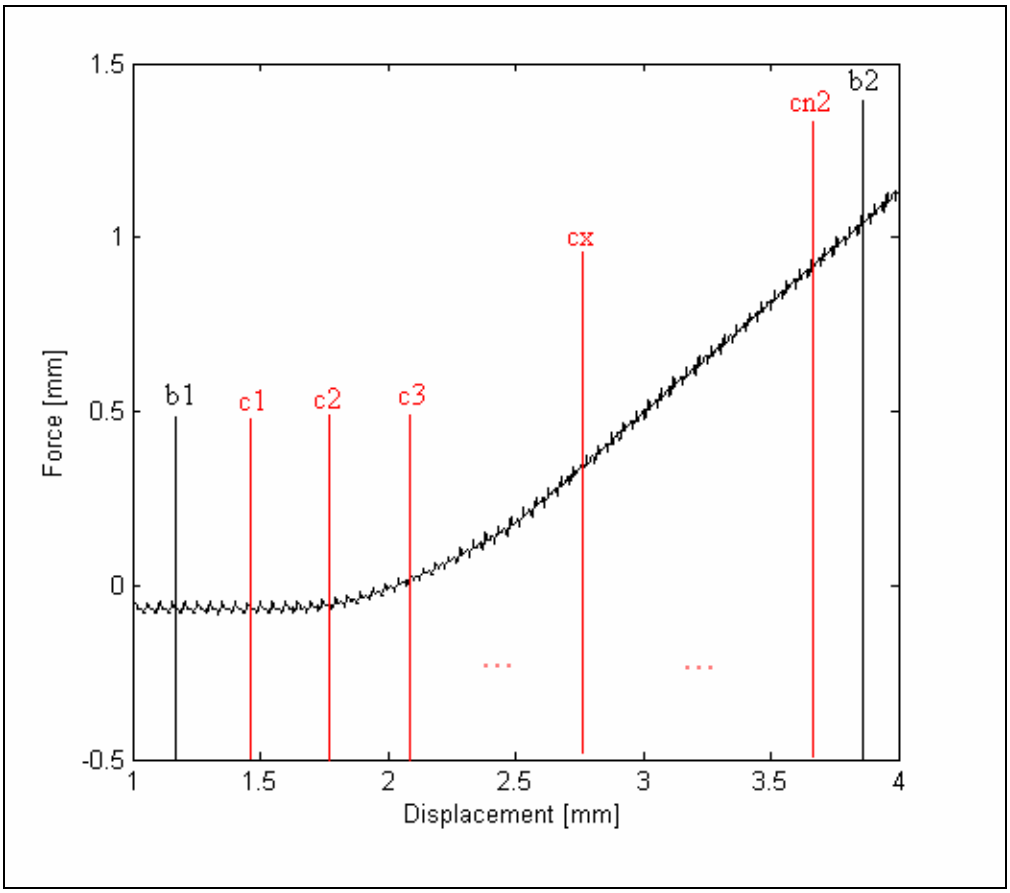

Figure 3.42 It is the portion where the difference between the points is bigger than the determined constant. And later in this portion also, N2 number equal interval points are marked and the differences between these successive points are compared with the second constant determined by the user.

During the studies, this algorithm has proved to be working well when compared with manual contact detection. The critical point is the selection of constants by the user, in a proper way. Selection is carried out by trial and error, and if the contact point is found much before than the real contact point a increase the constant and if it is found much later a decrease constant and the procedure is repeated (Figure 3.43).

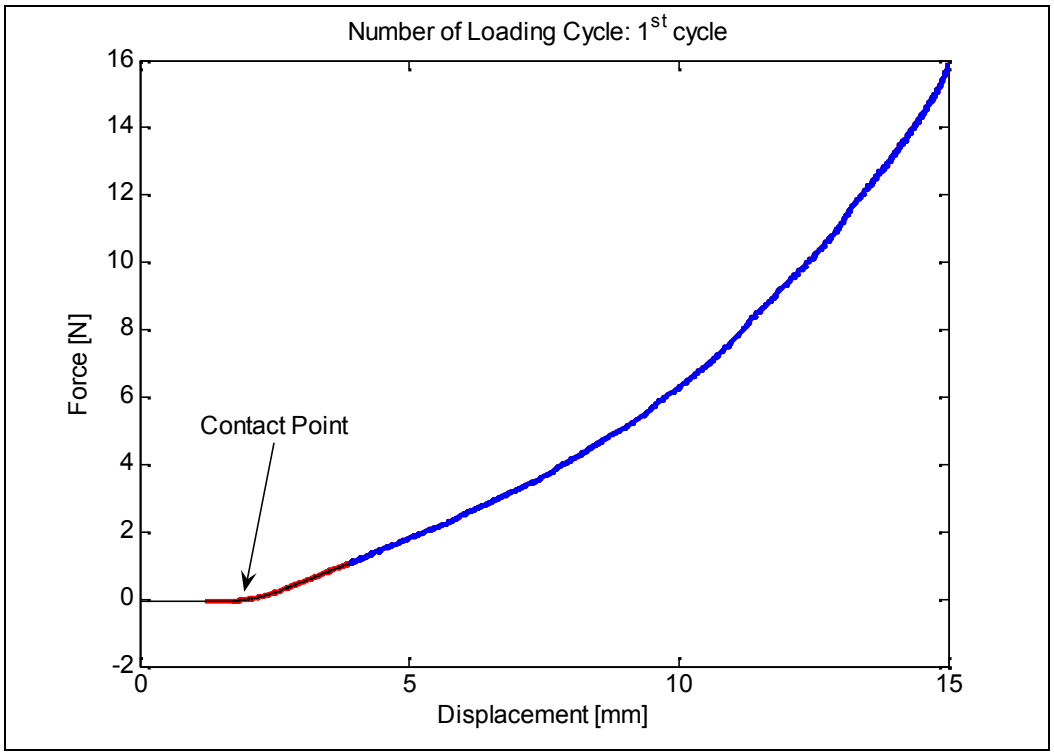

Figure 3.43 Keeping the constant small, causes the sighting of the contact point much before the real point (red data) and keeping it big, causes the sighting of contact point much after the real point(blue data).

Since the above mentioned algorithm (Appendix B) was transformed into a function by Matlab, this process could be achieved rather quickly. During the studies it was observed that, process worked substantially well, when the first constant was taken as 0.07, second constant as 0.02, first number of points as 40 and the second number of points as 1. Results can be seen in Figure 3.44.

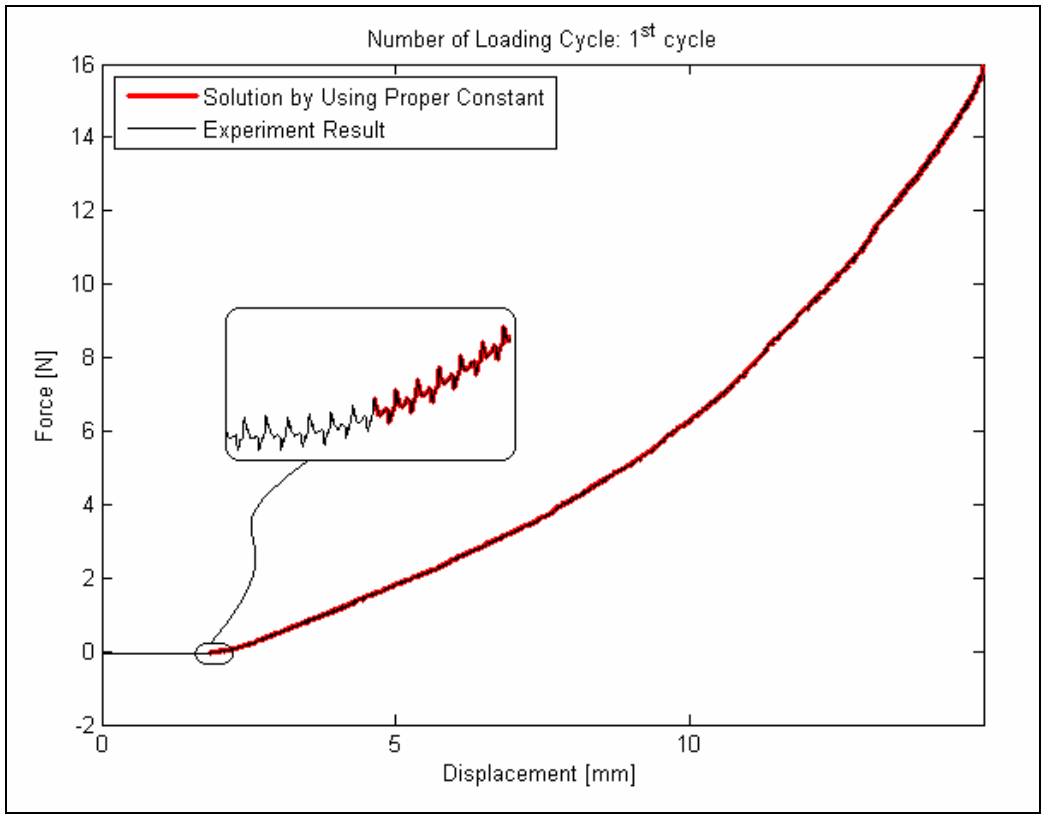

Figure 3.44 Good results are obtained by using appropriate constants and proper number of intervals.

Other observation was that, the contact point might display difference from cycle to cycle. In addition to that, the forward movement contact point took place earlier compared to that of the backward movement. This is the result of that the soft tissue is not an elastic material and also the test location is effected from the compression of the indenter tip which may causes some minor permanent deformation on the tissue (which would take considerably long time to recover when compared to experimental time). Therefore, two functions were identified. These are,

st (c1, c2, n)

st2 (c1, c2, n)

where,

c1 = First constant

c2 = Second constant

n = the old and the new curves are showed on the same graph for each loading and unloading curves, if n is entered as 1 (Figure 3.43, 3.44).

Contact points for each cycle and forward backward movements are separately determined by using the st function (Figure 45-a, b).

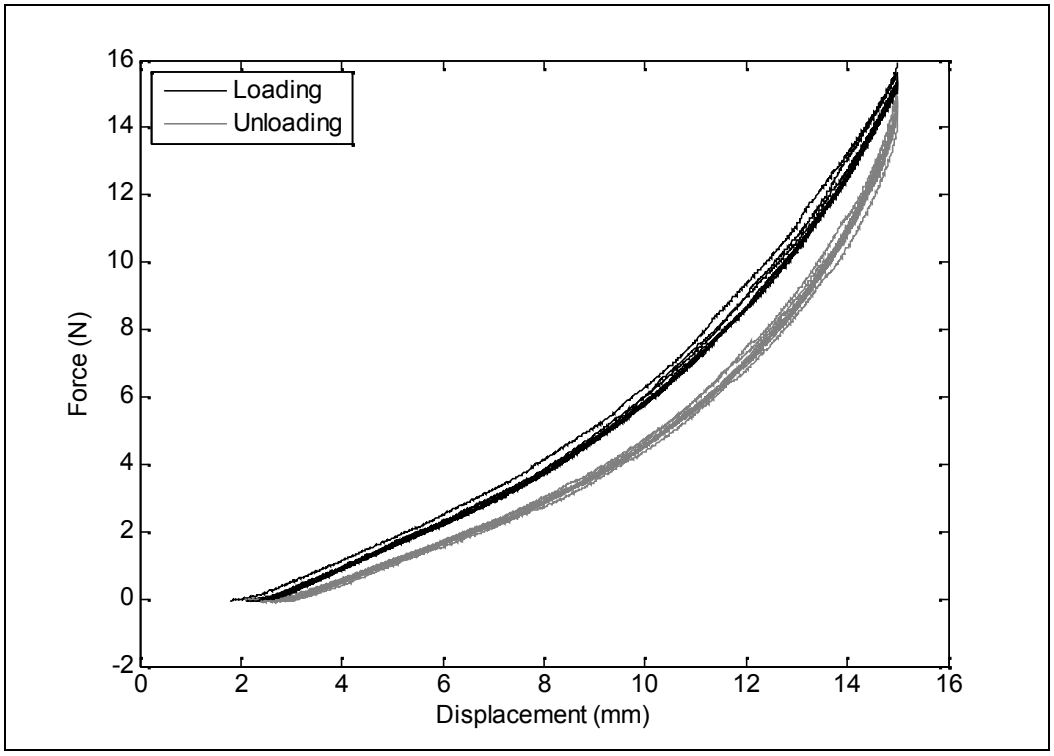

Figure 3.45-a Graph obtained when the contact point is determined independently for each cycle, by using the st function (Appendix B).

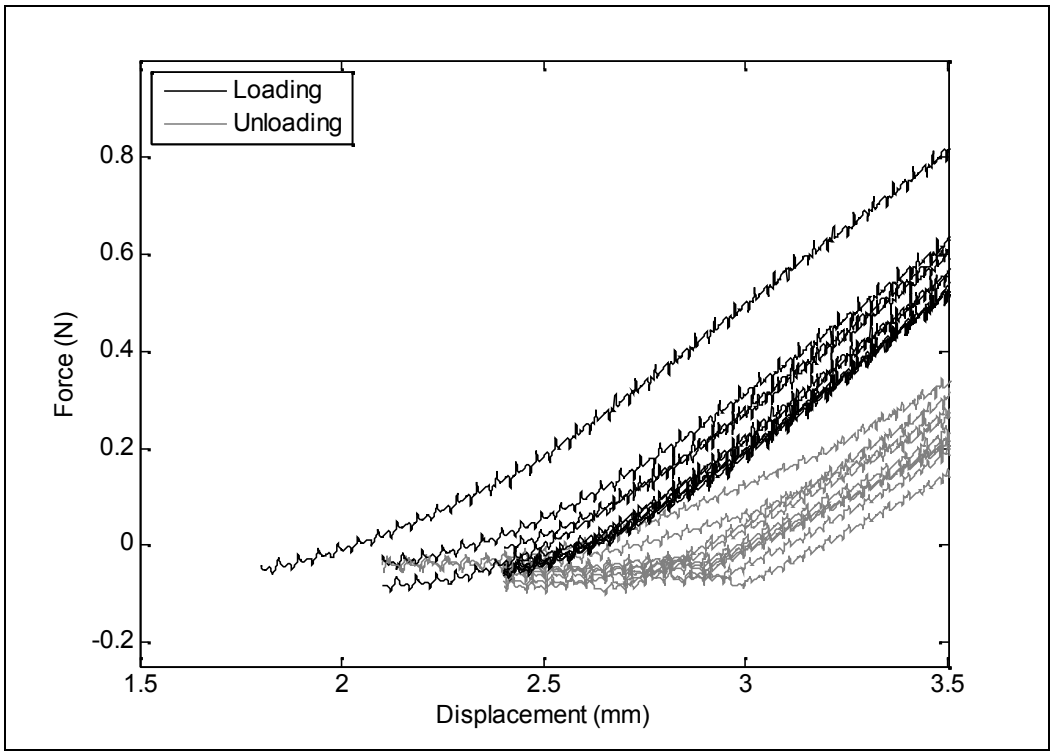

Figure 3.45-b Detailed view from the Figure 45-a. in this graph, different contact points determined can be seen.

On the other hand, by using st2 function, mean values of the separately determined contact points were calculated. Then, the calculated value was taken as overall contact point (Figure 3.46).

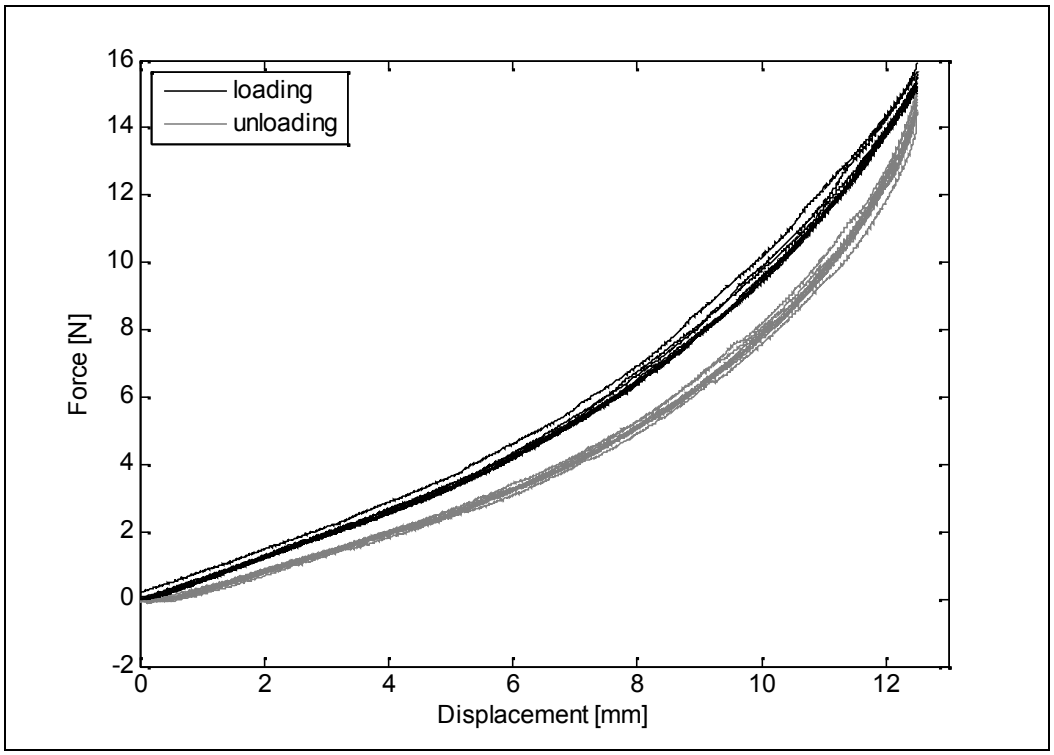

Figure 3.46 Graph obtained through the determination of the contact point by the help of the average value by using the st2 function (Appendix B).

Depending on the type of study, it was possible to use both of these functions.

CHAPTER 4

SOFT BIOLOGICAL TISSUE TESTS

4.1 Introduction

By the improvement of the software controlling the indenter test device mentioned in Chapter 3, and by producing a new connection system, proper tests directed to the aimed targets were commenced. In these tests, behavior of the soft biological tissues under cyclic loading were observed and the responses to relaxation and creep were studied. In relation to these, some related behaviors and anisotropic features of the tissues were also observed.

Tests were carried out in-vivo on forearm. Advantages and disadvantages of the in-vivo testing were discussed in detail in Chapter 2.

The reasons why the tests were carried out on forearm are as follows:

- Ease of working on forearm, speedy and easy achievement of the successive tests
- More comfortable control on the forearm
- When the work is carried out on the forearm, simpler design, low cost and small dimensions of the attachments to the test device
- More precise tests to be carried out

In the above mentioned points, especially the last issue is very important. Conduct of tests in in-vivo conditions, makes the fulfillment of the precision requirements in tests difficult to achieve. Tissues being alive cause the measurement to be influenced from slightest movement encountered. Difference

in the position of the tissue from its previous position, no matter how small this difference is may influence the test data.

Tests were started prior to a complete contact of the indenter tip with the tissue when there remains a predetermined distance in between. This is done so to avoid preloading and to be capable of observing all of the range of behavior starting from "*zero strain*"[2]. Later the test portion up to contact of the indenter tip to soft tissue was discarded by the help of the function described in Chapter 3. Thus, the preservation of this gap in measurements of the same test groups and in successive measurements is extremely important. Even in deviations less than 1 mm, test data is too much influenced from this, resulting with the build-up of additional loadings.

When the test was carried out on the forearm, this would be controlled more easily, speedy corrections in successive tests where the time is very important would be made and in general test arrangement speeds would be higher. This way, more speedy and dependable tests were carried out in a daytime.

4.2 Conducting In-vivo Indenter Tests and the Points to be Paid Attention

As explained in Chapter 2.5 in detail, besides the advantages rendered by in-vivo tests, it brings important difficulties during the course of the tests due to the livelihood of the tissue. In this section, it will be beneficial to discuss how these tests are conducted and to which points attention is paid.

4.2.1 Protocol Followed in the Conduct of Before the Tests

1. After the test system is powered up, it is waited for half an hour and the system is allowed to warm up to reach a steady state. Tests conducted within this duration are questionable and would nod be taken into consideration.

[2] Actually the tissue has some non-zero physiological stress and strain however the externally applied strain is zero for no-contact conditions.

2. At the end of this duration, a couple of trial tests are carried out and the system's proper performance is checked. Trial tests are carried out with due regard to the method intended to be employed in the tests. That is, in case it is indented to conduct the cyclic loading test, then, this test protocol is employed.

3. When the measurements are completed with one tests protocol, and a different test protocol is to be commenced, trial tests for this different protocol are carried out and the proper performance of the system is rechecked.

4. Parameters pertinent to the protocol to be employed are entered by the help of the interface (Figure 4.2). These parameters are;

For the cyclic loading test; motor speed, displacement amount of the indenter tip, number of cycles (See Section 4.3).

For the relaxation test; motor speed, displacement amount of the indenter tip, relaxation duration (See Section 4.4).

For the creep test; motor speed, target force, creep duration, and gain (See Section 4.5).

5. Forearm on which tests will be applied, are secured with the help of the arm rests (See Chapter 3.1.5).

6. By using the indenter tip positioner, indenter tip is positioned and secured to the point where the test will be applied.

7. In this securing, attention is paid on the indenter tip to be in perpendicular position to the surface of the tissue in concern.

8. In order to avoid any data loss, a certain distance is allowed in between the indenter tip and the tissue

9. After these positioning are being done, force zeroing is being carried out. Calibration is repeated for each measurement.

10. The test is started by pushing the button initiating the related protocol from the interface.

4.2.2 Protocol Followed in the Conduct of During the Tests

1. With the commencement of the test, any movement should be avoided. Speaking, movement of head to right or left, movement of fingers, forceful breathing should be avoided as far as possible.

2. When the group tests are conducted, during the successive measurements of the group, utmost attention is paid to preserve the body, arm and hand position.

3. When a measurement is completed and prior to the start of another measurement, position of the indenter tip should be checked. If the tip is left in forward, it should be backed up. Whether a slip at the test point exists or not is controlled.

4.2.3 Protocol Followed in the Conduct of After the Tests

1. Individual is released from the system

2. Data obtained is recorded with due regard to the chronology of tests and the related parameters

3. In case the test data is intended to be used in the computer simulations, for the determination of the tissue thickness, the test point is marked.

4. Tissue thickness is determined by the ultrasonography device existing in the Health center, located in the METU campus.

5. As the thickness of the tissue at the test point is determined, the probe of the ultrasonography device must not be pressed on to the tissue. If probe

is pressed in, tissue thickness will be measured to be thinner than it actually is.

6. To this end, for the determination of the tissue thickness is best way, probe is initially pressed in for a certain degree, to clearly see the bone tissue. Following this, the pressure applied by the probe on the tissue is relieved and the image is freezed at the last point where the bone is seen. Here, tissue thickness is measured (Figure 4.1). This way, variation of the tissue thickness due to the pressure to probe is minimized.

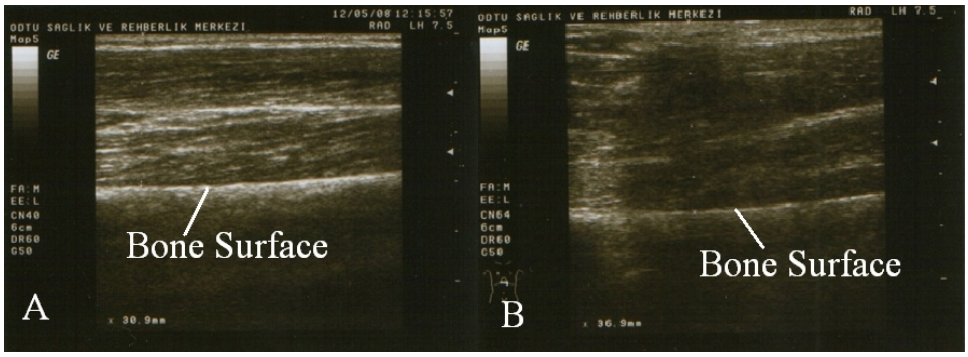

Figure 4.1 Tissue pressed by the probe to see the bone surface clearly (A) After seeing the bone clearly, the pressure applied by the probe is relieved (B)

7. Other important point which deserves attention when the tissue thickness is being determined is that, the arm muscles must not be squeezed and that the arm must be kept in the position in conformance with the tested position as far as possible. Squeezing the arm muscles will result with obtaining a tissue thickness more than the actual thickness of the tissue in the tests.

4.3 Cyclic Loading Tests and Observations

Cyclic loading tests are the measurements by loading and unloading of the measured tissue as the indenter tip periodically moves forward and backwards.

Prior to the test, movement distance of the indenter tip, motor speed and cycle amount information are entered by the interface (Figure 4.2) and following this, the test is started.

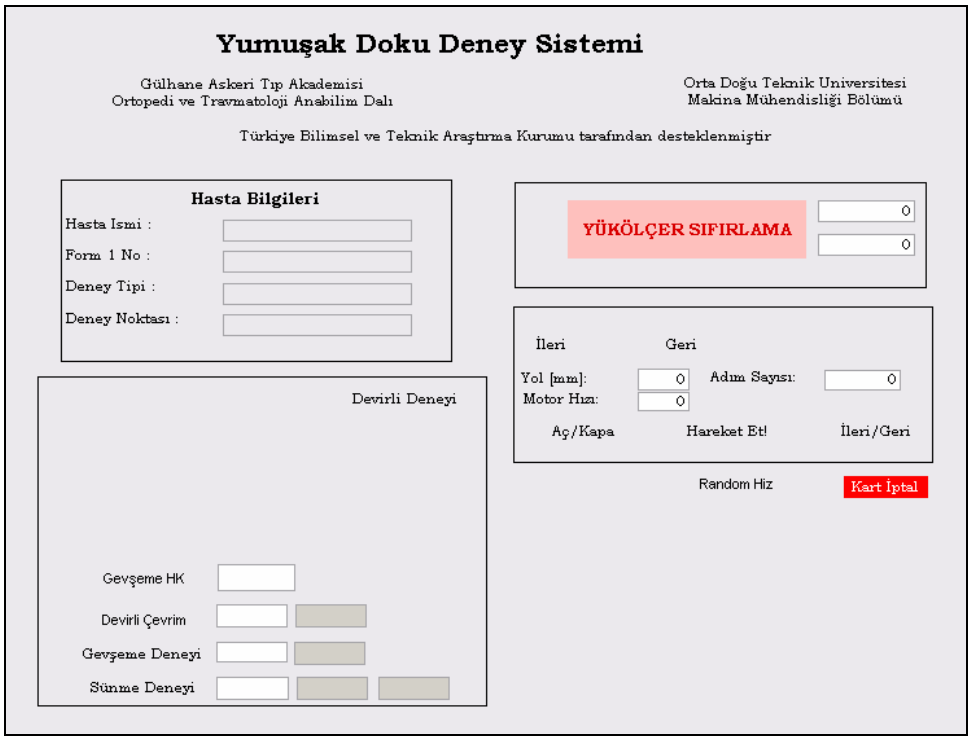

Figure 4.2 The require parameters are entered by the help of the interface prepared by using Matlab GUI

At the end of the tests, two groups of data were collected. These were the force-time and force-displacement data. By the use of these data, various observations were made.

4.3.1 Preconditioning Effect

Soft biological tissues display preconditioning (Mullin's) effect under cyclic loading. At the end of this behavior, tissue which was more resistant in the first couple of cycles, in the consecutive cycles showed repeatable and a compliant

response. This was believed to be happening due to the spread of the tissue fluids to surrounding areas.

In the in-vivo tests, due to different factors, preconditioning effect was not a phenomena observed at every measurement. Two basic causes of this were,

- Continuation of tissue to display its preconditioning feature as a consequent of the successive tests
- Unintentional variations in the muscle activations or deviations in the position of the tested organ that is the forearm.

Another phenomenon encountered with the preconditioning effect were the formation of differing cases pertinent to the force – time and force – displacement data. Preconditioning effect in the force – time data was encountered as the decrease in the resistance of tissue with progressing cycles and as getting constant after a certain number of cycles (Figure 4.3).

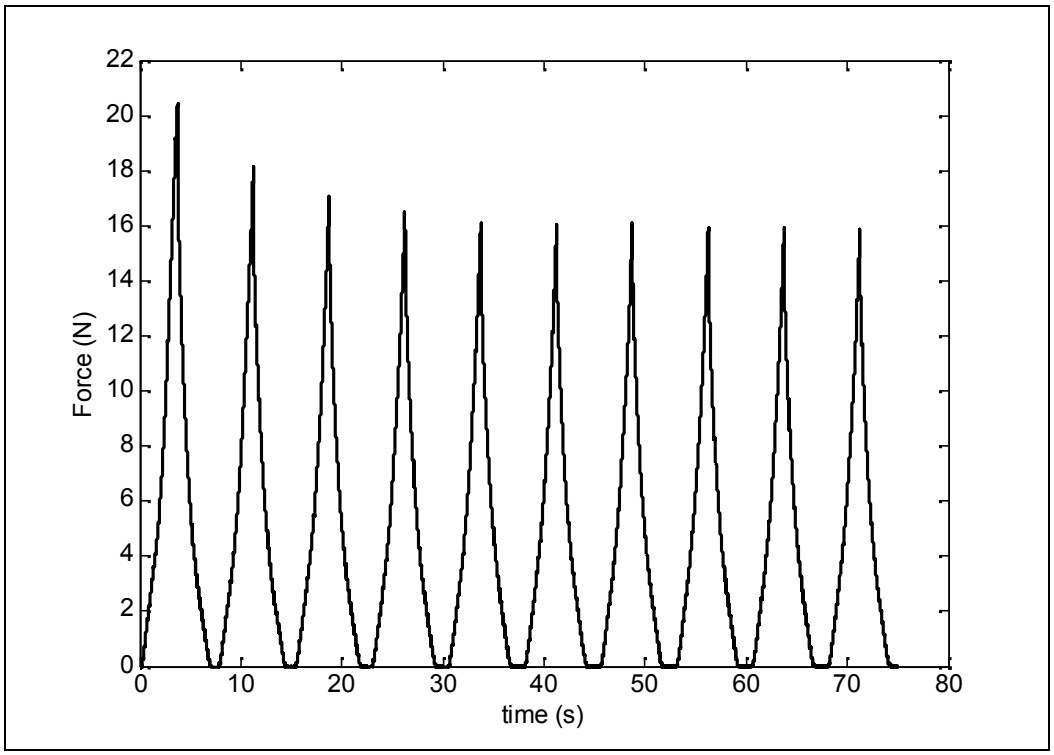

Figure 4.3 Preconditioning effect observed in the cyclic loading test, conducted for 4 mm/s motor speed and 14 mm displacement

In the force – displacement curves on the other hand, the situation was encountered was somewhat different. Therefore, discussing initially, the general properties of the force – displacement data will help for a better understanding of the subject matter. Sample force - displacement curve obtained through the cyclic loading tests can be seen in Figure 4.4.

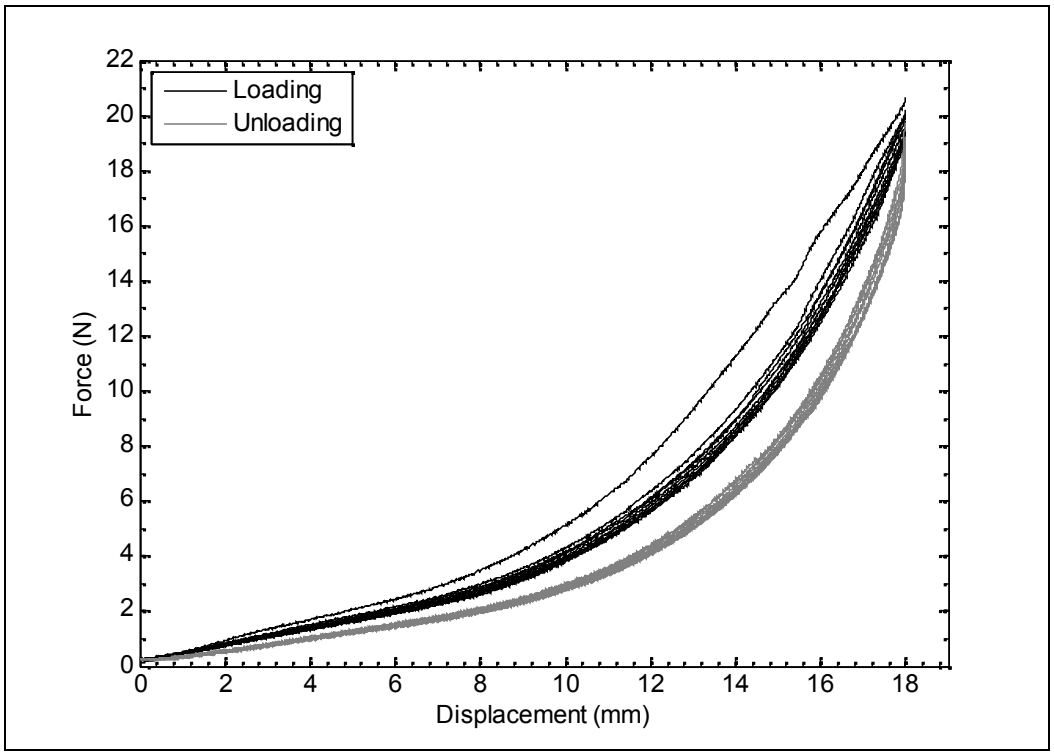

Figure 4.4 Displacement – force graph obtained for 4 mm/s motor speed and 18 mm displacement

In these curves, a cyclic graph was formed for each cycle. One side of this curve was formed for loading and the other for unloading. In between these two curves an area called hysteresis shows the mechanical energy loss during loading and unloading (Figure 4.5).

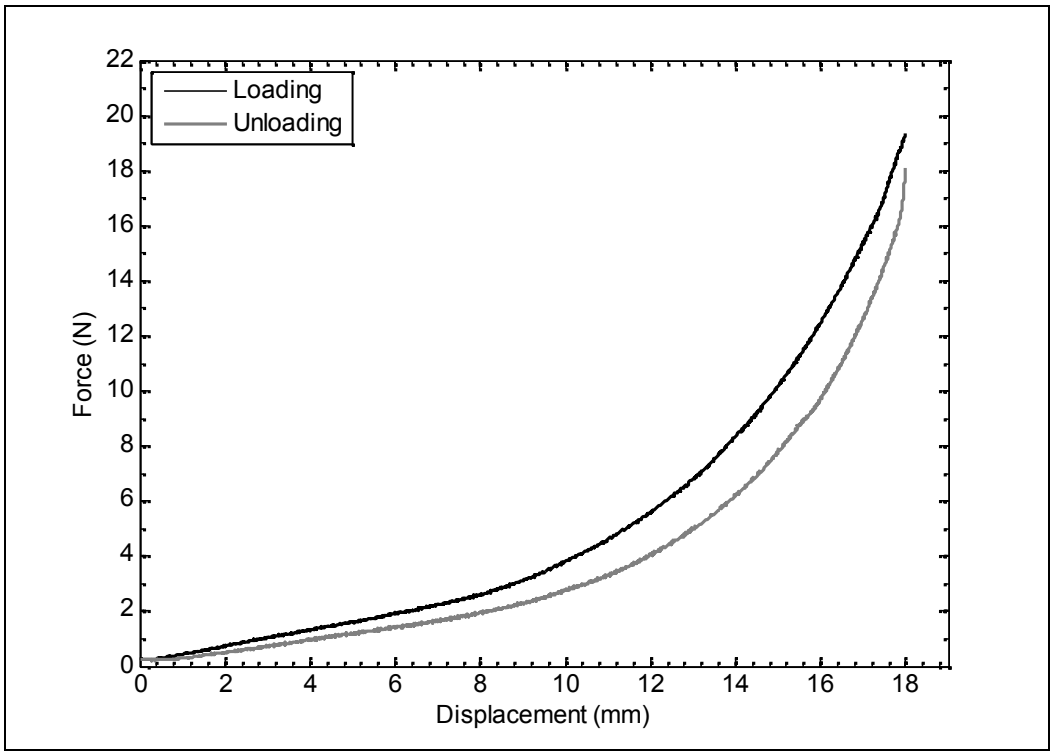

Figure 4.5 Loading and unloading curves pertinent to graph given in Figure 4.4

In these data, with increasing cycle loading and unloading sides progress in the directions shown in Figure 4.6, and towards the last cycles almost repeating cycles occur. This is a phenomena results from the preconditioning effect (Mullin's effect).

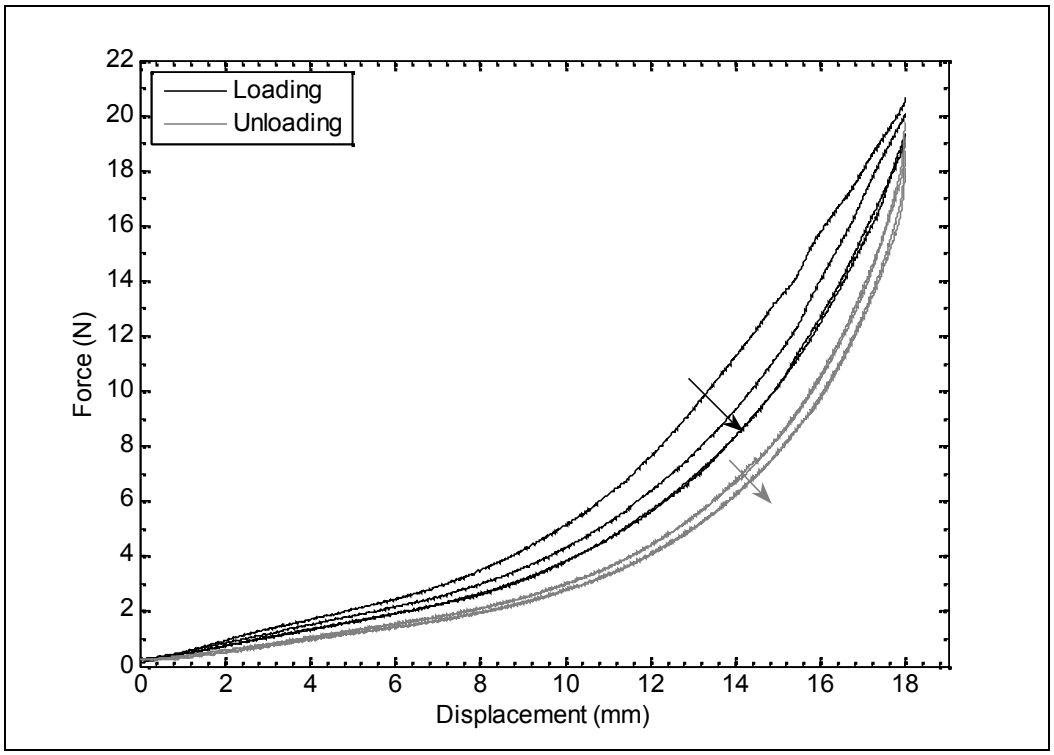

Figure 4.6 Preconditioning (Mullin's) effect observed in the Figure 4.3 data

Here, the point which must be considered is that, the meaning of the preconditioning effect observed in the force – time relation is different than the meaning of the preconditioning effect in the force – displacement curves. Preconditioning effect observed in the force – time relation is encountered in the last portion of the force – displacement curves shown in Figure 4.7.

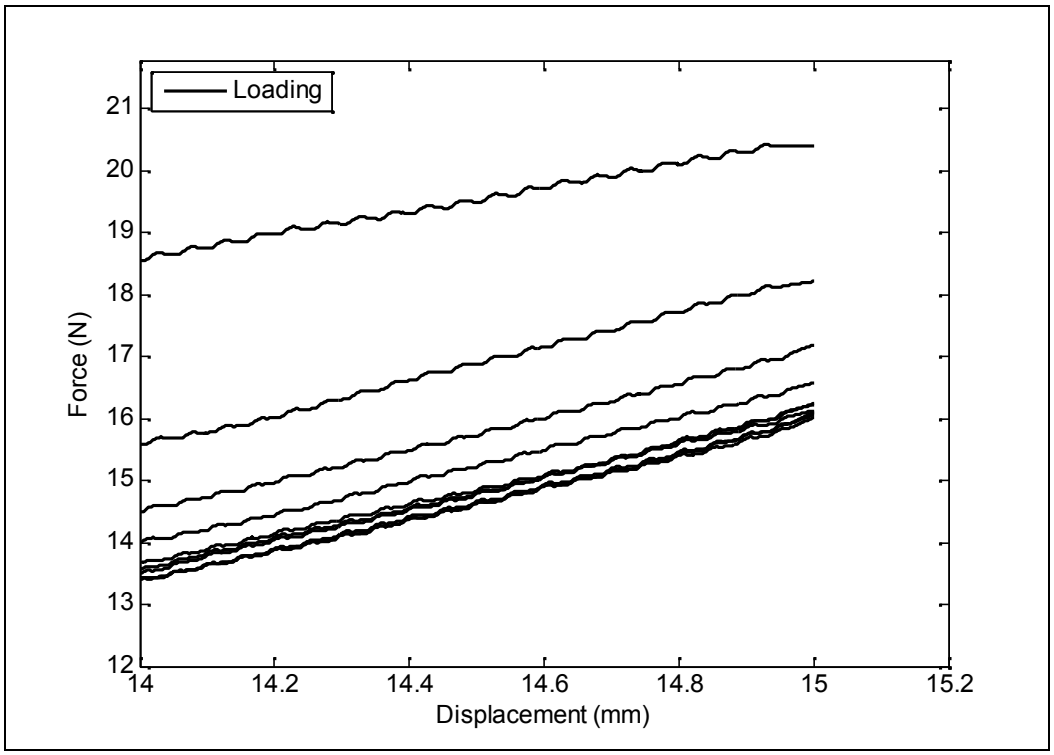

Figure 4.7 Displacement - force graph pertinent to test given in Figure 4.2. In the last portion of the graph, preconditioning effect attributed to force is observed

The phenomena here is the change in the maximum forces developing in each cycle. Thus, in the force – displacement curves, in addition to this phenomena, an areal change occurs and these areas represent the magnitude of hysteresis. The magnitude of the hysteresis area decreased with the increasing number of cycles and approached to a repeatable level (Figure 4.8).

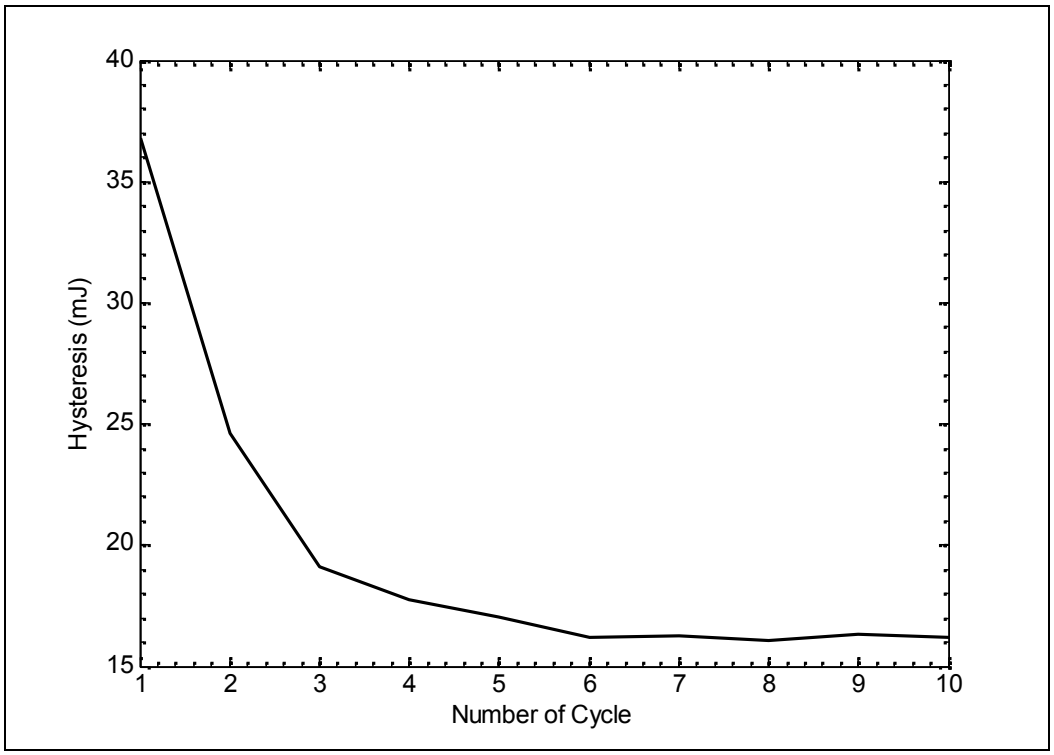

Figure 4.8 Change of the hysteresis magnitudes observed in Figure 4.4, with the increase in the progressing cycle

Critical and relatively important point here was that, this situation was encountered independent of the preconditioning effect observed in the force – time curves. That is to say, while no preconditioning effect was observed in the force – time curves, on hysteresis magnitude related preconditioning effect was encountered in the force – displacement curves (Figure 4.9 and 4.10).

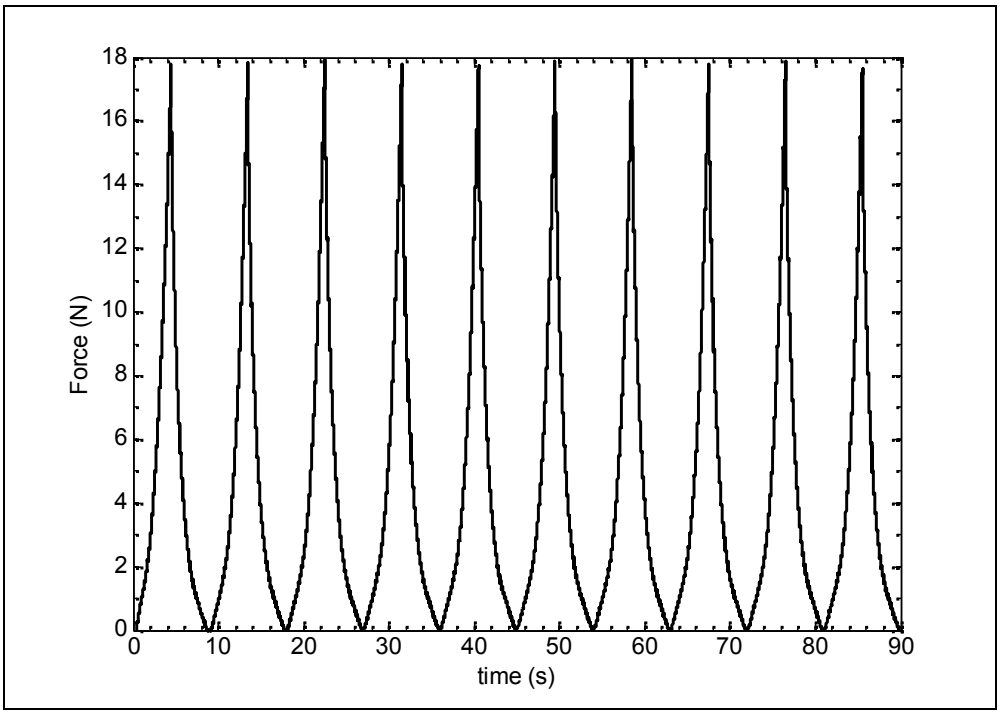

Figure 4.9 Cyclic loading test achieved for 4 mm/s motor speed and 18 mm displacement

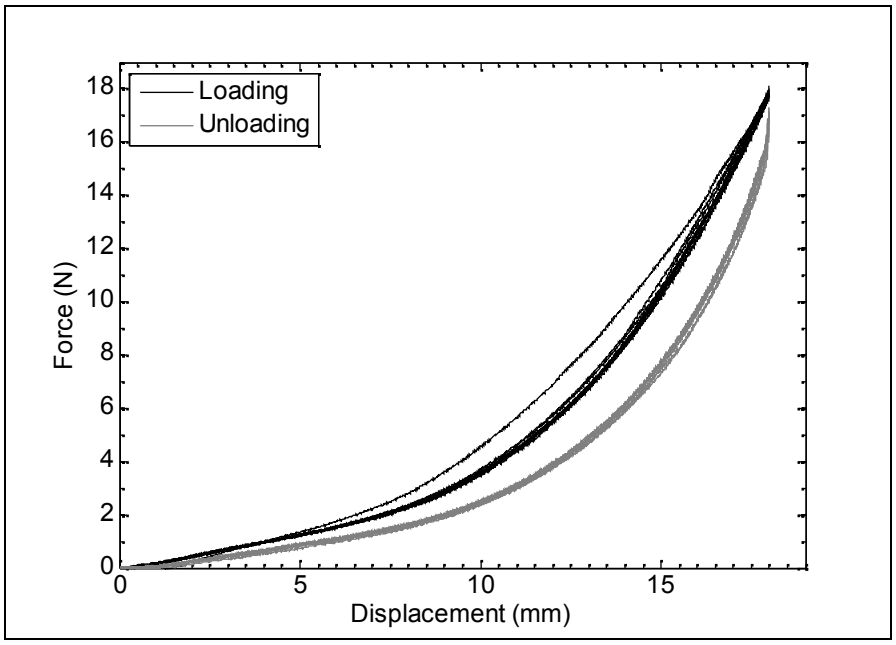

Figure 4.10 While no preconditioning effect was observed. In Figure 4.9**,** a preconditioning effect depending on the hysteresis areas in the force displacement graph was encountered

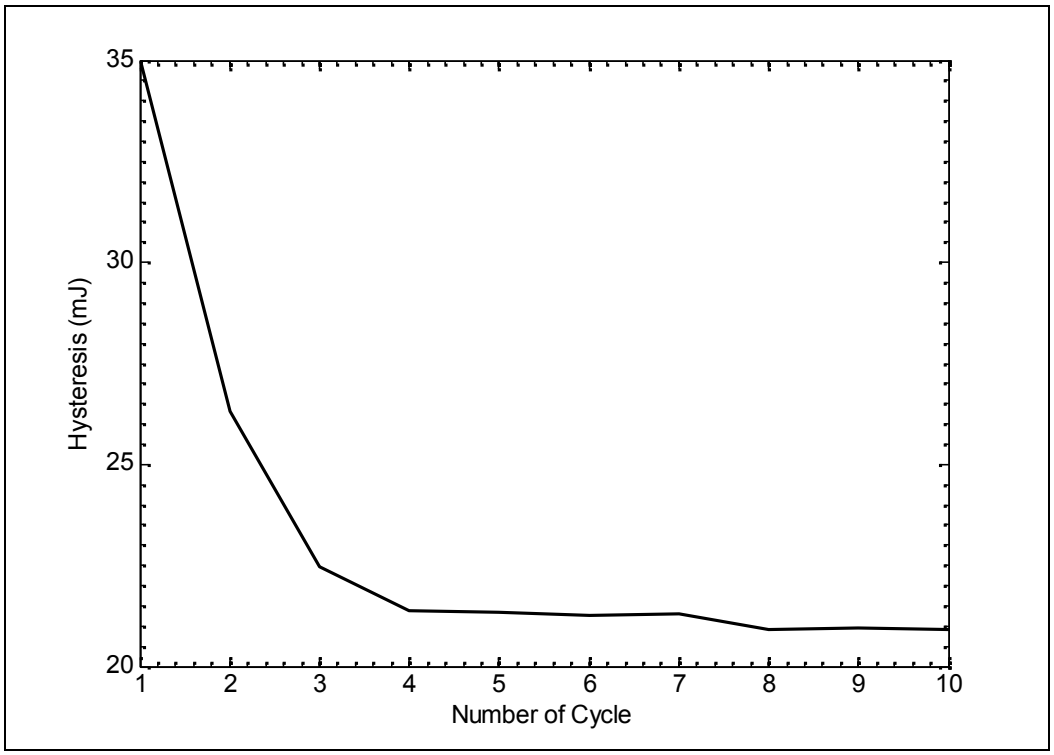

Figure 4.11 Change in the hysteresis magnitude with the progressing cycles (For the case in Figure 4.10)

The exceptional case where this phenomena would not be observed was, depending on the changes in the muscle tonus, in the progressive cycles of the cyclic loading data, forces displayed sudden increases. Hysteresis areas, when these force increases were encountered, also increased in amounts depending on the intensity of these force increases (Figure 4.12 and 4.13).

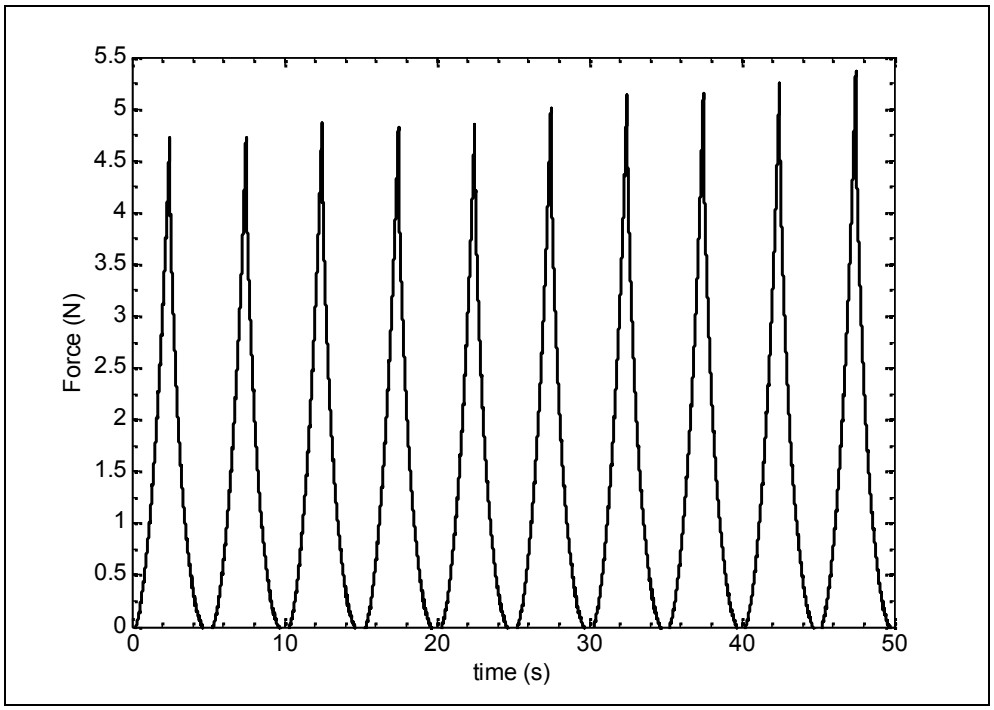

Figure 4.12 Force – time graph pertinent to cyclic loading test conducted for 20 mm displacement at 8 mm/s motor speed.

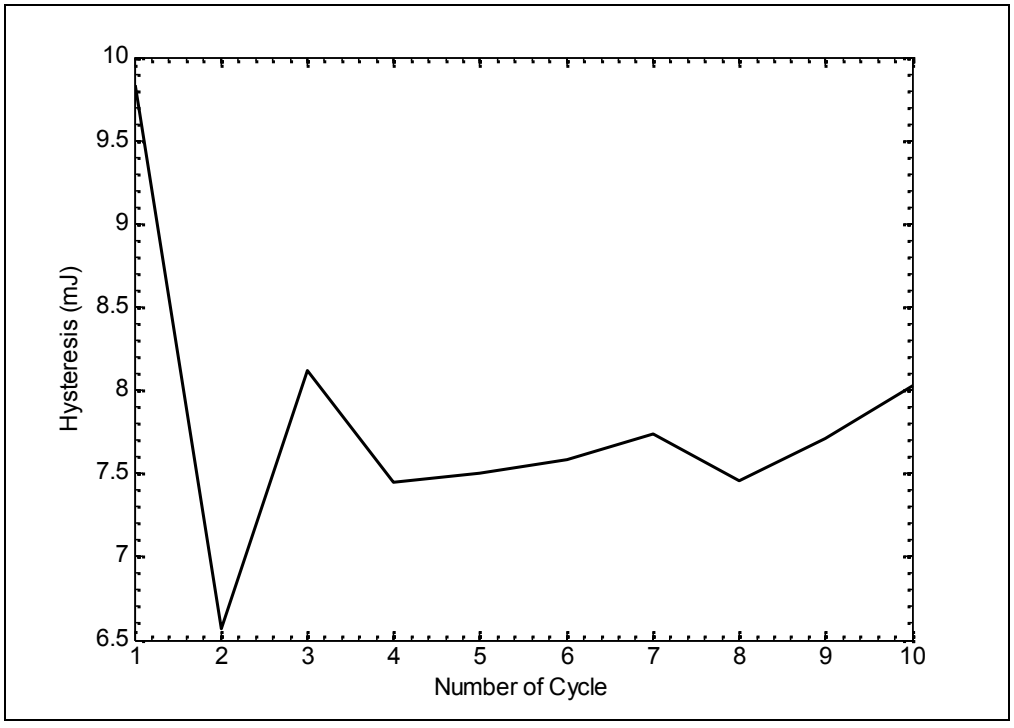

Figure 4.13 Change in the hysteresis magnitude with the progressing cycles

4.3.2 Investigation of Speed Dependency in the Cyclic Loading Tests

In the cyclic loading tests, one of the issues to be observed, is the influence of speed on the data obtained. Therefore at 25 mm displacement magnitude and 1, 2, 4 and 8 mm/s motor speeds tests were carried out on the forearm, using a 10 mm circular tip. Tests were carried out in three groups, no lag was given between the tests and group measurements. The reason for this was that, the aim of these observations was solely the investigation of the speed dependency. Therefore, it was not necessary that, the tissue would recover itself and display a preconditioning effect. Portions where the preconditioning effect presently takes place would also be discarded. These groups were set as,

- 1, 2, 4 and 8 mm/s speed orders
- 8, 4, 2 and 1 mm/s speed orders
- 8, 2, 4, 8, 4, 1, 4, 8, 2, 4, 8, 1 mm/s random speed orders

In the cyclic loading tests, 10 cycles were applied and in the tests no preconditioning effect was encountered. Random speeds in the 3rd group were determined by the software given in Appendix B. In these tests also, like in all other tests, maximum attention was spared for the preservation of arm position and muscle volume.

Scrutiny required for the comparison of the data was carried out as follows. Initially, maximum forces pertinent to each cycle were determined by the help of the software prepared (Appendix B). Later, average of these forces was determined and the forces showing maximum duration above and below these average values were eliminated. Following this, average of the remaining 8 values was taken and thus, the force value to be used in the test was determined. This process was repeated for all tests. Finally, motor speed graph, corresponding to these forces, were drawn (Appendix E). As can be noted from these figures, a speed related regular trend was not observable. It is anticipated that, this was due to small changes in the muscle tonus, occurring during tests. In

addition to that, unknown influences pertaining to the physiology at the test point generated from the livelihood of the tissue must also be taken into consideration.

At this point, it was decided that, the result to be considered by taking the average of the force data obtained for the same speeds, and the average force – motor speed graphs were drawn (Figure 4.14 and 4.15).

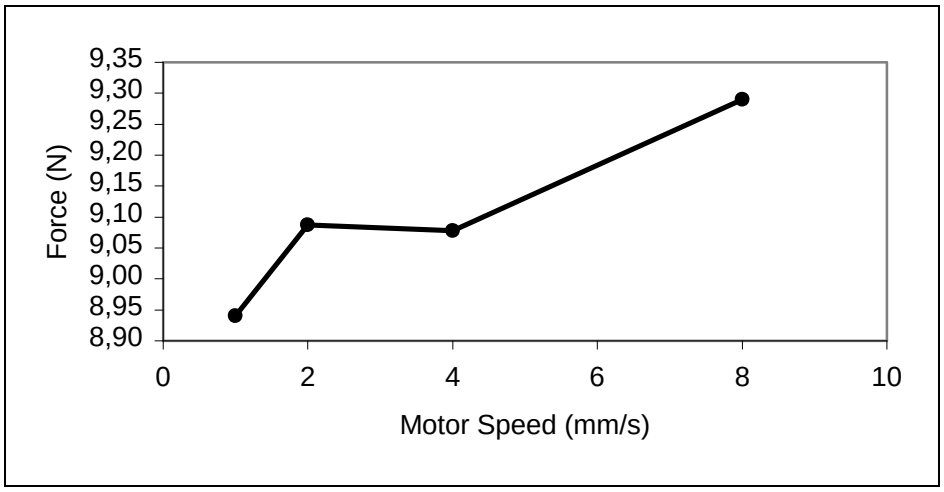

Figure 4.14 Force–motor speed graph for the first grub measurement (Appendix E)

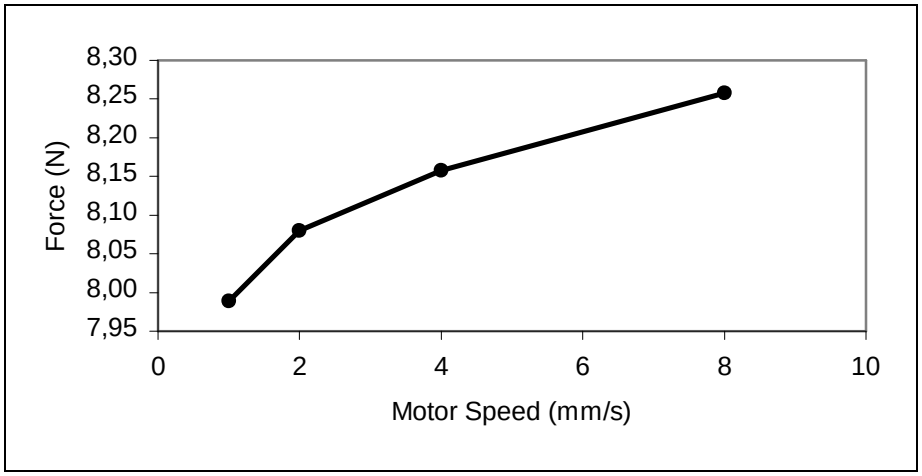

Figure 4.15 Force–motor speed graph for the 2nd grub measurement (Appendix E)

At the end, a graph almost linear and where the average forces increased with the speed was obtained. This is an expected situation for the viscoelastic materials. Yet, in the in-vivo tests, variable and hard to control behaviors of the soft biological tissues, as mentioned above, made the observation of this tendency extremely difficult if not impossible.

Another study, related to speed, was observation of the variation of hysteresis areas depending on the speed. Another important observation relevant to hysteresis area was that the extend of these areas increased almost linearly with the increase in speed magnitude. For this observation, hysteresis areas of the tests conducted the same day were calculated and their averages were taken. Later, these results corresponding to same speeds are grouped together, and their average was recalculated. Finally, observations presented in Figure 4.16 was obtained. As can be seen also from Figure 4.16, hysteresis magnitudes increases almost linearly with the increase in the speed. Observing such a behavior of tissue, that is increase in the hysteresis magnitude with increase in speed, is an important conclusion.

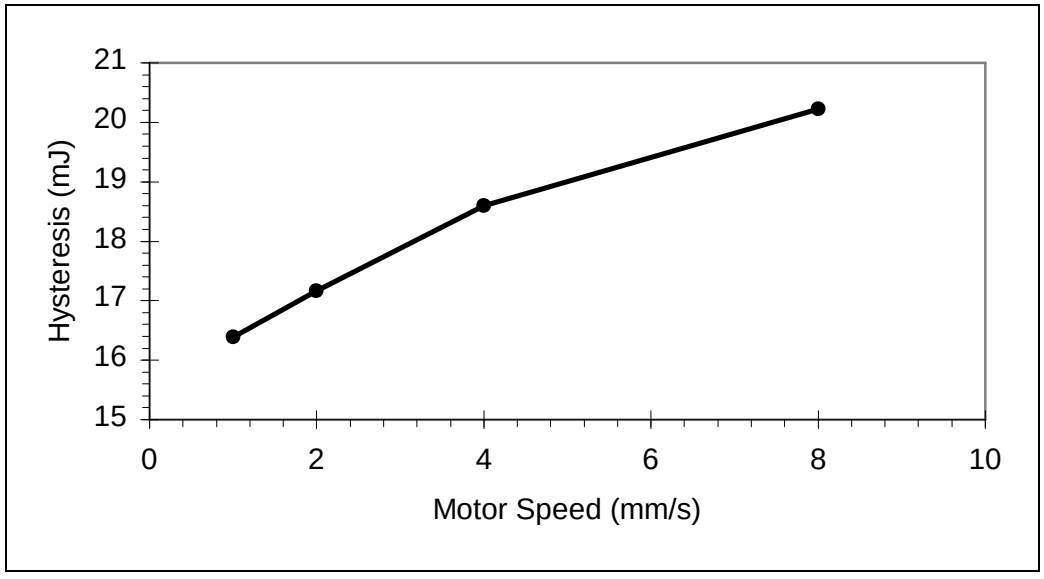

Figure 4.16 Hysteresis - motor speed graph

In great many number of studies carried out, it is concluded that, hysteresis loops are either independent or nearly independent from the strain rates (Rubin and Bodner, 2002). Common point of these studies are that, as reference, they take the Fung's studies (Fung, 1993). In Zhang et al., (2007) study, which is one of these studies, it is stated that, some biological materials may display rate – sensitive behavior (Kiss et al., 2004). Yet, in these studies where the hysteresis cycles are said to be independent of the strain rate, nothing is mentioned or no result is presented with regard to the hysteresis magnitudes. Therefore, referring these studies, it is not possible to conclude anything about how the hysteresis magnitudes vary in relation to speed.

In this study, on the other hand, it was observed that, hysteresis magnitude rises almost proportionally with rising speed (Figure 4.16, Appendix G). Here, the important point is that, hysteresis magnitude increased independently from the force variations observed in relation to the speed. That is, for instance, even if the reaction force showed a trend of decrease with increasing speed, hysteresis still got larger (Appendix G). This, in fact, is an important conclusion. Particularly, when in-vivo tests were being conducted, difficulty of preserving the tissue tonus and the consequences of this were discussed. Therefore, to have a clear observation or to draw a firm conclusion with regard to the mode of responses of the tissue under different speeds, was not feasible.

In conclusion, as in the preconditioning effect observations, indentation speed studies made by using the hysteresis data, give us much clearer information about the soft biological tissues. The hysteresis magnitudes obtained by using the force – displacement data were influenced much less than the problems such as the preservation of the muscle tonus which is in fact a substantial problem encountered in the in-vivo tests. Therefore, especially in the in-vivo studies, utilizing the results obtained by using hysteresis data, in the advanced applications such as various modelling and computer simulations, will assure much more dependable and realistic outcomes.

4.3.3 Causes of Force Decrease During Transition from Loading to Unloading, in the Cyclic Loading Tests

In the cyclic loading tests, at the transition from loading to unloading a fall in the force is encountered. This fall was observed clearly in the tests conducted at 8 mm/s speed (Figure 4.17).

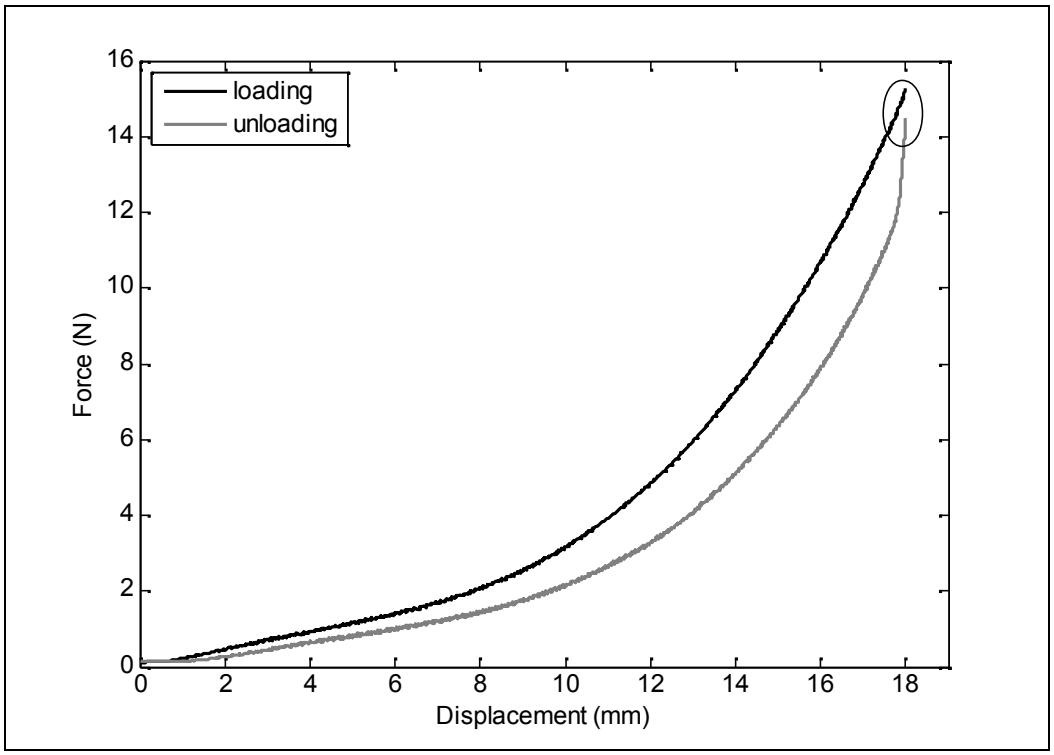

Figure 4.17 Inability of the tissue to keep continuously in touch with the tip, during the cyclic loading test at 8 mm/s

It was therefore has been a matter of consideration and solution to this problem was tried to be sought. Yet, despite all efforts, a clear result was not attained.
In the further stages of the study, during the literature search, a conclusion of Zheng et al., 1999 was encountered. In this study where Zheng has carried out tests on the forearm, he has noted that, in the cyclic loading tests realized at 7.5 mm/s speed, in the unloading phase, skin surface could not follow the indenter

tip (Zheng et al., 1999). It was therefore contemplated that, in our tests also, such a contact loss phenomena took place and it was decided to make studies on this matter to inquire its relevancy. At this point, force falls occurring in the speeds at which the cyclic loading tests had been conducted, were overviewed. To this end, cyclic loading tests carried out successively in a day were brought to scrutiny. These tests comprise of 10 cycles at 1, 2, 4 and 8 mm/s speeds. For the observation, force differences taking place in each cycle were computed and their average was taken. This procedure was repeated for all speeds and for the sake of ease, results were obtained by using a software (Appendix B). Finally, graph in Figure 4.18 was obtained.

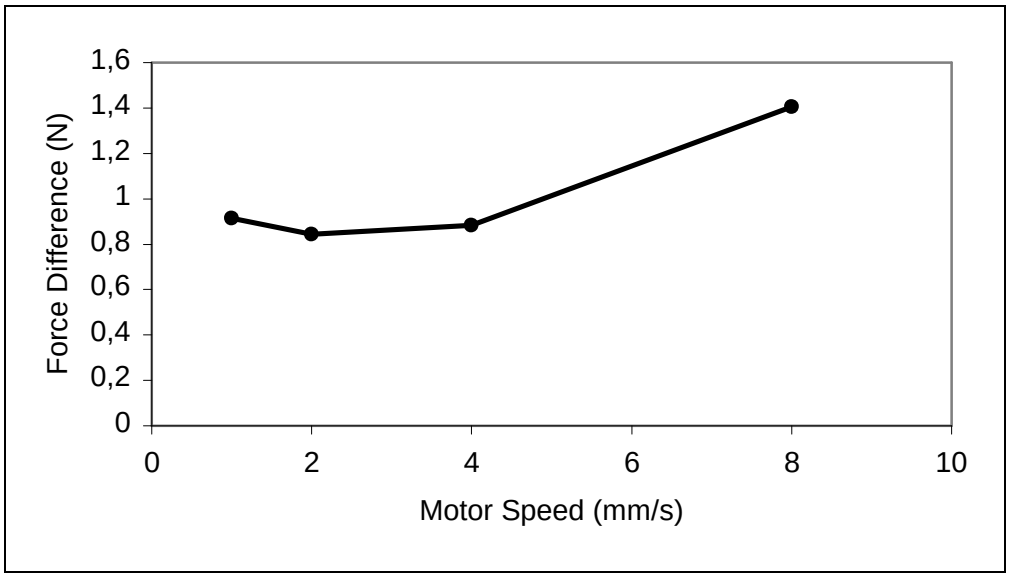

Figure 4.18 Particularly at 8 mm/s speed, tissue can not keep its contact with the indenter tip for a longer duration

As seen from the graph, almost same amount of force difference occurred in 1, 2 and 4 mm/s speeds. At 8 mm/s speed, on the other hand, a sudden increase took place. Thus, a result supporting the matter described by Zheng was evident. Yet, normally in tests conducted at speeds other than 8 mm/s, force difference was not notable in the end graphs and consequence a certain level of force

differentiation was observed with this study. This phenomena, at first instance, was interpreted as the no conformance of the skin surface with the indenter tip. Yet, the consultation on this matter, revealed the possibility that this could have been originated from a different reason. In the cyclic loading tests, indenter tip stops for a very short time during the transition from loading to unloading phase. Thus, at this instant, it is anticipated that, tissue displays the same behavior as in the relaxation tests and that, it relaxes at a certain extent. In order to inquire this conclusion, 9 successive tests comprising 1 cycles each, within the interval of 0.5 and 8 mm/s speeds were carried out. For each speed, force differences were calculated and the graph shown in Figure 4.19 was obtained.

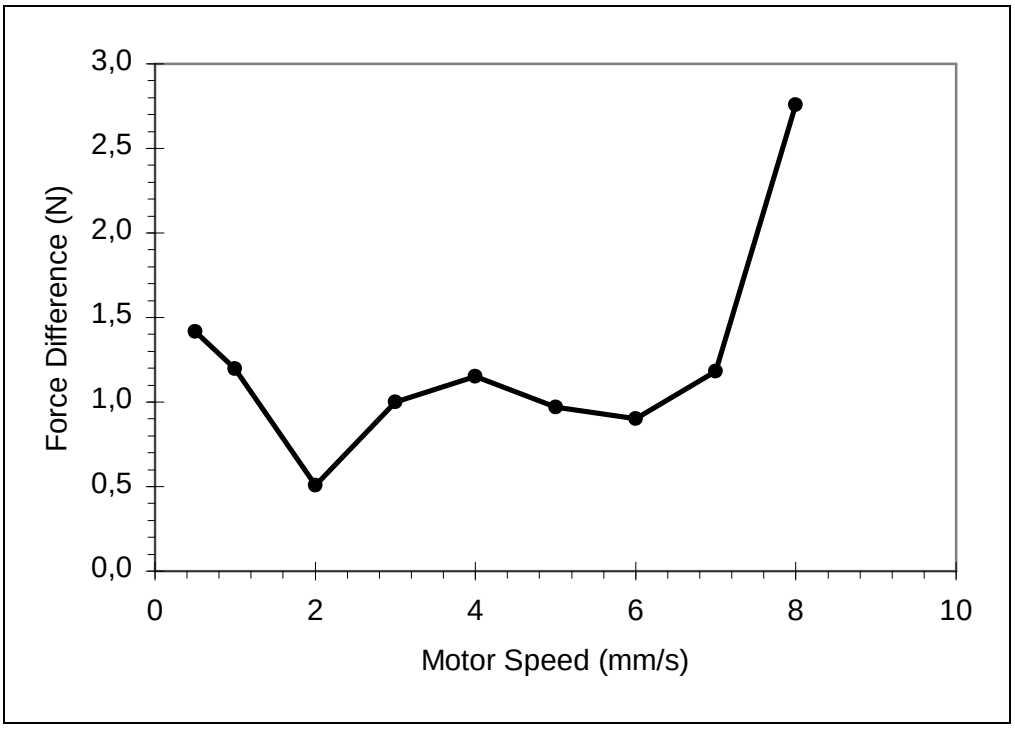

Figure 4.19 Motor speed versus force difference graph

Consequently, a case similar to that in Figure 4.18 was revealed. That is, force differences at 0.5 mm/s to 7 mm/s speed range were almost same but sudden increase in 8 mm/s speed was encountered. Therefore, it is hard to state that, a

force difference occurs only due to speed. Because, force difference occurring in a very low speed of 0.5 mm/s is same with that difference occurring in 7 mm/s speed. If the force difference would originate from speed, force difference should have increased with the increased speed. Furthermore, force difference should have been near to zero at such a low speed of gained weight and proved to be relevant. In other words, in the cyclic loading tests, at the instant of passage from loading to unloading an instantaneous stopping occurred, and in consequence, the tissue relaxed. This in turn, caused the occurrence force difference. It was understood that, additionally, standing from 8 mm/s speed on, at the verge of transition to reserve movement, surface of the tissue could not follow the indenter tip for a small duration and an additional force built up would take place.

4.4 Relaxation Tests

In the relaxation tests, indenter tip indents the tissue at the desired speed and displacement, and when the desired displacement is reached, displacement is kept constant for desired duration of time. During the whole process the tissue behavior was observed. Therefore, in relaxation tests, displacement, motor speed and relaxation time are the parameters to be entered in the interface. Tests were carried out in displacement amounts varying in between 10 to 25 mm interval and 1, 2, 4 and 8 mm/s indenter speeds. In most of the tests, 120 seconds were selected as relaxation time. The reason for this preference was that, 120 seconds rendered to be sufficient to observe the relaxation behavior of tissue and also the discomfort and uneasiness displayed by the individual during long waiting times were avoided.

In the relaxation tests, with the holding the indenter tip, a considerable fall in the reactionary force displayed by the tissue was observed, and with the progressing time force data approached to an equilibrium position (Figure 4.20).

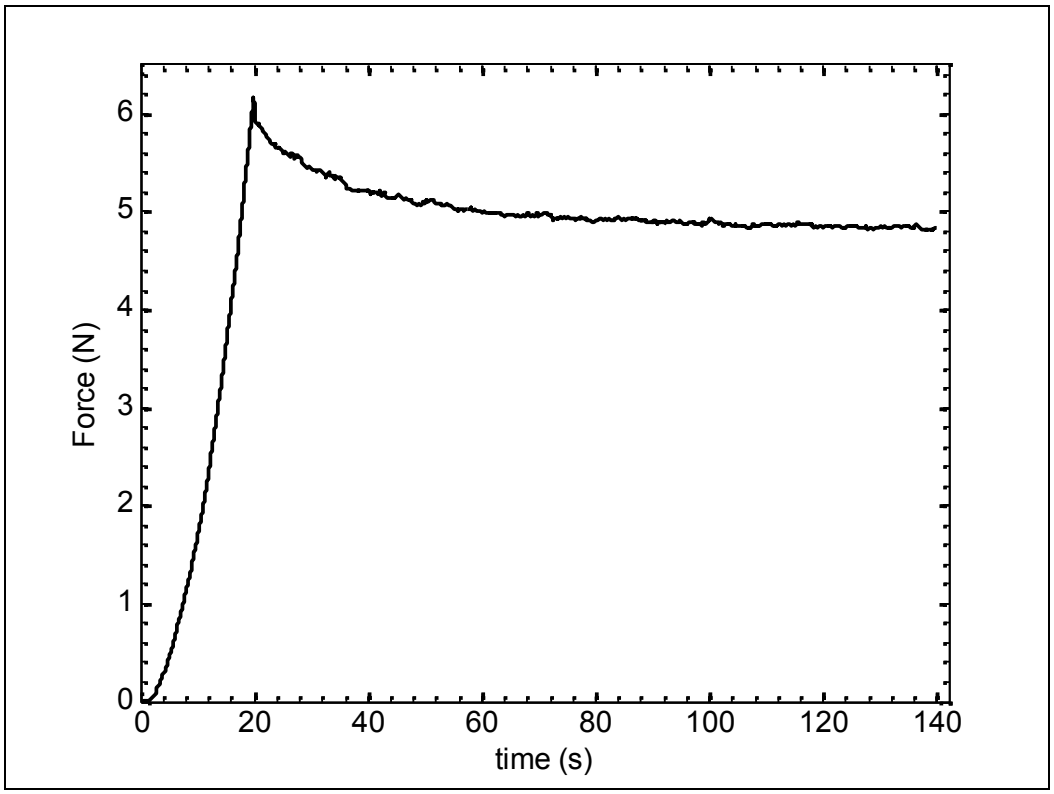

Figure 4.20 Relaxation test conducted for 1 mm/s motor speed, 20 mm displacement and 120 second relaxation duration

Although observation in the relaxation tests could have been done at 1 mm/s, in order to observe the influence of speed on the relaxation data, observations were carried out at four different speeds, namely 1, 2, 4 and, 8 mm/s.

Yet, at the end of the tests carried out, any trend attributable to speed could not been observed (Section 4.6.3.1). It is believed that, this was due to the same reasons faced in the cyclic loading. That is, variations in the muscle tonus in the course of the tests, small variations at the point subjected to test, or the reasons attributable to tissue physiology might have contributed to this conclusion. Yet, since speed dependent behaviors of the soft biological tissues were already determined by using the hysteresis data, they were not considered to be overemphasized.

4.4.1 Influence of Pulse and Breathing on the Relaxation Test Results

In some relaxation test results, unexpectedly unclean data were encountered (Figure 4.21 and 4.22). Although the causes were guessable, in order to firmly determine the source of this, some studies were carried out.

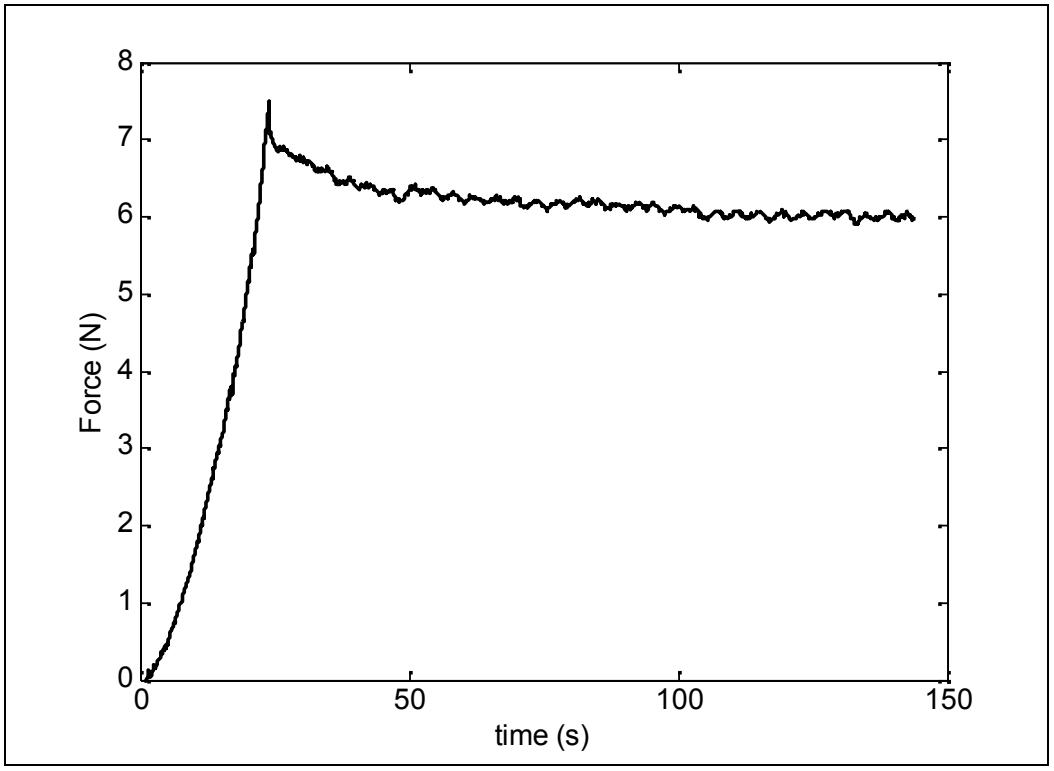

Figure 4.21 Unclean data observed at relaxation tests

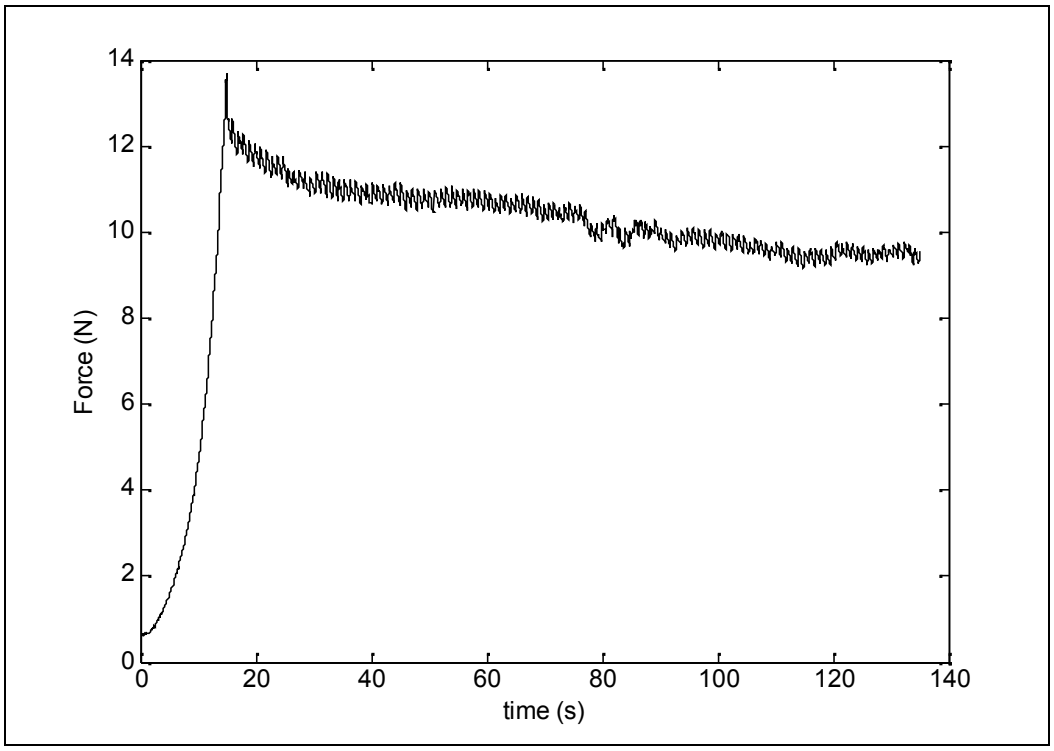

Figure 4.22 Unclean data observed at relaxation tests

First point determined for the unclean data was that the characteristics displayed were same. It was therefore understood that, the uncleanness originated from a certain source. It was anticipated that, basically two sources may have caused uncleanness. These are,

- Noise which may be attributed to the electronic fittings of the test device, and,
- Various movements of the test specimen or the physiology of the tested point

At this stage, it was decided to inquire whether a problem originating from the test system existed or not. Reason for that decision was the possibility of anticipating and investigating numerous causes attributable to the tissue and the test specimen. In case this caused by a device originated noise a considerable

time would have been lost. Even if logical finds, showing that, cause originated from tissue or tested individual, were encountered, without conducting an investigation with regard to the test system, a clear statement would not have been possibly made because, the test data has a noise originated format. In this context, in order to determine whether a test device originated noise is prevalent or not, it was decided to carry out a test on sponge. In this way, it was aimed that, no effect originating from the tested individual or tissue would be reflected on the test data, and that, any noise originating from the test device would be detected without interference. More than 10 tests were carried out on the sponge at speed of the relaxation tests speeds and the characteristic data given in Figure 4.23 were obtained.

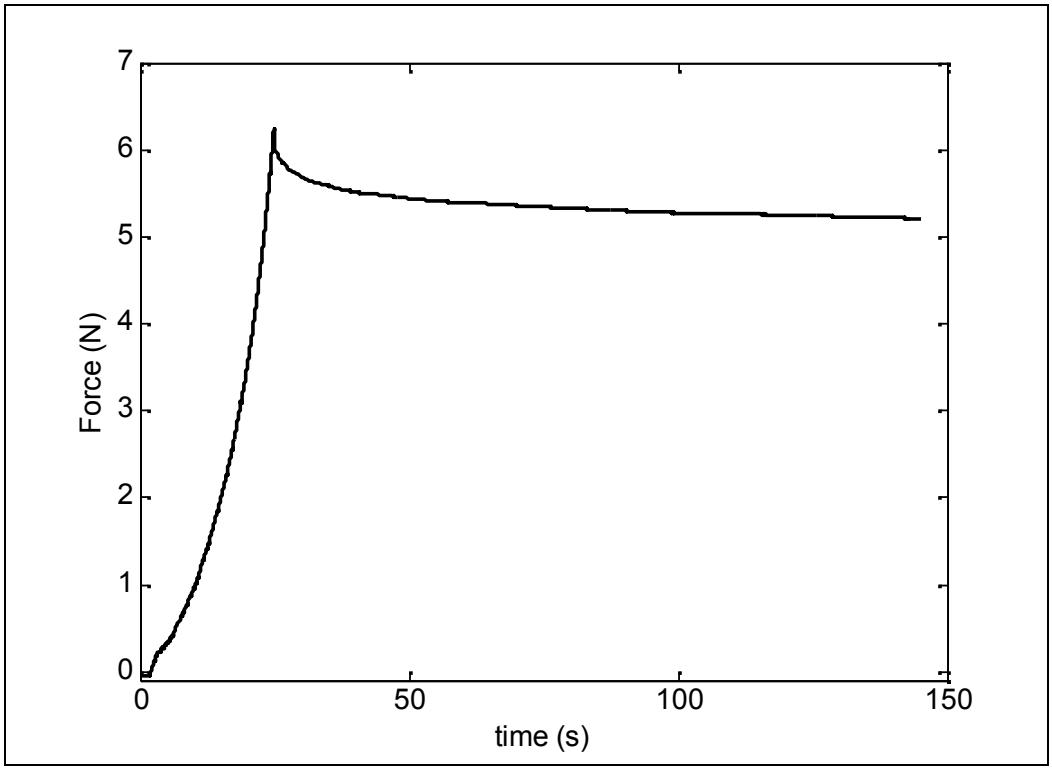

Figure 4.23 Result of the relaxation test carried out on sponge.

As seen from the Figure 4.23, no noise attributable to the test device was detected and very clean graphs were obtained. At this point, it was anticipated that, the prevalent condition of the data could be attributed to either the tested individual or the tissue physiology.

In the case of Figure 4.21, in a certain period, fluctuations in the relaxation data were observed. In Figure 4.22, on the other hand, fluctuations were encountered in even smaller periods.

Relaxation tests are greatly influenced by the muscle movements. Therefore, tests were carried out with attention and in a noiseless media. During the tests carried out to determine the cause of fluctuations in data, same attention was spared. Therefore, the movements in the body of the individual originating from his breathing were noted and it was anticipated that, the source of fluctuations in Figure 4.21 was suspected to be these movements. At this point, it was decided to compare the number of fluctuations observed throughout the relaxation test and the number of inhaling and exhaling.

It was observed that the number of breathing was in harmony with the fluctuations (Figure 4.24). Also, it was observed that fluctuations increased depending on the breathing intensity (Figure 4.25). Consequently, it was understood that the observation seen in Figure 4.21 was caused by breathing.

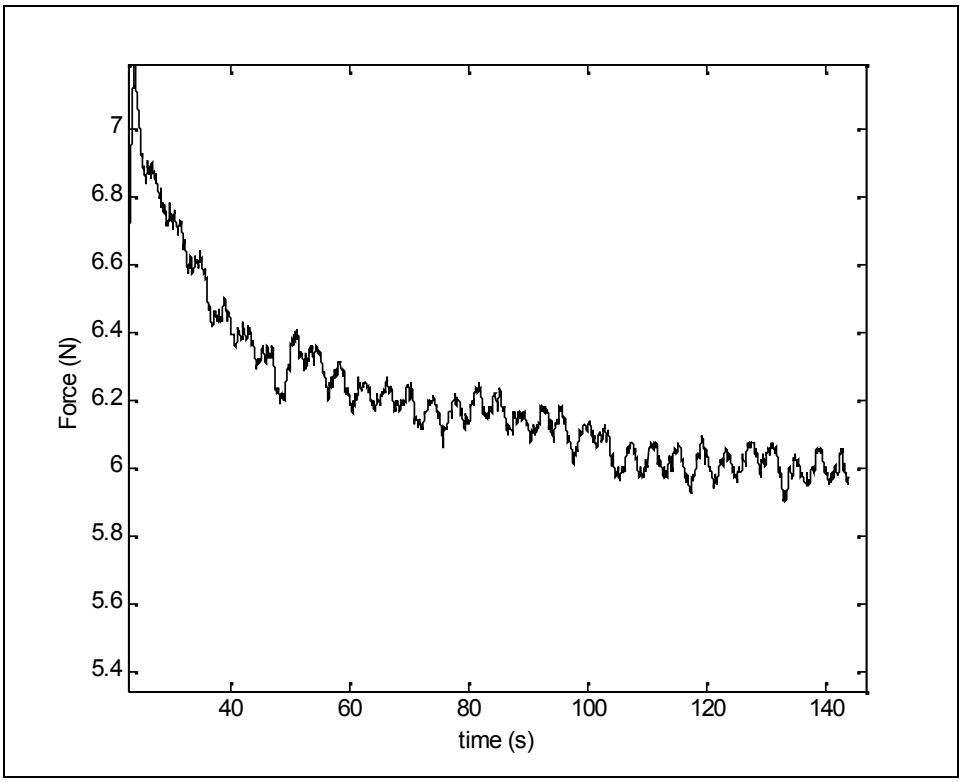

Figure 4.24 Detail of the test result given in the Figure 4.21. The number of breathings during the experiment is 31 and it shows compatibility with the fluctuation in the data

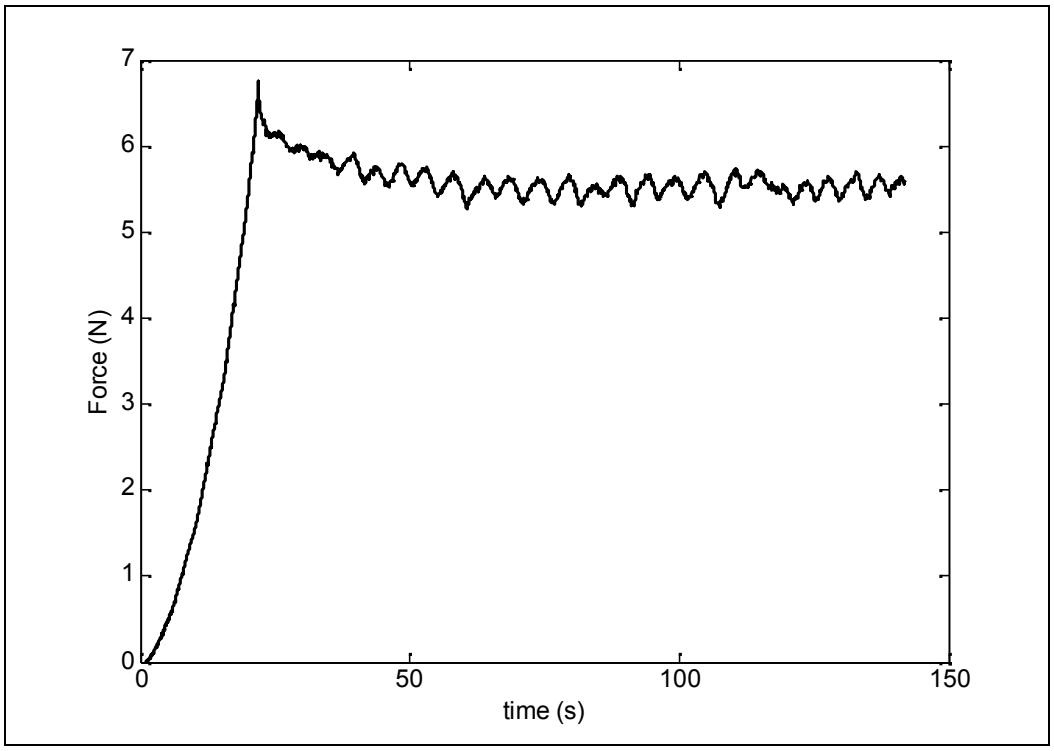

Figure 4.25 Increased fluctuation intensity with increasing breath

In the case of Figure 4.22, as mentioned before, spreading of fluctuations to smaller periods, were observed. This type of fluctuations could have been origined from pulse, as had been anticipated in the previous studies (Tönük, 2004). It was therefore decided to investigate whether the status of this data originated from pulse or not. In a healthy individual, pulse varies within the range of 60 to 100 (Fox, 1992). In order to make a comparison in this context, fluctuations in data within a duration of 10 seconds were counted and noted as values varying between 10 and 12 (Figure 4.26). Thus, the number of fluctuations taking place in a minute was fixed as 60 – 72 and it was understood that, the situation of the data originated from pulse. It was then understood that, the indenter tip coincided with an artery and therefore the pulse was reflected on the data collected.

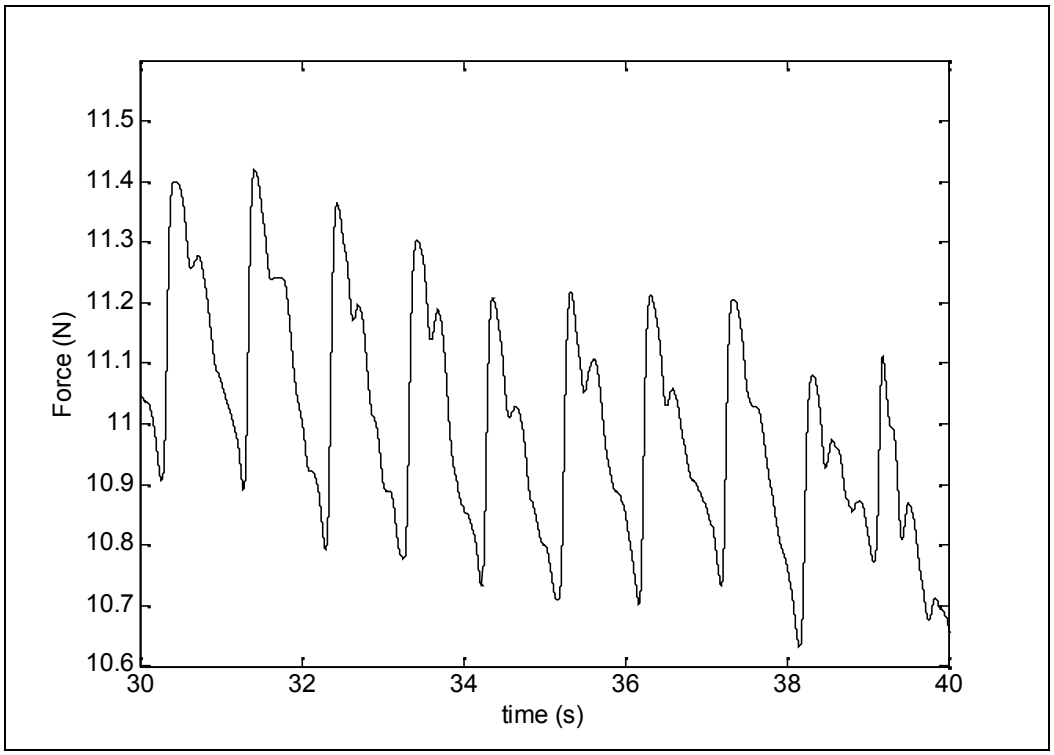

Figure 4.26 Fluctuations caused by the pulse.

4.5 Creep Tests

In the creep tests, initially, target force which will be applied to the tissue, is determined. With the start of the test, indenter tip is loaded to the tissue at entered motor speed, until this target force is reached. With reaching the target force, with small forward and backward movements of the tip achieved by the proportional close loop control cycle, this target force is maintained throughout the desired creep duration. Simultaneously, the displacement of the tissue under constant force is measured. The parameters which need to be entered through the interface, prior to tests are target force, creep duration, motor speed during initial indentation and the gain of the proportional closed loop control system. Selecting gain values close to 0.25 gave proper results. Due to capacity of the computer used, creep duration is taken 120 seconds at the most. Yet, in order to the creep characteristic of the tissue, this duration renders to be sufficient. Motor speed, due to the limitations pertinent to software and equipment (See Chapter 3.6) was

taken as 1 mm/s. Therefore, for the creep tests, tests could not have been carried out at different initial loading speeds.

At the end of the creep tests two different groups of data are obtained. These are the force – time (Figure 4.27) and displacement – time (Figure 4.28) graphs.

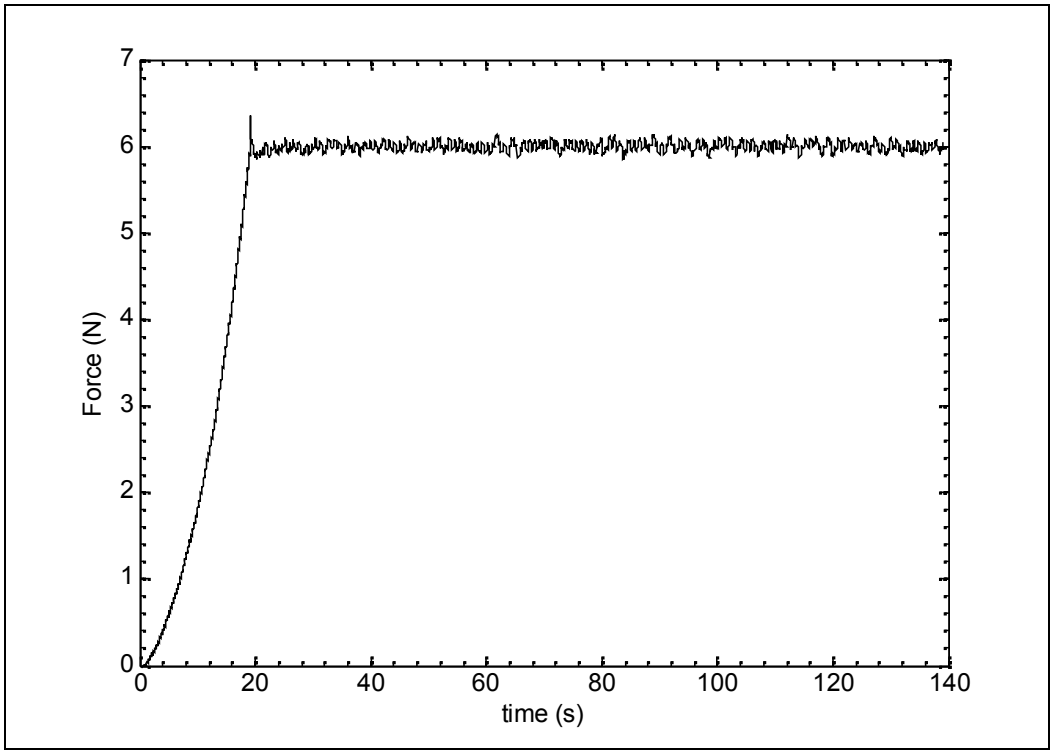

Figure 4.27 Force – time graph obtained for 1 mm/s motor speed, 120 second creep duration and 6 N target force. As seen, force gets fixed around 6N.

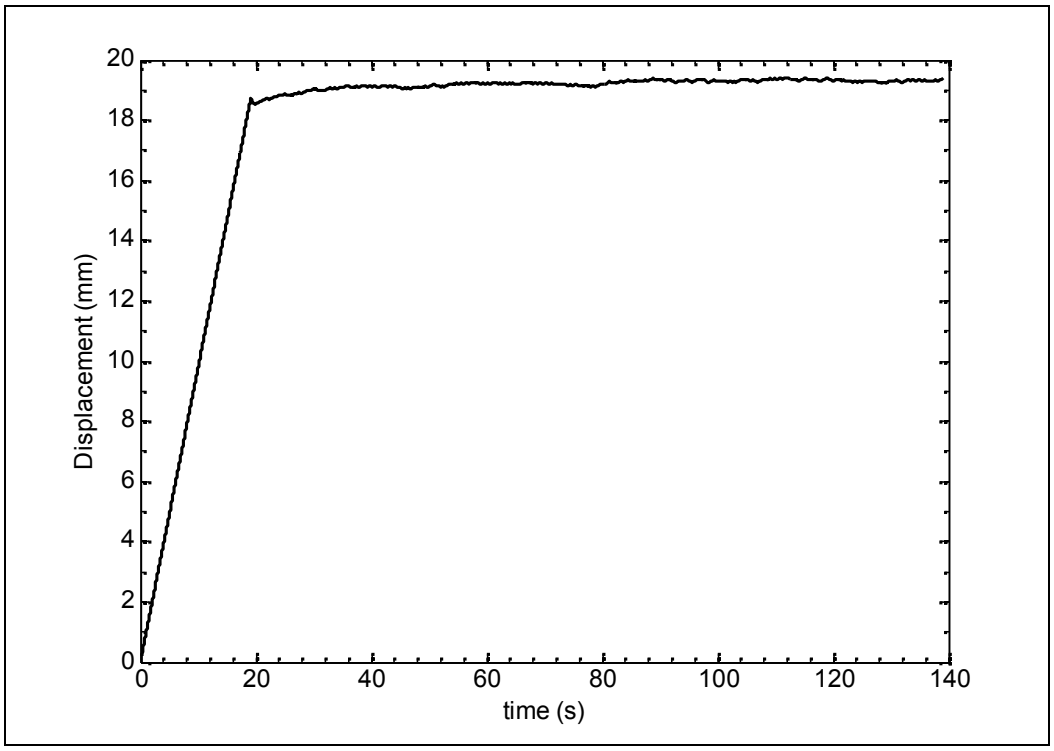

Figure 4.28 Displacement – time graph obtained in the test given in Figure 3.20.

Force – time graphs constitutes to be a control data for the target force. The more important data which needs to be evaluated is the displacement – time graph. Creep behavior is also observed through this graph. Starting with the attainment of the target force, the data group formed throughout the creep duration yields the creep behavior of the tissue (Figure 4.29). Thus, by using this data, various constants needed to be used in the subsequent computer simulations, are determined (Chapter 4.6).

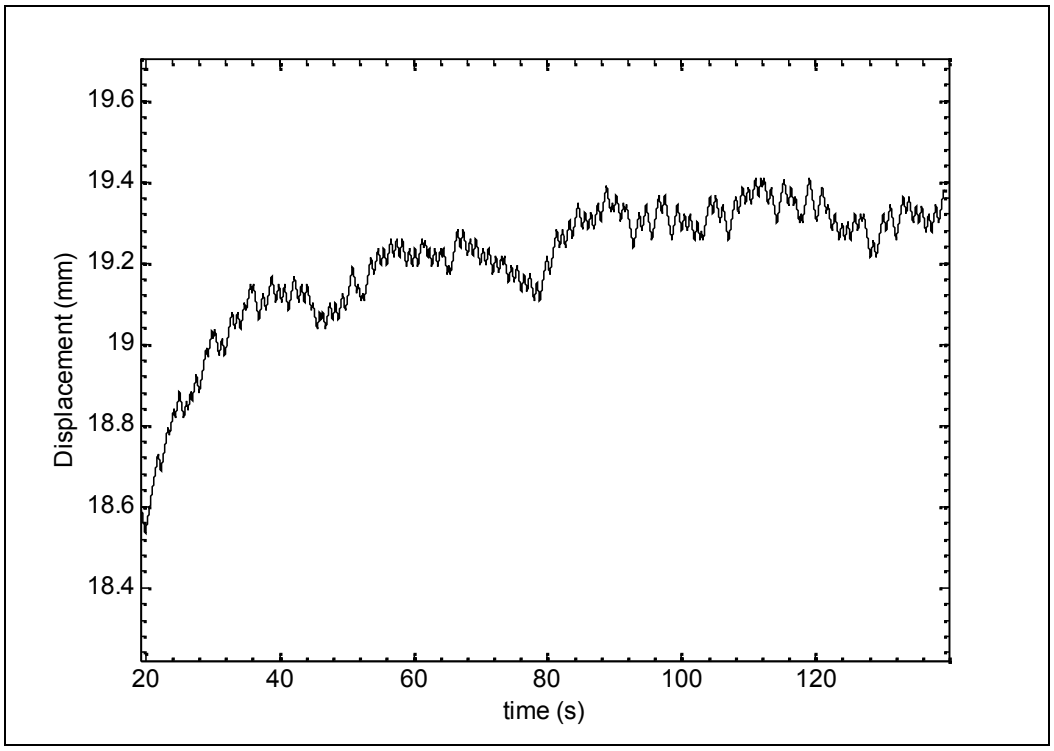

Figure 4.29 Behavior of the tissue during the creep duration

As in the cyclic loading and relaxation tests, in the creep tests also, data reflecting foreseeable and known trends were not obtainable. As mentioned quiet frequently, this is a consequence of carrying out the tests in-vivo.

4.6 Constitutive Equations and Curve Fitting Functions for the Relaxation and Creep Data and the Determination of the Related Constants

From past to date, great many numbers of constitutive equations have been tested for the simulation of the mechanical behaviors displayed by the soft biological tissues. Majority of these models which are important for their utilization in the computer simulations bear certain limitations.

In a proper constitutive equation, following points are to be valid.

1. It must be predictive, that is, the material model determined by one test protocol must predict all (if not possible, a wide range of) different test results and mechanical situations.

2. Parameters of the model in concern, must have physical meanings and should be determined by simple experiments if possible.

Constitutive equations used, contain various constants. By changing these constants, test data giving the characteristics of the soft biological tissues are worked out through the mathematical models. Thus, it is very important that, for understanding and explanation of the behaviors of the soft biological tissues, these constants should have physical meanings. Explaining this point by a simple example will make it more comprehensible. For the modeling the linear elastic materials consider the one-dimensional Hooke's Law. This law is expressed by the following equation;

$\sigma = E\varepsilon$ ..... (4.1)

where;

σ = Stress

ε = Strain

E= Modulus of elasticity

According to this equation, stress is obtained as a linear function of strain and a parameter called the modulus of elasticity. That is, this parameter reflects a unique feature of the elastic material observed. This feature is stiffness of a material. Every linear elastic material has unique modulus of elasticity value and while stiffer materials like steels take higher elasticity values, spongy materials take low values (Hibbeler, R. C, 1999).

Similarly, parameters of the constitutive equations used for the modelling of the soft biological tissues should contain a certain physical meaning and should make the behavior of the soft biological tissues more comprehensible if it is possible. In other words, these parameters should be interrelated to certain behaviors of the soft biological tissues.

4.6.1 Constitutive Equations Used for the Simulation of the Soft Biological Tissues

Mathematical models used in this study can be considered under three groups. These may be expressed as curve fitting equations, medium level constitutive equations and complex constitutive equations.

4.6.1.1 Equations Used for Curve Fitting

Curve fitting equations posses none of the qualities carried by a good mathematical model. Constants within these coefficients do not posses any physical meaning at all, and they are not appropriate for any predictions. Their modelling of the experimental data are not proper. Instead of modelling the soft biological tissues, these mathematical expressions are used to compare the experimental data obtained, and to make observations to diagnose the interrelations. In our study, in this context, two equations were used. First one of these equations is as follows,

$$F = at^{-b} \quad \text{.....(4.2)}$$

where,

F = Force,

t = time,

a & b = constants

With the help of this equation, only the relaxation of the soft biological tissues can be roughly fitted (Figure 4.30).

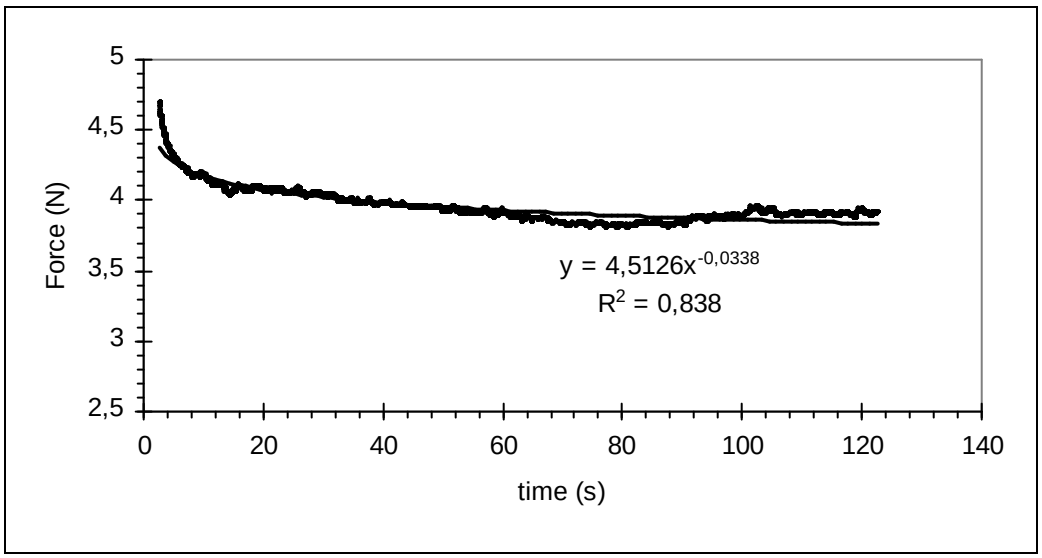

Figure 4.30 Curve fitting of test carried out for 8 mm/s motor speed, 25 mm displacement and 120 second relaxation period, by using the Equation 3.2

Second curve fitting equation is given below,

$$y = y_0\left(1 + at^{-b} + ct^{-d}\right) \quad \text{.....(4.3)}$$

where,

y = output data (force for relaxation, displacement for creep, force for preconditioning effect)

t = time

a, b, c, d = constants

With the help of Equation 4.3**,** relaxation, creep and preconditioning test results of the soft biological tissues can be fitted (Figure 4.31, 4.32, 4.33).

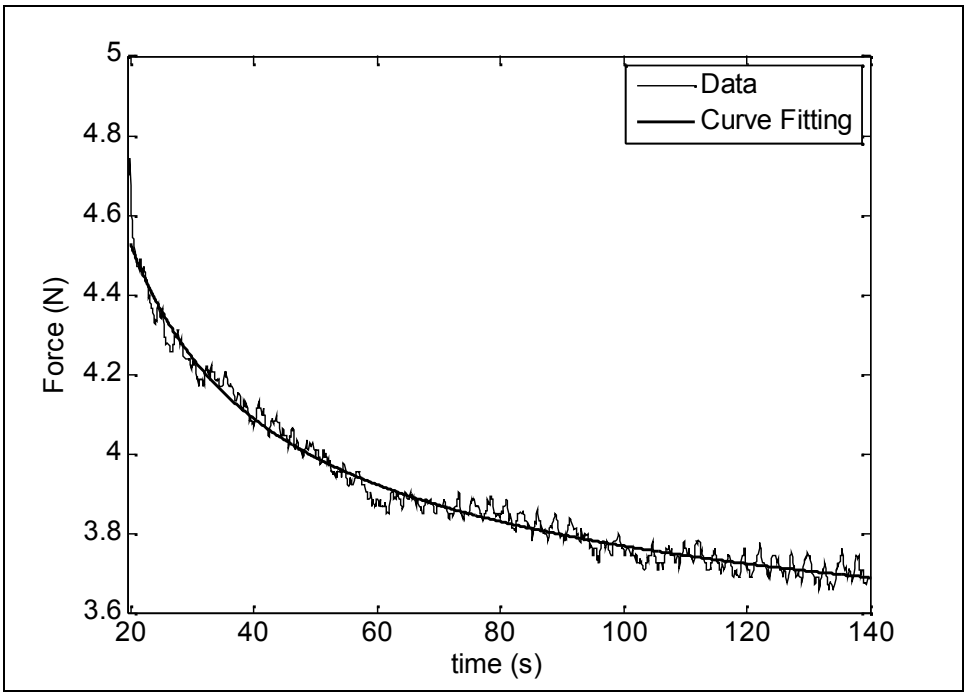

Figure 4.31 Curve fitting of graph obtained for 1 mm/s motor speed, 20 mm displacement and 120 second relaxation period by the help of Equation 3.3

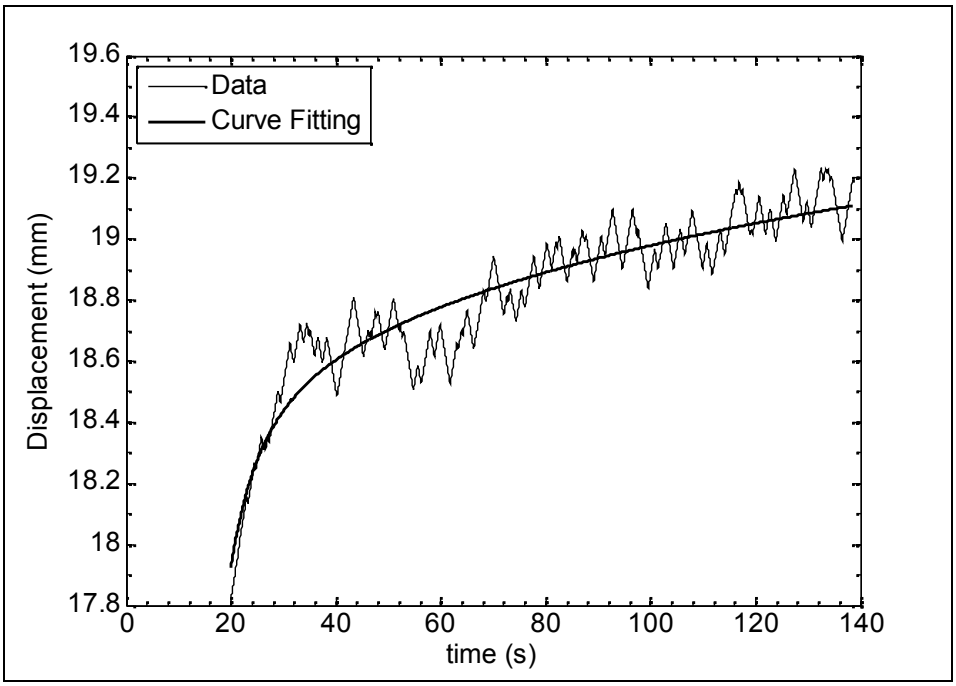

Figure 4.32 Curve fitting of data obtained for 1 mm/s motor speed, 5 N target force and 120 second creep duration, by the help of the power equation

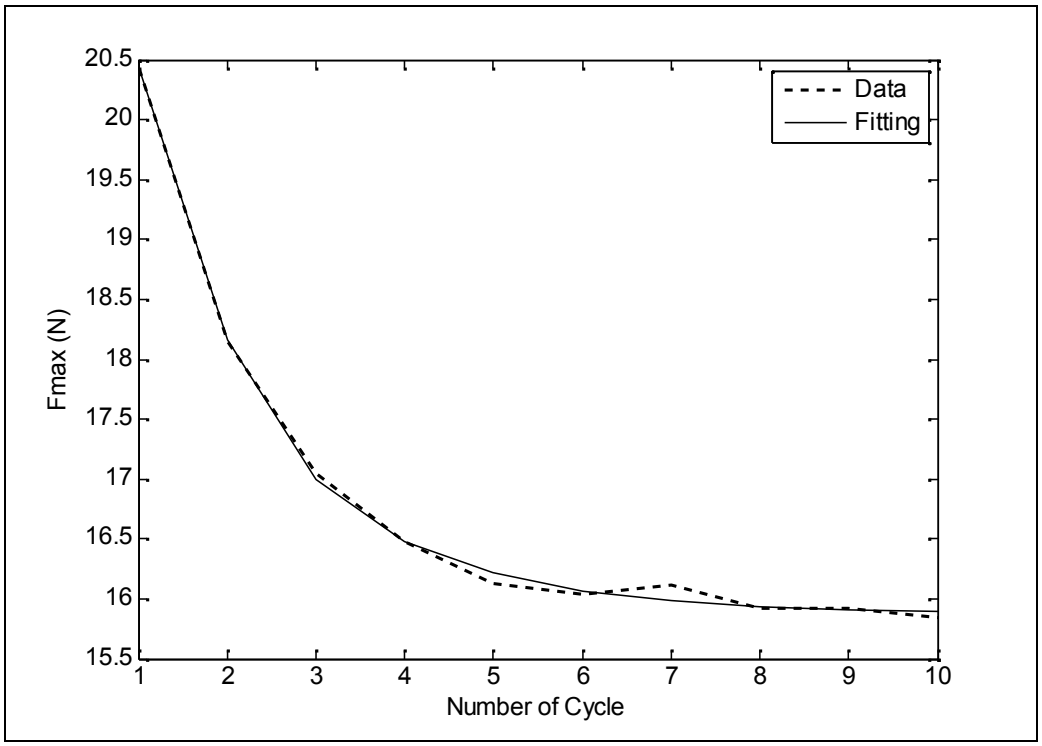

Figure 4.33 Curve fitting of the preconditioning effect observed in Figure 4.2

It was an important shortcoming that, constants did not correspond to any meaningful parameter and that they were variable. Yet, due to being a very flexible expression, curves very close to the experimental data could be obtained by this equation (Figure 4.31, 4.32, 4.33).

4.6.1.2 Medium Level Constitutive Equations

These are the models possessing at least one of the qualities sought in a good constitutive equation. Depending on the structure of these equations, they can simulate more than one feature of the soft biological tissues. Parameters in the model have a physical meaning. By using these equations, curves very close to the experimental data can be obtained. In this study, one medium level constitutive equation was used. This equation is the expressions known to be as the Prony series.

General form of this equation is,

$$y(t) = y_0\left[1 + \delta_1 e^{-t/\tau_1} + \delta_2 e^{-t/\tau_2} + ...\right] \quad (4.4)$$

where,

y (t) = Output data

y_0 = y value at t = t_0

δ_1 = Short-term magnitude depending on the test method

τ_1 = Short-term time constant

δ_2 = Long-term magnitude

τ_2 = Long-term time constant

t = time

Relaxation and creep behaviors of the soft biological tissues can be simulated by the help of the Prony series. Parameters in the equation have certain meanings based on the viscoelastic material model (Tönük and Silver-Thorn, 2004). Constants used for relaxation and creep are different. Therefore, when we consider these equations one by one,

For the relaxation, equations,

$$f(t) = f_0\left[1 - \delta_1 e^{-t/\tau_1} - \delta_2 e^{-t/\tau_2} - ...\right] \quad (4.5)$$

is used. Where,

f (t) = Output force

f_0 = Force at the start of relaxation

δ_1 = Short-term relaxation magnitude

τ_1 = Short-term relaxation time constant

δ_2 = Long-term relaxation magnitude

τ_2 = Long-term relaxation time constant

t = time

For the creep, equation,

$$d(t) = d_0\left[1 + \delta_1 e^{-t/\tau_1} + \delta_2 e^{-t/\tau_2} + ...\right] \quad (4.6)$$

is used. Where,

f (t) = Output force

f_0 = Force at the start of relaxation

δ_1 = Short-term creep magnitude

τ_1 = Short-term creep time constant

δ_2 = Long-term creep magnitude

τ_2 = Long-term creep time constant

t = time

For linear viscoelastic material models one set of coefficients may be obtained from the other set of coefficients (Tönük and Silver-Thorn, 2004) however for the nonlinear case this conversion procedure fails. With the help of these equations, substantially close results to the relaxation and creep data extracted from the tests, are obtained (Figure 4.34, 4.35).

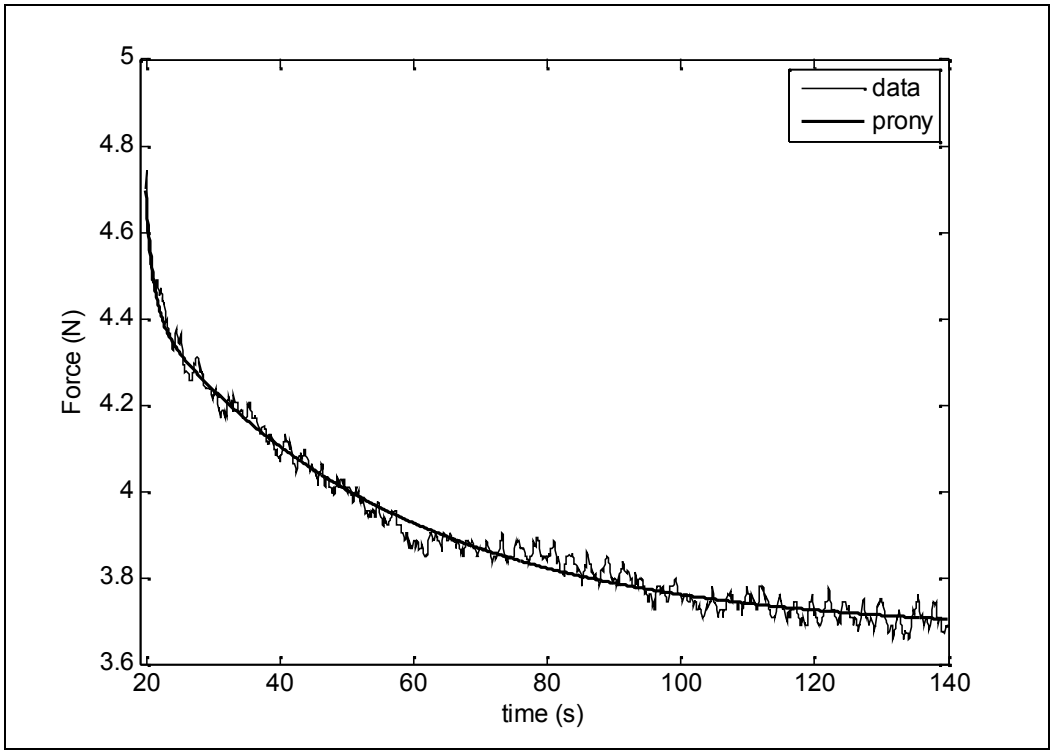

Figure 4.34 Modelling of the graph obtained for 1 mm/s motor speed, 20 mm displacement and 120 second relaxation duration, by Prony series. Equation 4.11-d was used for modelling.

Related constants and r-square values are given below for the Figure 4.34.

Table 4.1 Constants and r-square value related to the Figure 4.34.

δ_1	τ_1	δ_2	τ_2	δ_3	τ_3	R-Square
46,48846	2,85361	0,25775	39,46564	-46,5433	0,03201	0,985268356

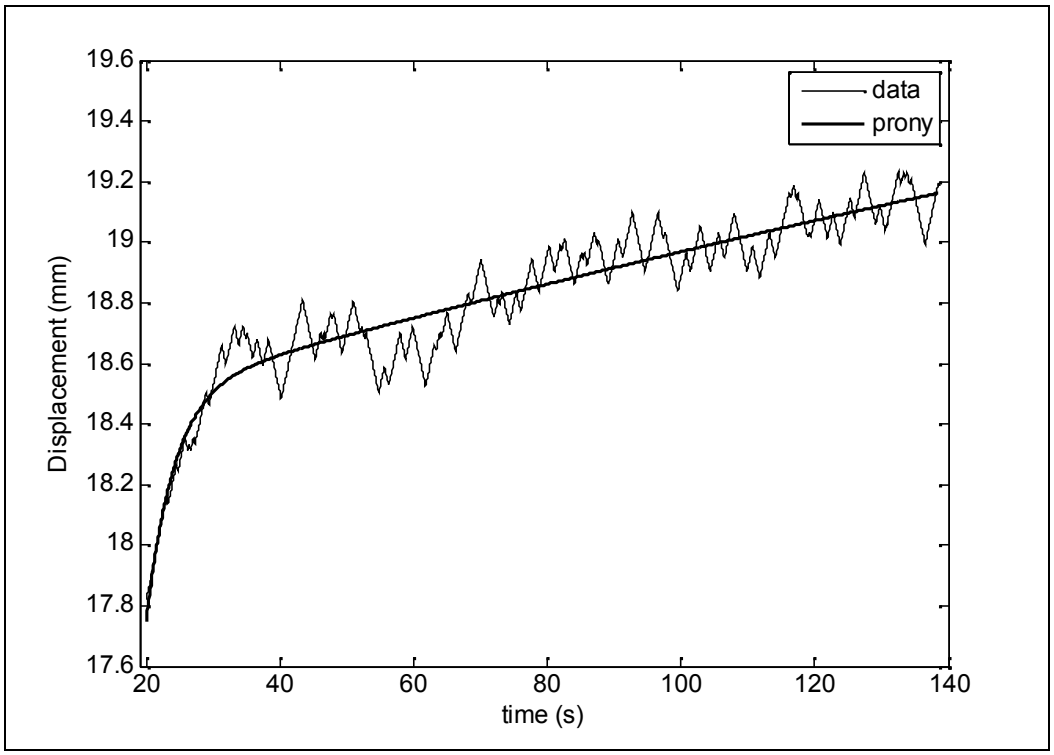

Figure 4.35 Modelling of the graph obtained for 1 mm/s motor speed, 5 N target force and 120 second creep duration, by Prony series. Equation 4.11-d was used for modelling.

Related constants and r-square values are given below for the Figure 4.35.

Table 4.2 Constants and r-square value related to the Figure 4.35.

δ_1	τ_1	δ_2	τ_2	δ_3	τ_3	R-Square
-0,18549	529,022	3,29397	0,00508	-2,89046	4,63512	0,911944717

Test given in Figure 4.34 and 4.35 were carried out at the same location by using the same tips. It was therefore decided to use the linear viscoelasticity material hypothesis. Behavior of the materials displaying linear viscoelasticity is described by Maurel et al., (1998), as follows,

"Practical experience with materials which exhibit these behaviors suggest that they remember the previous deformations to which they have been subjected. This leads to formulate the general linear viscoelastic behavior as a relationship between the stress, the strain and their derivatives with respect to time in the form:

$$\left[a_0 + a_1\frac{\partial}{\partial t} + a_2\frac{\partial^2}{\partial t^2} + \ldots\right]\sigma(t) = \left[\alpha_0 + \alpha_1\frac{\partial}{\partial t} + \alpha_2\frac{\partial^2}{\partial t^2} + \ldots\right]\varepsilon(t) \quad \text{"p.43}$$

On the basis of this hypothesis, constants found for Figure 4.34 were used as initial guesses for the creep test given in Figure 4.35. Consequently, result given in Figure 4.36 and the constants given in Table 4.3 were obtained.

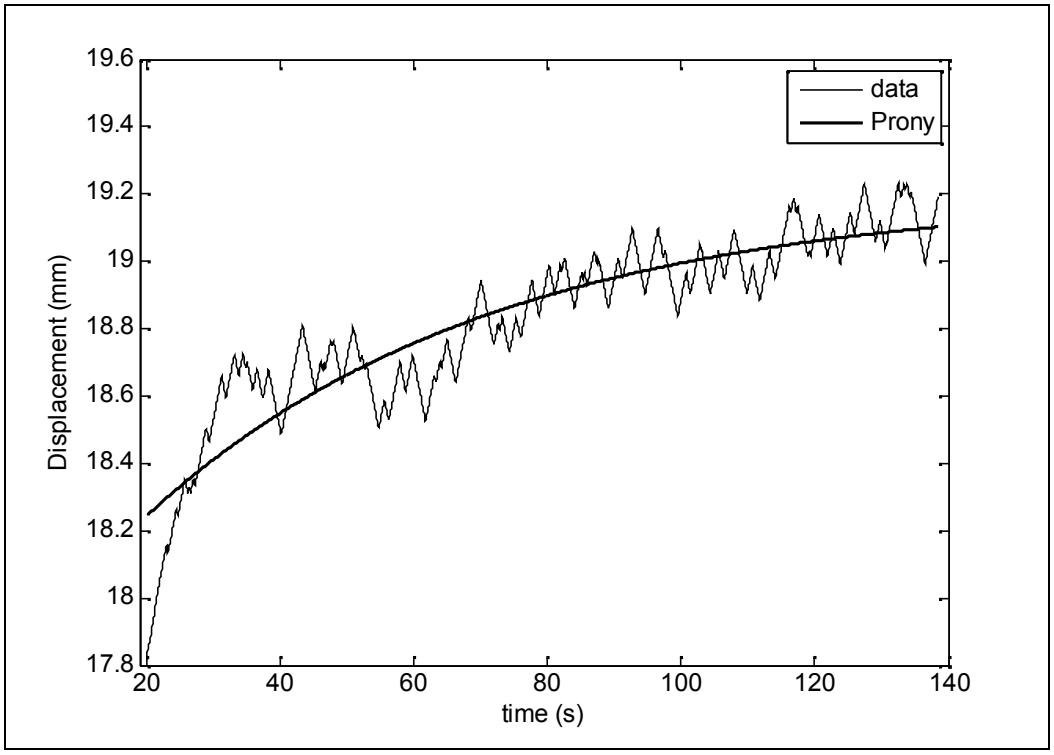

Figure 4.36 Graph drawn as a consequence of finding constants for creep by the help of the constants of relaxation, obtained by using the linear viscoelasticity hypothesis.

Table 4.3 Constants and r-square value related to the Figure 4.36.

δ_1	τ_1	δ_2	τ_2	δ_3	τ_3	R-Square
47.68	0.73472	-0.079047	51.919	-47.523	0.041152	0.84156

As can be seen from Figure 4.36, constants necessary for the creep were found by the help of the constants found for the relaxation test. Besides this, these constants found came out to be quite close to the relaxation constants. On the other hand, when r-square values for two creep series were compared value found for first constants was better.

It is possible to lay down the Prony series in a different form (Tonuk and Silver-Thorn, 2004)**.** In such case, relaxation and creep equations can be written as;

$$f(t) = f_0\left[1-\delta_1\left(1-e^{-t/\tau_1}\right)-\delta_2\left(1-e^{-t/\tau_2}\right)-...\right] \quad (4.7)$$

$$d(t) = d_0\left[1+\delta_1\left(1+e^{-t/\tau_1}\right)+\delta_2\left(1+e^{-t/\tau_2}\right)+...\right] \quad (4.8)$$

In the study, both forms were used, and it was observed that the second form gave better results (See Chapter 4.6.3.2).

4.6.1.3 High Level Constitutive Equations

They pose all qualifications of a good constitutive equation. Structurally, these equations are complicated and they posses such important qualifications as the capability to simulate different features of the soft biological tissues and their constants to be meaningful and identifiable.

Such an expression (enhanced quasi-linear viscoelastic model) was found in the study constituting the other branch of the soft biological tissues mechanical behaviors and containing the computer simulations (Üsü, 2008).

$$T_{xx}=\left(p^2\times\frac{\varepsilon_x^2}{a^2+b^2+c^2}\right)\times\left(\frac{A}{1+C\times\ln\left(\frac{\tau_1}{\tau_2}\right)}\right)\times$$

$$\left(\begin{array}{l}\left(\begin{array}{l}e^{(B\times\dot{\varepsilon}\times t_0)}-1+C\times\left(\frac{e^{(-t/\tau_1)}}{\tau_1}\right)\times\left(e^{(B\times\dot{\varepsilon}+1/\tau_1+t_0)}\times\frac{(\tau_1\times(t_0+\tau_1-t))}{(t_0-t)^2}\right)-\tau_1\\ \times\frac{((B\times\dot{\varepsilon}\times\tau_1+1)\times t_0+\tau_1)-(B\times\dot{\varepsilon}\times\tau_1+1)\times t}{((B\times\dot{\varepsilon}\times\tau_1+1)\times(t_0-t))^2}+\frac{\tau_1}{t}\times\left(1-\frac{\tau_1}{t}\right)-\frac{\tau_1}{((B\times\dot{\varepsilon}\times\tau_1+1)\times t)}\times\\ \left(1-\frac{\tau_1}{((B\times\dot{\varepsilon}\times\tau_1+1)\times t)}\right)\end{array}\right)+e^{(-t/\tau_2)}\times\\ \left(\begin{array}{l}e^{((B\times\dot{\varepsilon}+1/\tau_2)\times t_0)}\times\frac{\tau_2}{((B\times\dot{\varepsilon}\times\tau_2+1)\times(t_0-t))^2}\times((B\times\dot{\varepsilon}\times\tau_2+1)\times(t_0-t)+\tau_2)+\frac{\tau_2}{(B\times\dot{\varepsilon}\times\tau_2+1)\times t}\times\\ \left(1-\frac{B}{(B\times\dot{\varepsilon}\times\tau_2+1)\times t}\right)\end{array}\right)-\\ \left(e^{(B\times\dot{\varepsilon}\times t_0)}\times\left(\gamma-\ln(\tau_2)+\frac{t_0}{\tau_2}+\ln(t-t_0)-\frac{t}{\tau_2}\right)+\ln(\tau_2)-\gamma+\frac{t}{\tau_2}-\ln(t)\right)\end{array}\right)\quad\ldots(4.9)$$

where,

T_{xx} = Stress along the material axis x

p (a, b & c) = Material parameter that reflect the unit cell dimension. It depends on the material axis

ε_x = Principal strain along the material axis x

A & B = Elastic material parameters

C = Material parameter related to the viscous damping

$\dot{\varepsilon}$ = Strain rate

γ = Shear Strain

t_0 = Beginning of relaxation

t = time

τ_1 & τ_2 = Material parameters related to the strain rates

Another important feature of this equation is that, it can simulate the anisotropic behaviors of the soft biological tissues. Thus, with the help of this equation, preconditioning effect, relaxation, creep and anisotropic behavior of the soft biological tissues can be modeled.

Obtaining the constants of Equation 4.9 by using the experimental data in hand, directly is not possible. Because, as our experimental data contains the displacement – time or force – time expressions, Equation 4.9 contains the stress, strain and time expressions. Therefore, constants are obtainable only through computer simulations conducted by using the inverse finite element method (Üsü, 2008).

4.6.2 Determination of the Equation Constants and the Results

To determine the constants in the equations three different software were used. One of them is Excel Trendline and the other two are curve fitting programs named as uifit GUI and Ezyfit toolbox used in Matlab 7.1.

Determination of constants of the Equation 4.2 which is a curve fitting equation is made by using the power option of the Excel trendline.

In the solution of the Equation 4.3 and the Prony Series, uifit GUI prepared by Michael Rousseau and which was available from the Matlab File Exchange Site was utilized (Appendix D).

Another code used for these equations is the Eazyfit Toolbox operating again in Matlab 7.1 (Appendix D). This toolbox, prepared by Assistant Professor Frederic Moisy from University Paris-Sud, is a free curve fitting toolbox which can be downloaded from the internet. By using this software, compared to uifit GUI, it is possible to obtain a result, initial guesses made for the constants must be good.

uifit GUI is more tolerant in this respect. Even if the initial guesses are not hot precise, result is obtainable by repeating the curve fitting efforts.

4.6.3 Results

4.6.3.1 Results Pertinent to the Curve Fitting Equation 4.2

Examination and comparison of the test data as a raw data, makes certain observations rather difficult and clear conclusions are not attainable. This problem was encountered when the variation of the relaxation data in relation to speed was tried to be observed. In the final graph formed by drawing the data of the same group measurements on the same graph, this situation was more clearly seen (Figure 4.37).

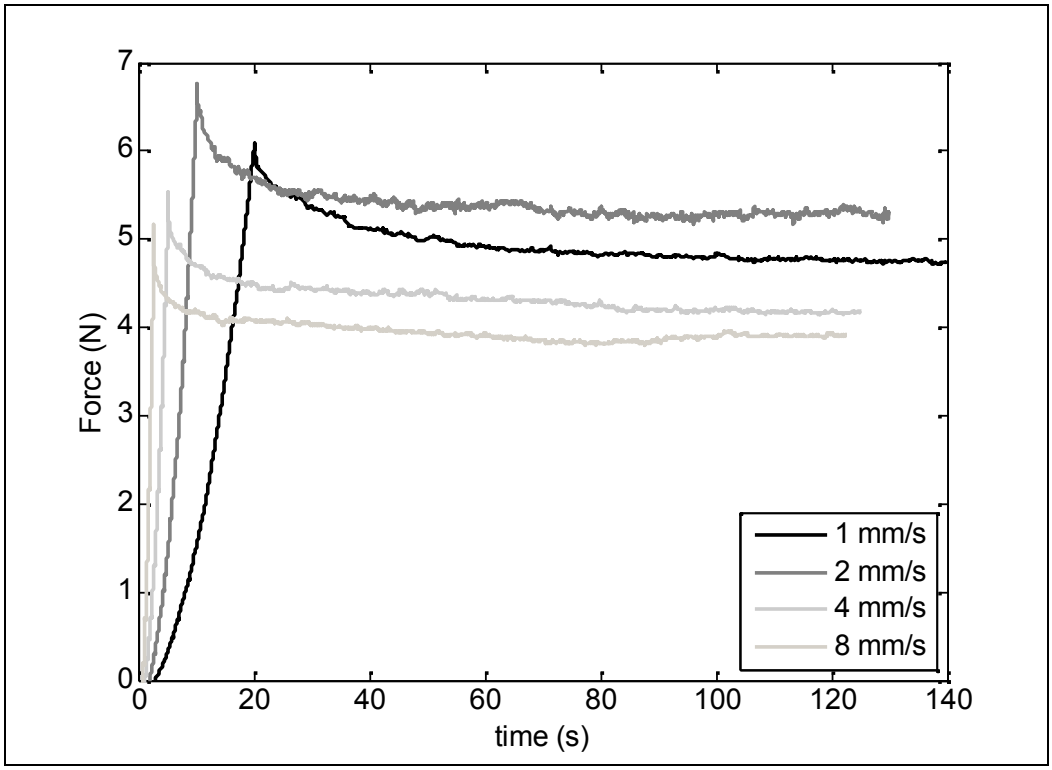

Figure 4.37 Relaxation data pertinent to the same group measurement

In this graph, 120 seconds relaxation data where the displacement amount was 20 mm is shown. Although it was possible to conclude that the lowest force is formed at 8 mm/s speed, a clearcut and explicit examination was not possible therefore, relaxation portions of the graphs were fitted by the help of the power function (Equation 4.2), using the Excel Trendline (Figure 4.30, Appendix C).

At the end, the constants, a and b of the Equation 4.2 were determined and graph showing their variation with speed were drawn (Figure 4.38, 4.39 and Appendix C).

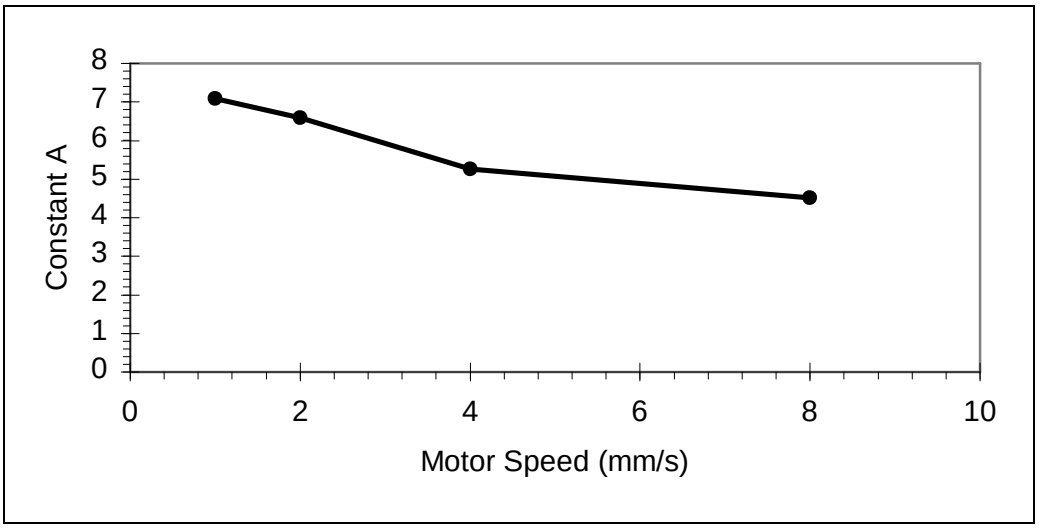

Figure 4.38 Variation of A constant with motor speed

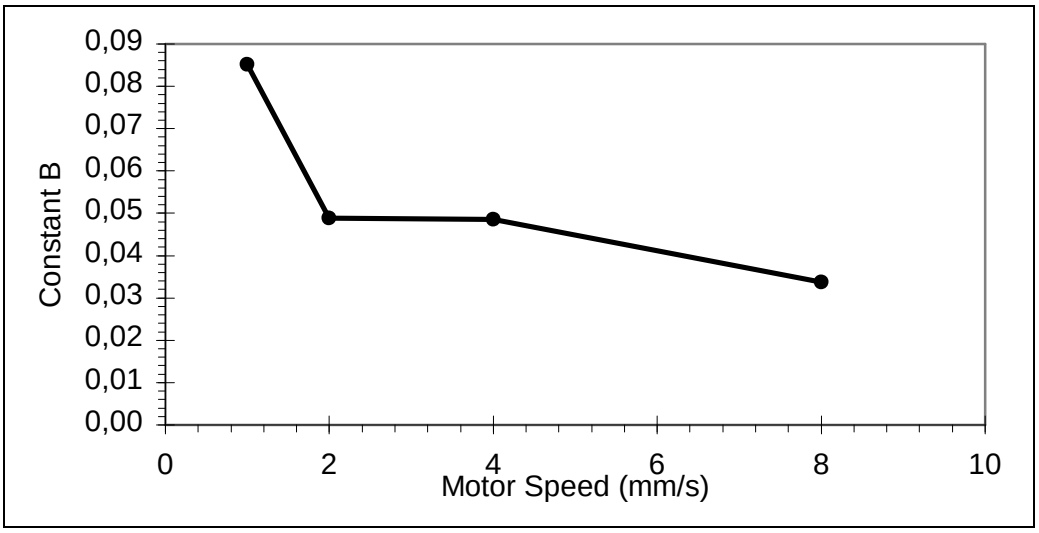

Figure 4.39 Variation of B constant with motor speed

As can be realized from the figures, A and B coefficients decreased with increasing speed. Yet, this result was somewhat different from the graphs presented in Appendix C and an increase in the coefficients pertinent to 8 mm/s speed. Therefore, at this point, it will be prudent not to draw a firm conclusion. As explained in detail previously**,** in the in-vivo tests, force data is extremely sensitive, and can be influenced even by very small muscle movements and minor deviations of the location of the indenter tip on the soft tissue tested. Therefore, interpretation of the speed related interactions of the soft biological tissues on the basis of hysteresis magnitudes, resulted with obtaining much clearer and dependable information.

4.6.3.2 Results Pertinent to the Constitutive Equations and Equation 4.3

With the study made, coefficients related to the equations were determined and the handicaps pertaining to the models were diagnosed (Section 4.6.4). Equation forms used in the simulations are given below in relation to the number of terms.

$$y(t) = y_0\left(1 + at^{-b} + ct^{-d} + et^{-f} + gt^{-h}\right) \quad \text{..... (4.10)}$$

$$y(t) = y_0\left[1 \pm \delta_1 e^{-t/\tau_1} \pm \delta_2 e^{-t/\tau_2}\right] \quad \text{(4.11-a)}$$

$$y(t) = y_0\left[1 \pm \delta_1 e^{-t/\tau_1} \pm \delta_2 e^{-t/\tau_2} \pm \delta_3 e^{-t/\tau_3}\right] \quad \text{(4.11-b)}$$

$$y(t) = y_0\left[1 \pm \delta_1\left(1 \pm e^{-t/\tau_1}\right) \pm \delta_2\left(1 \pm e^{-t/\tau_2}\right)\right] \quad \text{(4.11-c)}$$

$$y(t) = y_0\left[1 \pm \delta_1\left(1 \pm e^{-t/\tau_1}\right) \pm \delta_2\left(1 \pm e^{-t/\tau_2}\right) \pm \delta_3\left(1 \pm e^{-t/\tau_3}\right)\right] \quad \text{(4.11-d)}$$

As can be noted above, as the relaxation is simulated the in term designation is - and as creep simulated it is +. Besides this, 4.11-a and b equations and the 4.11-c and d equations were formed by writing the Prony series in two different forms. In the Tables given below**,** coefficients determined, can be seen.

Table 4.4 Coefficients of Equation 4.10 for the relaxation data

T.No	a	b	c	d	e	f	g	h
R.1	0,488	-4,045	-4,596	-1,326	0,094	-0,452	0,248	-0,109
R.2	-0,586	-2,701	-4,397	-1,584	-0,550	-0,403	0,290	-0,013
	-2,0E+05	-4,331	485,137	-1,868	-68,553	-1,000	13,595	-0,620
R.3	-3,131	-1,816	4,259	-1,264	0,041	0,349	-6,454	-1,254
	-21,247	-1,803	0,217	-0,442	0,014	0,545	0,056	-0,576
	-5340,1	-3,790	43,844	-23,855	0,025	0,452	-31,750	-27,782
R.4	0,270	-3,048	-1,527	-2,370	0,155	0,089	-2,820	-0,948
R.5	-1,5E+07	-4,1E+04	-1,0E+07	-1,8E+07	0,018	0,485	-8,0E+07	-7,047
R.6	-2,797	-3,204	1,367	-2,528	0,271	0,010	-1,924	-0,692
	-5,6E+05	-5,096	85,151	-1,440	3,873	-0,395	-29,629	-0,872
R.7	1,115	-5,836	-3,774	-4,754	0,756	-0,265	-5,040	-0,922

Table 4.5 Coefficients of Equation 4.10 for the creep data

T.No	a	b	c	d	e	f	g	h
C.1	0,000	0,197	1,684	-0,272	14379	-4,081	-2,110	-0,413
C.2	-0,092	0,079	0,073	-2,521	-1,351	-2,542	0,143	-0,070
C.3	-0,017	0,263	-197184	-770	100423	-4,859	265581	-648
C.4	-0,337	0,064	0,357	0,017	4554	-4,036	2832	-3674
C.5	-1,522	-0,695	29,378	-1,646	-115	-5912	0,000	1,603
C.6	-12,104	-21,931	8,131	-16,464	-0,264	-0,244	51,975	-1,949
C.7	-2662	-53,782	13103	-4,137	-0,007	0,545	-1606	-10,270

Table 4.6 Coefficients of Equation 4.11-b for the relaxation data

Test No	δ_1	τ_1	δ_2	τ_2	δ_3	τ_3	R-Sq.
Relax. 1	0,15093	44091,4	19993,14	0,00046	-746,872	2,11105	0,337
Relax. 2	0,15203	3029258	-60373,8	0,00325	-0,36056	8,50492	
	0,23255	895,3	-0,20324	46,31593	-1347151	1,19126	0,841
Relax. 3	0,18024	3688,2	-104,431	3,2899	-834,976	1,35744	
	0,25696	992903,4	-0,24176	69,28676	-159883	1,35938	0,984
Relax. 4	0,21783	49166982	-983855	1,19715	-0,26538	37,52988	0,985
Relax. 5	0,6181	32651902	-4788,66	1,814	-0,56328	465,4394	0,913
Relax. 6	0,22683	2018759	-0,27695	38,35479	-196917	1,33351	0,981
Relax. 7	0,15311	2531,594	10612,59	0,00524	-0,78876	11,51369	0,844

Table 4.7 Coefficients of Equation 4.11-b for the creep data

Test No	δ_1	τ_1	δ_2	τ_2	δ_3	τ_3	R-Square
Creep 1	0,313	396,641	-145,844	2,61803	-0,32311	168,1461	0,965
Creep 2	0,991	143,637	-1,00579	129,5022	-216,004	0,0055	
	0,893	145,095	-0,9075	129,355	-1,2E+09	0,86302	0,611
Creep 3	0,110	12872,7	-3,83966	4,67835	-0,07389	287,6471	0,718
Creep 4	0,202	-1,4E+10	-5,15544	4,16783	-0,17066	469,4644	0,913
Creep 5	0,230	752,050	-0,2783	136,6843	-13,4158	3,69945	0,944
Creep 6	0,256	116,503	-0,28958	41,92991	-0,29032	9,96561	0,881
Creep 7	0,133	395,767	0,53704	152,2655	-0,68694	116,1829	0,834

Table 4.8 Coefficients of Equation 4.11-a, c, d for the relaxation data

Eq. Type	δ_1	τ_1	δ_2	τ_2	δ_3	τ_3	R-Square
a	0,22671	1342495	-0,25819	57,98248			0,976167188
c	0,25817	57,97436	-0,03149	0,00444			0,976168053
d	1,56642	5,85771	0,24128	101,5282	-1,52783	0,32682	0,985188468
a	0,287	458,0344	-0,35526	49,13241			0,976513174
c	0,29882	33,63308	-0,10064	0,01613			0,980651584
d	46,48846	2,85361	0,25775	39,46564	-46,5433	0,03201	0,985268356
a	0,21459	3067775	-0,30838	34,55			0,974739293
c	0,30837	34,54799	-0,09379	0,14746			0,974739206
d	1,74852	0,37361	0,30837	34,54799	-1,84232	0,02545	0,979877964

Table 4.9 Coefficients of Equation 4.11-a, c, d for the creep data

Eq. Type	δ_1	τ_1	δ_2	τ_2	δ_3	τ_3	R-Square
a	0,09428	32732,08	-0,12213	67,38226			0,95841017
c	0,22527	0,05836	-0,12059	89,91842			0,96247160
d	0,3191	0,67925	-0,09384	0,00146	-0,12059	89,91841	0,96247134
a	0,05666	760844,1	-0,29114	11,88716			0,60881047
c	0,34848	0,01159	-0,29184	11,87273			0,60888831
d	0,07237	0,07707	0,27611	0,24539	-0,29184	11,87273	0,60888831
a	0,07754	3088054	-0,07905	51,92429			0,84238221
c	0,22588	0,01092	-0,16055	18,53549			0,76774173
d	-0,18549	529,022	3,29397	0,00508	-2,89046	4,63512	0,91194472

4.6.4 Evaluation of the Results

Results were evaluated under two considerations. Firstly, whether the constants of the relevant parameters showed stable behaviors or not, and whether values of the same parameters obtained for different graphs deviated from each other substantially or not, were inquired. Secondly, the r-square values were calculated in order to observe how well the equations modeled the related graphs.

Firstly, let us clarify that, we meant the color when we stated it to be unstable. As an example let us consider the equation among the second group measurements given in Table 4.8. As can be seen from the table, short term time

constant τ_1 is determined to be 458 s. In order to obtain a better result, by using the constants determined for this "a" equation, when curve fitting process is repeated by the help of uifit GUI, τ_1 was found to be 9074493 s. When the same process was repeated again, τ_1 is found as 9.88E15 s. In other words, this constant did not stay stable in a fixed value but showed an ever-increasing trend. Thus, in some of the equation forms used, such a case was observed and the term to describe this case was stated as unstable. Finally, if the constants showed an increasing trend with repeated curve fitting process, the equation used was termed as unstable and if not it was denoted as stable.

For the second case, on the other hand, whether the pertinent parameters were guessable or not was meant. That is, when determining the parameters of the equations used for the experimental data in hand, whether our initial guesses for these parameters were, under the experience of previous observations, close enough to be sought parameters. Naturally, the fact that, the tests were being carried out in-vivo, made this case a difficult one, but nevertheless, for some equation forms such an approach was employed.

Coefficients of the Prony series and power equations were observed to show extremely unstable behaviors. In particular coefficients of the power equations showed extremely dispersed and unstable behaviors and it was revealed that, the coefficients in concern were unestimatable (Table 4.4, 4.5). In the Prony series, on the other hand, situation was somewhat different. Results of the Prony equations with different forms were also different. In this context, best results were obtained when the Prony series given in Equation 4.11-c was used. The constants obtained for the relevant parameters were, within certain limits, estimatable (Table 4.8, 4.9). It was observed that, the form given in Equation 4.11-b gave the worst results. It was concluded that, the constants obtained through this form were unestimatable, and that parameters such as τ_1, δ_1 displayed unstable behaviors (Table 4.6, 4.7). In the forms of equations a and c,

better results were obtained, but still, variable behaviors and deviations were commonplace.

Another parameter, used for the evaluation of the results is the r-square value. In this context, r-square values were calculated. Results can be seen in Figure 4.40 and 4.41.

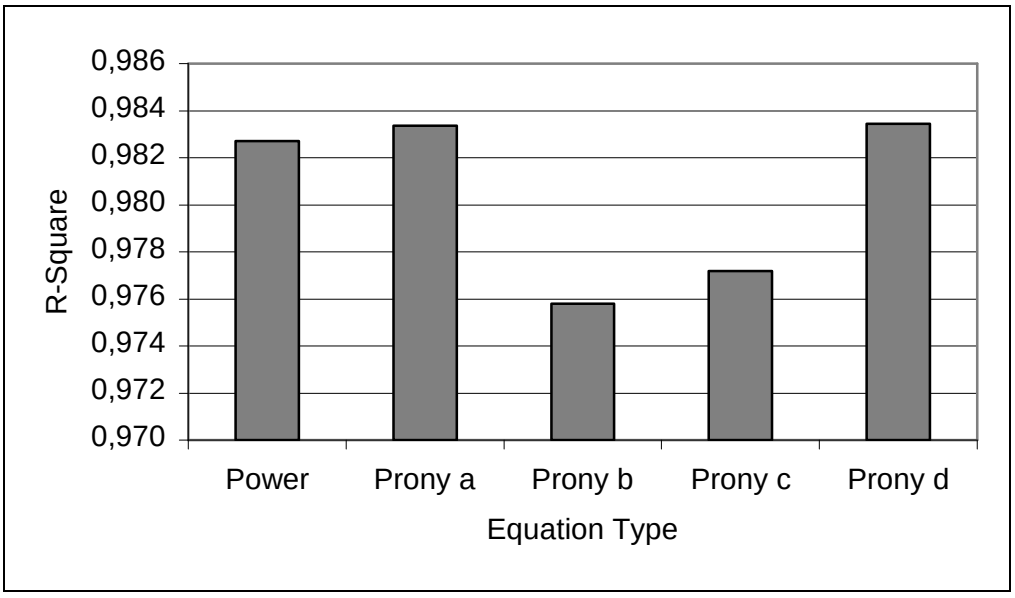

Figure 4.40 R-square values of the models used for the relaxation data

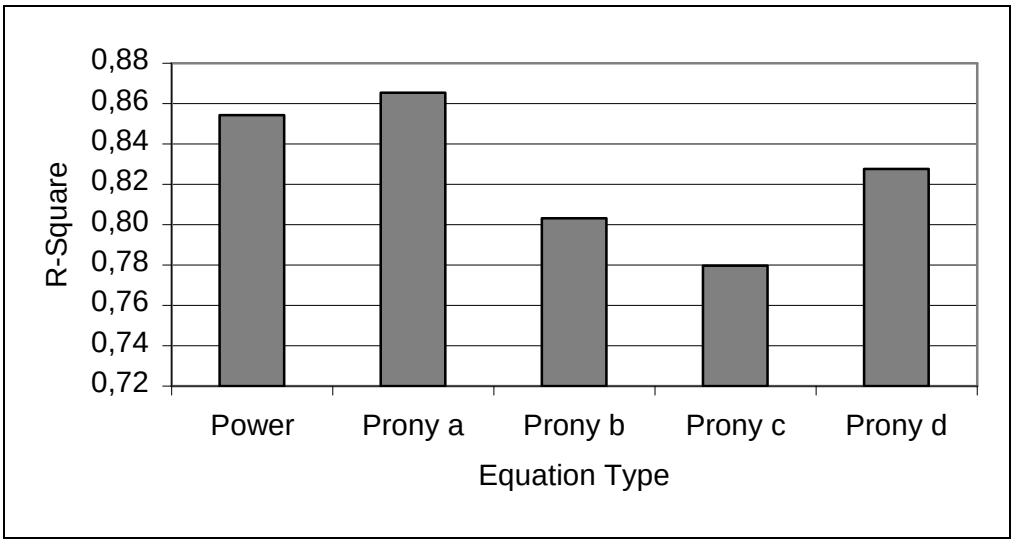

Figure 4.41 R-square values of the models used for the creep data

R-square values given in the graphs were determined by using 3 each relaxation and creep graphs where clean data were obtained. R-square values for different models were calculated by using these and, graphs were drawn by taking their average values.

As can be seen in Figure 4.40, best result was obtained for the Prony equation in "4.11-d" form. For the creep tests, on the other hand, best result was yielded by the Prony equation in "4.11-a" form.

4.7 Examination of the Anisotropic Behaviors of the Soft Biological Tissues

Soft biological tissues are bodies displaying anisotropic behaviors. That is, responses given to loads coming from different directions are also different. In the indenter tests, these behaviors of the soft biological tissues can not be determined by the axi-symmetric tips. Examples of these tips are the spherical and cylindrical tips. Therefore, ellipsoid tips which are theoretically examined by Bischoff, (2004), were used.

4.7.1 Ellipsoid Tips

Ellipsoid tips possess ellipsoidal form and designed according to two basic length parameters. These lengths are the long and short axis lengths (Figure 4.42).

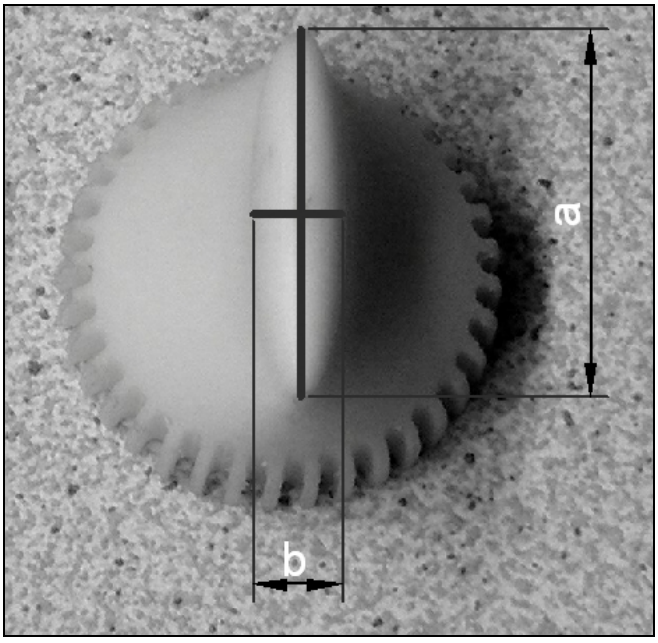

Figure 4.42 a and b give the lengths of the long and short axis respectively. Edges are prepared and produced according to these dimensions

For the tests, three ellipsoid tips in different dimensions were produced (Figure 4.43).

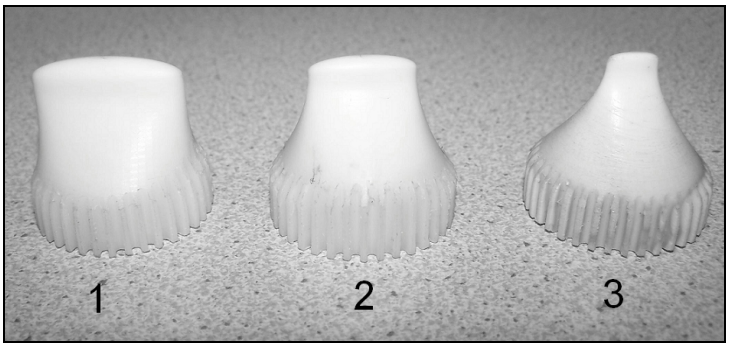

Figure 4.43 Ellipsoidal tips of different dimensions. Tip dimensions; a =24 mm, b = 6 mm (1) a = 16 mm, b = 4 mm (2) a = 8 mm, b = 2mm (3)

The reason for producing different dimensioned tips was to be able to perform measurements fit to the tissue physiology at different locations. It was necessary to use small sized tips for the points where thick tissues prevailed and large sized tips for the points of thin tissues. At the points where thick tissue took place, it is feasible to work with larger displacement amounts and in such places using small sized tips brings the risk of damaging the tissue. Independent of the tissue thickness, to work with small sized tips as small displacement amounts are applied, is more suitable. Another criteria decisive for the selection of the indenter tip is the size of the organ tested. For instance, small indenter tips are used for the fingers, cheeks or heel showing high degree of curvature. Using the medium and big sized tips in such organs causes deficiency in full contact between the tissue and the indenter tip. Furthermore, the variance of the tissue thickness underneath a large sized tip creates a problem for obtaining the tissue thickness parameter which is very important for the computer simulations. For large organs like arms and legs, provided that the tissue thickness is sufficient, it is possible to work with medium. On the periphery of the indenter tips produced, 36 notches, one at each 10º increment, were made (Figure 4.40). Ellipsoidal tips could be placed in desired angles by the help of the aligning element attached to the indenter tip (Figure 4.44).

Figure 4.44 By the help of the alignment edge and routes, measurements at 10º intervals could be made

4.7.2 Tests Carried Out with Elliptical Tips and Their Results

At the same test point, by 10º and 30º angular increments, tests were carried out and the anisotropy of tissue in the plane of the skin surface was determined. Ellipsoidal indenter tip was placed parallel to the longer axis of the forearm, that is parallel to the contraction direction of the muscle fibers. Following this, the necessary indenter tests were carried out by positioning of the indenter tip at the desired angular positions (Figure 4.45).

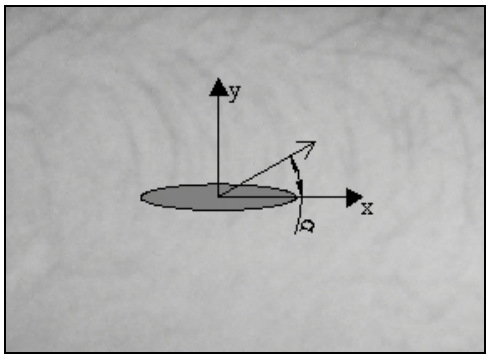

Figure 4.45 Response of the tissue under different angles is examined by aligning the ellipsoidal tip at α angle

Tissue anisotropies were examined separately for the cyclic loading, relaxation and creep test protocols.

4.7.2.1 Cyclic Loading Tests

Basic measurements were performed at 8 mm/s motor speed by 10º increments within the 0º and 170º interval. In addition to these angles, measurements for control purposes 180º, 210º, 240º and 270º angle tests were also conducted. These positions coincide with the first 0º, 30º, 60º, and 90º positions of the indenter tip. Later the basic measurements were compared with the control measurements. In the tests, closeness of the control data to the basic measurements indicated that these measurements were dependable. Yet, a great variation between the control measurement and the basic measurement or the deviation of graph form the general tendency, marked that test point was dislocated or the muscle volume was altered.

In these tests where observing the preconditioning effect is not a matter of importance, the tests were conducted consecutively without waiting for the soft tissue to recover. Measurements consisting of 10 cycles were carried out, and method used in the examination of the influence of speed on the soft biological tissues was employed (Chapter 4.3.2). That is, maximum forces for each cycle were determined, and later their averages were taken. Following this, highest and lowest values above and below these average values were eliminated and the average of the remaining values were recalculated. This procedure was repeated for all angle values and the graph of the soft tissue response force versus the angle of the angle of elliptical indenter tip was drawn (Figure 4.46).

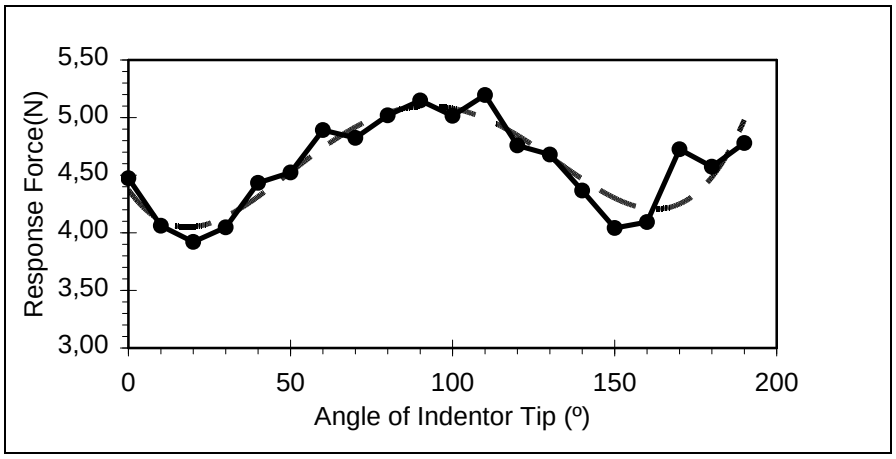

Figure 4.46 Anisotropic behavior of the tissue in relation to the varying angles in cyclic loading. Tests were carried out under the 8 mm/s speed and 16 mm tissue displacement

As can be seen from the Figure 4.46, response of the tissue increased from 0º to 90º and decreased from 90º to 180º. Thus, maximum force developing in the tissue occurred when the indenter tip was positioned perpendicular to the contraction direction of the muscle fibers. Again, result of a similar measurement can be seen in Figure 4.47.

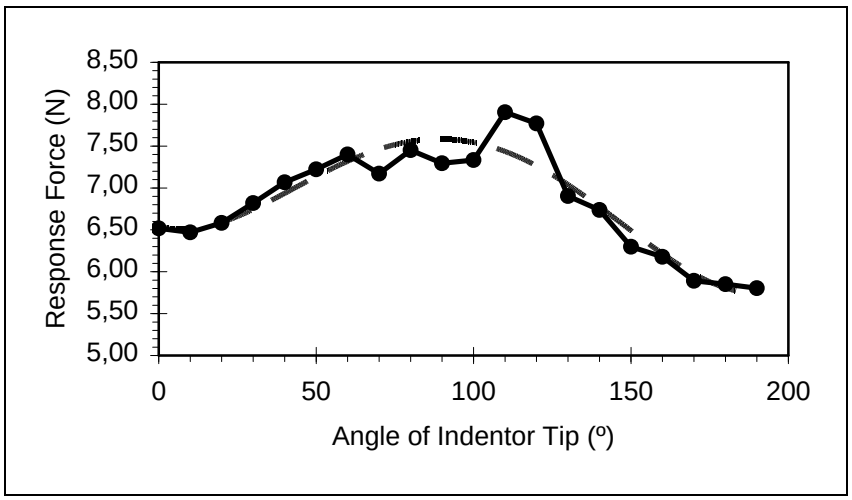

Figure 4.47 Anisotropic behavior shown by the tissue, at another cyclic loading test

To obtain consistent results, while rotating the indenter tip in between the tests, the test point on the tissue should not be changed. Due to long duration of the tests, the muscle tonus should be kept the same during the tests. These tests were substantially time taking tests and in case the necessary diligence was not dedicated, data would be greatly influenced. Despite all these, the general tendency discussed above, were observed also in this type of uneasy data (Figure 4.48).

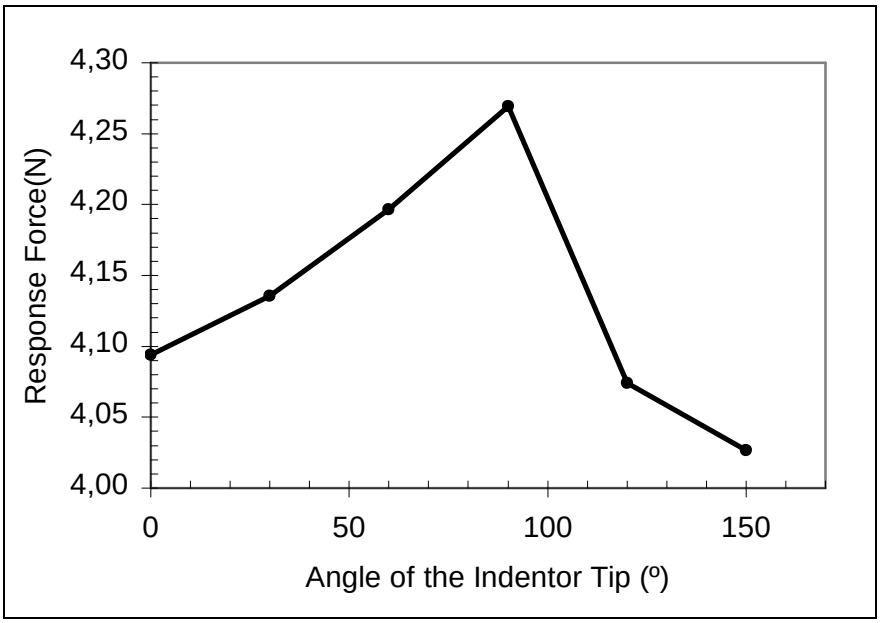

Figure 4.48 Anisotropic behavior observed in the cyclic loading tests conducted at 16 mm displacement and 8 mm/s motor speeds.

4.7.2.2 Examination of the Tissue Anisotropy Related to the Relaxation Behavior

In order to examine the tissue anisotropy as related to relaxation behavior, 7 successive tests with 30º interval increases between 0 and 210º angles, were carried out. In these tests, 1 mm/s motor speed, 120 second relaxation duration and 17-22 mm displacement amounts were applied. Anisotropy investigations

for the relaxation behavior were carried out in two ways. First of this was may by the comparison of forces at the end of the creep duration, end the other, by driving and comparing the constants of the two term Prony Equation (Equation 4.11-c)

4.7.2.2.1 Observed Anisotropy Related to the Force Values at the End of the Relaxation Time

In order to comfortably observe the anisotropy behavior, force values at the end of the relaxation time were determined and force – indenter tip angle graphs were drawn (Figure 4.49, 4.50).

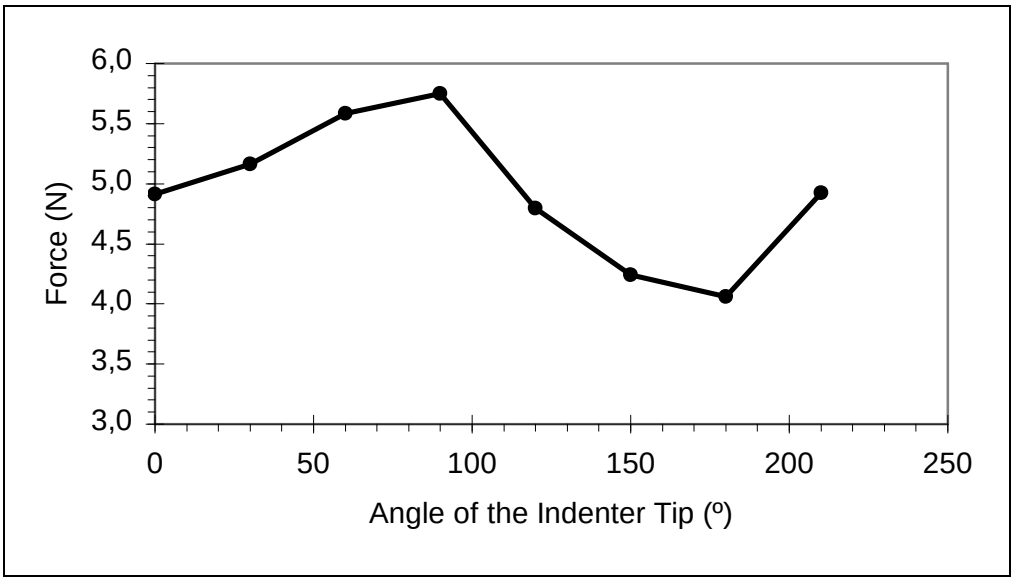

Figure 4.49 Anisotropic response attributed to relaxation behavior. In the test data a 22 mm displacement is applied

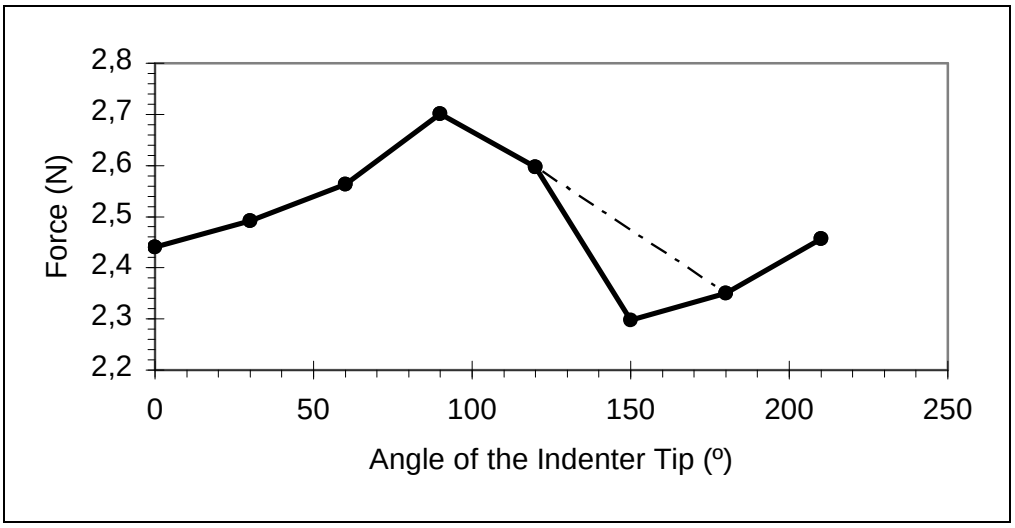

Figure 4.50 Anisotropic response attributed to relaxation behavior. In this test a 17 mm displacement is applied

As can be seen from the figures, in the relaxation tests also, results similar to those of the cyclic loading tests, were obtained. Response force displayed by the tissue increased from 0º to 90º degrees and decreased from 90º to 180º degrees. After 180º, another increase was observed. Again, maximum force was encountered when the indenter tip placed perpendicular (90º) to the contract direction of the muscle.

In the Figure 4.49, at 150º a deviation attributed to the muscle activity was encountered and by eliminating this value, expected result was obtained (dashed line).

4.7.2.2.2 Examining the Relaxation Dependent Anisotropy Behavior by Using the Prony Equation

Another examination pertinent to anisotropic behavior displayed by the tissue was carried out by using the Prony series. Constants of Equation 4.11-c were determined by using the test data and the graphs showing the variation of constants in relation to the angle of the ellipsoid tip, were drawn.

4.7.2.2.2.1 Graphs Pertinent To the Test Results Given in Figure 4.49

In the following graphs, it was given the variation of the coefficients (Table 4.10) belonging to Equation 4.11-c with the indenter tip angle.

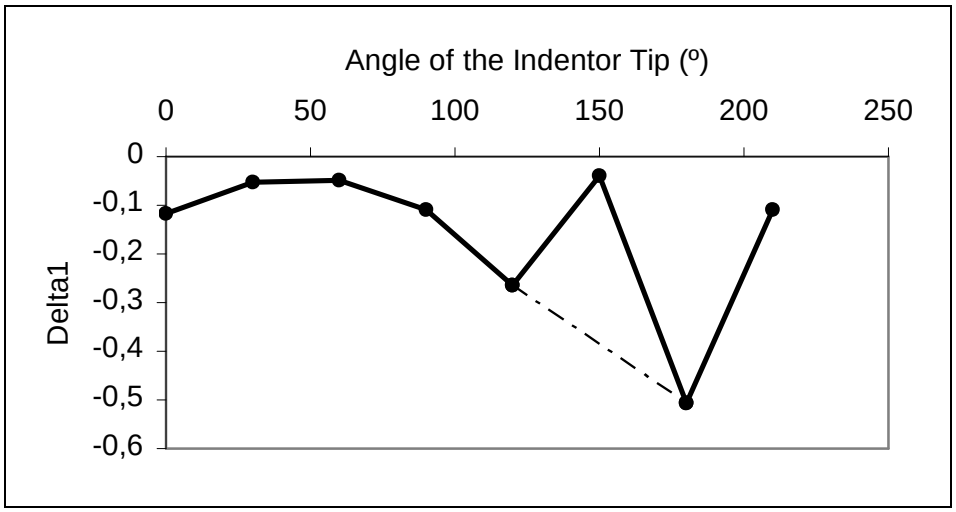

Figure 4.51 Angle of the indenter tip versus δ_1 graph

As it can be seen from the Figure 4.51, an interesting result was obtained. The short term relaxation magnitude degreased gradually with the increasing tip angle. Only a high deviation was observed at 150º. This was most probably caused by the muscle tones changes. The other probability was the physiology under the indenter tip at this angle. It was observed a high deviation at 150º in the other test result given in Section 4.7.2.2.2.2. The control value observed at 210º nearly took same value with the magnitude of δ_1 at 0º.

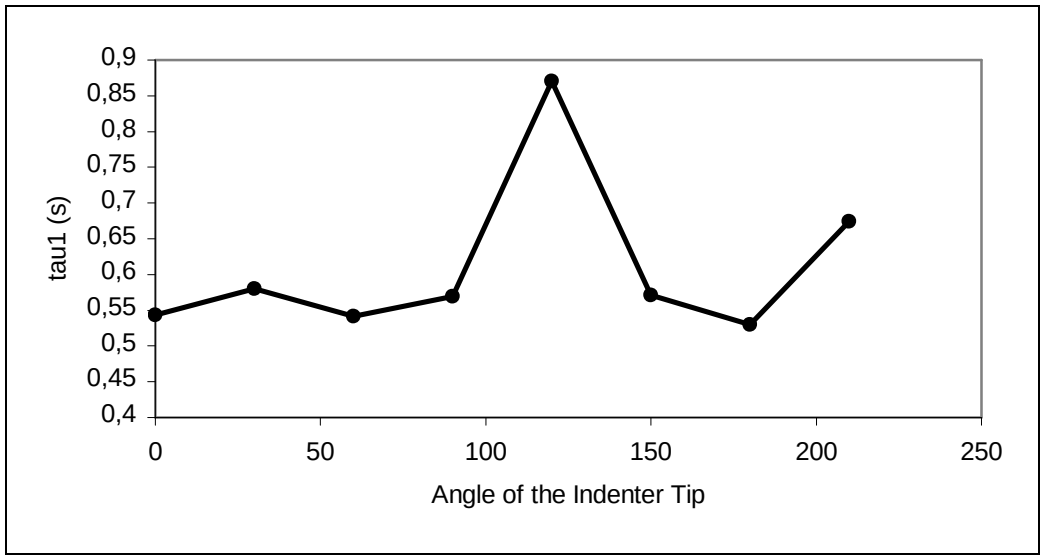

Figure 4.52 Angle of the indenter tip versus τ_1 graph

As it can be seen from the Figure 4.52, the short term relaxation time constants changed around the 0.55 s with the increasing tip angle. Two high deviations were observed in this result. These points were 120º and the control measurement at the 210º.

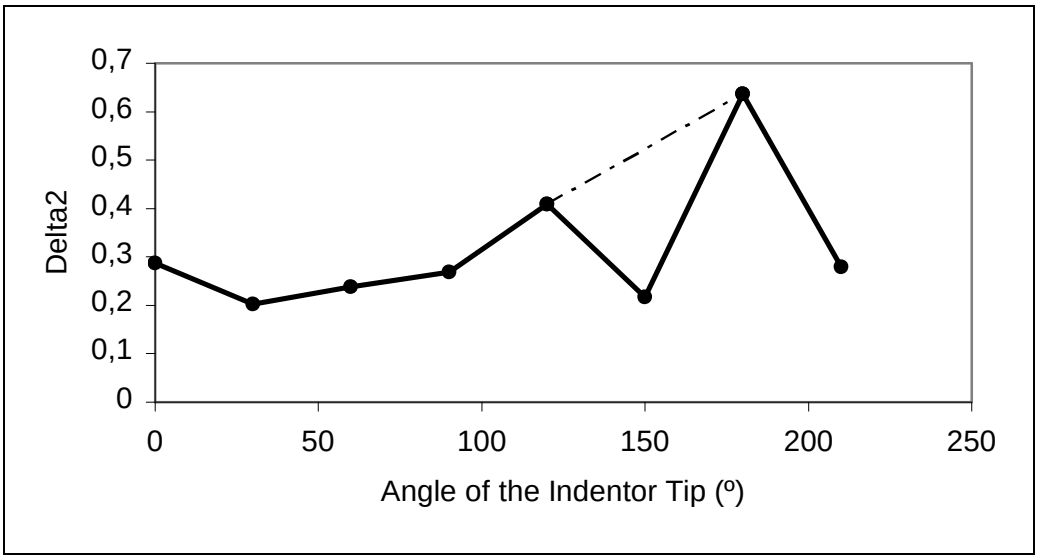

Figure 4.53 Angle of the indenter tip versus δ_2 graph

The results for the long term relaxation magnitude showed a parallel result with the short term relaxation magnitude. Only the sign of the values were positive. Other then the sign, the general characteristic of δ_2 were observed same with δ_1.

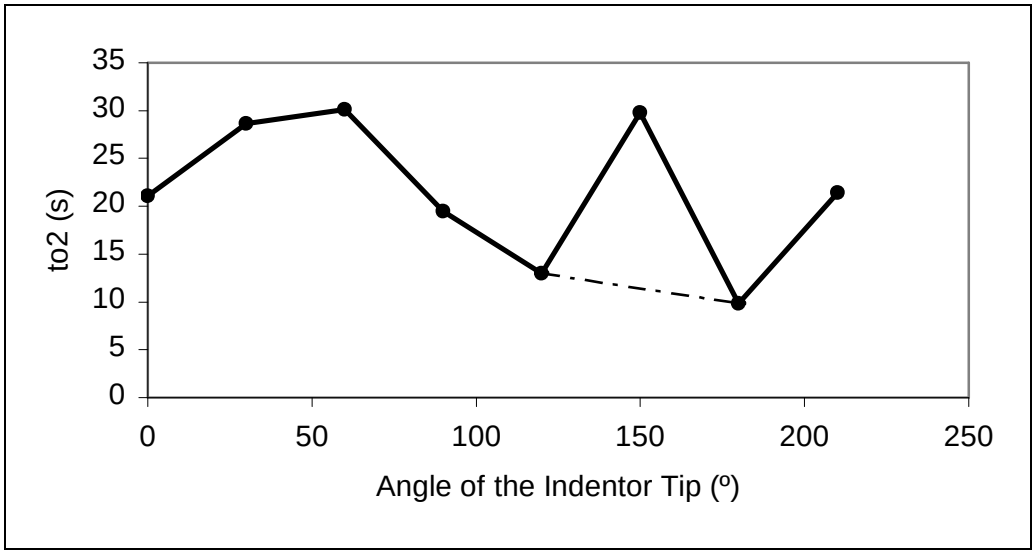

Figure 4.54 Angle of the indenter tip versus τ_2 graph

Unlike the short term relaxation time constant, long term time constant τ_2 showed similar characteristic with the increased tip angle as observed in Figure 4.51 and Figure 4.53.

In conclusion, it was not able to see a pure observation about anisotropy as it was for the force dependent anisotropy research given in Figure 4.49 and Figure 4.50. On the other hand, it was still observed trends especially in the Figures 4.51, 4.53 and 4.54. Also, it was obtained parallel results for these figures.

Table 4.10 Coefficients for the relaxation tests

Angles of the Indenter Tip (º)	δ_1	τ_1 (s)	δ_2	τ_2 (s)	R-Square
0	-0,11672	0,54357	0,2873	21,107	0,96657
30	-0,05208	0,58054	0,20246	28,634	0,97232
60	-0,04918	0,5419	0,23865	30,146	0,98301
0	-0,10974	0,56943	0,26826	19,454	0,95771
120	-0,26395	0,87049	0,40823	12,965	0,98165
150	-0,03967	0,57082	0,21676	29,749	0,94956
180	-0,50647	0,52973	0,63635	9,8382	0,90638
210	-0,10914	0,67428	0,27956	21,388	0,95355

4.7.2.2.2.2 Graphs Pertinent To the Test Results Given in Figure 4.50

Below the coefficient (Table 4.11) graphs pertinent to test results given in Figure 4.50 can be seen.

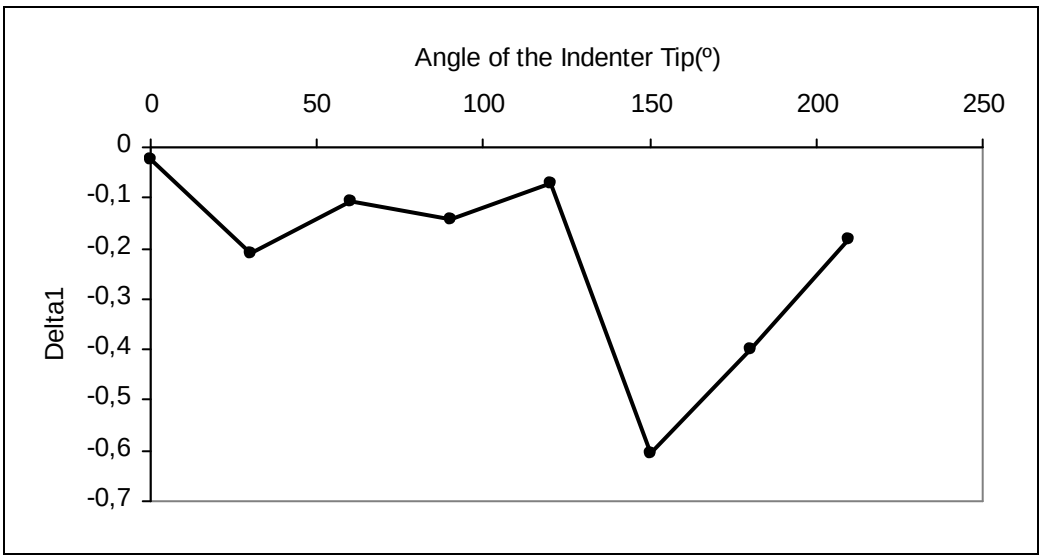

Figure 4.55 Angle of the indenter tip versus δ_1 graph

The result obtained for the short term relaxation magnitude was given in Figure 4.55. There was no regular trend observed for the δ_1 unlike the previous study. Consequently, it was not possible to make an inference about anisotropy for the δ_1 values.

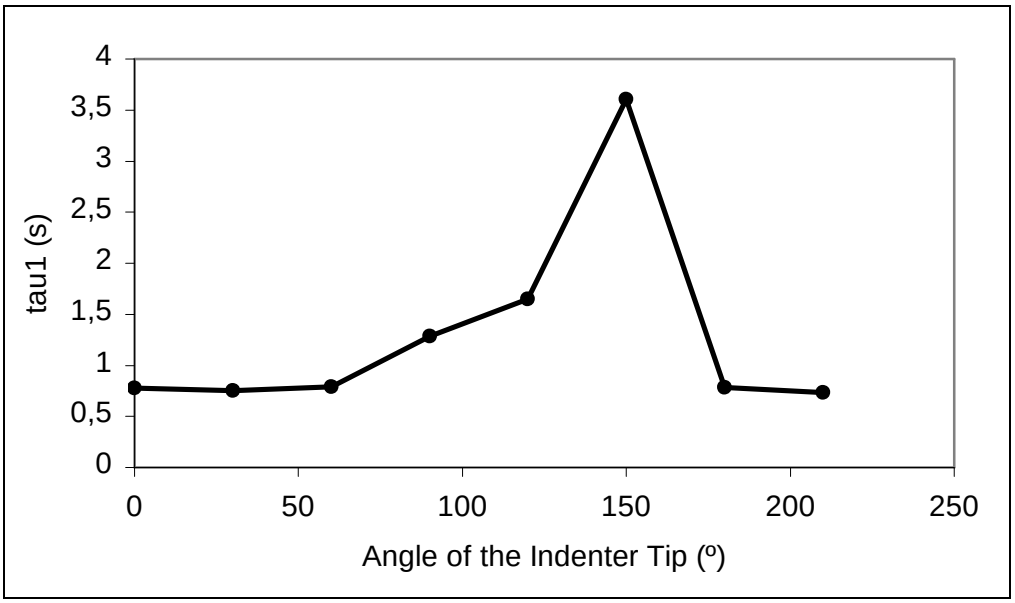

Figure 4.56 Angle of the indenter tip versus τ_1 graph

Short term time constants were showed barely same character with the results given in Figure 4.52. However, for the angles started from 90º and ended with 150º was showed an increase gradually. After the angle 150º similar values was obtained for τ_1 with the beginning angles. Thus, if the results given in Figure 4.52 were also considered, it could have been concluded that τ_1 took values the 0.77 s with the increasing tip angle.

Figure 4.57 Angle of the indenter tip versus δ_2 graph

The result obtained for the long term relaxation magnitude was given in Figure 4.57. A similar observation was made for δ_2 with the result given in Figure 4.55. On the other hand, there was no trend obtained with the increasing indenter tip angle.

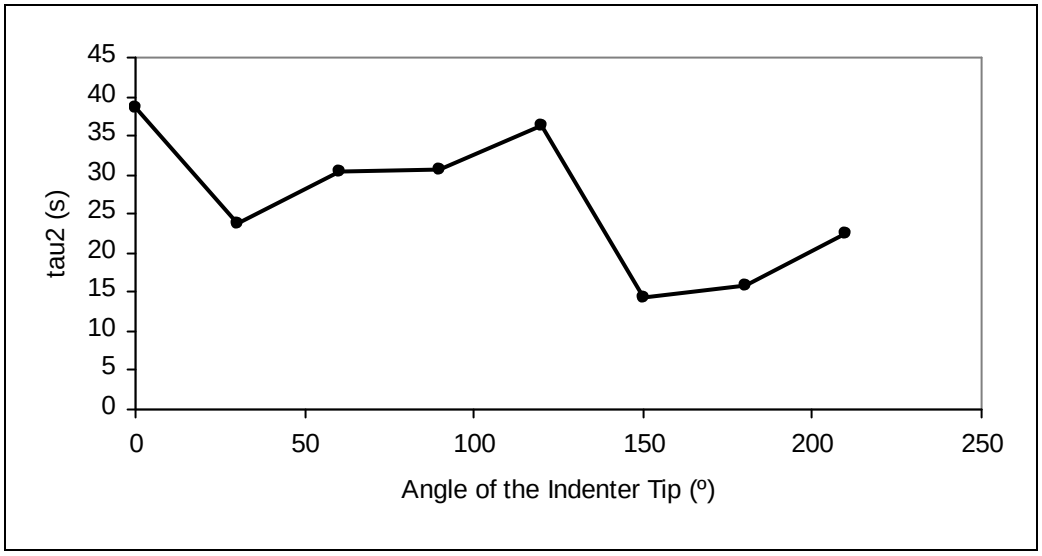

Figure 4.58 Angle of the indenter tip versus τ_2 graph

The result obtained for the long term relaxation time constant was given in Figure 4.58. Like the other given results for the coefficients, it was not possible to say about the changes of the τ_2 with the increasing indenter tip angle. On the other hand, with the careful looking, W shaped appearance could have been observed between the angles 0º and 180º. If the deviation appeared at 120º was not considered, this shape was more comprehensible. However, this is a bit enforcement conclusion, and at this point it is better to aware of such a conclusion.

Because of the characteristic of the experimental measurements, the results obtained for the coefficients of the related Prony series did not show a clear result about the tissue anisotropy. The results given in Chapter 4.7.2.2.2.2 showed better behavior related to the tissue anisotropy. This result can also be seen from the anisotropy results pertinent to the force magnitudes. It was observed a deviation at 150º from the general trend in Figure 4.50.

Table 4.11 Coefficients for the relaxation tests

Angles of the Indenter Tip (º)	δ_1	τ_1 (s)	δ_2	τ_2 (s)	R-Square
0	-0,02428	0,77957	0,20978	38,664	0,92778
30	-0,20779	0,75047	0,37282	23,66	0,98695
60	-0,10534	0,79106	0,284	30,462	0,98047
90	-0,14111	1,2877	0,35818	30,796	0,98541
120	-0,07176	1,6498	0,28154	36,377	0,98204
150	-0,60429	3,6038	0,77677	14,443	0,95864
180	-0,40114	0,7828	0,57358	15,959	0,96663
210	-0,18074	0,73348	0,34259	22,553	0,97557

4.7.2.3 Examination of the Tissue Anisotropy Related to the Creep Behavior

For the examination of the tissue anisotropy in relation to the creep behavior, as in relaxation case, 7 successive tests with 30º interval increases between 0º and 180º angles, were carried out. Motor speed of 1 mm/s, creep duration of 120 seconds and target force of 5 N were used.

4.7.2.3.1 Observed Anisotropy Related to the Displacement Values at the End of the Relaxation Time

For the observation of the tissue anisotropy related to the creep behavior, displacement amounts at the end of the creep duration were determined for each test and the displacement – indenter angle graphs were drawn (Figure 4.59).

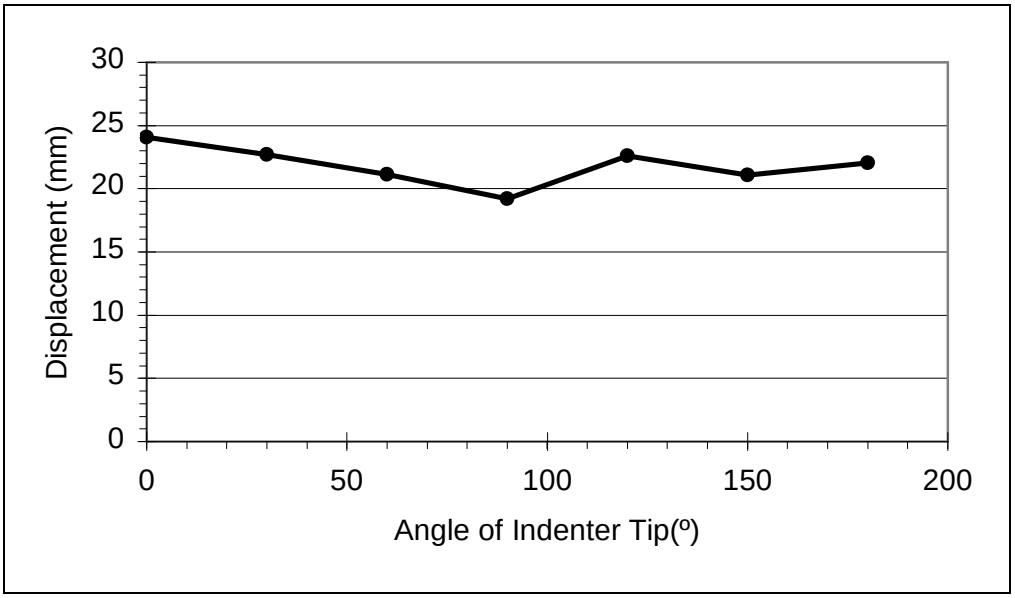

Figure 4.59 Anisotropic behavior observed, in relation to the creep behavior

As can be noted from Figure 4.59, result obtained is consistent with the situation observed in the cyclic loading and relaxation behaviors. Tissue behaved stiffer around 90º, and in consequence, the target force was reached in a shorter distance. Again, the stiffness of the tissue progressively decreased from 90º to

180º. At 120º, a small deviation in the obtained data was encountered. As discussed in the previous sections, this deviation may be attributed to the changes in the tonus of the muscle.

4.7.2.3.2 Examining the Creep Dependent Anisotropy Behavior by Using the Prony Series

A second observation related to anisotropy pertinent to creep tests were made by using Prony series (Equation 4.11-c). Relevant constants were determined by using the test data and the graphs incorporating the variations of these constants in relation to the tip angles were drawn.

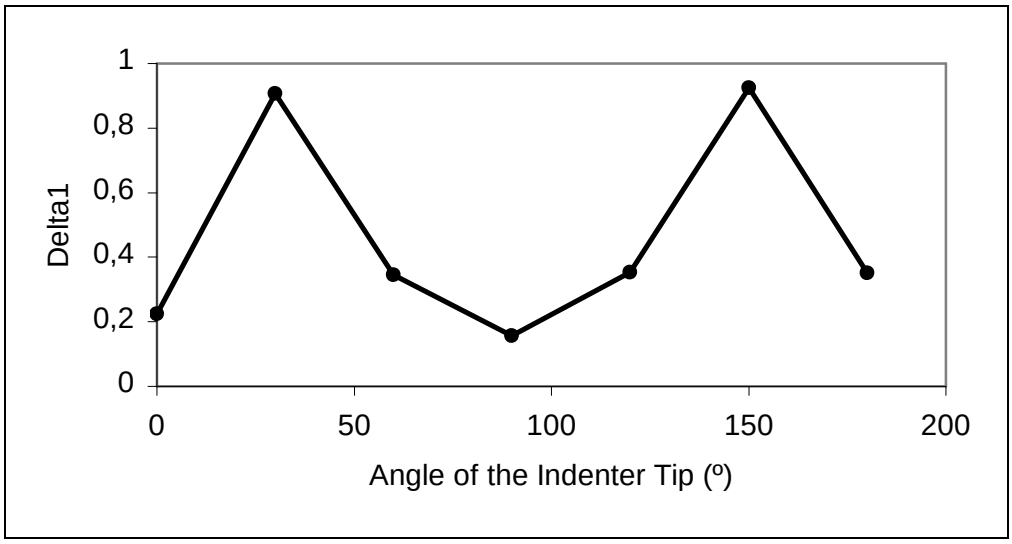

Figure 4.60 Angle of the indenter tip versus δ_1 graph

The result obtained for the short term creep magnitude was given in Figure 4.60. As it can be seen from the Figure 4.60, an M shaped behavior related to tissue anisotropy was obtained.

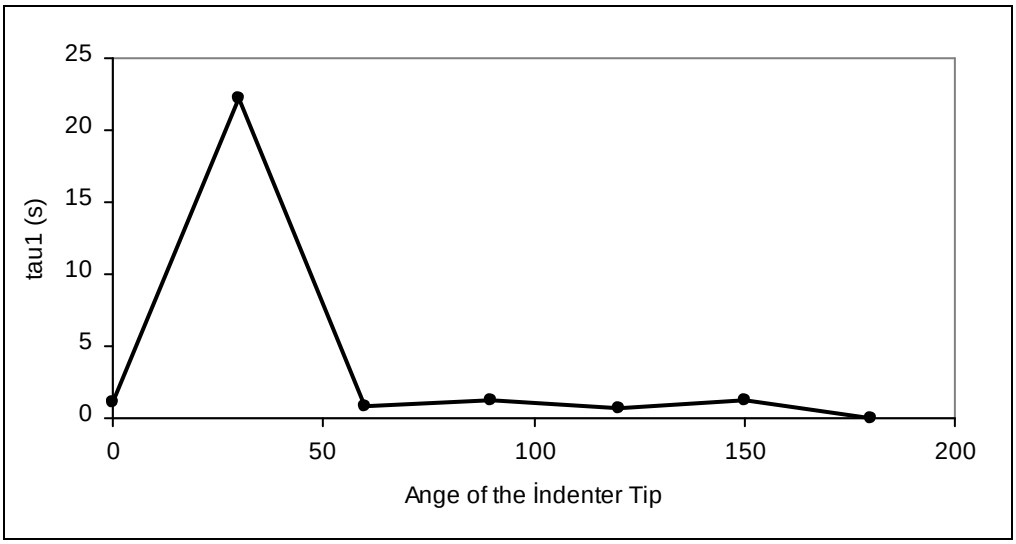

Figure 4.61 Angle of the indenter tip versus τ_1 graph

Changing of the short term time constant with the increasing indenter tip angle was given in the Figure 4.61. As it can be seen from the Figure 4.61, it was not observed a proper changing depending on the tissue anisotropy with the increasing indenter tip angle. This was mainly due to the high deviation in the values of the coefficients pertinent to the angles 30º and 180º from the other coeffecients (Table 4.12).

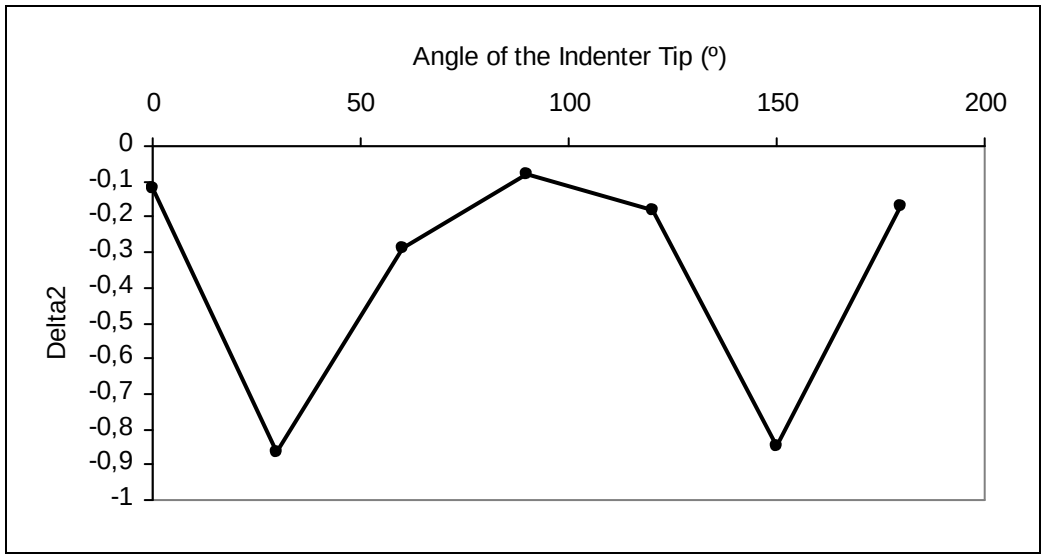

Figure 4.62 Angle of the indenter tip versus δ_2 graph

The results for the long term relaxation magnitude showed a parallel result with the short term relaxation magnitude. Only the sign of the values were positive. Other then the sign, the general characteristic of δ_2 were observed same with δ_1.

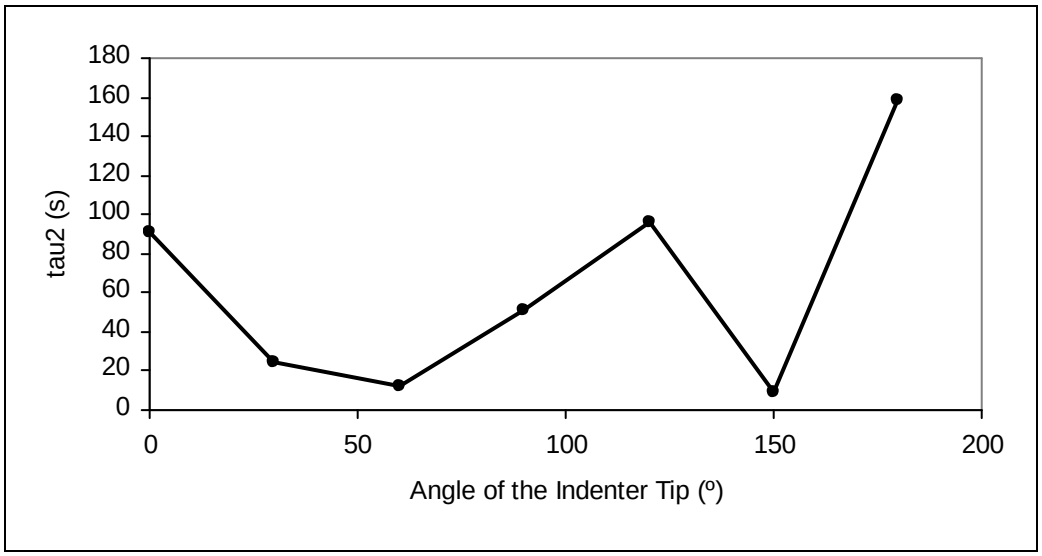

Figure 4.63 Angle of the indenter tip versus τ_2 graph

Result obtained for the long term creep time constant was given in the Figure 4.63. As it can be seen from the Figure 4.63, a decrease was obtained between the angles 0º and 60º after this point τ_2 values was increased gradually except the value at 150º.

Table 4.12 Coefficients for the creep tests

Angles of the Indenter Tip (º)	δ_1	τ_1 (s)	δ_2	τ_2 (s)	R-Square
0	0,22423	1,1524	-0,1205	90,523	0,98109
30	0,9077	22,213	-0,86563	24,919	0,80003
60	0,34436	0,8466	-0,28794	11,94	0,7781
90	0,15724	1,3007	-0,07952	51,172	0,9177
120	0,35278	0,73646	-0,18009	96,432	0,95432
150	0,92546	1,1843	-0,84652	9,2868	0,88219
180	0,35189	3,68E-09	-0,17097	158,5	0,92629

CHAPTER 5

DISCUSSION AND CONCLUSION

5.1 Summary

Study basically consisted of two phases. In the first phase of the study, for conducting dependable and precise experiments, improvements in the existing test system were achieved. In the second phase of the study, by using this improved test device, to observe the soft biological tissue behaviors under various conditions, systematic experiments were carried out.

In the first phase, two basic points were inquired. These may be set forth as the improvement of the movement precision of the indenter tip and improvement of the load measurement precision. As a result of the efforts made, both precision were substantially improved. Deviations displayed by the indenter tip was within the range of 0.05 mm to 4.42 mm before the study and this deviations were drawn back to the range of -0.11 mm to +0.12 mm. the force data, on the other hand, was confined to the range of -0.25 N to + 0.43 N and it was observed that, the average deviation remained at + 0.19 N as a result of the efforts given in this study.

Again, the works carried out in this study are presented item by item below.

- A new connection system, for achieving smooth and correct measurements, was developed
- A filtering procedure was developed to clean the noisy data
- A Matlab code to determine the point of contact of the indenter tip with the tissue, and to discard the data just before this point was formulized.

- Also, Matlab codes serving different goals and rendering considerable time conservations were prepared.

- Necessary arrangements for the simultaneous commencement of the force data collection and the indentor's tip movement were made

In the second phase of the study, cyclic loading, relaxation and creep tests on the forearm were carried out. In order to observe the anisotropic behavior of the tissue, ellipsoid tips which provided measurements in different angles, were designed and produced. With the tips prepared, anisotropy experiments on the tissue were conducted. By using the relaxation and creep data, constants of the Prony series capable of modelling these data were determined and the Prony series of different forms were compared. Anisotropic response of the tissue was examined by utilizing the constants found for the Prony series.

Now, let us consider the results obtained in the second phase, in more detail.

5.2 Results and Discussion

The most fundamental observation made at the end of the experiments was the non linear behavior displayed by the tissues. In other words, it was observed that, hysteresis developed at the cyclic loading, stress decreased under constant strain, that is, relaxation, and the strain increased under constant stress, that is the creep. Again, under cyclic loading, tissue has displayed the preconditioning (Mullin's) effect. It was contemplated that, this phenomena was not always observable and it was seen more clearly in the healthy physiologies with better conditions. Another important conclusion derived with regard to the preconditioning effect was that, the preconditioning effect related to the hysteresis magnitudes was more clearly obtainable. Preconditioning effect was not observed amply in the force – time graphs. This was origined from the fact that, test were carried out in –vivo and therefore, the force data was influenced greatly from the muscle movements. Yet, in the scrutinizes made with the hysteresis magnitudes, this sensitivity was found to be much less critical.

Another study on the soft biological tissues was carried out to observe the effect of speed on the tissue behavior. In this context, the response force displayed by the tissue and the hysteresis magnitudes, as just like in the preconditioning effect, were examined separately. The result was that of the preconditioning effect. That is, a clear conclusion was not attainable in the investigation of the effect of speed on the tissue, by just looking at the force magnitudes. Yet, it was observed that, the hysteresis magnitudes increased almost linearly with the rising speed. Here, the important point was that, this increase in hysteresis occurred independently from the variations in force. In other words, hysteresis displayed an increase tendency with the rising speed independent of the force which might have been lower or higher in a low speed in the measurements of the same group.

In the in-vivo experiments, where the realistical behavior of the tissue is best followed, it is anticipated that, observing the impact of preconditioning effect and speed in relation to the hysteresis magnitudes is two very important conclusions. In simulations where the impact of the preconditioning effect and speed will be considered, it will be safer and more correct to use the results pertinent to the hysteresis magnitudes.

In this study, anisotropic behaviors of the soft biological tissues were also examined. When the anisotropic response of the tissue were investigated, separate evaluations were carried out for the cyclic loading, relaxation and creep tests and results in parallel with each other were obtained. According to these results, as the angle between the long axis of the ellipsoid tip and the contraction direction of the muscle increases, the resistance of the tissue increased and reached its maximum at 90º angle in between. This behavior showed a periodical character and it tended to decrease again in the interval starting from 90 º and ending with 180º.

The last observation made in the study was realized by determining the constants of the Prony series, capable of modelling the relaxation and creep experimental

data obtained. In the modelling, Prony series in various forms were used and they were compared among each other. Best results were obtained for the Prony series with three terms, given in Equation 4.11-d. Yet, the constants obtained for this form, could have displayed unstable behaviors. Best results with regard to the stability, were obtained for the Prony series with two term, given in Equation 4.11-c. additionally, by using these coefficients pertaining to the relaxation and creep data, anisotropic behavior was examined. Yet, by utilizing these constants, a clear-cut result was not obtained. Therefore, in the in-vivo experiments, examination of the anisotropic behavior was better to be achieved by observing the force data.

In conclusion, with the experiments carried out, behaviors of the soft biological tissue were investigated in detail. Besides this, behaviors of the soft biological tissues were better understood. Application of the results obtained in these studies, to the simulations particular to the computer environment, will make the observing of the soft biological tissue behaviors in imaginary medium with mush better and more realistical outcomes.

5.3 Future Works

Test system is deficient with regard to its hardware. The most components belong to hardware of experiment system was taken in the years 2001-2002. The communication between the computer and control unit has been providing through the port USB 1.1. The maximum data transfer rate via this port can be 12 Mbits/second (Chiu and DeVercelly, 2006).

These deficiencies in the experiment system, caused to happen problems especially when added some new experiment protocols. Particularly, they were caused not to work properly the force controlled test protocols or collecting missing data. If it is necessary to give an example, in relaxation experiments, in order to be started the beginning of relaxation as linked to the target force, it was studied to prepare a Matlab code. But, in order to be the relaxation experiment done in an ideal way, the prepared code, was caused to problems during

apparatus working. Therefore, the codes were modified in order to make the apparatus working properly. Yet, this caused to loss of experiment data and, the observations were not done in required characteristics, either. A similar problem, was faced during preparing codes for the cyclic loading experiment linked to target force.

Also, this deficiency sometimes results with problems arising during the experiments. This, in consequence, results with time loss and in certain cases, becomes deteriorating for the testes individual and the conductor of the tests, due to the long lasting efforts spent. Further to that, the performance of the test protocols needed to be annexed may be impaired due to this deficiency.

Therefore, in this context, by changing the hardware components and fittings other than the test unit itself, much better experiments and different observations will be possible to be achieved.

REFERENCES

Alexander, H., Cook, T. H., 1977. Accounting for natural tension in the mechanical resting of human skin. The Journal of Investigative Dermatology 69, 310-314

Bischoff, J. E., 2004. Static Indentation of Anisotropic Biomaterials Using Axially Asymmetric Indenters-a Computational Study. Journal of Biomechanical Engineering 126, 498-505

Bönniger, M., 1905. Die elastische Spannung der Haut und deren Beziehung zum Oedem. Ztschr. F. Exper. Path. U. Therapie 1, 163-183

Chapra S. C., Canale, R. P., 1998. Numerical Methods for Engineering. McGraw Hill, 3th ed., Singapore.

Chiu, I., DeVercelly, W., last revision date: 31/08/2006. USB 2.0, Hi Speed USB FAQ. http://www.everythingusb.com/usb2/faq.htm, last accessed date: 25/09/2008

Choi, A. P. C., Zheng, Y. P., 2005. Estimation of Young's modulus and Poisson's ratio of soft tissue from indentation using two different sized indenters : finite element analysis of the finite deformation effect. Medical & Biological Engineering & Computing 43, 258-264.

DiSilvestro, M. R., Suh, J. F., 2001. A cross-validation of the biphasic poroviscoelastic model of articular cartilage in unconfined compression, indentation, and confined compression. Journal of Biomechanics 34, 519-525

Felmlee, J.P., Greenleaf, J.F., Ehman, R.L., 2001. Magnetic resonance elastography: Non invasive mapping of tissue elasticity. Medical Image Analysis, Vol.5, pp.237-254

Fox, S. I., 1992. Human Physiology. McGraw-Hill, 4th ed., Iowa.

Fung, Y. C., Zweifach, B. W., Intaglietta, M., 1966. Elastic environment of capillary bed. Circulation Research 19, 441-461.

Fung, Y. C., 1984. Structure and Stress-Strain Relationship pf Soft Tissues. American Zoologist 24, 13-22.

Fung, Y. C., 1993. Biomechanics: Mechanical Properties of Living Tissues. Springer-Verlag, 2nd ed., New York.

Gefen, A., Megido-Ravid, M., Azariah, M., Itzchak, Y., Arcan, M., 2001. Integration of Plantar Soft Tissue Stiffness Meausurements in Routine MRI of the Diabetic Foot. Clinical Biomechanics 16, 921-925.

Gefen, A., Margulies, S. S., 2003. Are in vivo and in situ brain tissues mechanically similar? Journal of Biomechanics 37, 1339-1352

Geyer, M. J., Brienz, D. M., Chib, V., Wang, J., 2004. Quantifying Fibrosis in Venous Disease: Mechanical Properties of Lipodermatosclerotic and Healthy Tissue. Advances Skin & Wound Care 17, 131-142.

Hibbeler, Y. C., 1999. Mechanics of Materials. Prentice Hall, 4th ed., New Jersey.

Holt, B. et al., 2008. Viscoelastic response of human skin to low magnitude physiologically relevant shear. Journal of Biomechanics, doi: 10.1016/j.jbiomech.2008.06.008

Kawchuk, G. N., Liddle, T. R., Fauvel, O. R., Johnston, C., 2006. The Accuracy of Ultrasonic Indentatıon in Detecting Simulated Bone Displacement: A Comparıson of Three Techniques. Journal of Manipulative and Physiological Therapeutics 29-2, 126-133

Kirk, E., Kvorning, S. A., 1949. Quantitative Measurements of the Elastic Properties of the Skin and Subcutaneous Tissue in Young and Old Individuals. Journals of Gerontology 4, 273-284.

Kiss, Z. K., Varghese, T., Hall, T. J., 2004. Viscoelastic characterization of in vitro canine tissue. Physics in Medicine and Biology 49, 4207-4218.

Korhonen, R. K., Saarakkala, S., Töyräs, J., Laasanen, M. S., Kiviranta, I., Jurvelin, J. S., 2003. Experimental and numerical validation fort he novel configuration of an arthroscopic indentation instrument. Physics in Medicine and Biology 48, 1565-1576.

Kroon, M., Holzapfel, G. A., 2008. A new constitutive model for multi-layered collagenous tissues. Journal of Biomechanics, doi: 10.1016/j.jbiomech.2008.05.033

Lawrence, A.J., Rossman, P.J., Mahowald, J.L., Manduca, A., Hartmann, L.C., Ehman, R.L., 1999. Palpating Breast Cancer by Magnetic Resonance Elastography. Proceedings of the 7th Annual Meeting of ISMRM, Philadelphia, 215.

Manduca, A., Oliphant, T.E., Dresner, M.A., Mahowald, J.L., Kruse, S.A., Amromin, E., Felmlee, J.P., Greenleaf, J.F., Ehman, R.L., 2001. Magnetic resonance elastography: Non-invasive mapping of tissue elasticity. Medical Image Analysis 5, 237–254.

Maurel, W., Wu, Y., Thalman, N. M., Thalman, D., 1998. Biomechanical Models for Soft Tissue Simulation. Springer, Germany.

Miller, K., 2000. How to test very soft biological tissues in extension? Journal of Biomechanics 34, 651-657.

Miller, K., Chinzei, K., 2002. Mechanical properties of brain tissue in tension. Journal of Biomechanics 35, 483-490

Miller-Young, J. E., Duncan, N. A., Baroud, G., 2002. Material properties of the human calcaneal fat pad in compression: experiment and theory. Journal of Biomechanics 35, 1523-1531

Moisy, F., 2008. ezyfit-A free curve fitting toolbox for Matlab. http://www.fast.u-psud.fr/ezyfit/, last accessed date: 19/09/2008.

Ottensmeyer, M. P., 2002. "In Vivo Measurement of Solid Organ Tissue Mechanical Properties," Studies in Health Technolgy and Informatics 85, 328-333.

Ottensmeyer, M. P., Kerdok, A. E., Howe, R. D., Dawson, S. L., 2004. The Effects of Testing Environment on the Viscoelastic Properties of Soft Tissues. International Symposium on Medical Simulation, 9-18.

Payne, P. A., 1991. Measurement of Properties and Function of Skin. Clinical Physics and Physiological Measurement 12(2), 105-129

Peña, E., et al., 2008. On modelling nonlinear viscoelastic effects in …. Journal of Biomechanics, doi: 10.1016/j.jbiomech.2008.06.019

Planar-Biaxial Soft Tissue Test System, 2004, http://www.instron.com.tr/wa/library/streamfile.aspx?doc=527, last accessed date: 19/09/2008.

Prete, Z. D., Antoniucci, S.,Hoffman, A. H.,Grigg, P., 2004. Viscoelastic properties of skin in Mov-13 and Tsk mice. Journal of Biomechanics 37, 1491-1497

Provenzano, P., Lakes, R., Keenan, T., Vanderby, R. Jr., 2001. Nonlinear ligament viscoelasticity. Annals of Biomedical Engineering 29, 908-914.

Rousseaou, J. M., 1999. Matlab central file exchange-uifit. http://www.mathworks.com/matlabcentral/fileexchange/loadFile.do?objectId=138&objectType=FILE, last accessed date: 19/09/2008.

Rubin, M. B., Bodner, S.R., 2002. A three - dimensional nonlinear model for dissipative response of soft tissue. International Journal of Solids and Structures 39, 5081-5099.

Sokolof, L., 1966. Elasticity of aging cartilage. Federation Proceedings 25, 1089-1095

Suha, J. F., Youna, I., Fub, F. H., 2001. An in situ calibration of an ultrasound transducer: a potential application for an ultrasonic indentation test of articular cartilage. Journal of Biomechanics34, 1347-1353

Tanaka , E., Tanaka, M., Aoyamaa, J., Watanabe, M., Hattori, Y., Asai, D., Iwabea, T., Sasaki, A., Sugiyama, M., Tane, K., 2002. Viscoelastic properties and residual strain in a tensile creep test on bovine temporomandibular articular discs. Archives of Oral Biology 47, 139–146

The MathWorks, 2008. Data Acquisition Toolbox. http://www.mathworks.com/access/helpdesk/help/toolbox/daq/index.html?/access/helpdesk/help/toolbox/daq/f5-32960.html&http://www.mathworks.com/cgi-bin/texis/webinator/search/?db=MSS&prox=page&rorder=750&rprox=750&rdfreq=500&rwfreq=500&rlead=250&sufs=0&order=r&is_summary_on=1&query=quantization+%22daq%22&query1=quantization&ResultCount=10&query2=%22daq%22&query3=&notq=, last accessed date: 19/09/2008.

Tönük, E., 2004. Dizaltı Protez Kullananlarda Yumuşak Doku Mekanik Özelliklerinin Belirlenmesi İçin İndentor. Project Result Report, project no: MİSAG-183. Makina, Kimyasal Teknolojiler, Malzeme ve İmalat Sistemleri Araştırma Grubu, TÜBİTAK.

Tönük, E., Silver-Thorn, M. B., 2004. Nonlinear viscoelastic material property estimation of lower extremity residual limb tissues. Journal of Biomechanical Engineering 126, 289-300.

Üsü, K., 2008. Identification of Soft Tissue Mechanical Material Model and Corresponding Parameters from In Vivo Experimental Data by Using Inverse Finite Element Method. M.Sc. thesis, Middle East Technical University, Ankara, Turkey.

Üsü, K., Tönük, E., 2008. Yumuşak Doku Bünye Denklemleri II: Geliştirilmiş Sanki-Doğrusal Viskoelastik Model. BİYOMUT 2008

Valtorta, D., Mozza, E., 2005. Dynamic measurement of soft tissue viscoelastic properties with a tensional resonator device. Medical Image Analysis 9, 481-490

Yin, Y., Ling, S., Liu, Y., 2004. A dynamic indentation method for characterizing soft incompressible viscoelastic materials. Materials Science and Engineering 379, 334-340.

Zhang, W., Chen, H. Y., Kassab, G. S., 2007. A rate – insensitive linear viscoelastic model for soft tissues. Biomaterials 28, 3579-3586.

Zheng Y. P., Mak A. F. T., Lue B. K., 1999. Objective assessment of limb tissue elasticity: development of a manual indentation procedure. Journal of Rehabilitation Research and Development 36, 71-85.

APPENDIX A

INDENTOR DEVICE MOVEMENT SENSITIVITY TEST RESULTS

Below, results of the tests carried out for the improvement of the movement precision of the indentor device as described in Chapter 3, are given

A.1 Entered Distance – Measured Distance Graphs for the Forward Movement

Below, test results showing the entered distance for the indentor tip forward movement versus the distance measured by dial gage are presented.

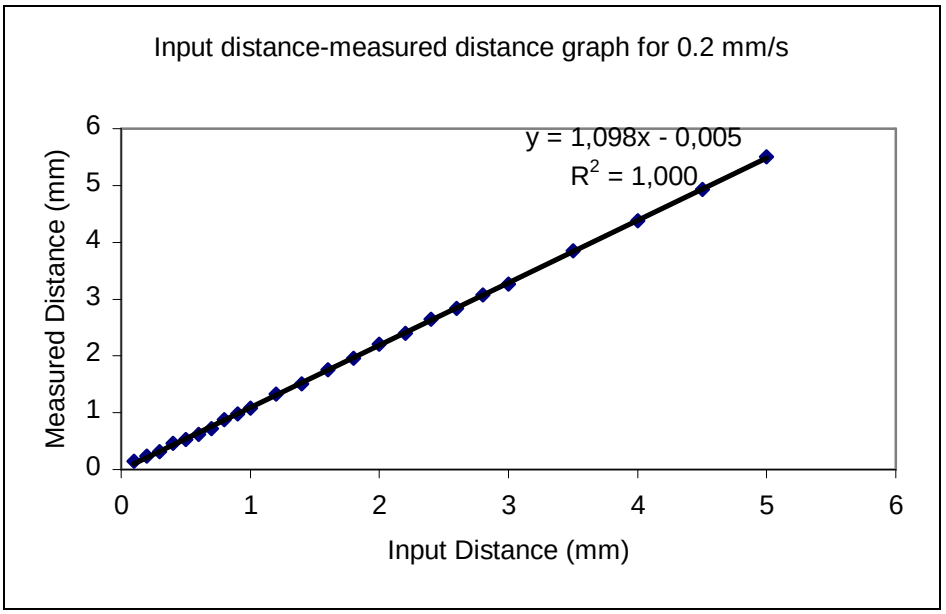

Figure A.1 Input distance versus measured distance graph for 0.2 mm/s

As it can be seen from the graph, it was obtained a linear relationship between the entered distance and measured distance for the 0.2 mm/s motor speed.

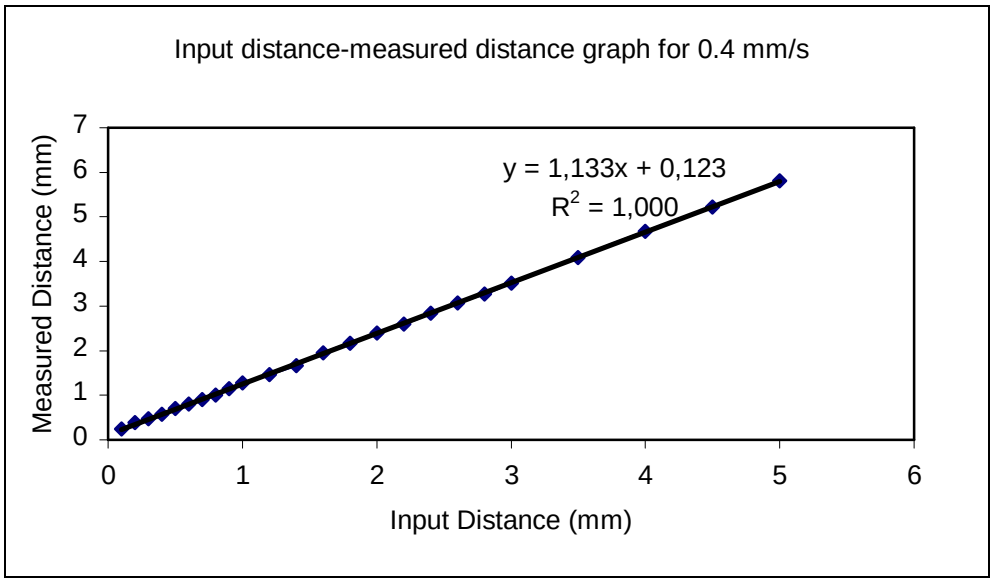

Figure A.2 Input distance versus measured distance graph for 0.4 mm/s

Similar result was also obtained for the 0.4 motor speed. It was obtained a linear relationship between the input distance and measured distance.

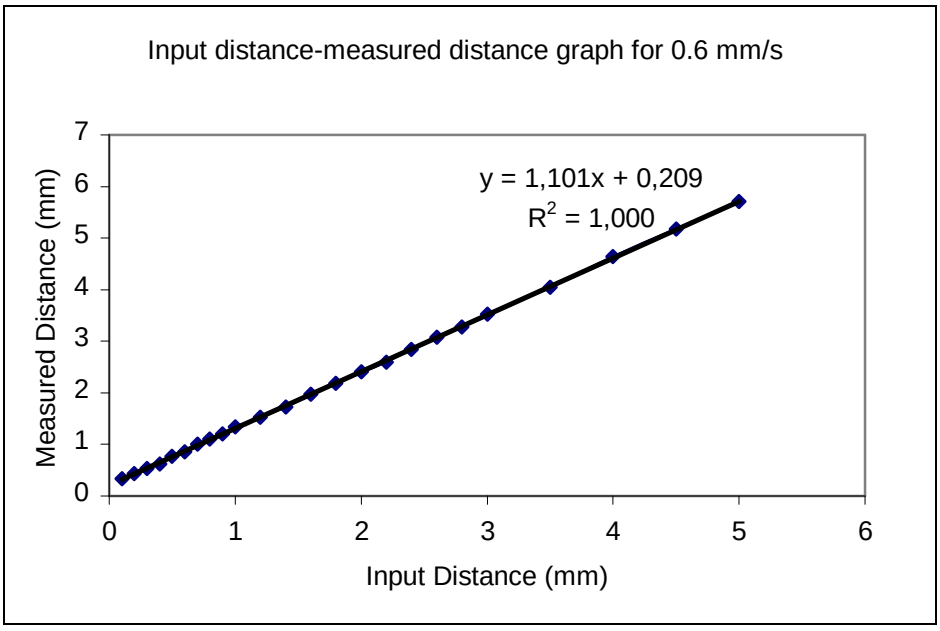

Figure A.3 Input distance versus measured distance graph for 0.6 mm/s

It was obtained a linear relationship for the 0.6 mm/s motor speed. Also, it was observed that the measured points were very close the trend line for the mentioned three graphs.

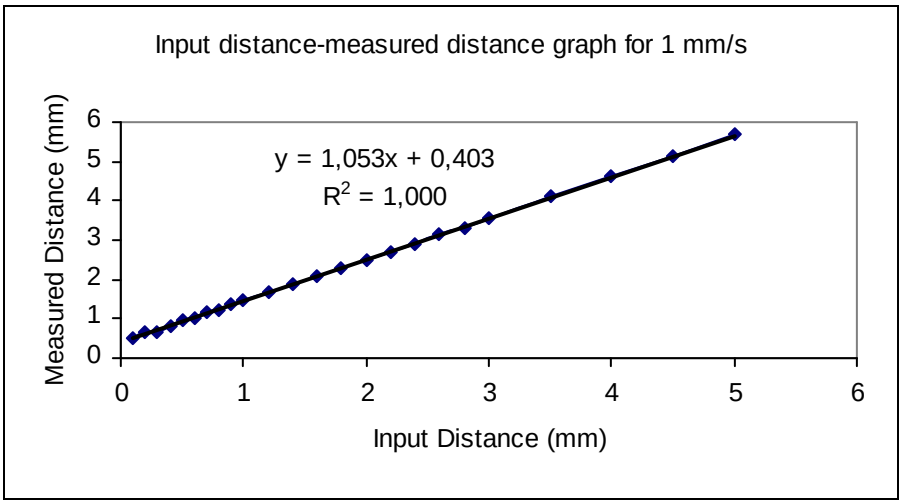

Figure A.4 Input distance versus measured distance graph for 1 mm/s

Although it was obtained a linear relationship between the input distance and measured distance, it was observed some minor deviations from the trend line especially for the distances below 1 mm input distance. On the other hand, it was obtained r-square value as 1.

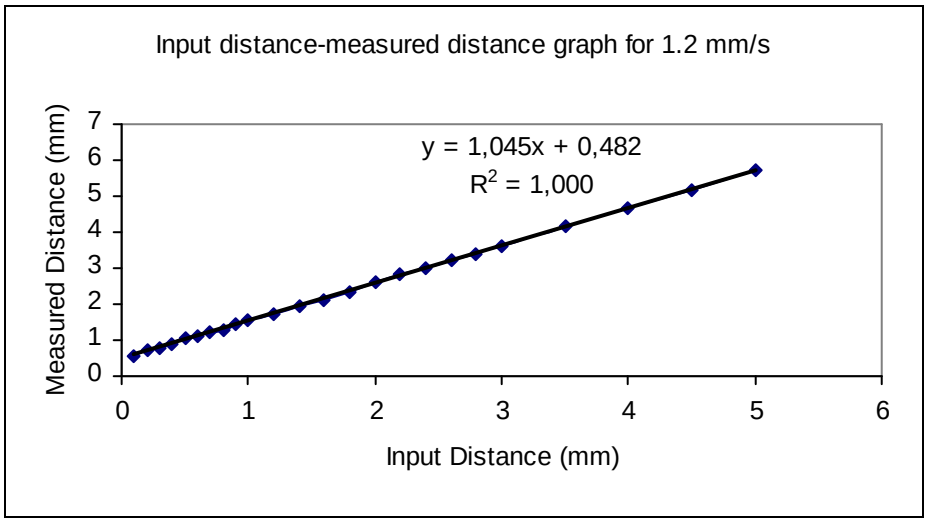

Figure A.5 Input distance versus measured distance graph for 1.2 mm/s

The graph obtained for 1.2 mm/s had same characteristic with the graph obtained for 1 mm/s.

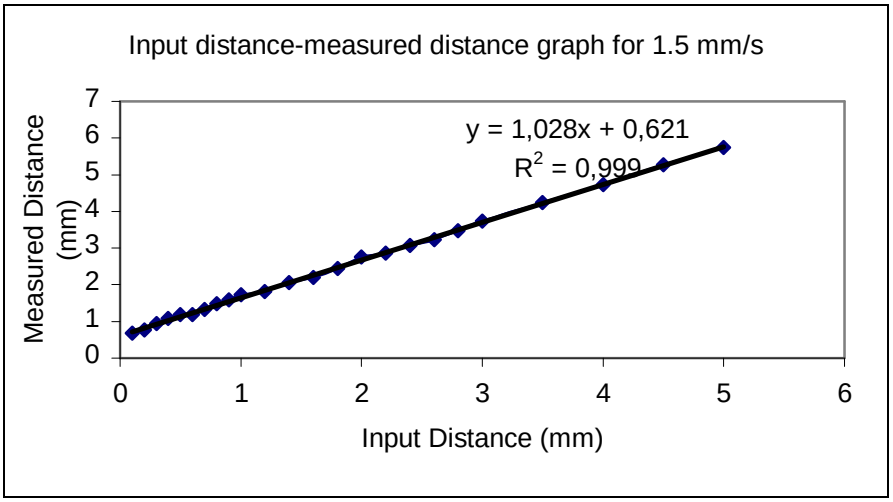

Figure A.6 Input distance versus measured distance graph for 1.5 mm/s

For the 1.5 mm/s it is observed that the input distances 0.5 and 0.6 mm was showed a clear quantization error. However, it was still obtained a linear relation between the input and measured distances.

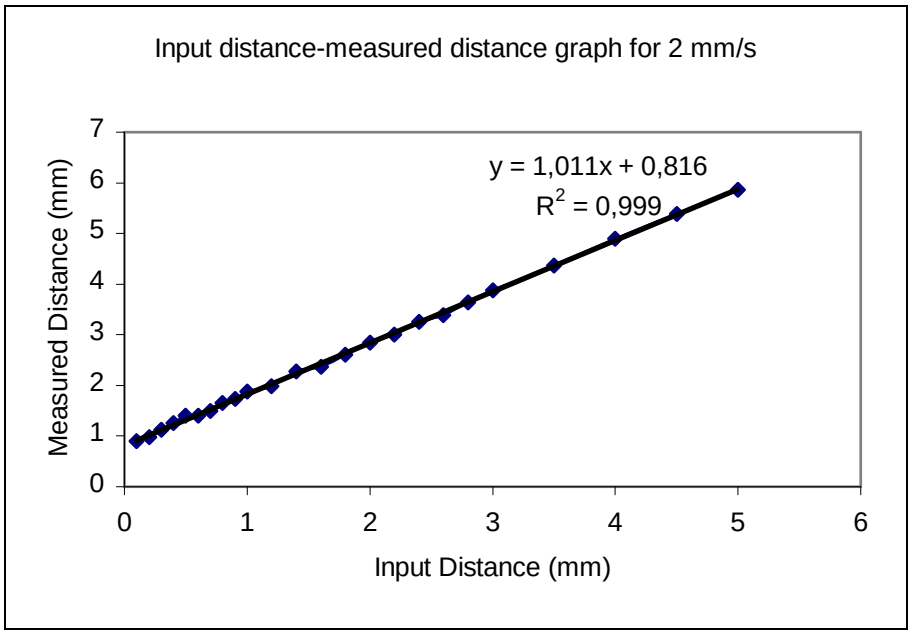

Figure A.7 Input distance versus measured distance graph for 2 mm/s

The same characteristic was observed for the motor speed 2 mm/s as mentioned for the 1.5 mm/s motor speed.

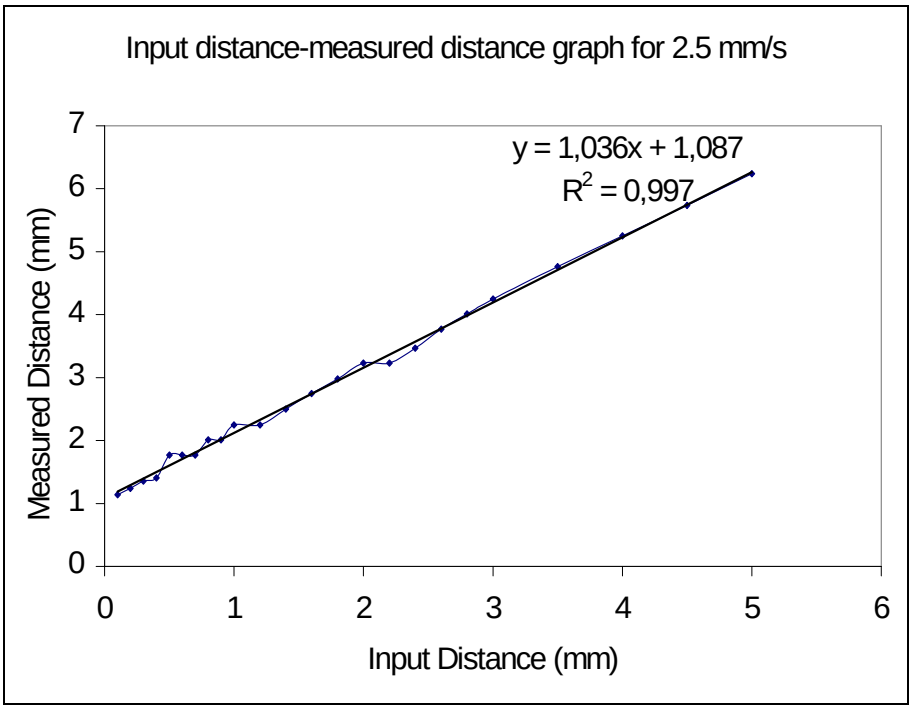

Figure A.8 Input distance versus measured distance graph for 2.5 mm/s

For the 2.5 mm/s motor speed, it was observed a clear quantization error. These errors were appeared at 0.5, 0.6, 0.7 mm as first group, 0.8, 0.9 mm as second group, 1, 1.2 mm as third group and 2, 2.2 mm as fourth group. It can be seen the same characteristics and errors at the speeds 3, 3.5, 4 and 4.5 mm/s from the following graphs.

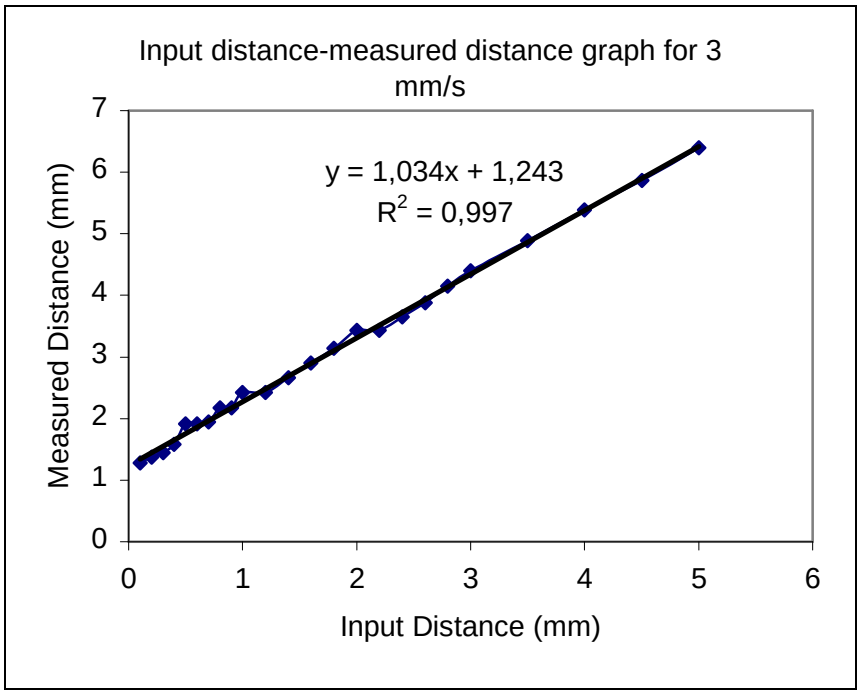

Figure A.9 Input distance versus measured distance graph for 3 mm/s

For the motor speed 3 mm/s, it was obtained a quantization error showing same characteristic with data obtained for 2.5 mm/s motor speed.

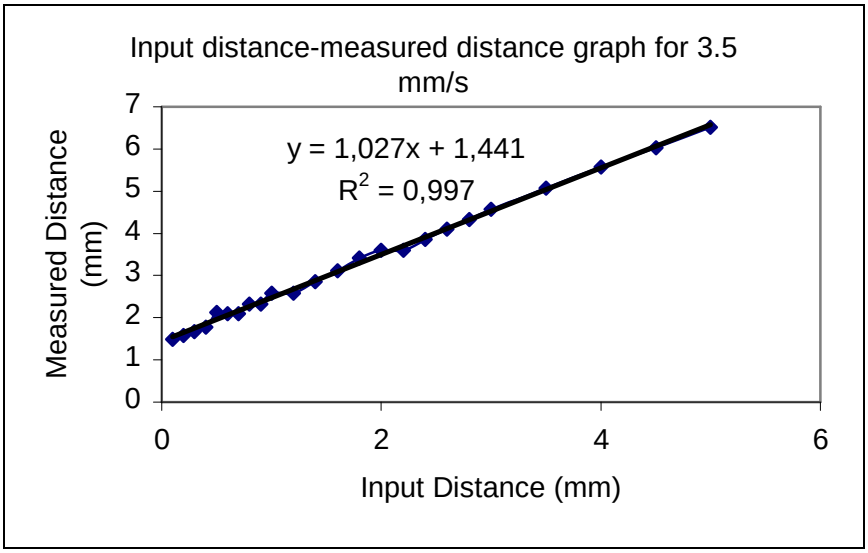

Figure A.10 Input distance versus measured distance graph for 3.5 mm/s

For the motor speed 3.5 mm/s, it was obtained a quantization error showing same characteristic with data obtained for 2.5 mm/s motor speed.

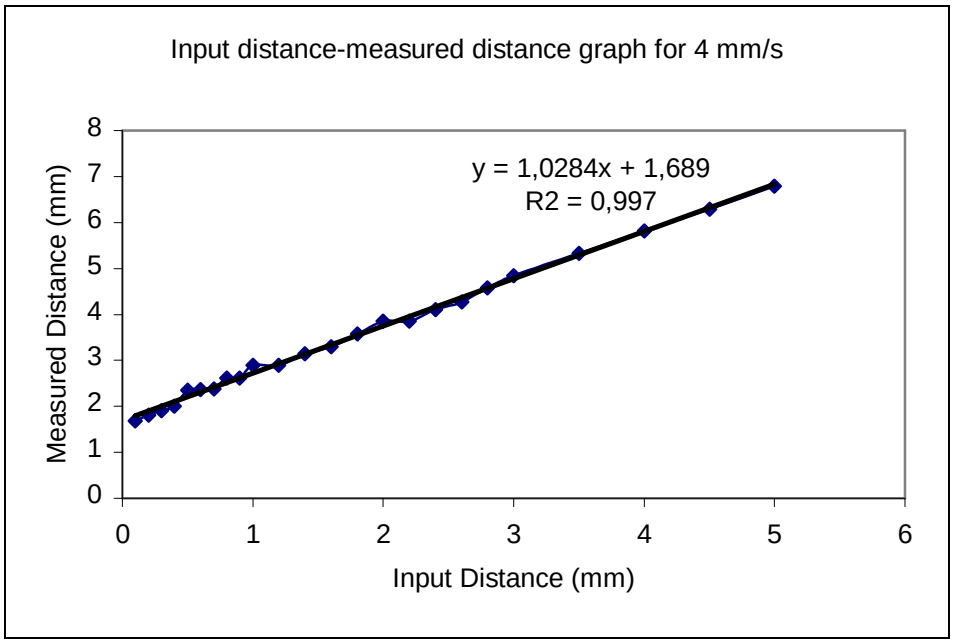

Figure A.11 Input distance versus measured distance graph for 4 mm/s

For the motor speed 4 mm/s, it was obtained a quantization error showing same characteristic with data obtained for 2.5 mm/s motor speed.

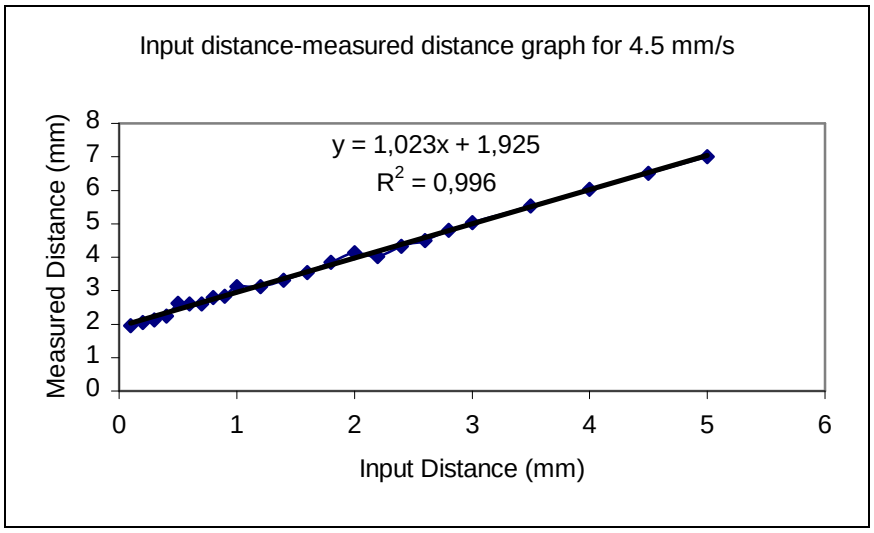

Figure A.12 Input distance versus measured distance graph for 4.5 mm/s

For the motor speed 4.5 mm/s, it was obtained a quantization error showing same characteristic with data obtained for 2.5 mm/s motor speed.

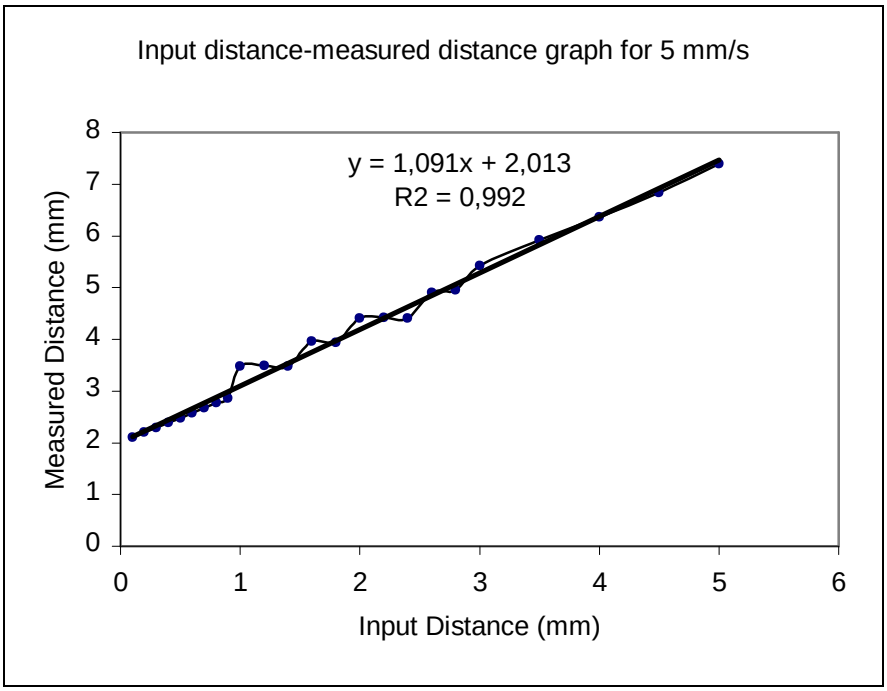

Figure A.13 Input distance versus measured distance graph for 5 mm/s

For the motor speed 5 mm/s, it was observed another quantization error characteristic. For this speed, measured distances took same value at the four input distance groups. Measured distances took same value at 1, 1.2, 1.4 mm; 1.6, 1.8 mm; 2, 2.2, 2.4 mm and 2.6, 2.8 mm input distances. On the other hand, a linear relationship between the input distance and measured distance was also observed.

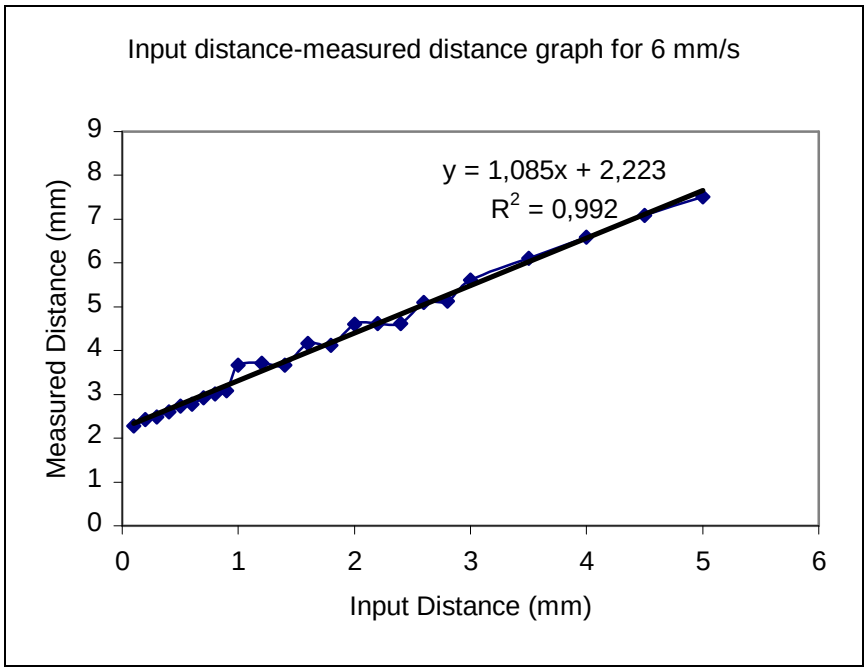

Figure A.14 Input distance versus measured distance graph for 6 mm/s

For the motor speed 6 mm/s, it was obtained a quantization error showing same characteristic with data obtained for 5 mm/s motor speed.

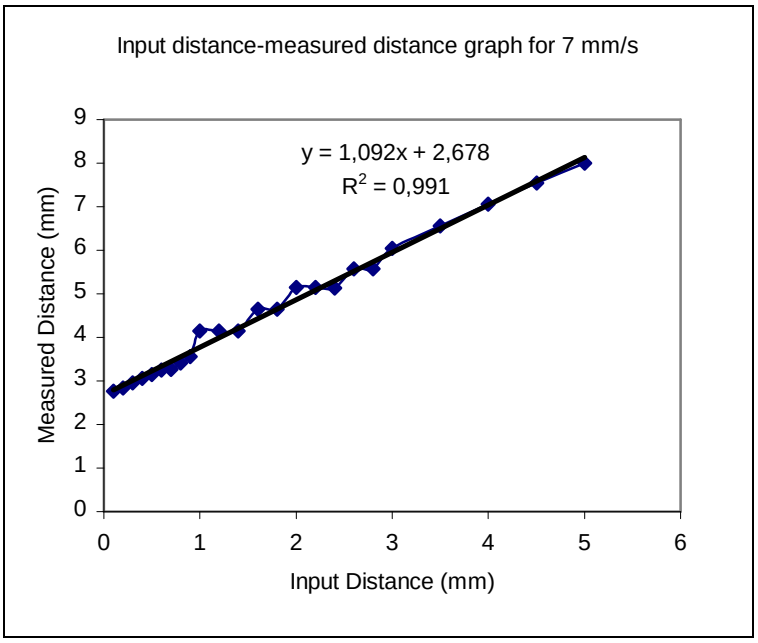

Figure A.15 Input distance versus measured distance graph for 7 mm/s

For the motor speed 7 mm/s, it was obtained a quantization error showing same characteristic with data obtained for 5 mm/s motor speed.

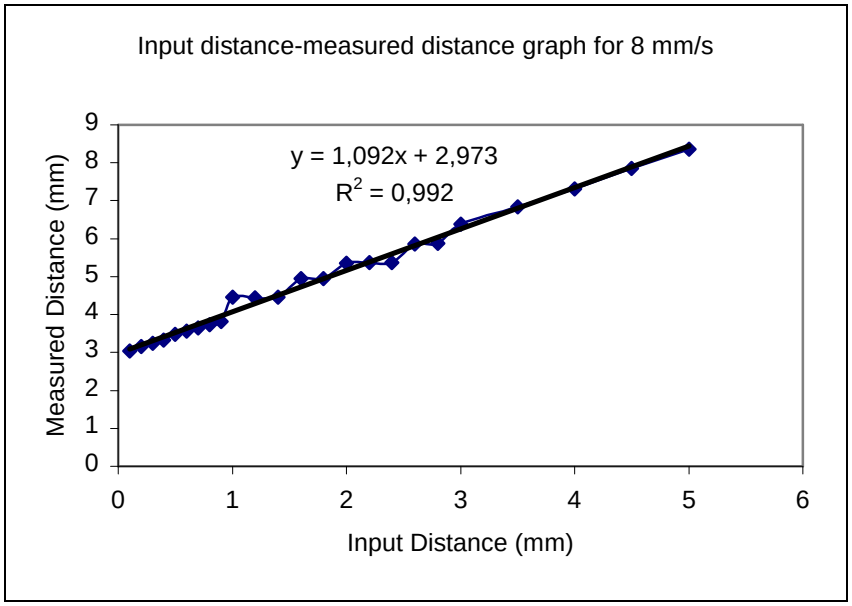

Figure A.16 Input distance versus measured distance graph for 8 mm/s

For the motor speed 8 mm/s, it was obtained a quantization error showing same characteristic with data obtained for 5 mm/s motor speed.

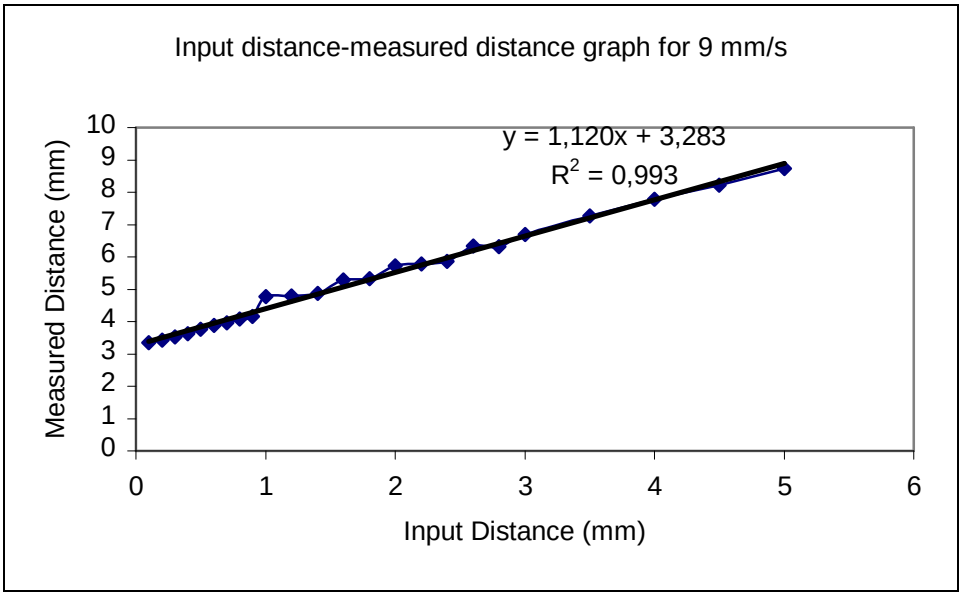

Figure A.17 Input distance versus measured distance graph for 9 mm/s

For the motor speed 9 mm/s, it was obtained a quantization error showing same characteristic with data obtained for 5 mm/s motor speed.

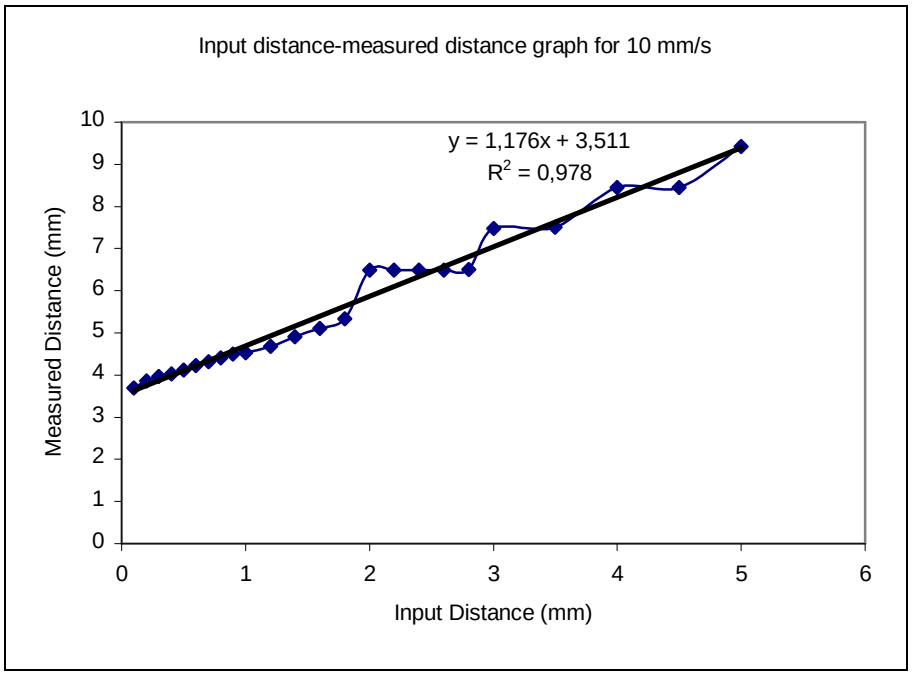

Figure A.18 Input distance versus measured distance graph for 10 mm/s

For the measurement done at 10 mm/s motor speeds, it was observed another type of quantization error. In this measurement measured distance took same value at the input distances 2, 2.2, 2.4, 2.6, 2.8 mm; 3, 3.5 mm and 4, 4.5 mm.

In conclusion, it was obtained a linear relationship between the input distance and measured distance for all motor speeds. On the other hand it was also obtained three different type of quantization error.

A.2 Entered Distance –Measured Distance Graphs for the Backward Movement

Below, test results showing the entered distance for the indentor tip backward movement versus the distance measured by dial gage are presented.

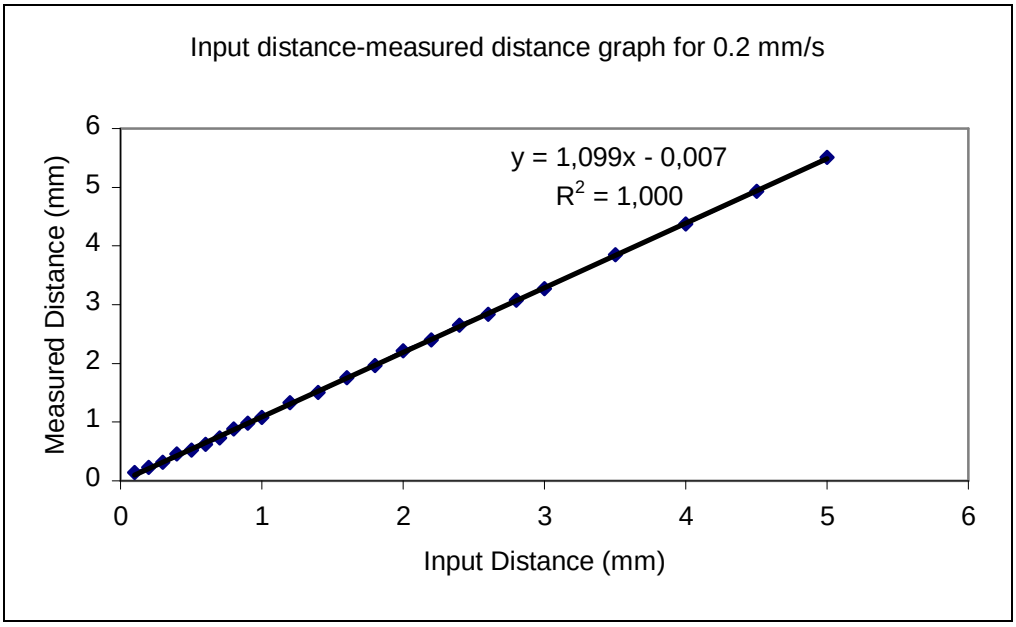

Figure A.19 Input distance versus measured distance graph for 0.2 mm/s

As it can be seen from the graph, it was obtained a linear relationship between the entered distance and measured distance for the 0.2 mm/s motor speed.

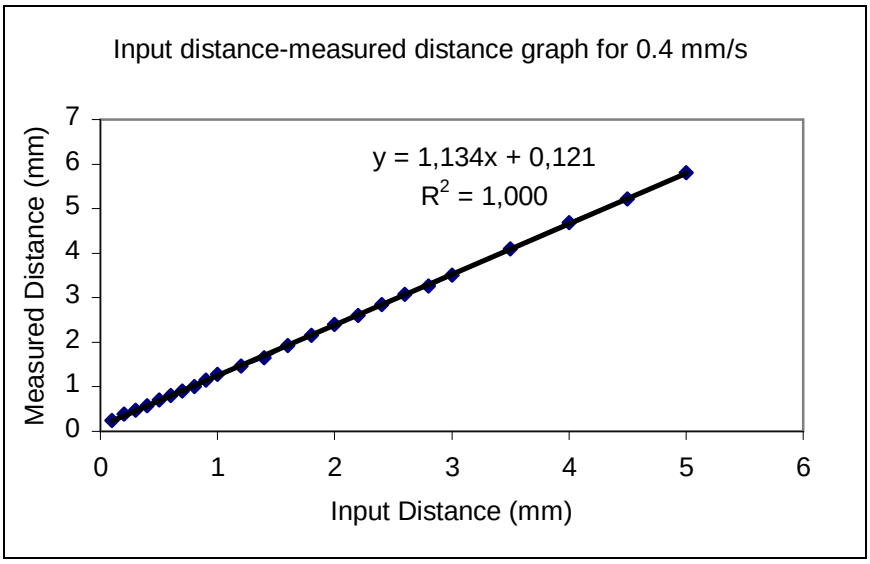

Figure A.20 Input distance versus measured distance graph for 0.4 mm/s

Similar result was also obtained for the 0.4 motor speed. It was obtained a linear relationship between the input distance and measured distance.

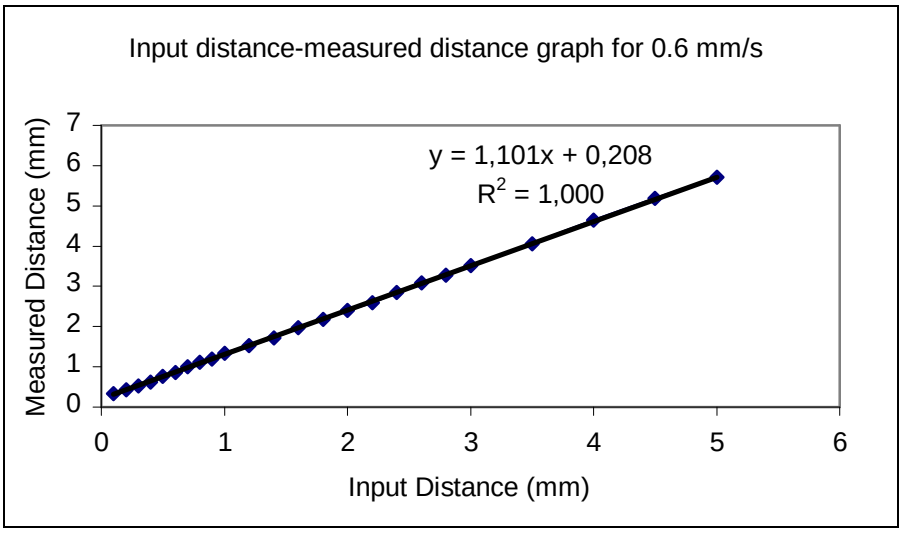

Figure A.21 Input distance versus measured distance graph for 0.6 mm/s

It was obtained a linear relationship for the 0.6 mm/s motor speed.

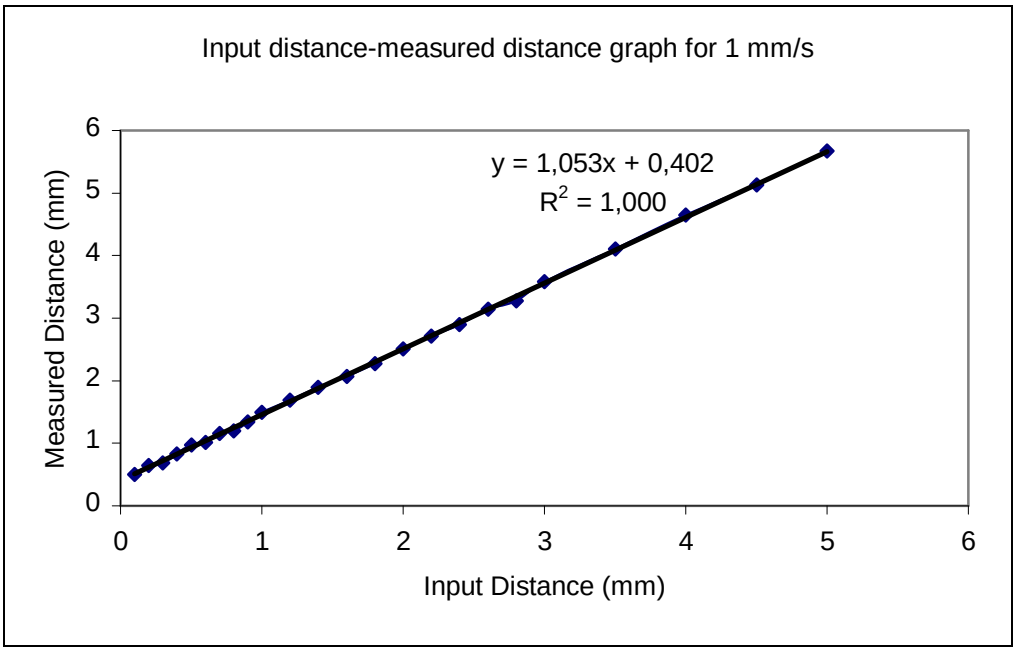

Figure A.22 Input distance versus measured distance graph for 1 mm/s

It was obtained a linear relationship between the input distance and measured distance for the motor speed 1 mm/s. Also a quantization error can be seen for the 0.2 and 0.3 mm input distances.

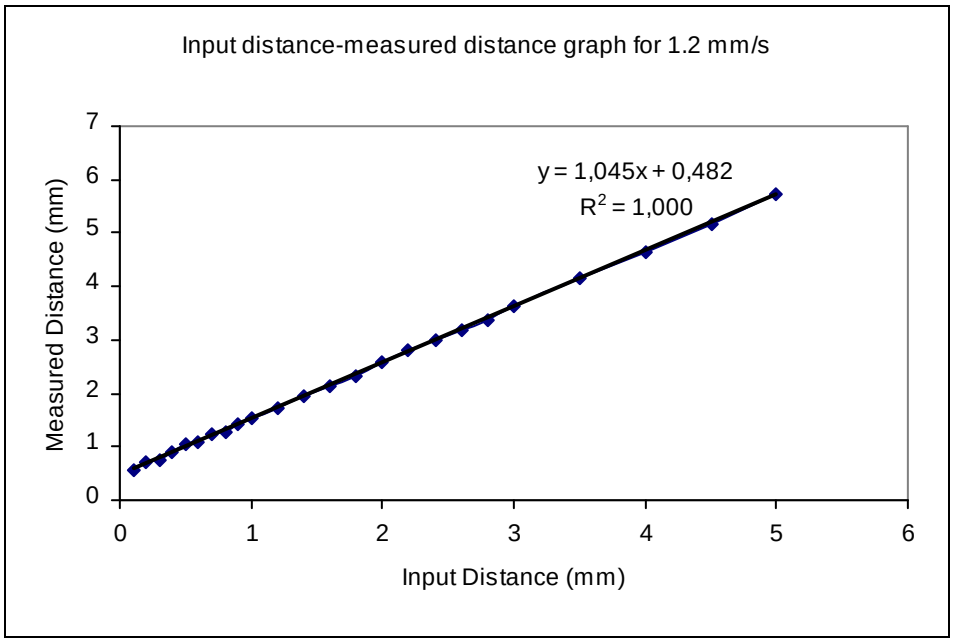

Figure A.23 Input distance versus measured distance graph for 1.2 mm/s

A linear relationship was obtained between the input distance and measured distance for the motor speed 1.2 mm/s.

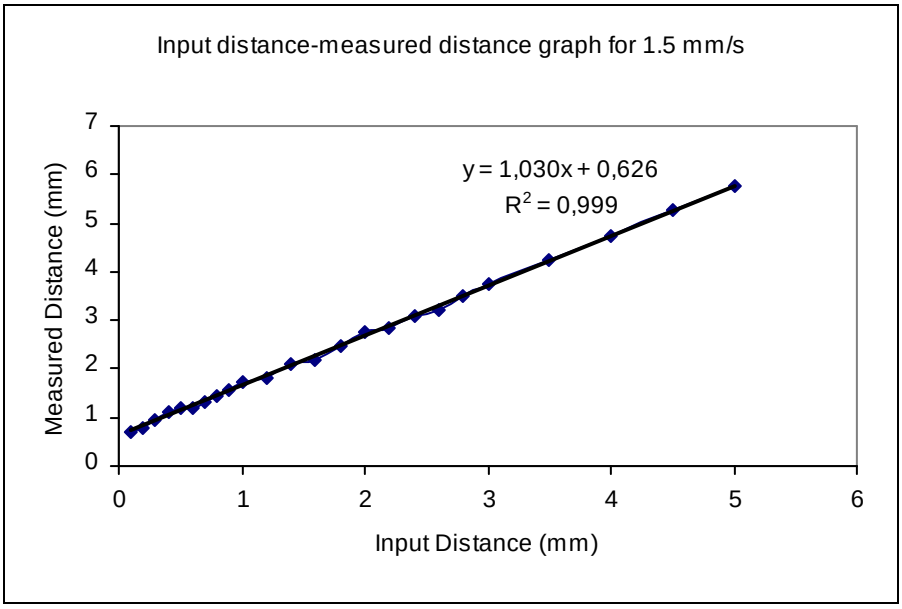

Figure A.24 Input distance versus measured distance graph for 1.5 mm/s

A linear relationship was obtained between the input distance and measured distance for the motor speed 1.5 mm/s. On the other hand, data obtained from the experiment was started show deviation from the trend line.

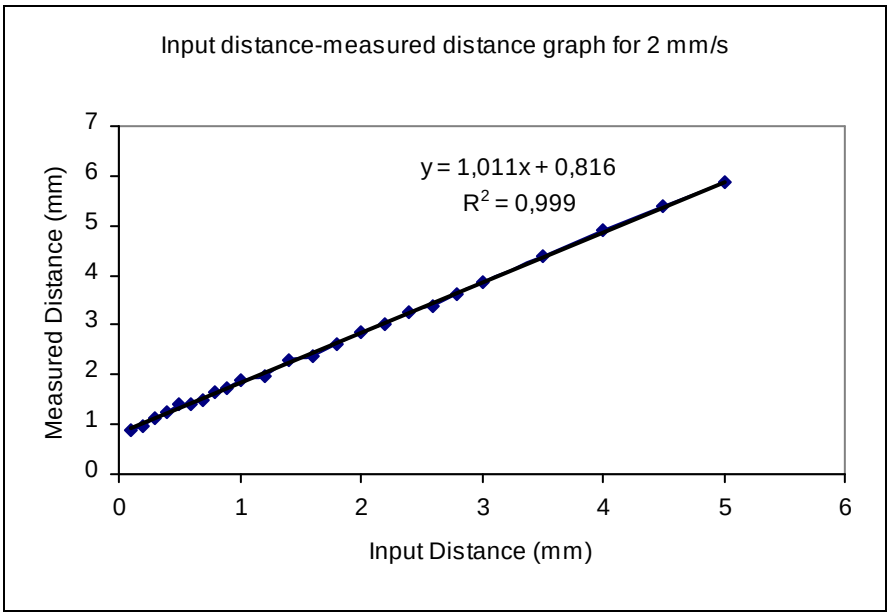

Figure A.25 Input distance versus measured distance graph for 2 mm/s

The deviation seen in Figure A.24 was also seen for the 2 mm/s input motor speed.

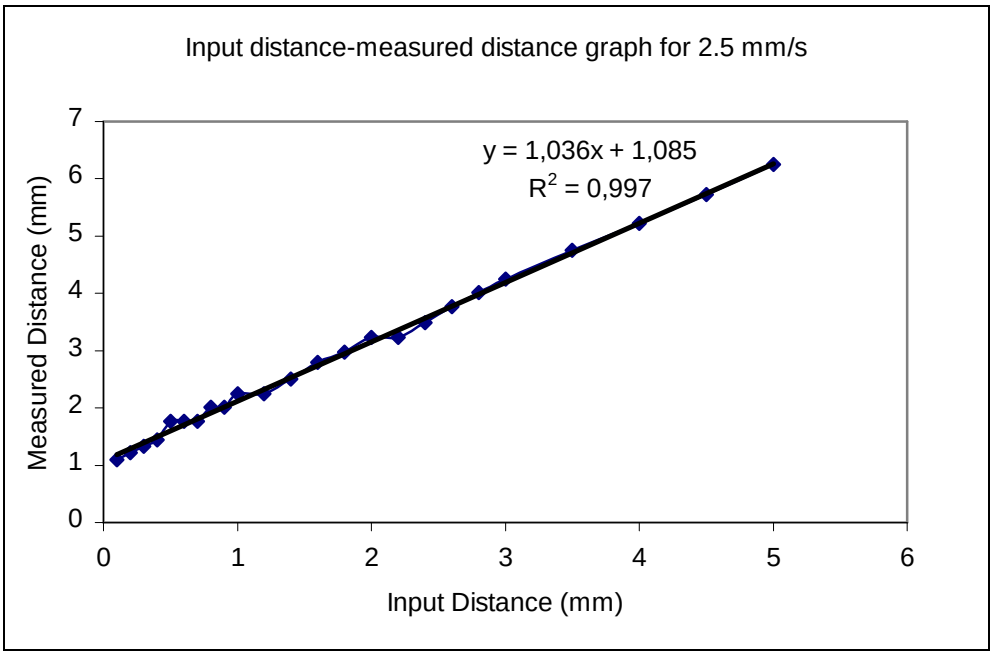

Figure A.26 Input distance versus measured distance graph for 2.5 mm/s

For the 2.5 mm/s motor speed, it was observed a clear quantization error. These errors were appeared at 0.5, 0.6, 0.7 mm as first group, 0.8, 0.9 mm as second group, 1, 1.2 mm as third group and 2, 2.2 mm as fourth group. It can be seen the same characteristics and errors at the speeds 3, 3.5, 4 and 4.5 mm/s from the following graphs.

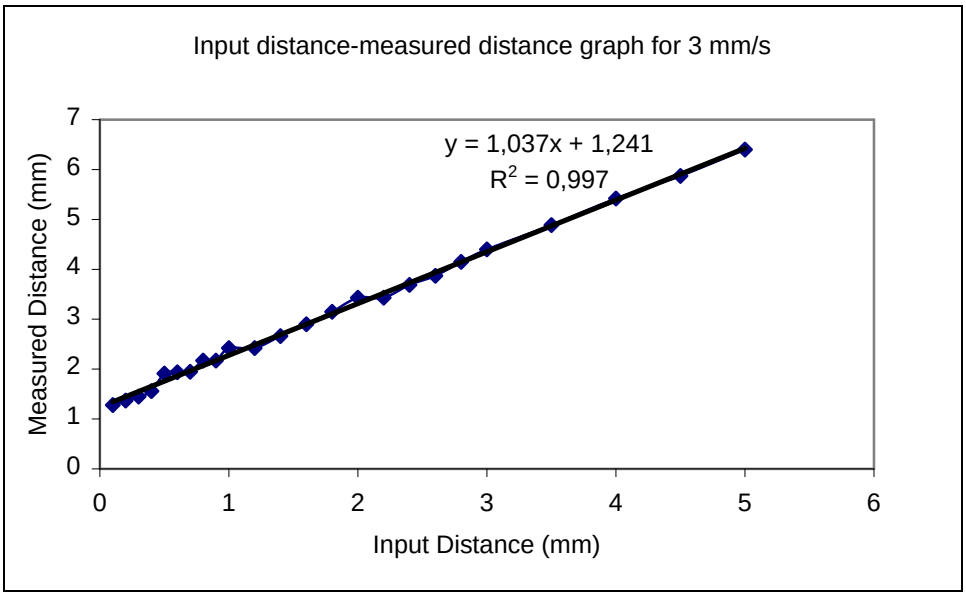

Figure A.27 Input distance versus measured distance graph for 3 mm/s

For the motor speed 3 mm/s, it was obtained a quantization error showing same characteristic with data obtained for 2.5 mm/s motor speed.

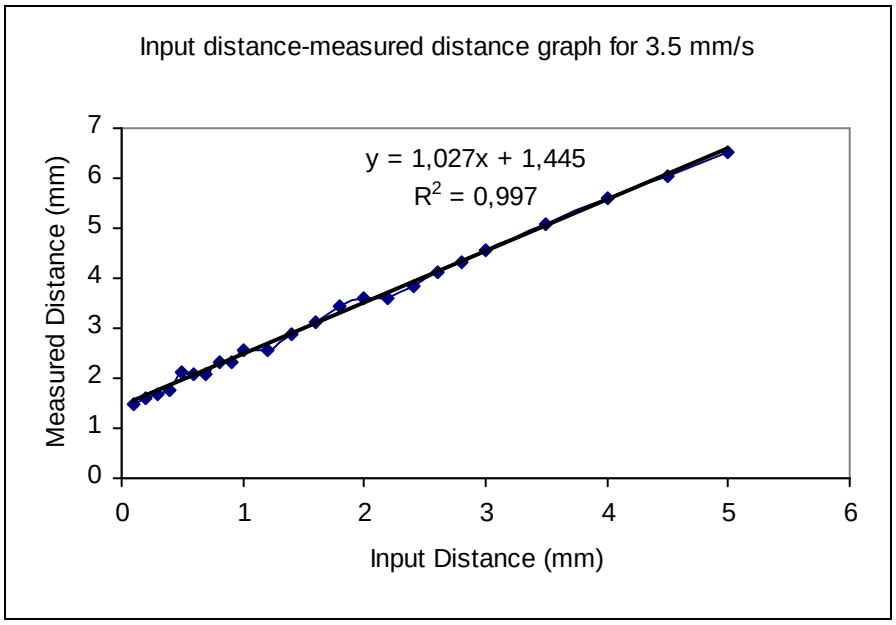

Figure A.28 Input distance versus measured distance graph for 3.5 mm/s

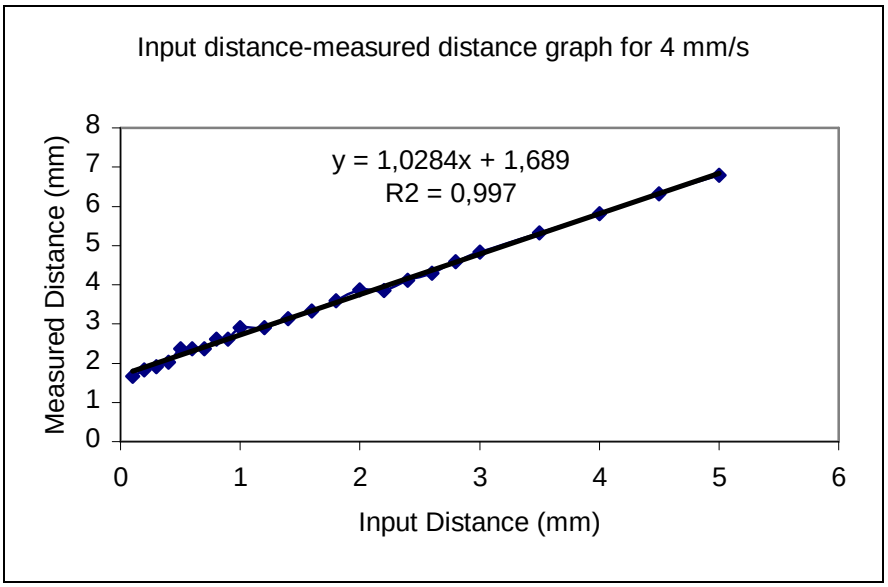

Figure A.29 Input distance versus measured distance graph for 4 mm/s

For the motor speed 4 mm/s, it was obtained a quantization error showing same characteristic with data obtained for 2.5 mm/s motor speed.

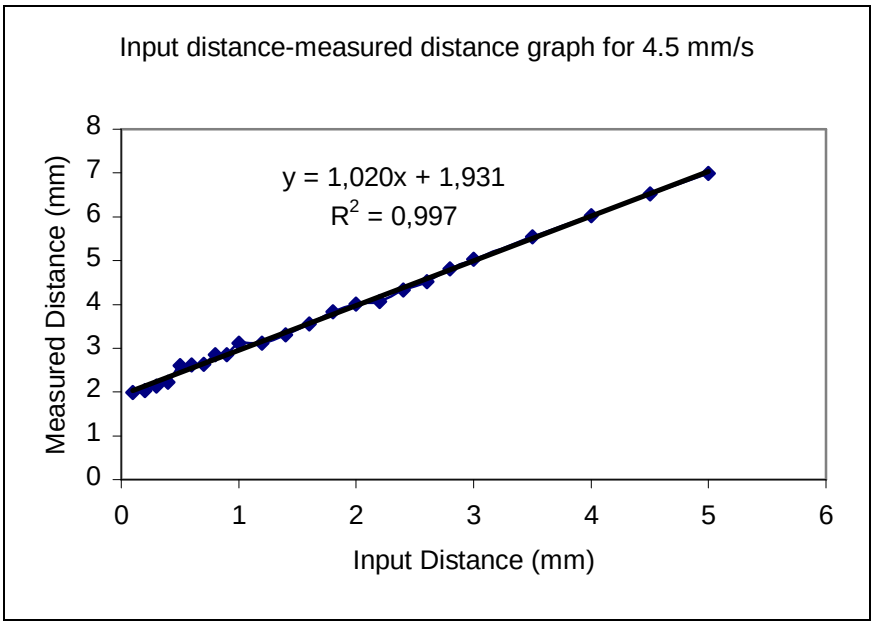

Figure A.30 Input distance versus measured distance graph for 4.5 mm/s

For the motor speed 4.5 mm/s, it was obtained a quantization error showing nearly same characteristic with data obtained for 2.5 mm/s motor speed.

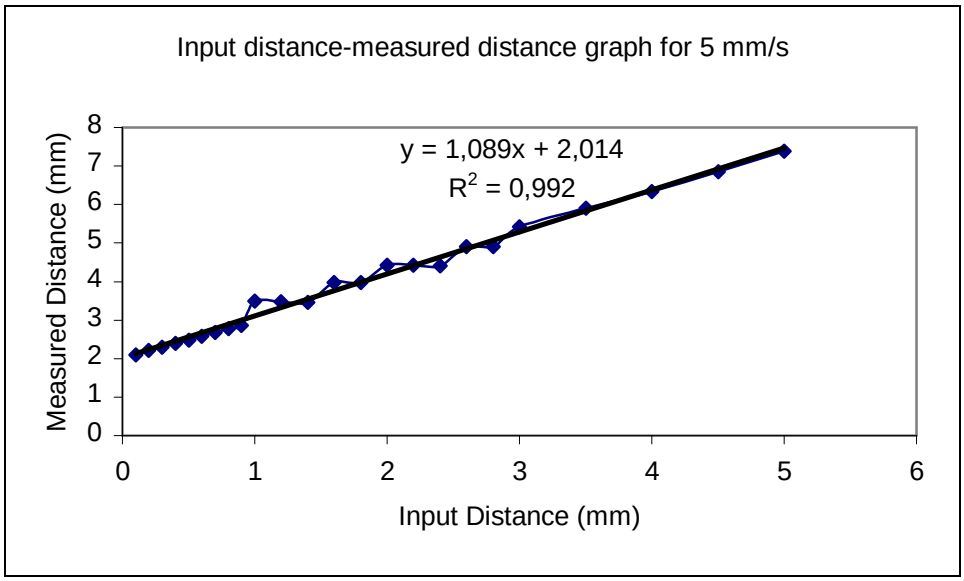

Figure A.31 Input distance versus measured distance graph for 5 mm/s

For the motor speed 5 mm/s, it was observed another quantization error characteristic. For this speed, measured distances took same value at the four input distance groups. Measured distances took same value at 1, 1.2, 1.4 mm; 1.6, 1.8 mm; 2, 2.2, 2.4 mm and 2.6, 2.8 mm. On the other hand, a linear relationship between the input distance and measured distance was also observed.

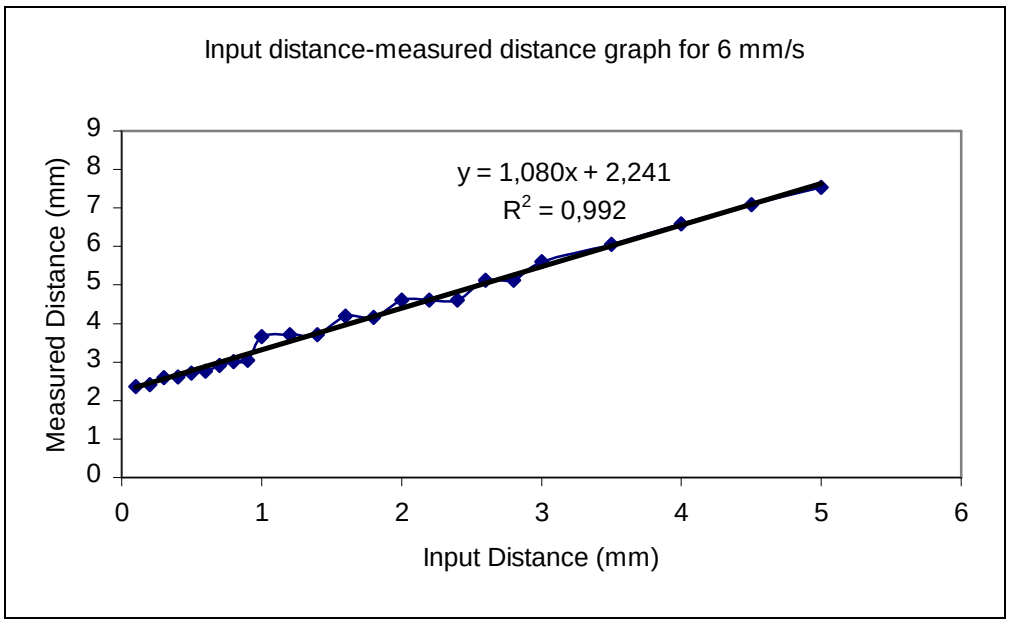

Figure A.32 Input distance versus measured distance graph for 6 mm/s

For the motor speed 6 mm/s, it was obtained a quantization error showing same characteristic with data obtained for 5 mm/s motor speed.

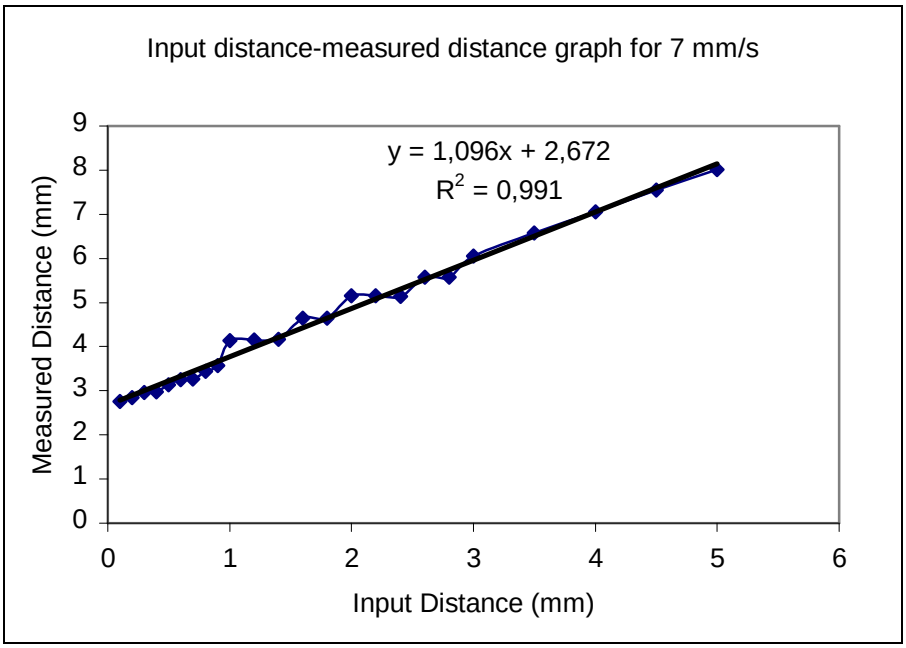

Figure A.33 Input distance versus measured distance graph for 7 mm/s

For the motor speed 7 mm/s, it was obtained a quantization error showing same characteristic with data obtained for 5 mm/s motor speed.

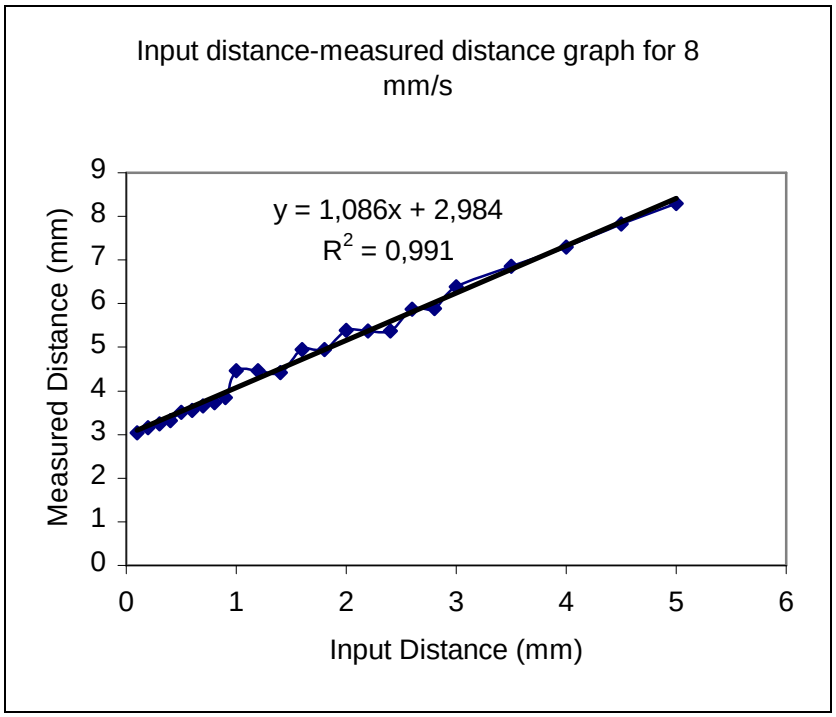

Figure A.34 Input distance versus measured distance graph for 8 mm/s

For the motor speed 8 mm/s, it was obtained a quantization error showing same characteristic with data obtained for 5 mm/s motor speed.

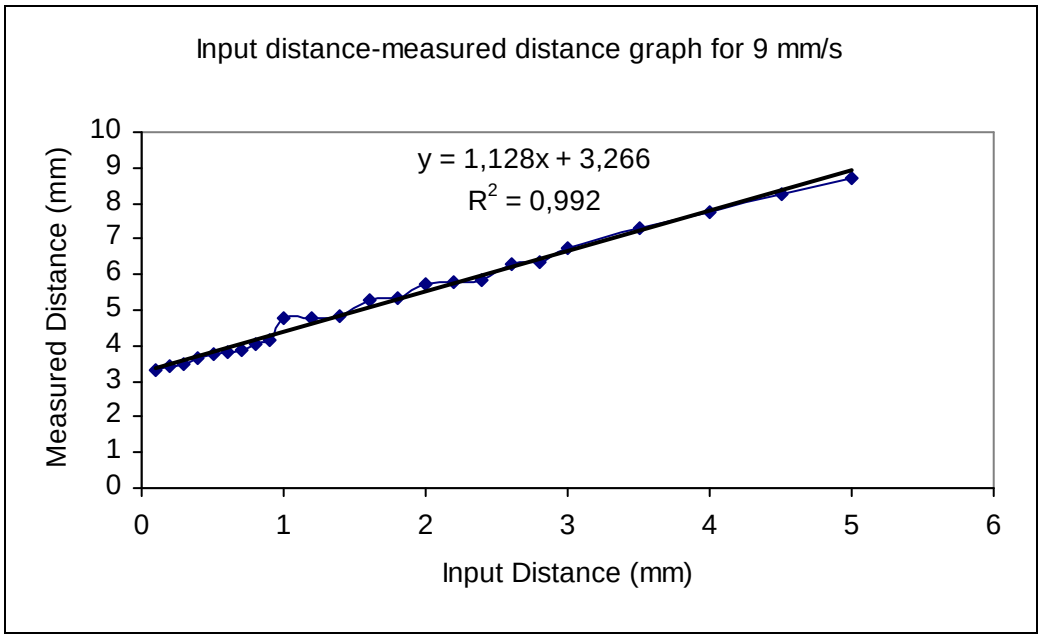

Figure A.35 Input distance versus measured distance graph for 9 mm/s

For the motor speed 9 mm/s, it was obtained a quantization error showing same characteristic with data obtained for 5 mm/s motor speed.

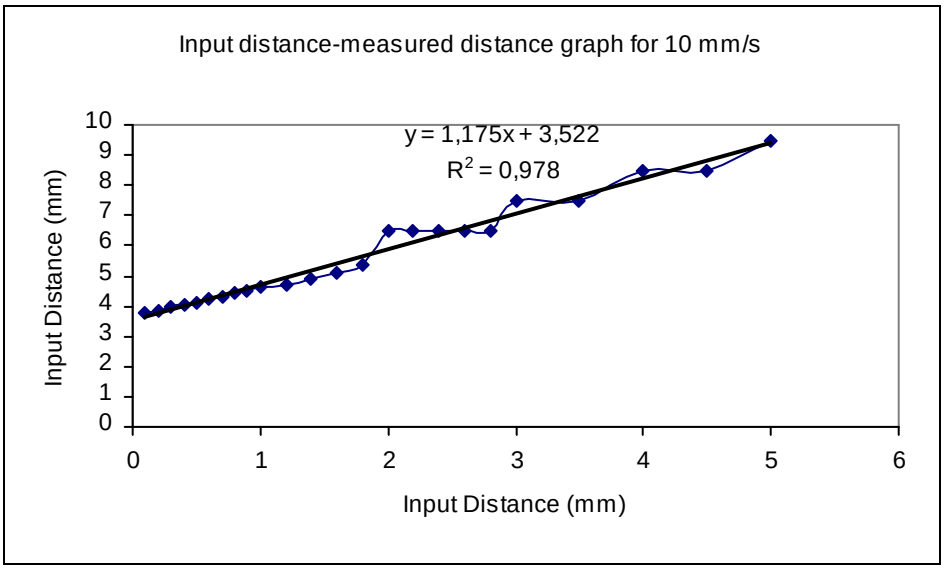

Figure A.36 Input distance versus measured distance graph for 10 mm/s

For the measurement done at 10 mm/s motor speeds, it was observed another type of quantization error. In this measurement measured distance took same value at the input distances 2, 2.2, 2.4, 2.6, 2.8 mm; 3, 3.5 mm and 4, 4.5 mm.

In conclusion, similar results were obtained with the forward movement. Consequently, it was obtained a linear relationship between the input distance and measured distance for all motor speeds. On the other hand it was also obtained three different type of quantization error.

A.3 Graphs Showing Calculated Motor Speed-Time Relation

Following graphs shows the relation of calculated motor speed with the input time. For all graphs same characteristic was observed. The relation of these parameters was explained with the Equation A.1 which was given as;

$$m = at^{-b} \quad \text{.....(A.1)}$$

where,

m = calculated motor speed (mm/s)

t = input time (s)

a, b = related coefficients.

This equation and related coefficients were directly calculated by using the Excel Trend line. As it can be seen from the following results, better r-square values were obtained with the increasing motor speed.

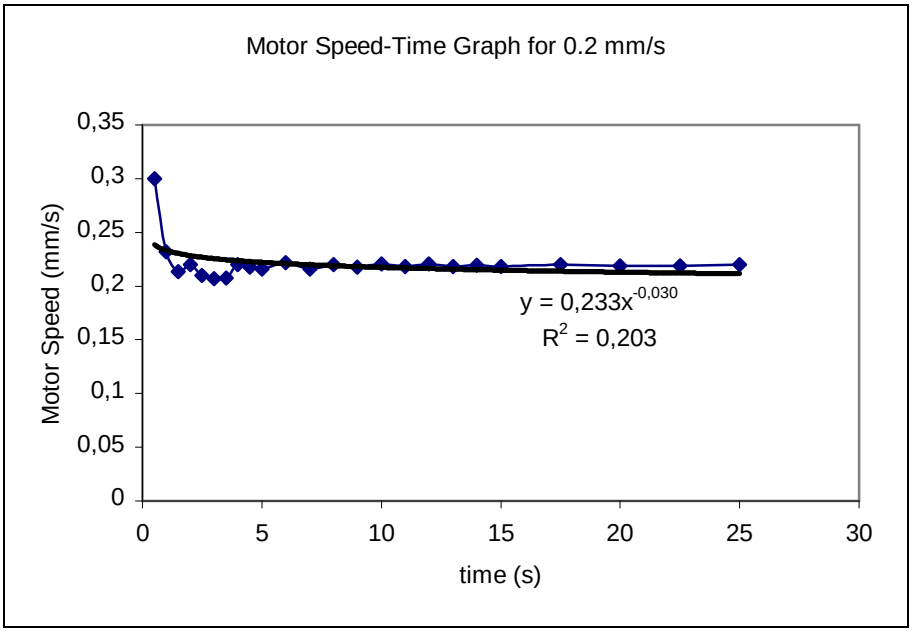

Figure A.37 time versus calculated motor speed graph for 0.2 mm/s

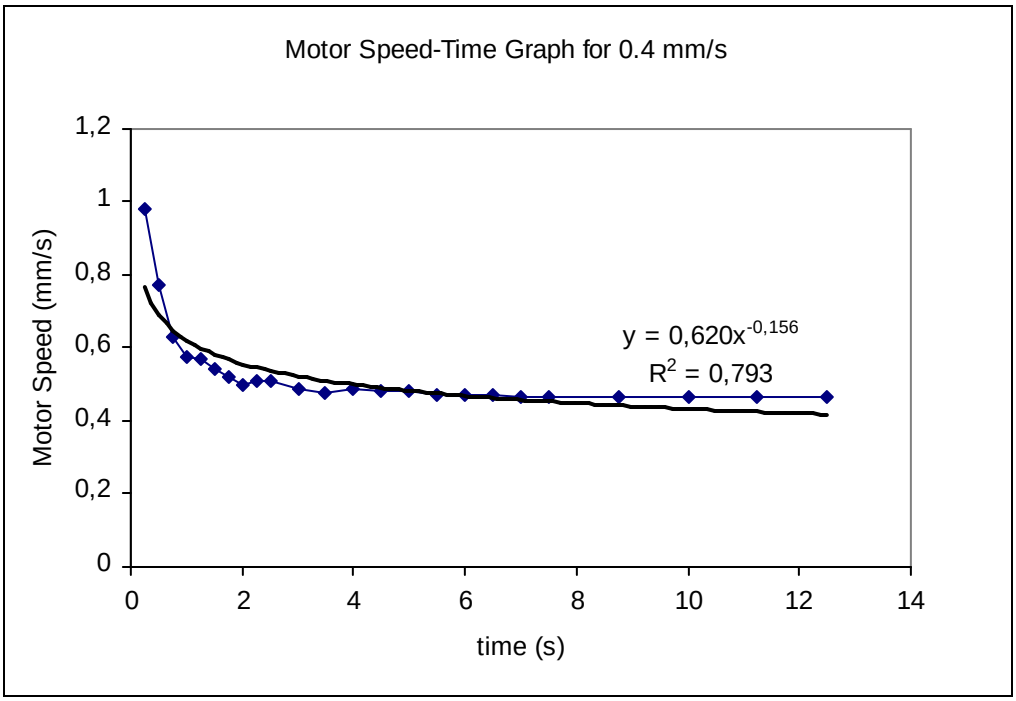

Figure A.38 time versus calculated motor speed graph for 0.4 mm/s

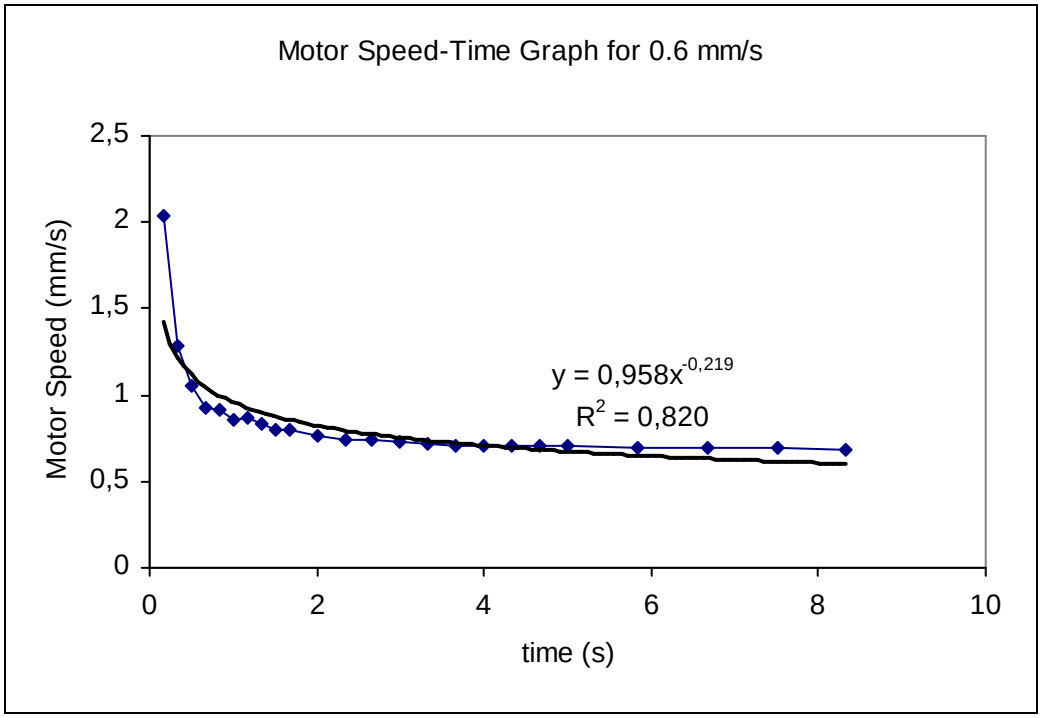

Figure A.39 time versus calculated motor speed graph for 0.6 mm/s

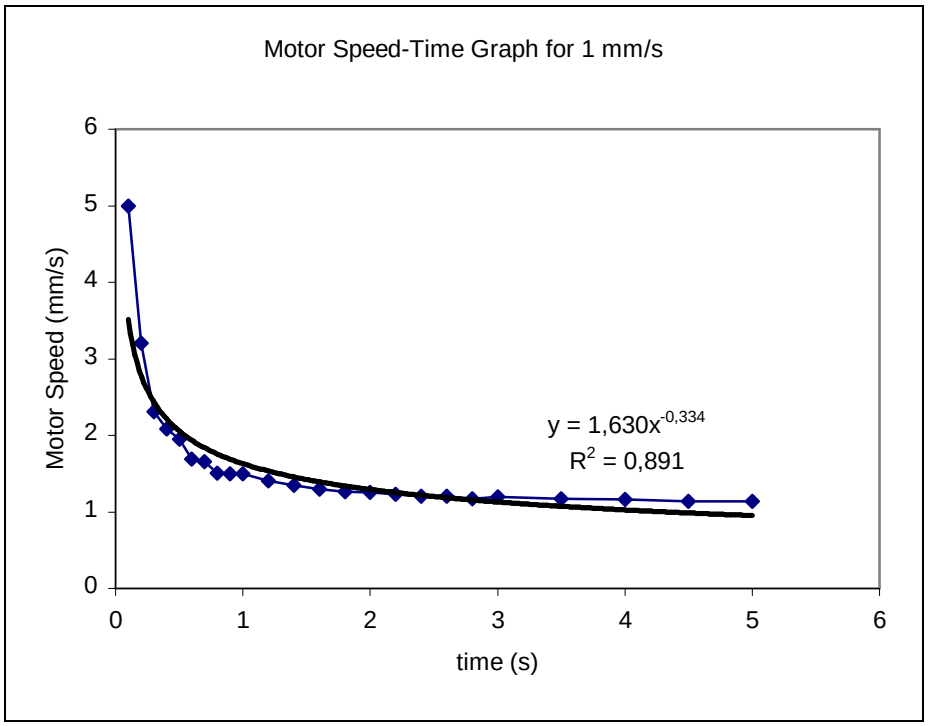

Figure A.40 time versus calculated motor speed graph for 1 mm/s

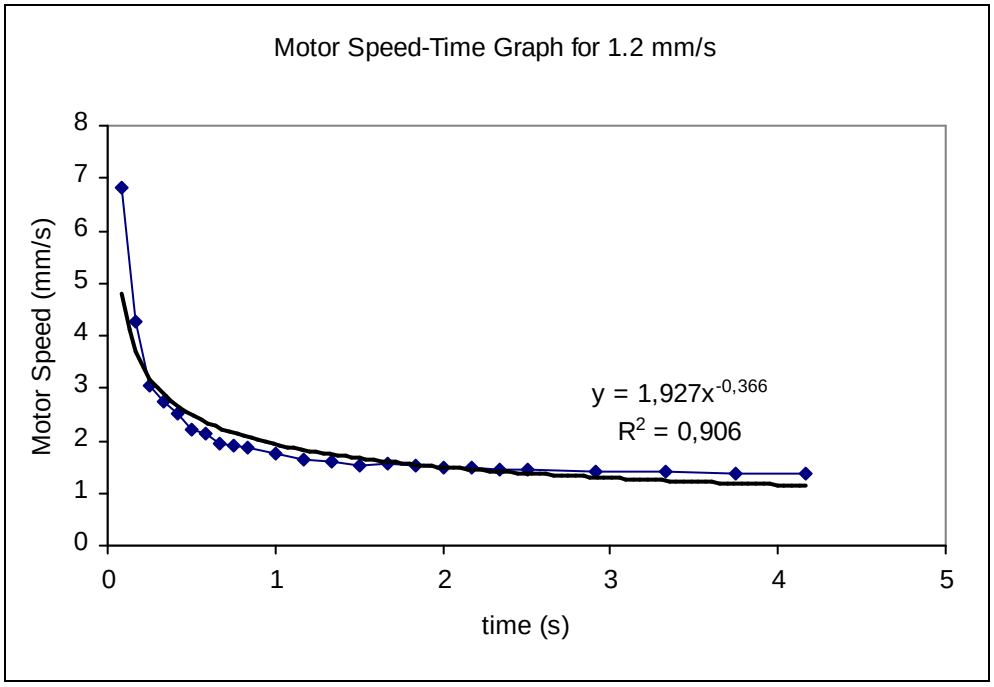

Figure A.41 time versus calculated motor speed graph for 1.2 mm/s

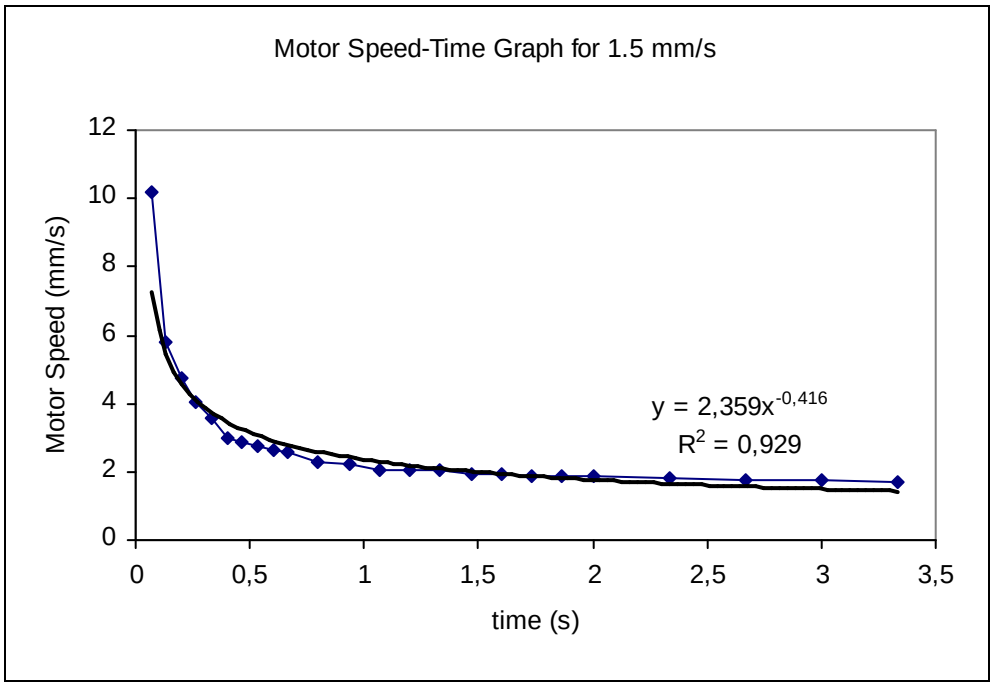

Figure A.42 time versus calculated motor speed graph for 1.5 mm/s

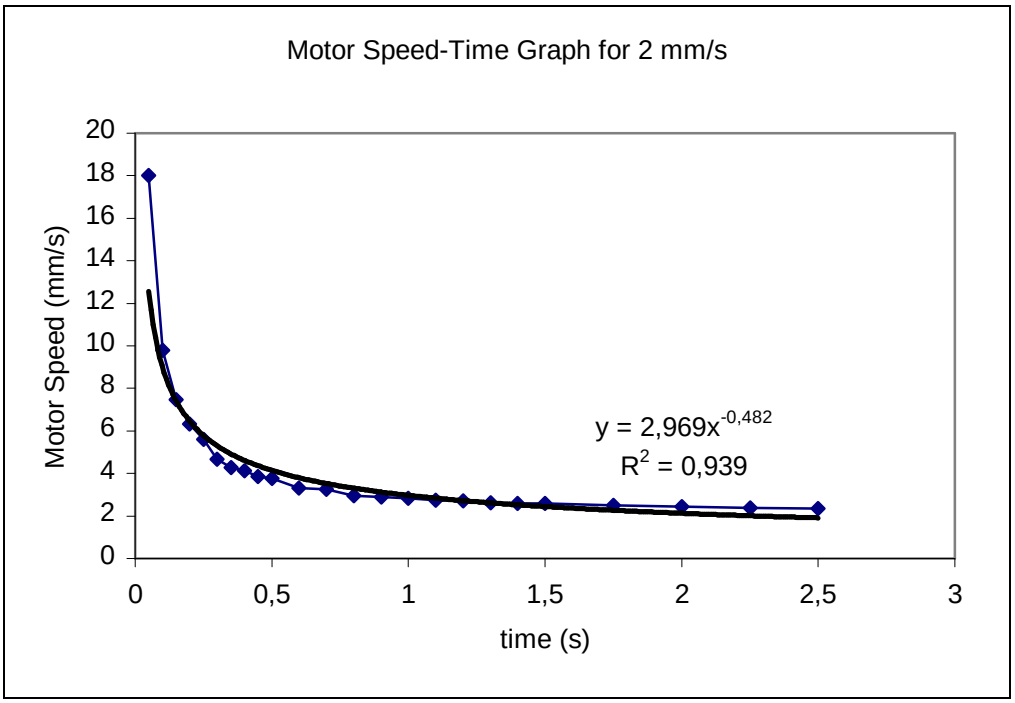

Figure A.43 time versus calculated motor speed graph for 2 mm/s

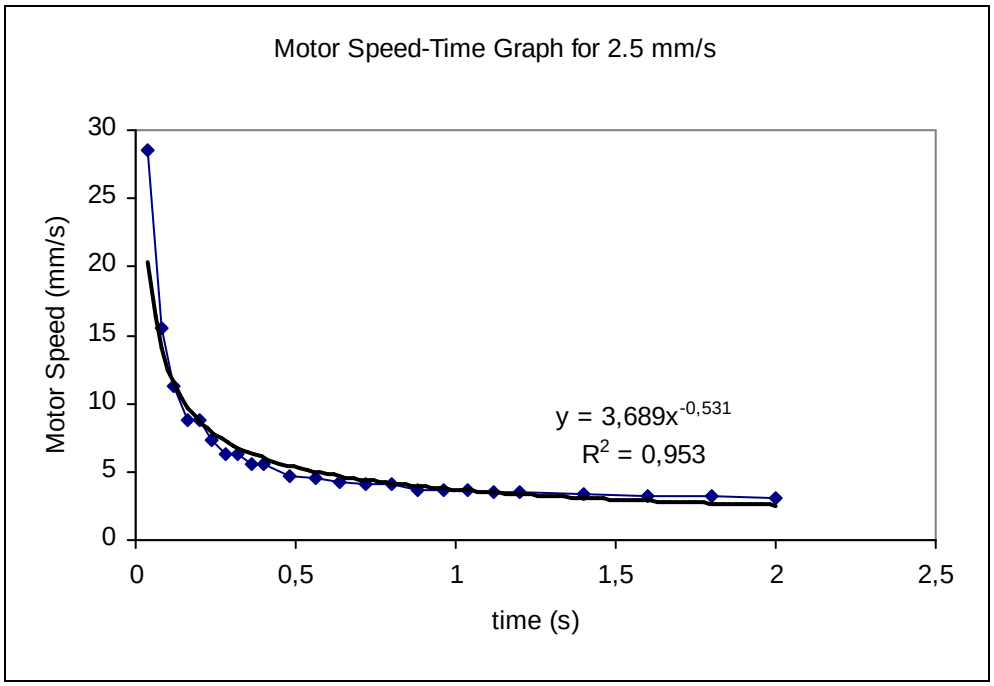

Figure A.44 time versus calculated motor speed graph for 2.5 mm/s

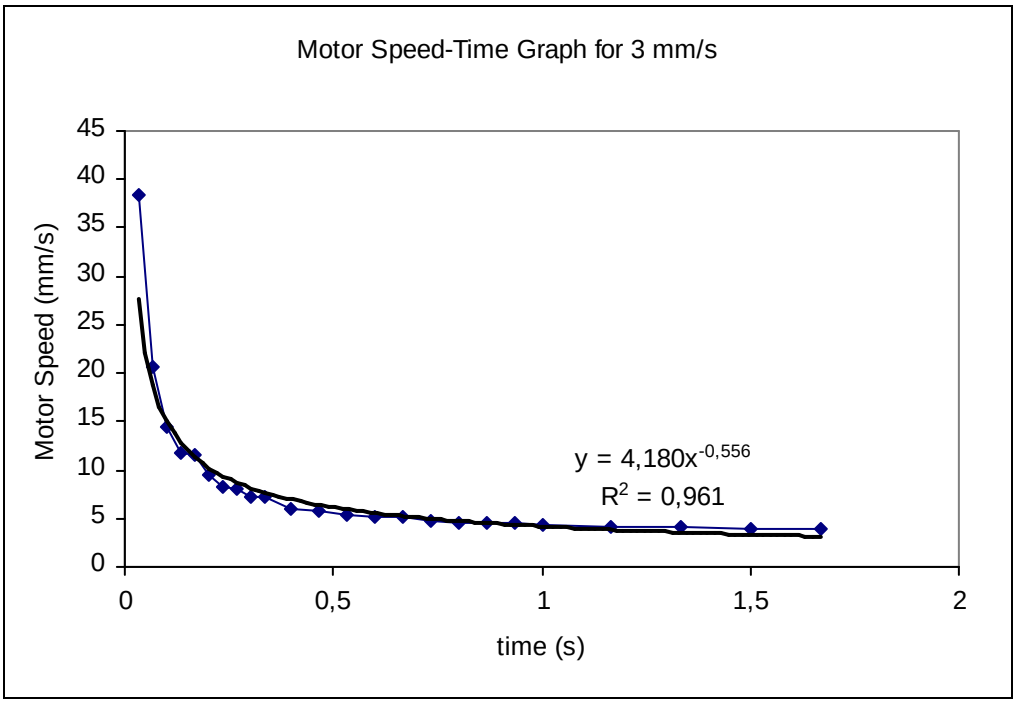

Figure A.45 time versus calculated motor speed graph for 3 mm/s

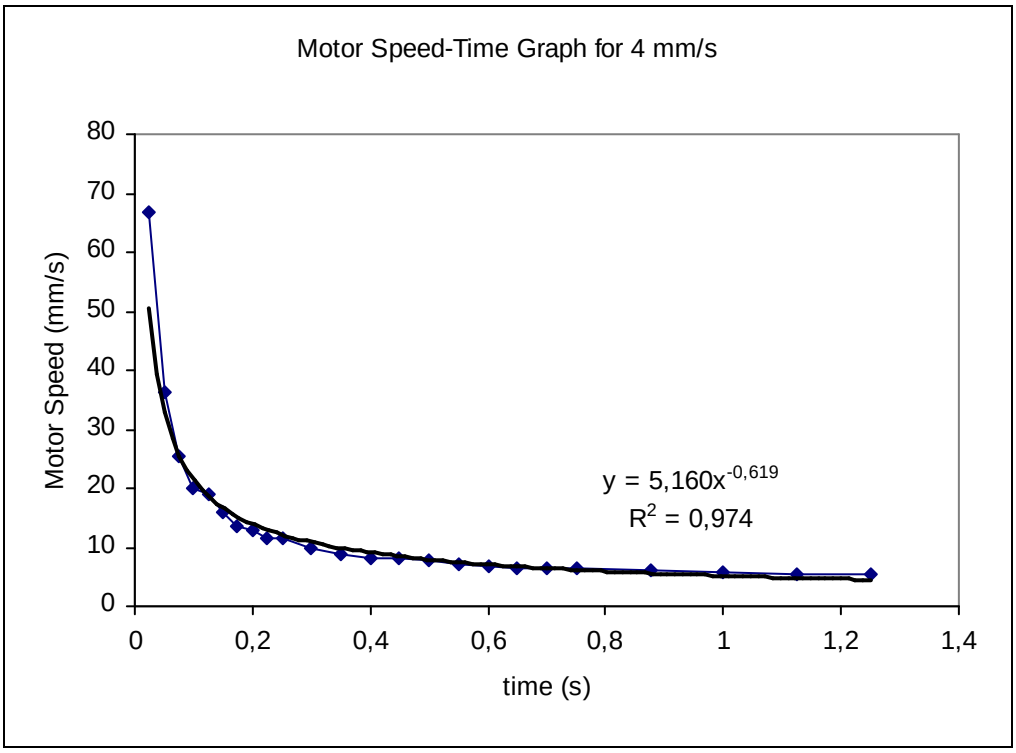

Figure A.46 time versus calculated motor speed graph for 4 mm/s

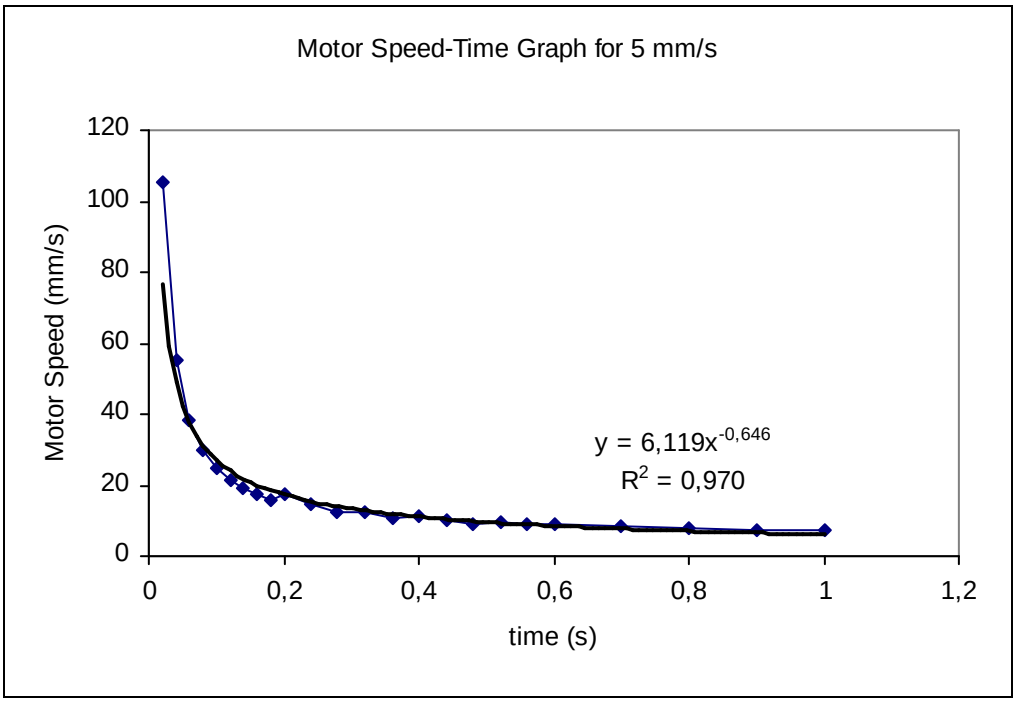

Figure A.47 time versus calculated motor speed graph for 5 mm/s

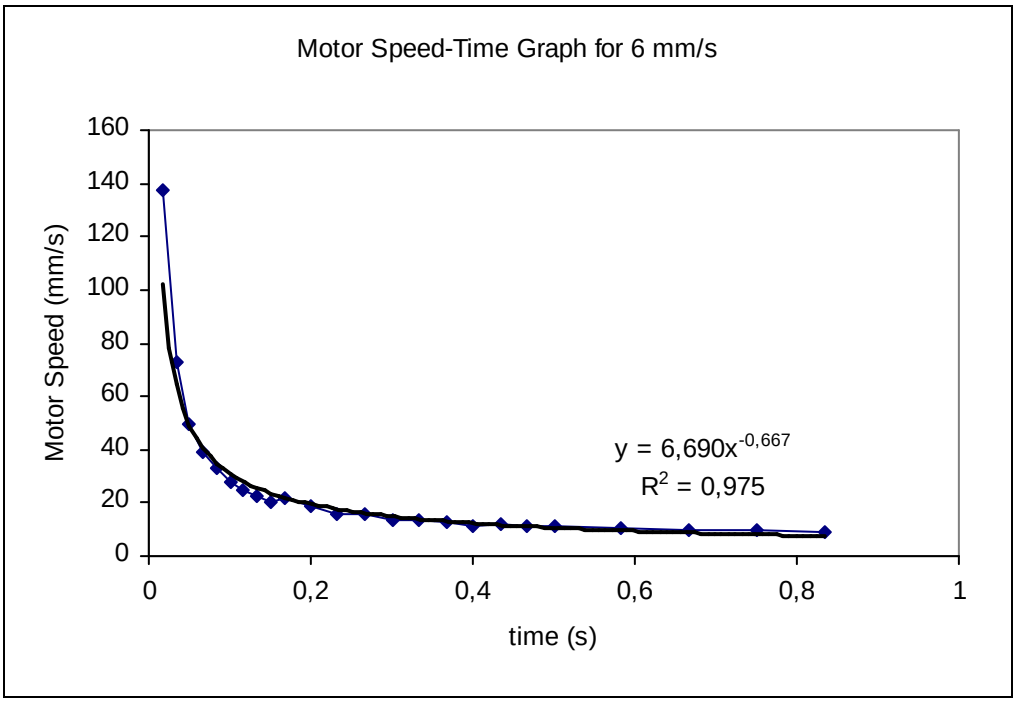

Figure A.48 time versus calculated motor speed graph for 6 mm/s

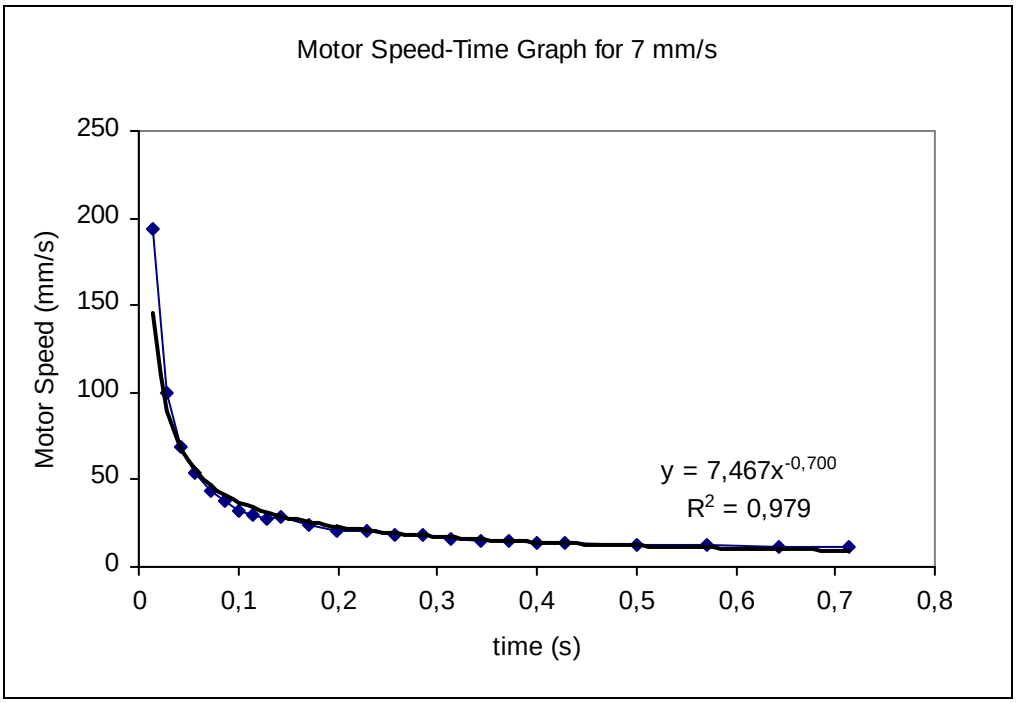

Figure A.49 time versus calculated motor speed graph for 7 mm/s

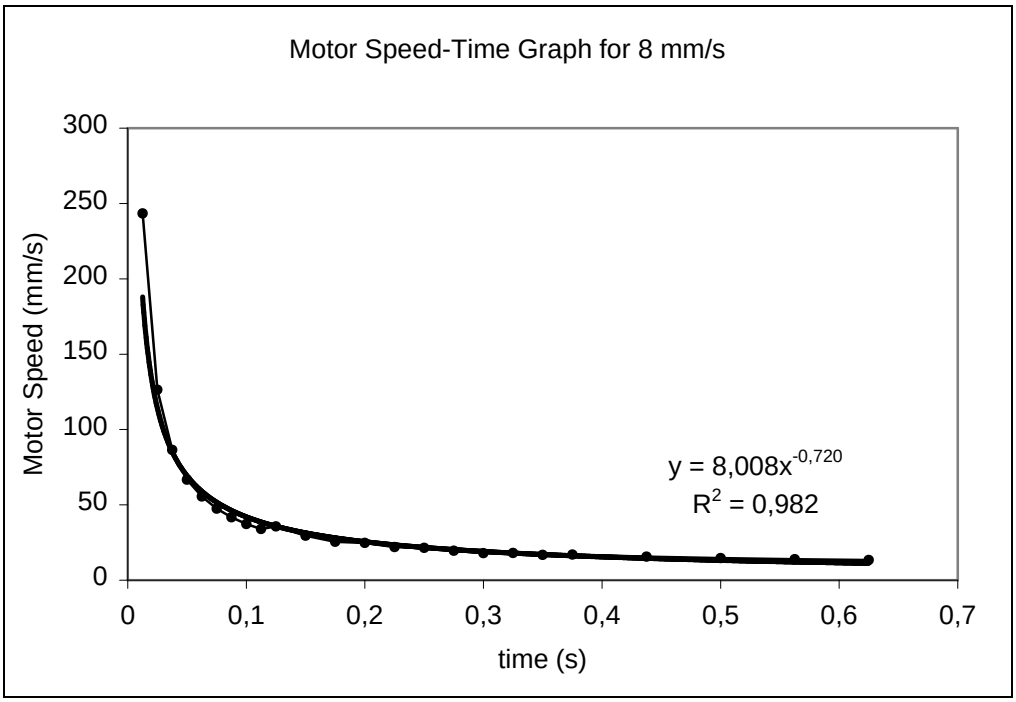

Figure A.50 time versus calculated motor speed graph for 8 mm/s

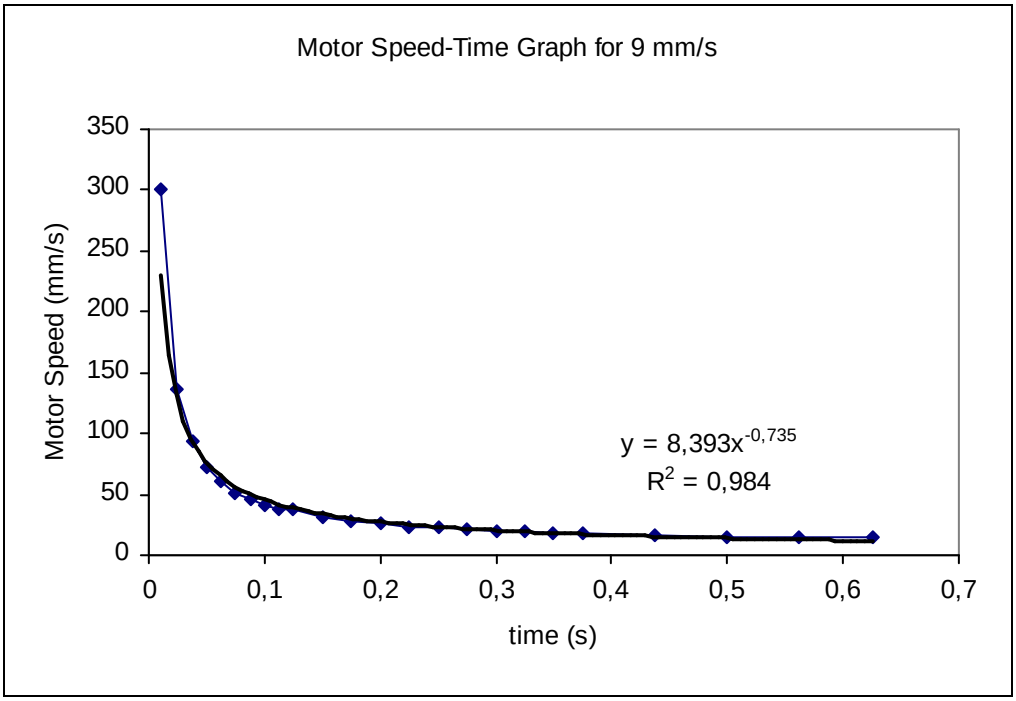

Figure A.51 time versus calculated motor speed graph for 9 mm/s

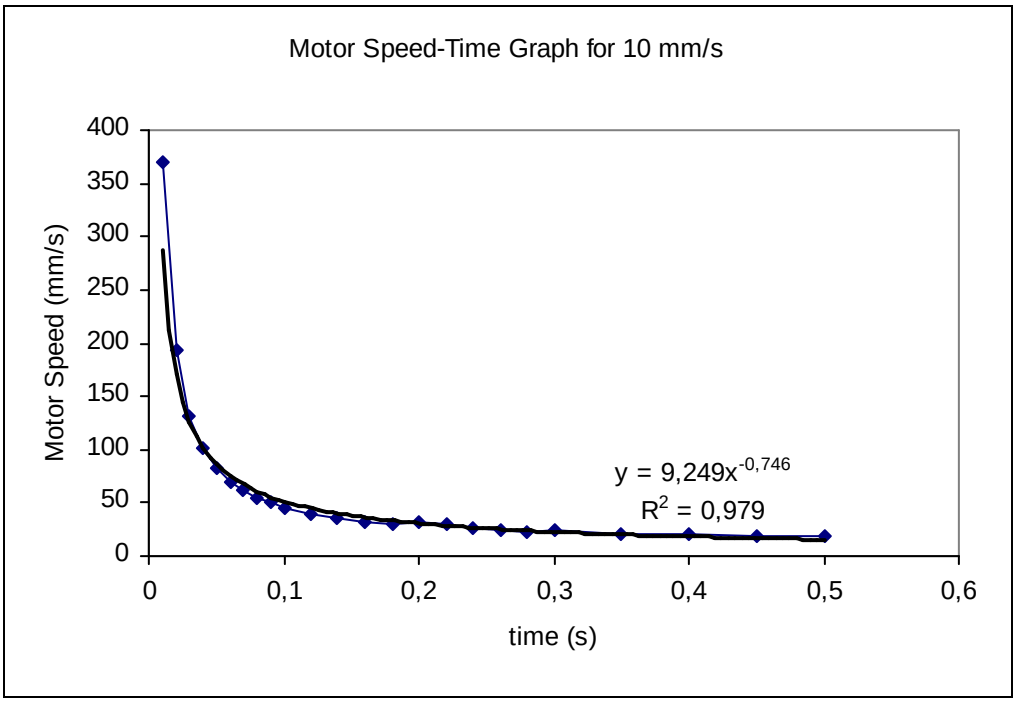

Figure A.52 time versus calculated motor speed graph for 10 mm/s

A.4 Graphs Showing Input Time-Output Time Relation

Below, graphs for the entered time versus times calculated from the measurements are given. It was observed that following graphs show totally same characteristic with the graphs given in the Appendix A.1 and A.2.

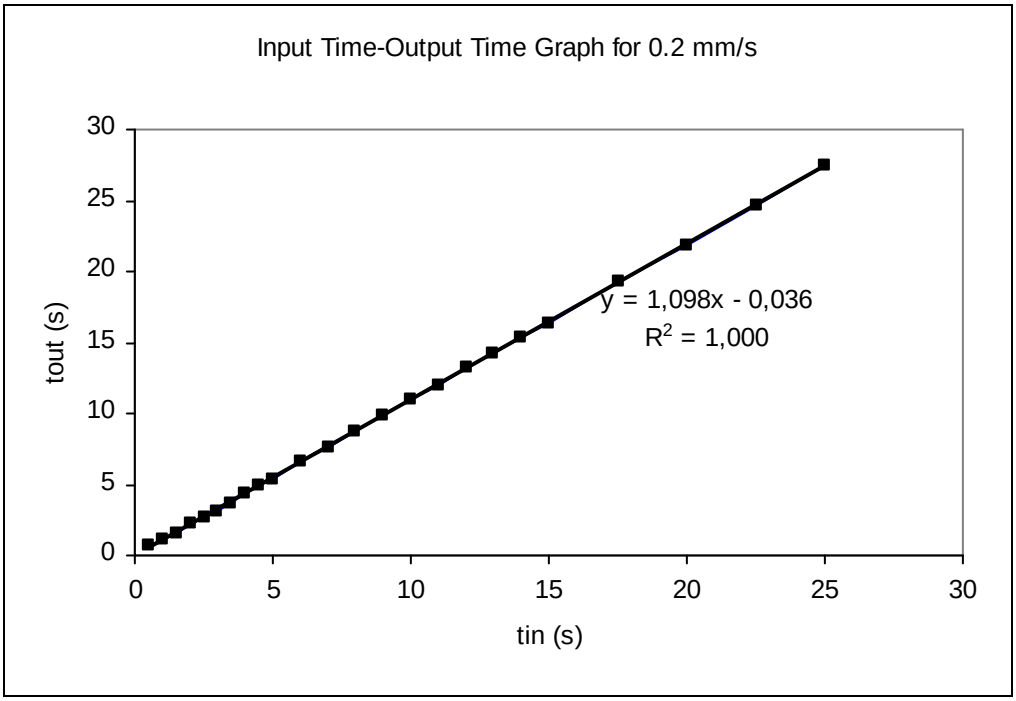

Figure A.53 Entered time versus calculated time graph for 0.2 mm/s

As it can be seen from the graph, it was obtained a linear relationship between the entered time and calculated time for the 0.2 mm/s motor speed.

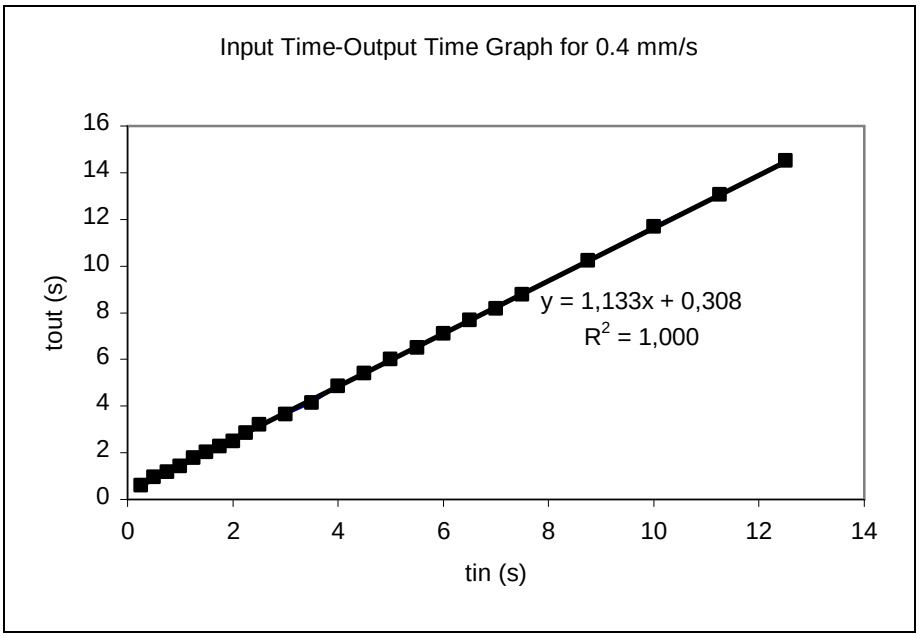

Figure A.54 Entered time versus calculated time graph for 0.4 mm/s

Similar result was also obtained for the 0.4 motor speed. It was obtained a linear relationship between the entered time and calculated time.

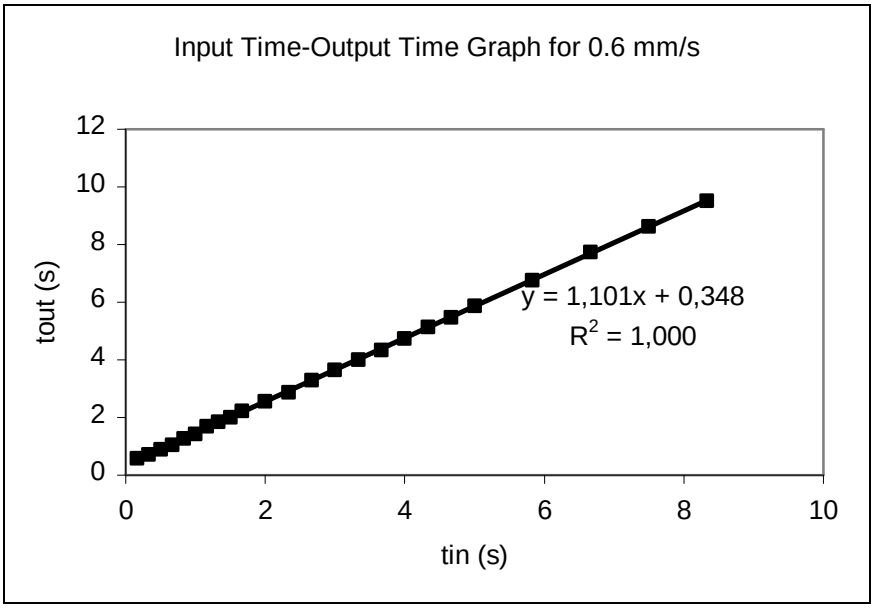

Figure A.55 Entered time versus calculated time graph for 0.6 mm/s

It was obtained a linear relationship for the 0.6 mm/s motor speed.

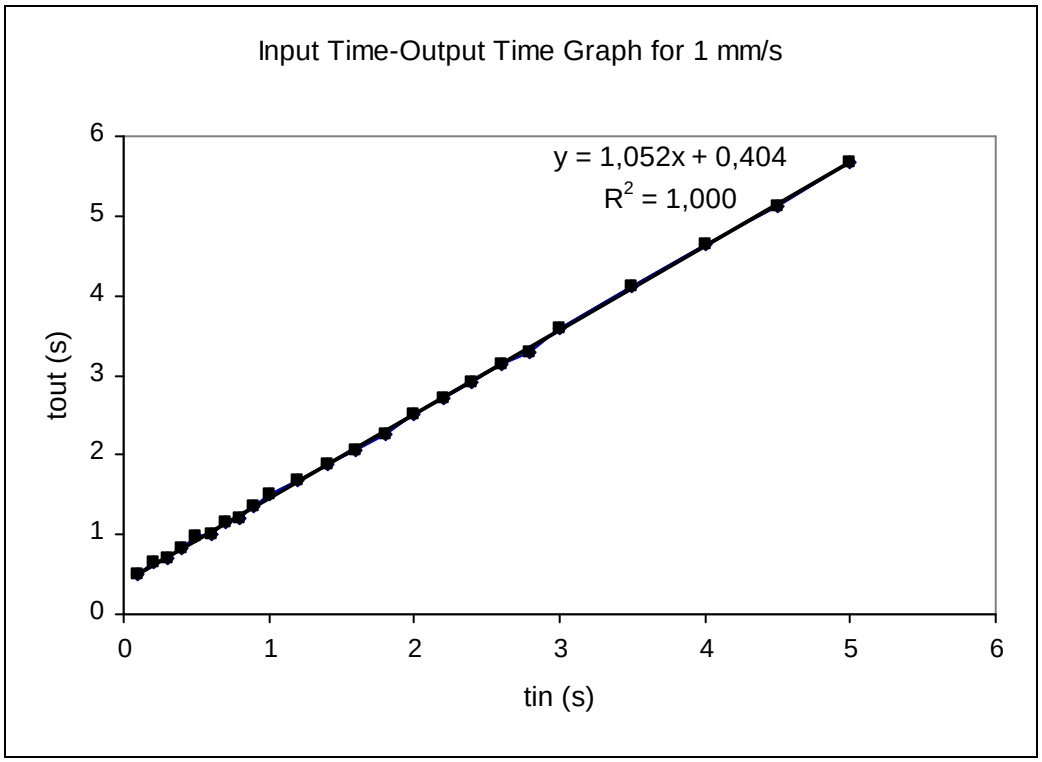

Figure A.56 Entered time versus calculated time graph for 1 mm/s

It was obtained a linear relationship between the entered time and calculated time for the motor speed 1 mm/s.

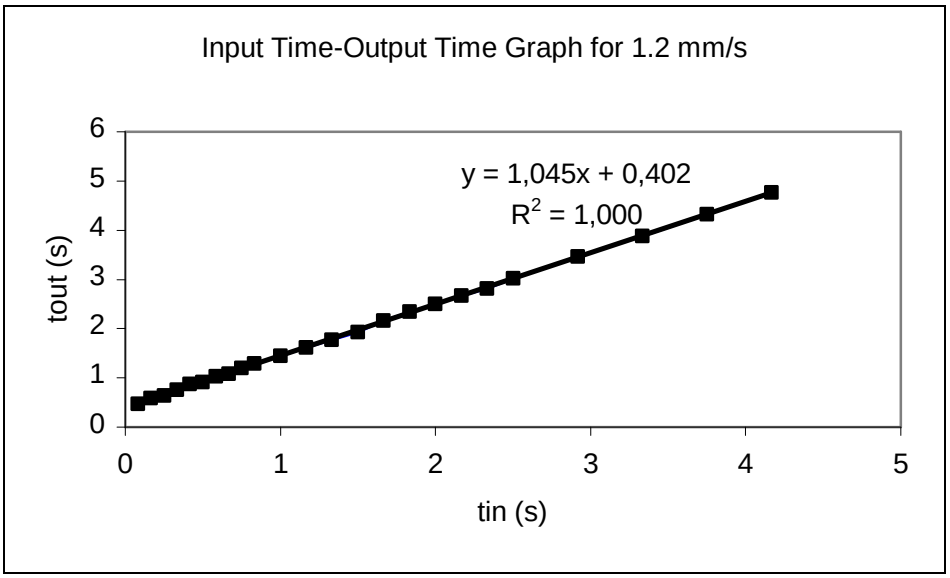

Figure A.57 Entered time versus calculated time graph for 1.2 mm/s

A linear relationship was obtained between the entered time and calculated time for the motor speed 1.2 mm/s.

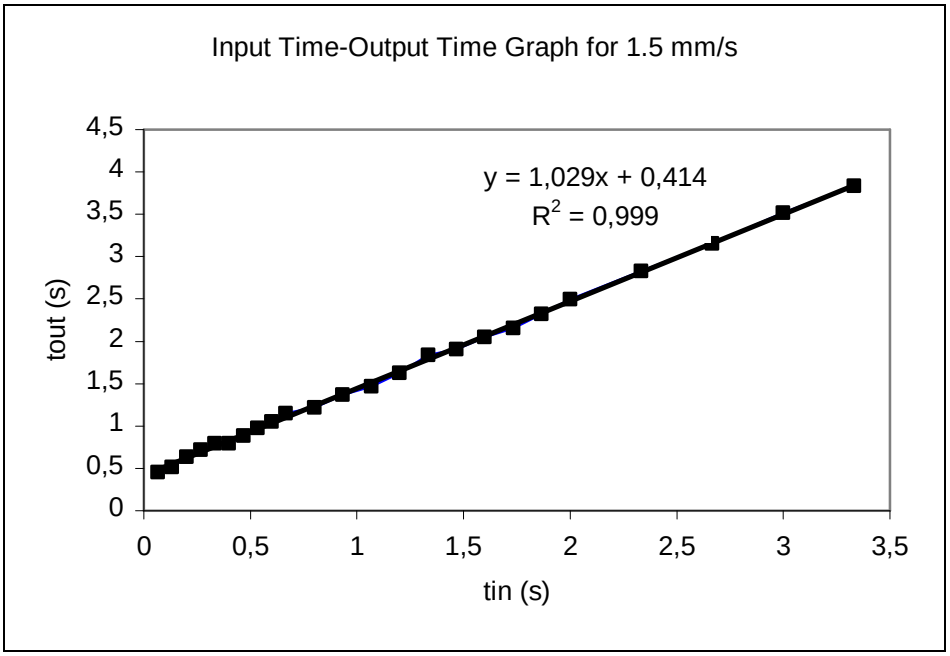

Figure A.58 Entered time versus calculated time graph for 1.5 mm/s

A linear relationship was obtained between the entered time and calculated time for the motor speed 1.5 mm/s. On the other hand, data obtained from the experiment was started show deviation from the trend line.

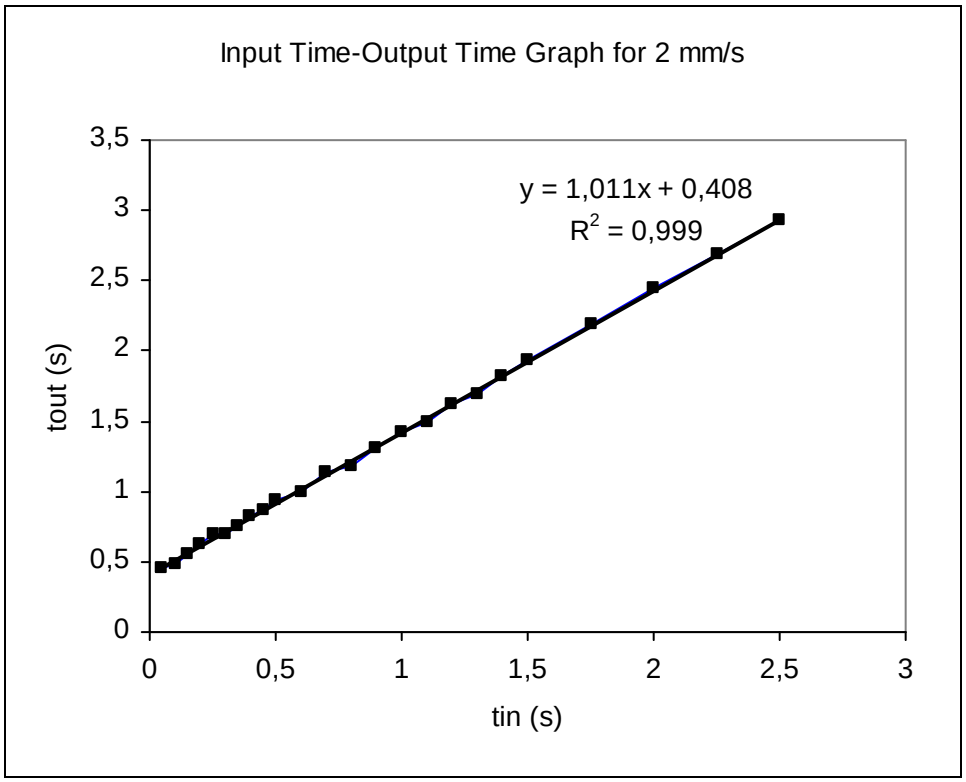

Figure A.59 Entered time versus calculated time graph for 2 mm/s

The deviation seen in Figure A.58 was also seen for the 2 mm/s input motor speed.

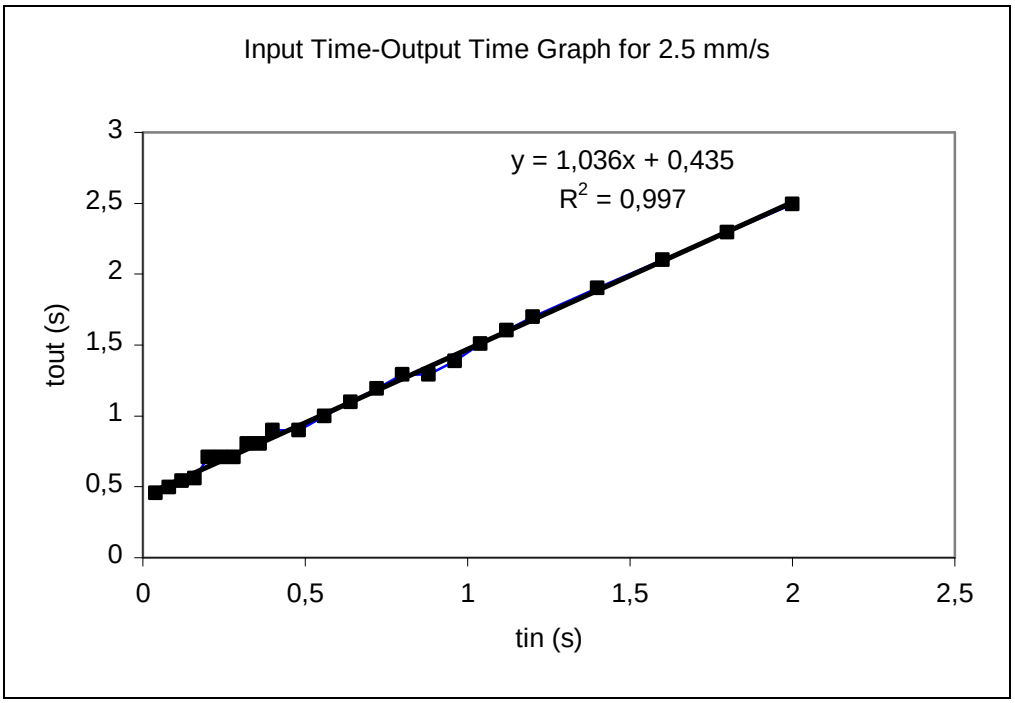

Figure A.60 Entered time versus calculated time graph for 2.5 mm/s

For the 2.5 mm/s motor speed, it was observed a clear quantization error. These errors were appeared at 0.2, 0.24, 0.28 s as first group, 0.32, 0.36 s as second group, 0.4, 0.48 s as third group and 0.8, 0.88 s as fourth group. It can be seen the same characteristics and errors at the speeds 3, 3.5, 4 and 4.5 mm/s from the following graphs.

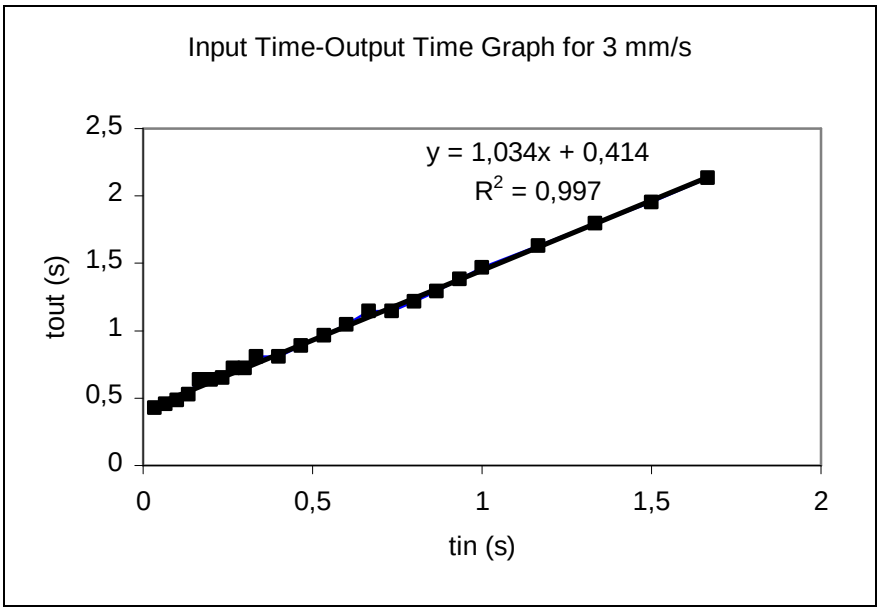

Figure A.61 Entered time versus calculated time graph for 3 mm/s

For the motor speed 3 mm/s, it was obtained a quantization error showing same characteristic with data obtained for 2.5 mm/s motor speed.

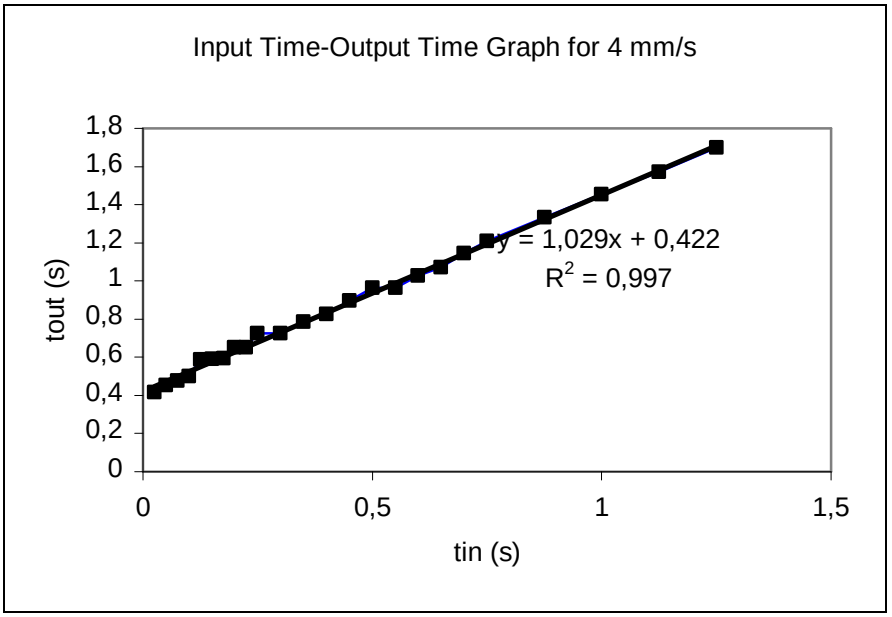

Figure A.62 Entered time versus calculated time graph for 4 mm/s

For the motor speed 4 mm/s, it was obtained a quantization error showing same characteristic with data obtained for 2.5 mm/s motor speed.

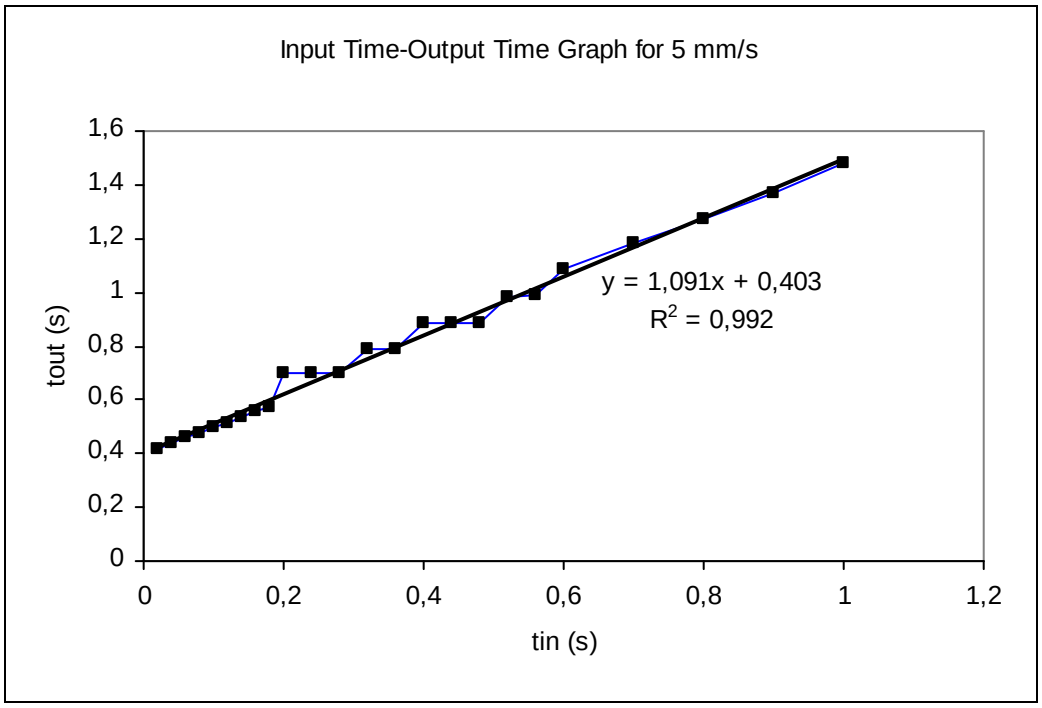

Figure A.63 Entered time versus calculated time graph for 5 mm/s

For the motor speed 5 mm/s, it was observed another quantization error characteristic. For this speed, measured distances took same value at the four entered time groups. Calculated time took same value at 0.2, 0.24, 0.28 s; 0.32, 0.36 s; 0.4, 0.44, 0.48 s and 0.52, 0.56 s. On the other hand, a linear relationship between the entered time and calculated time was also observed.

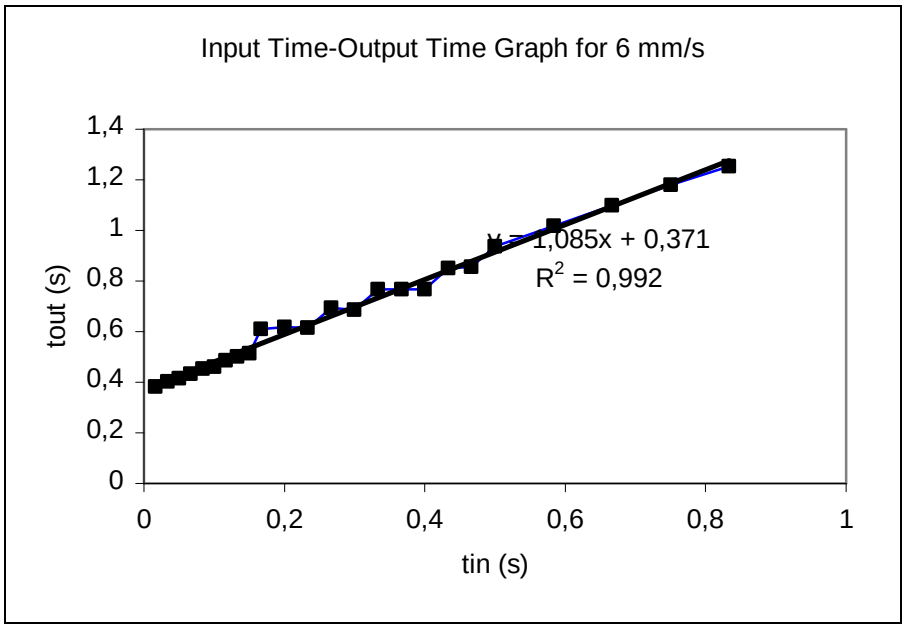

Figure A.64 Entered time versus calculated time graph for 6 mm/s

For the motor speed 6 mm/s, it was obtained a quantization error showing same characteristic with data obtained for 5 mm/s motor speed.

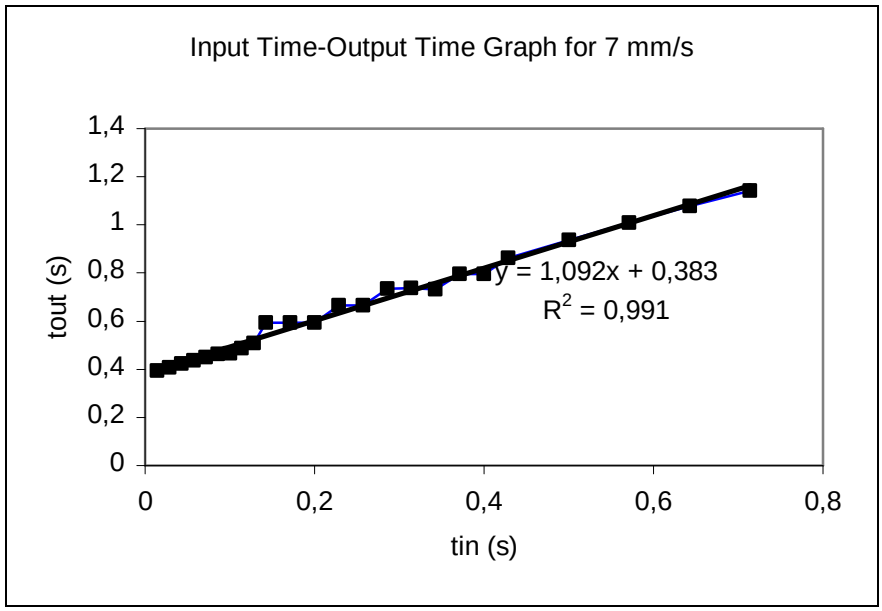

Figure A.65 Entered time versus calculated time graph for 7 mm/s

For the motor speed 7 mm/s, it was obtained a quantization error showing same characteristic with data obtained for 5 mm/s motor speed.

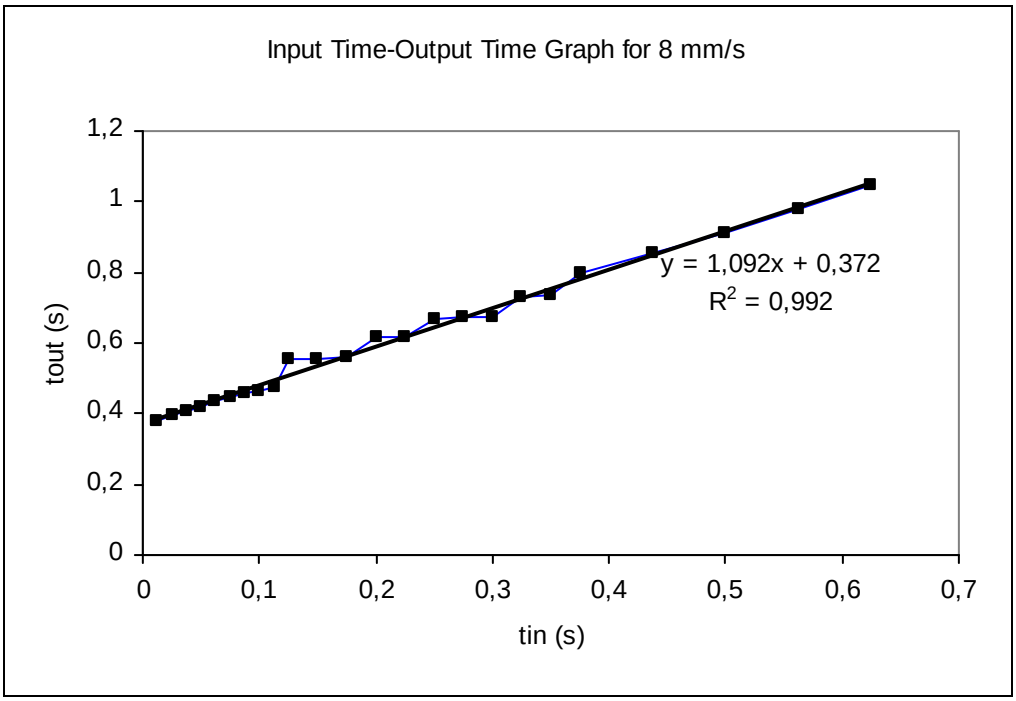

Figure A.66 Entered time versus calculated time graph for 8 mm/s

For the motor speed 8 mm/s, it was obtained a quantization error showing same characteristic with data obtained for 5 mm/s motor speed.

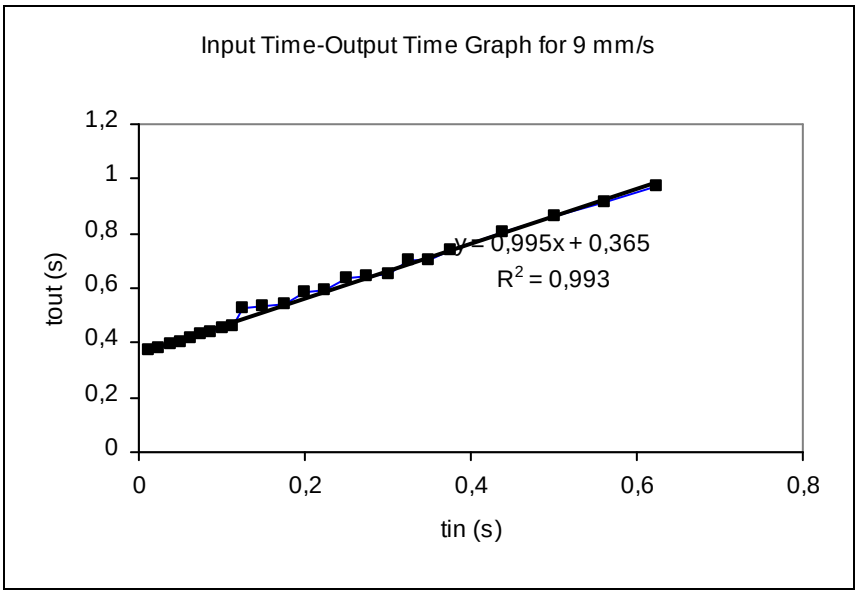

Figure A.67 Entered time versus calculated time graph for 9 mm/s

For the motor speed 9 mm/s, it was obtained a quantization error showing same characteristic with data obtained for 5 mm/s motor speed

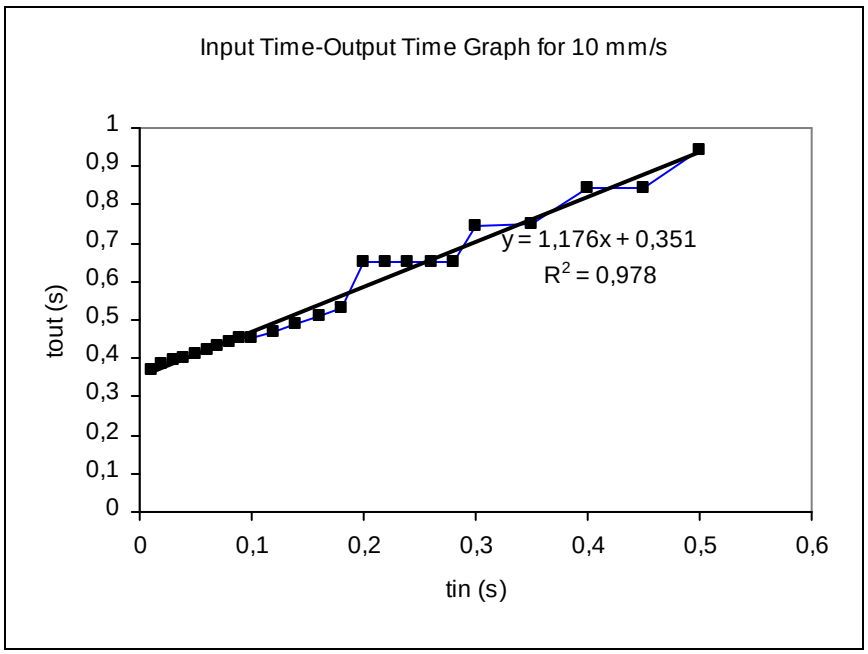

Figure A.68 Entered time versus calculated time graph for 10 mm/s

For the measurement done at 10 mm/s motor speeds, it was observed another type of quantization error. In this measurement calculated time took same value at the entered time 0.2, 0.22, 0.24, 0.26, 0.28 s; 0.3, 0.35 s and 0.4, 0.45 s.

A.5 Constant Graphs Obtained from Input Time versus Calculated Output Time Graphs

Graphs showing motor speed related variation of the slope and y-intersect obtained by the data pertinent to graphs in A.4, are given below

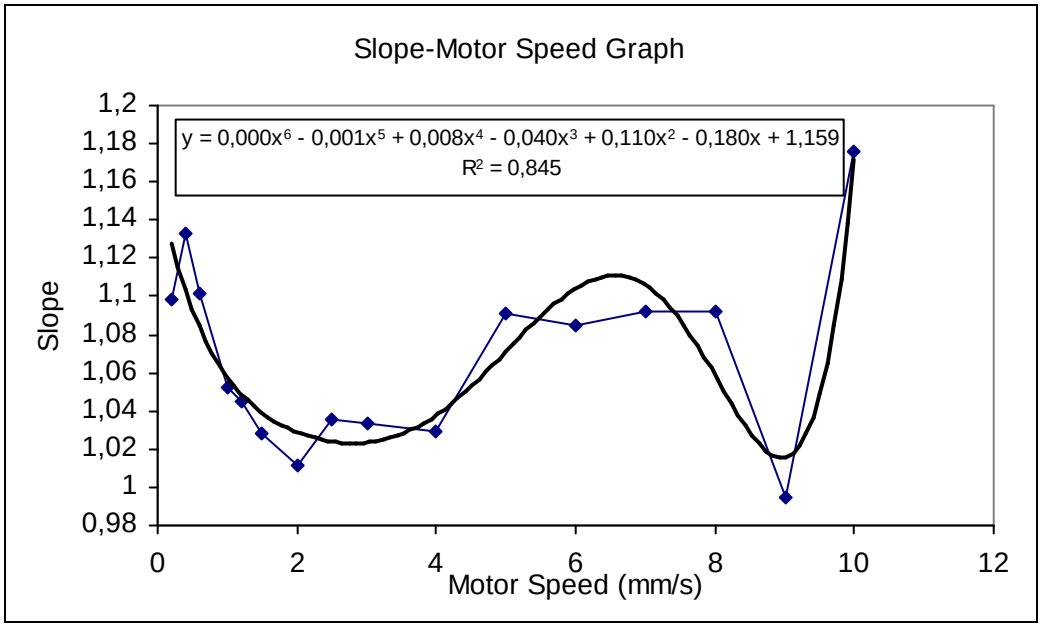

Figure A.69 Graph drawn for the slope of the equations for graphs shown in Appendix A.4

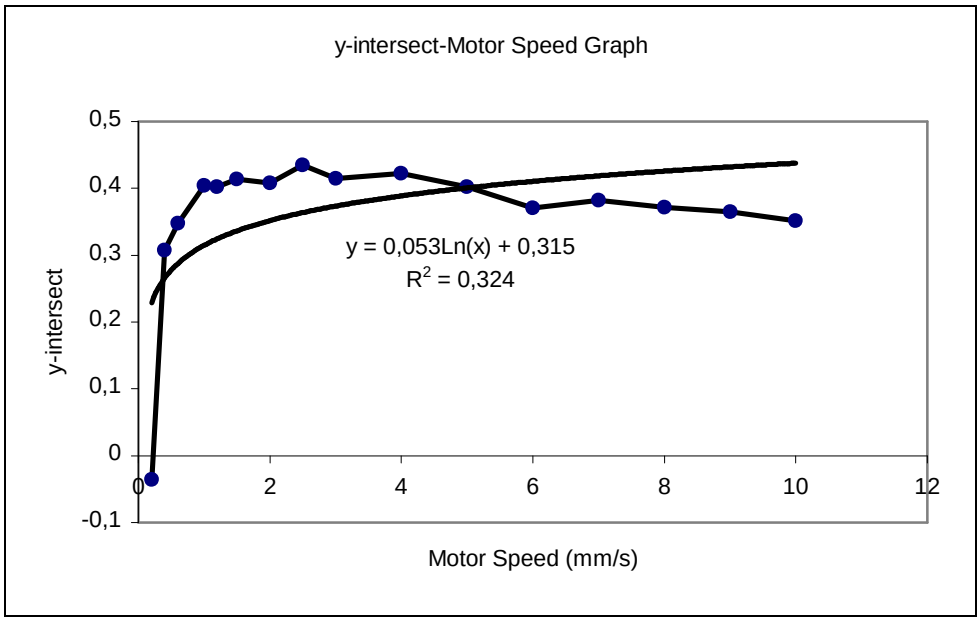

Figure A.70 Graph drawn for the y-intersect of the equations for graphs shown in Appendix A.4

A.6 Graphs Showing Displacement-Output Time Relation

Below, entered displacement versus the calculated time graphs were given. It was observed that following graphs show totally same characteristic with the graphs given in the Appendix A.1, A.2 and A.4.

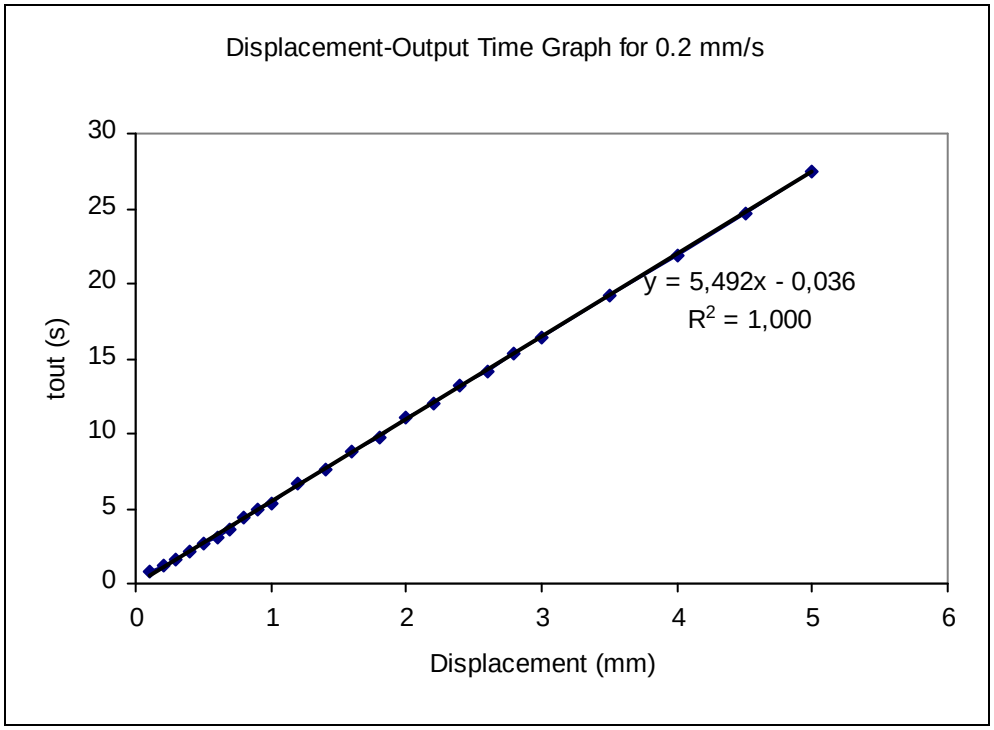

Figure A.71 Entered displacement versus calculated time graph for 0.2 mm/s

As it can be seen from the graph, it was obtained a linear relationship between the entered displacement and output time for the 0.2 mm/s motor speed

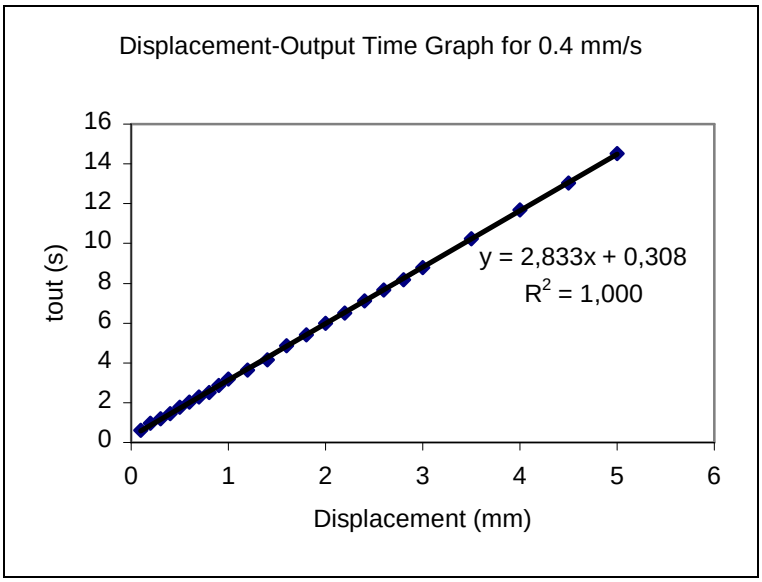

Figure A.72 Entered displacement versus calculated time graph for 0.4 mm/s

Similar result was also obtained for the 0.4 motor speed. It was obtained a linear relationship between the entered displacement and output time.

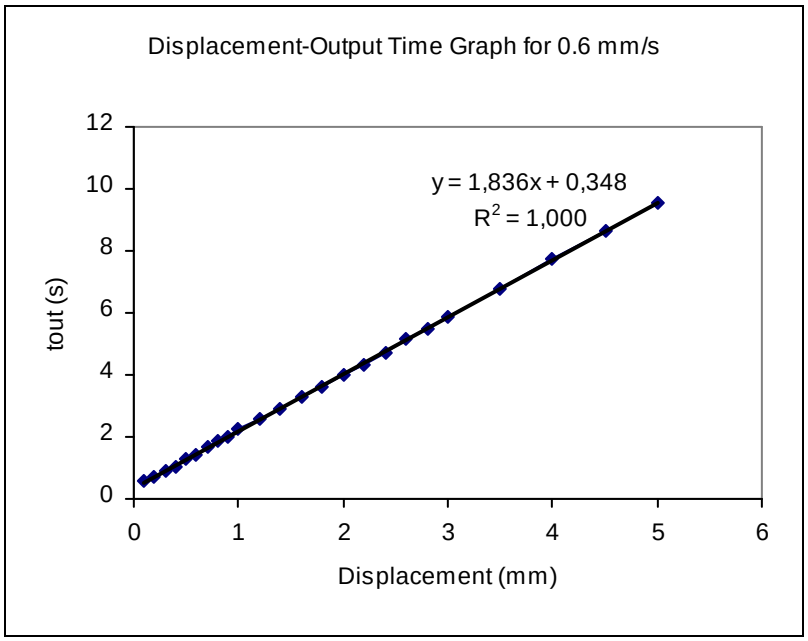

Figure A.73 Entered displacement versus calculated time graph for 0.6 mm/s

It was obtained a linear relationship for the 0.6 mm/s motor speed.

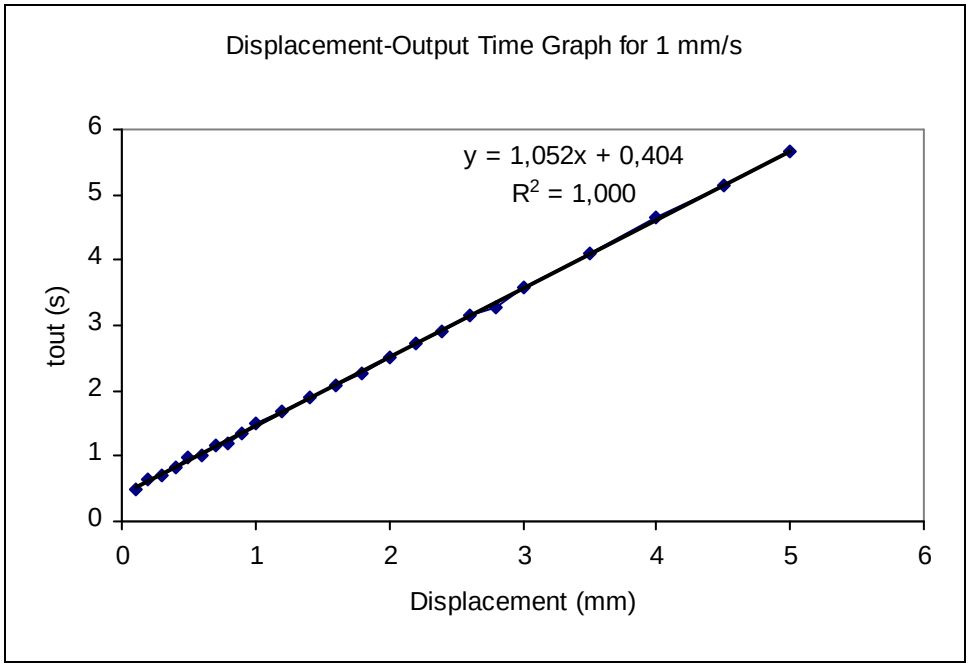

Figure A.74 Entered displacement versus calculated time graph for 1 mm/s

It was obtained a linear relationship between the input distance and output time for the motor speed 1 mm/s

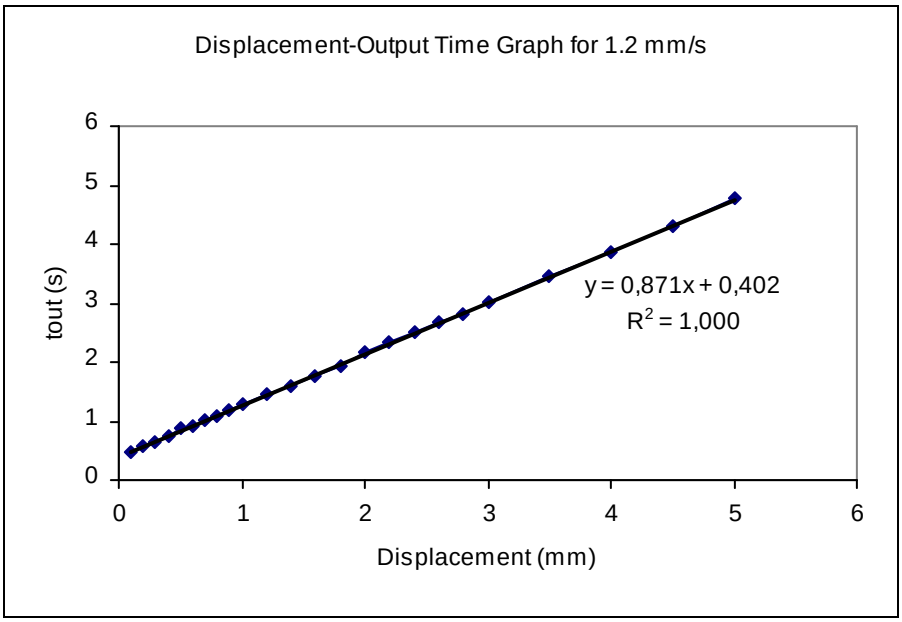

Figure A.75 Entered displacement versus calculated time graph for 1.2 mm/s

A linear relationship was obtained between the input distance and calculated time for the motor speed 1.2 mm/s.

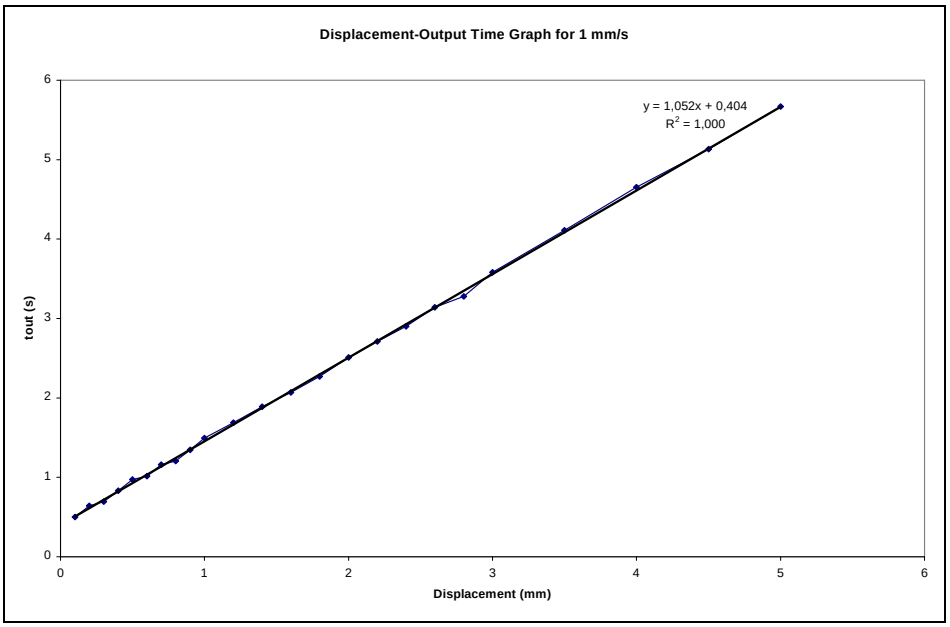

Figure A.76 Entered displacement versus calculated time graph for 1.5 mm/s

A linear relationship was obtained between the input distance and calculated time for the motor speed 1.5 mm/s. On the other hand, data obtained from the experiment was started show deviation from the trend line.

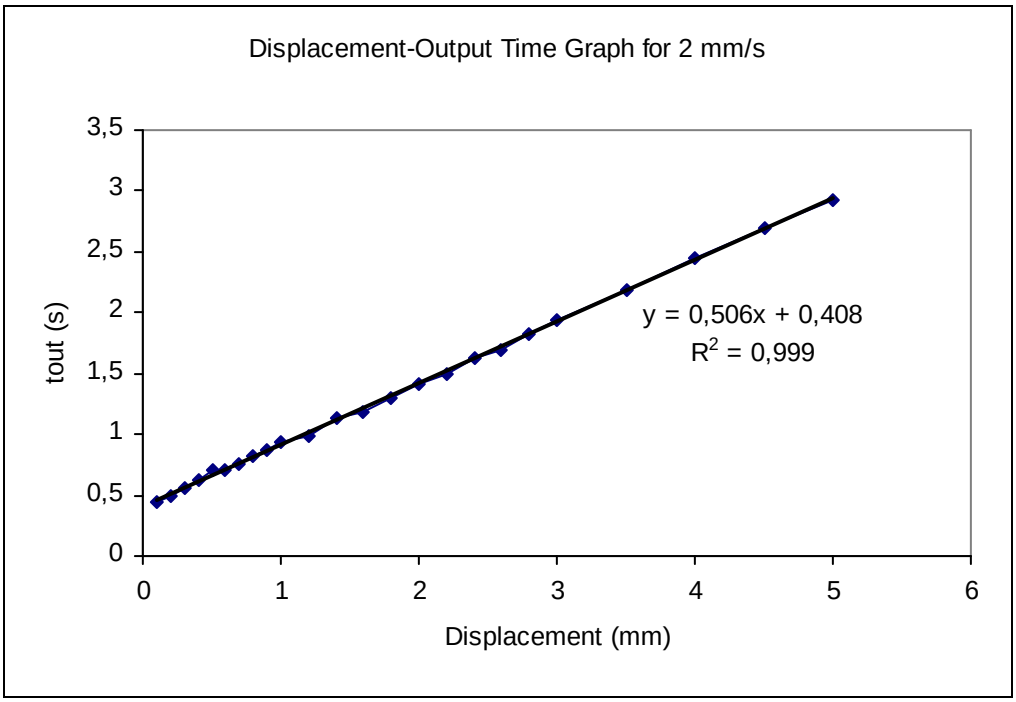

Figure A.77 Entered displacement versus calculated time graph for 2 mm/s

The deviation seen in Figure A.24 was also seen for the 2 mm/s input motor speed.

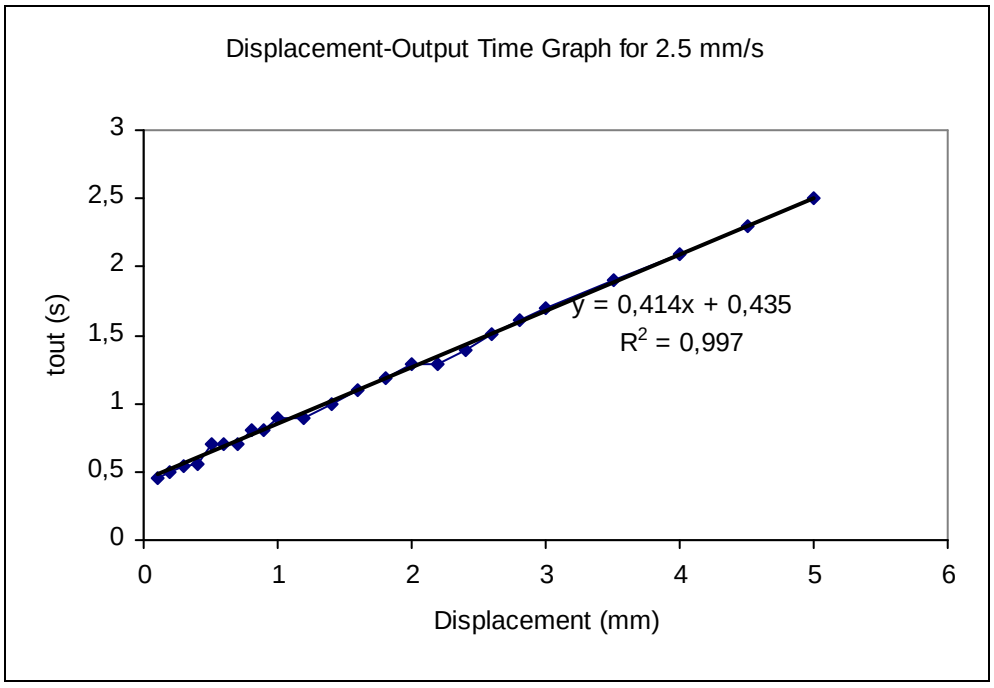

Figure A.78 Entered displacement versus calculated time graph for 2.5 mm/s

For the 2.5 mm/s motor speed, it was observed a clear quantization error. These errors were appeared at 0.5, 0.6, 0.7 mm as first group, 0.8, 0.9 mm as second group, 1, 1.2 mm as third group and 2, 2.2 mm as fourth group. It can be seen the same characteristics and errors at the speeds 3, 3.5, 4 and 4.5 mm/s from the following graphs.

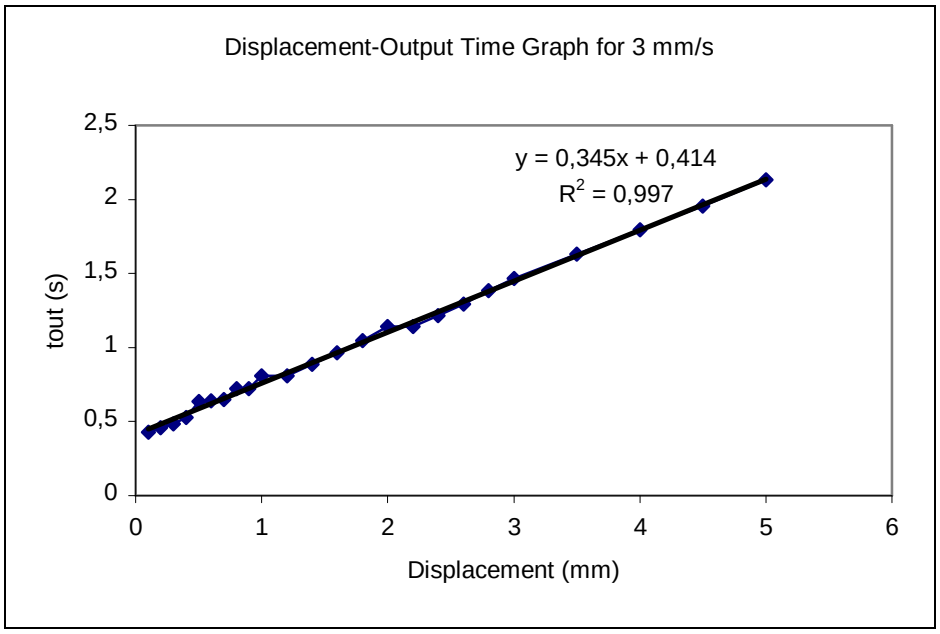

Figure A.79 Entered displacement versus calculated time graph for 3 mm/s

For the motor speed 3 mm/s, it was obtained a quantization error showing same characteristic with data obtained for 2.5 mm/s motor speed.

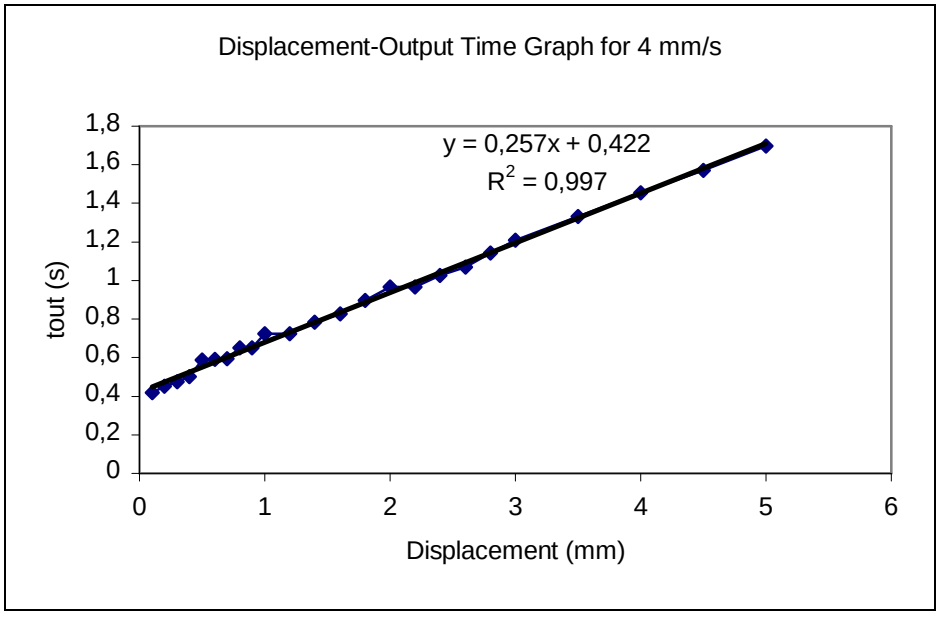

Figure A.80 Entered displacement versus calculated time graph for 4 mm/s

For the motor speed 4 mm/s, it was obtained a quantization error showing same characteristic with data obtained for 2.5 mm/s motor speed.

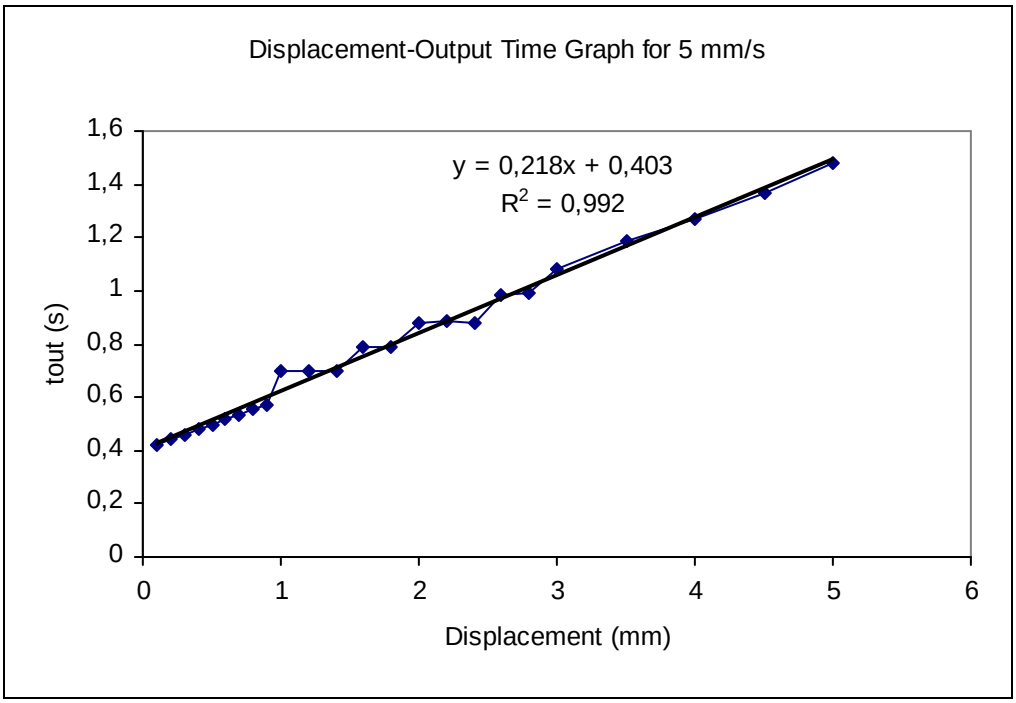

Figure A.81 Entered displacement versus calculated time graph for 5 mm/s

For the motor speed 5 mm/s, it was observed another quantization error characteristic. For this speed, calculated time took same value at the four entered displacement groups. Calculated time took same value at 1, 1.2, 1.4 mm; 1.6, 1.8 mm; 2, 2.2, 2.4 mm and 2.6, 2.8 mm. On the other hand, a linear relationship between the entered displacement and calculated time was also observed.

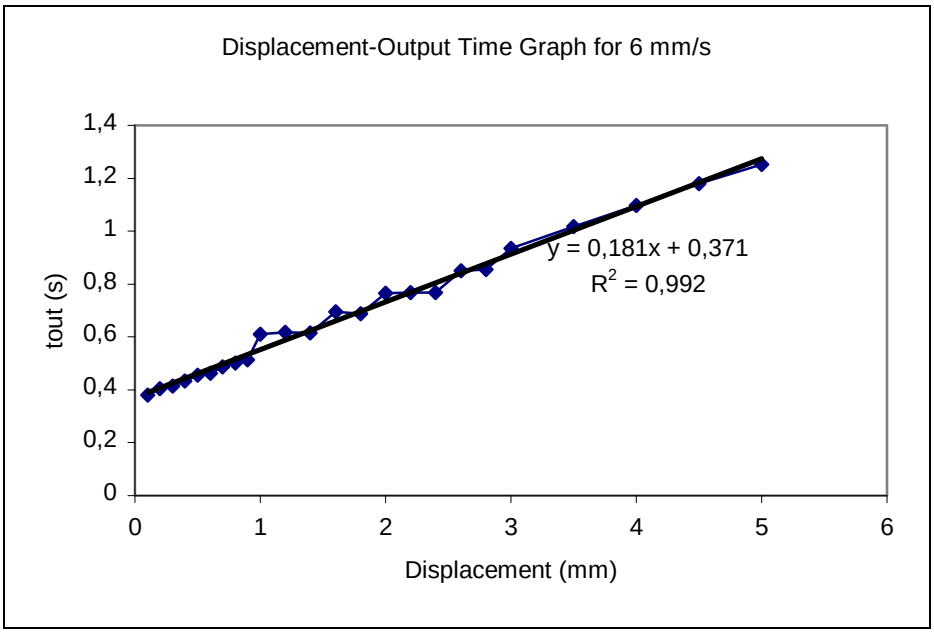

Figure A.82 Entered displacement versus calculated time graph for 6 mm/s

For the motor speed 6 mm/s, it was obtained a quantization error showing same characteristic with data obtained for 5 mm/s motor speed.

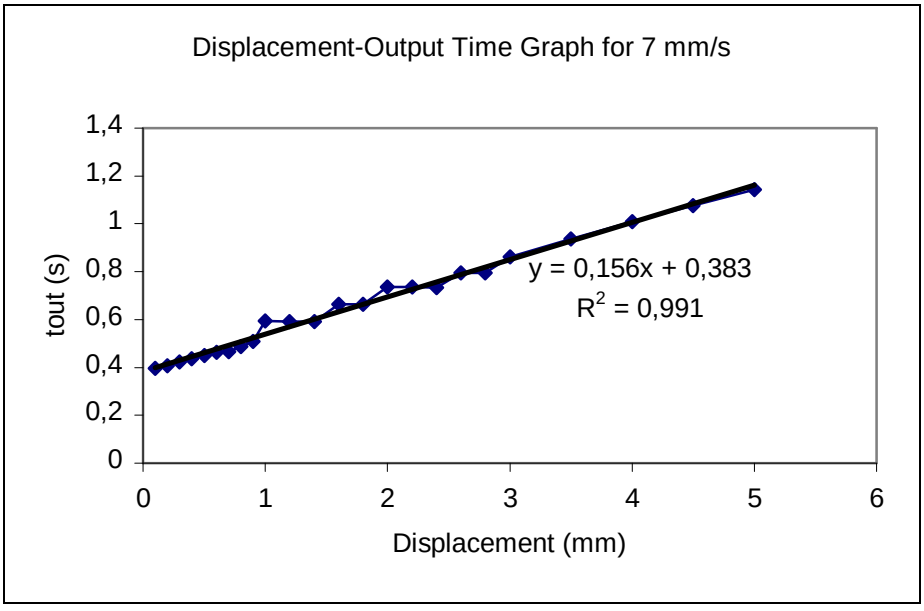

Figure A.83 Entered displacement versus calculated time graph for 7 mm/s

For the motor speed 7 mm/s, it was obtained a quantization error showing same characteristic with data obtained for 5 mm/s motor speed.

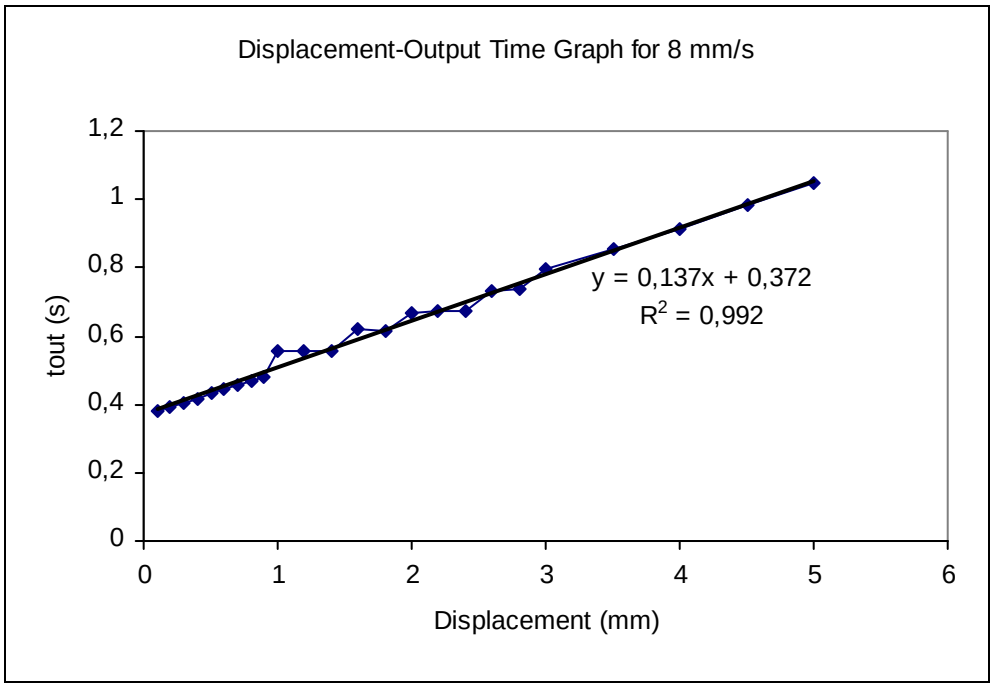

Figure A.84 Entered displacement versus calculated time graph for 8 mm/s

For the motor speed 8 mm/s, it was obtained a quantization error showing same characteristic with data obtained for 5 mm/s motor speed.

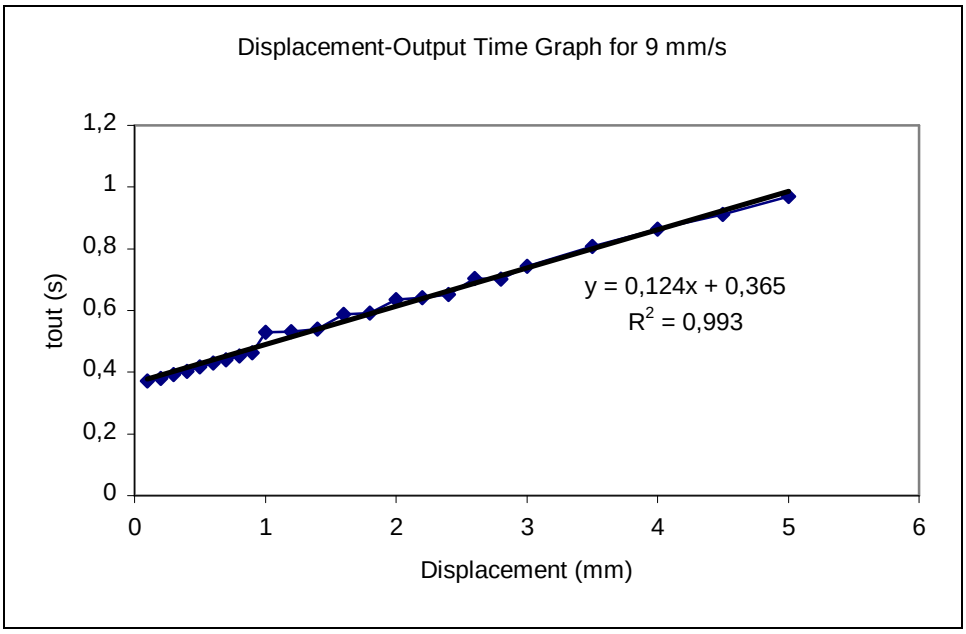

Figure A.85 Entered displacement versus calculated time graph for 9 mm/s

For the motor speed 9 mm/s, it was obtained a quantization error showing same characteristic with data obtained for 5 mm/s motor speed.

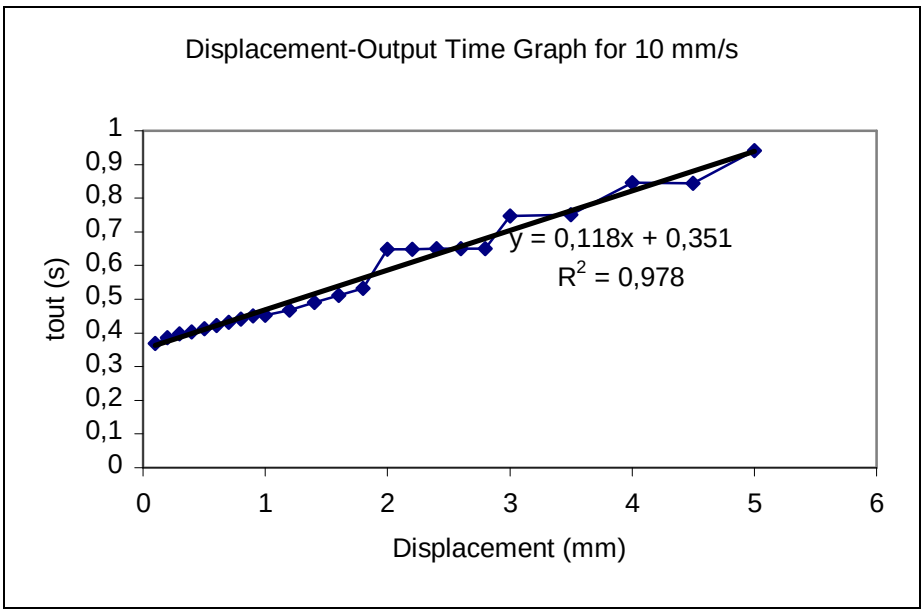

Figure A.86 Entered displacement versus calculated time graph for 10 mm/s

For the measurement done at 10 mm/s motor speeds, it was observed another type of quantization error. In this measurement calculated time took same value at the entered displacements 2, 2.2, 2.4, 2.6, 2.8 mm; 3, 3.5 mm and 4, 4.5 mm.

A.7 Constant Graphs Obtained from the Displacement-Output Time Graphs

Graphs showing motor speed related variation of the slope and y-intersect obtained by the data pertinent to graphs in A.6, are given below.

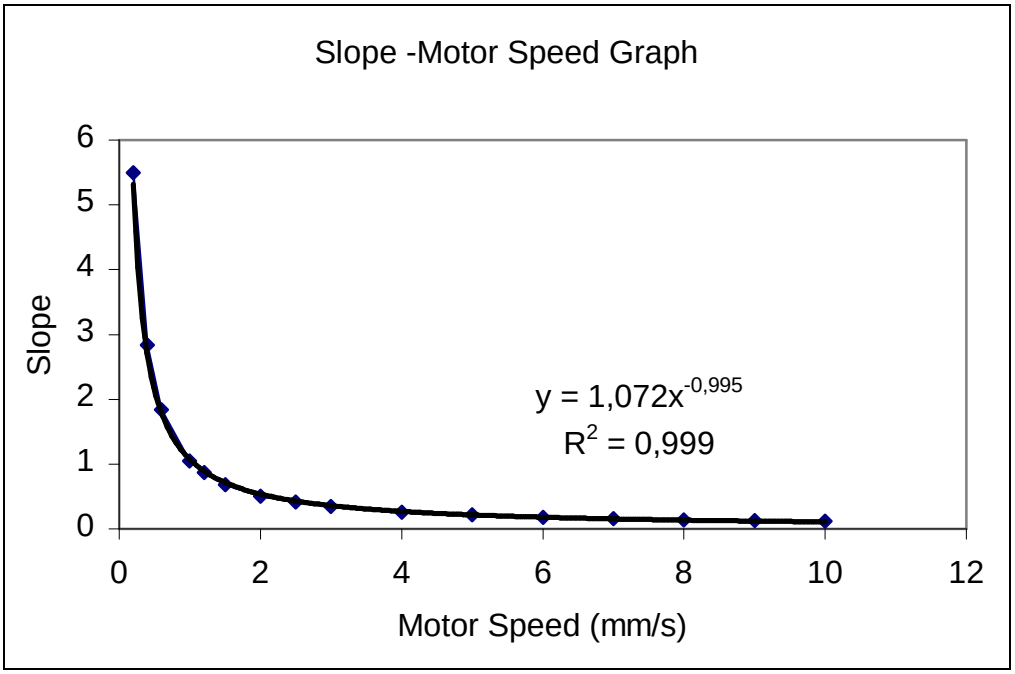

Figure A.87 Graph drawn for the slope of the equations for graphs shown in Appendix A.6

As it can be seen from the Figure A.89, slope values versus motor speed relation was perfectly fitted by using the power equation given in the Figure A.89.

The following Figure A.90 showing y-intercept – motor speed relation was obtained. The curve fitting function was found by using the Excel Trend line.

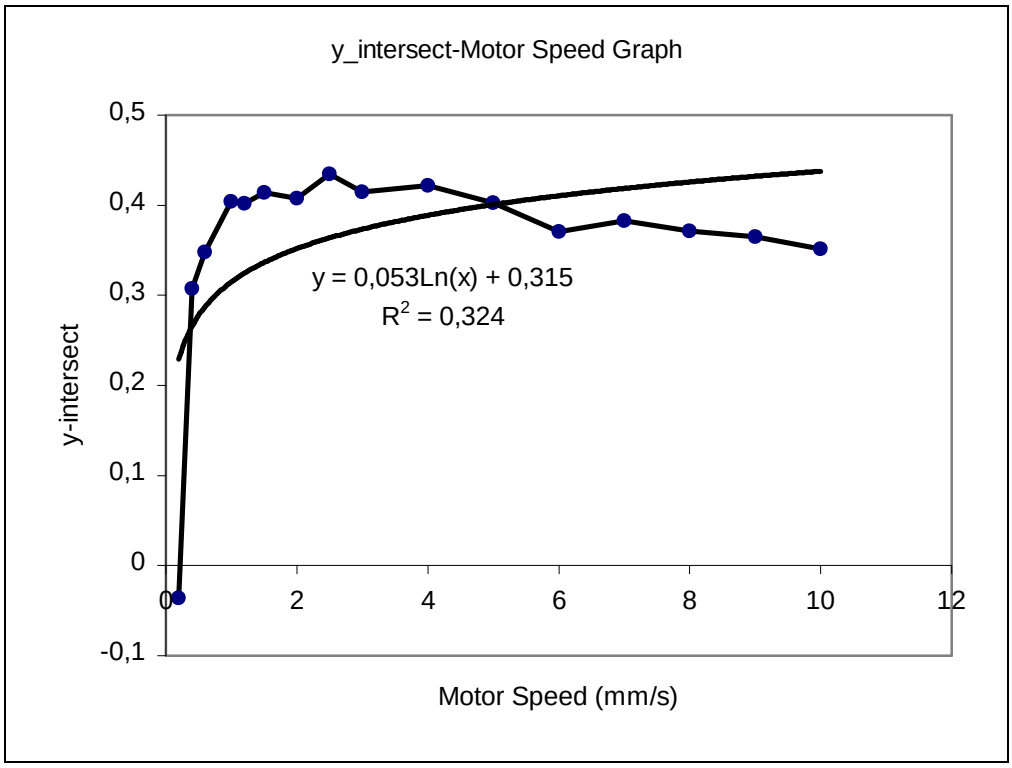

Figure A.88 Graph drawn for the y-intersect of the equations for graphs shown in Appendix A.6

APPENDIX B

CODES GENERATED

B.1 Matlab Code for Random Speed Generation

It was prepared the following software to select the motor speeds randomly. Motor speeds 1, 2, 4 and 8 mm/s were selected randomly by using this software. Thus, the effect of the motor speed on the tissue behavior was observed by making successive measurements at the different speeds showing no trend (Section 4.3.2).

```
global mothiz
for i=1:10000000
    mothiz=randint(1,1,[1,8])
    if mothiz==1
        set(handles.edit2, 'string', num2str(mothiz))
        break
    elseif mothiz==2
        set(handles.edit2, 'string', num2str(mothiz))
        break
    elseif mothiz==4
        set(handles.edit2, 'string', num2str(mothiz))
        break
    elseif mothiz==8
        set(handles.edit2, 'string', num2str(mothiz))
    break
elseif i==10000000
     errordlg('Istenen sayilar yakalanamadi. Lütfen tekrar
deneyin’,’Hatalı Giriş’,’modal’)
end
end
```

B.2 Matlab Code for Finding Maximum Force Values and Corresponding Times

The following software was prepared to find maximum forces for every cycle belonging to the force – time data obtained from the cyclic loading experiments (Figure B.1). These values which would normally be determined one by one from the graphs, would cause substantial time loss, especially when a great many

number of graphs would have been scrutinized. Yet, by using this software, this operation was completed within seconds and thus loss of time was avoided. This software was used for the observation of the effect of speed mentioned in Section 4.3.2 and 4.7.2.1 on the tissue behaviors and also for the observation of the anisotropy behavior studies.

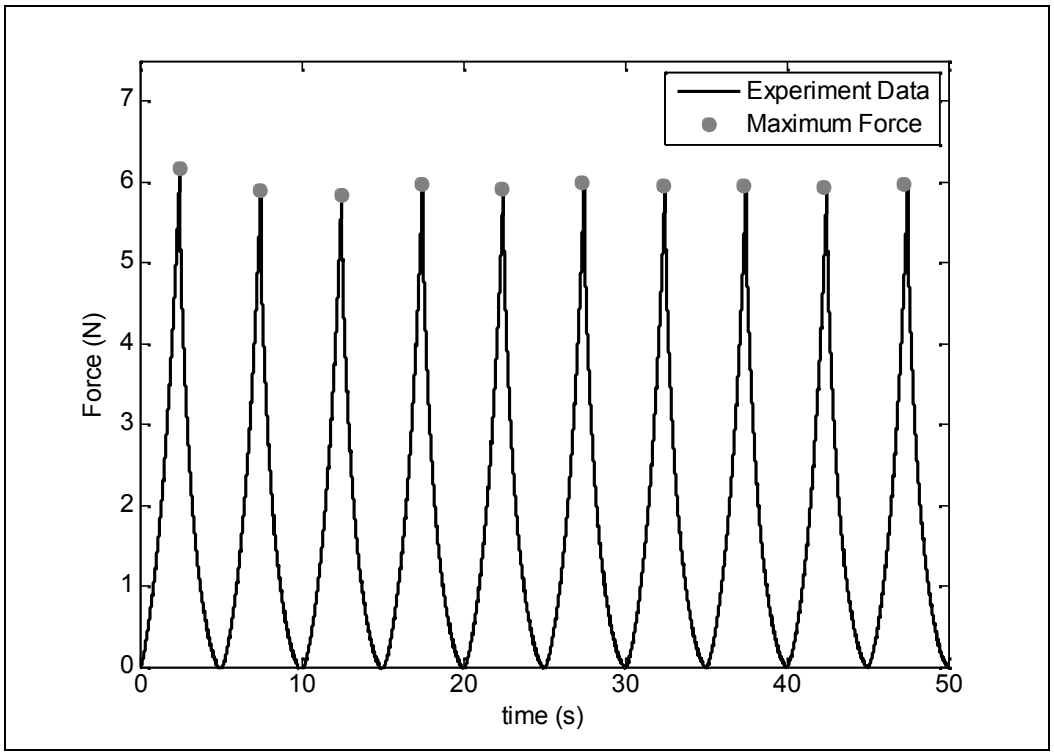

Figure B.1 Maximum force values

```
h1=findobj(gca,'Type','line');
y=get(h1,'YData');
x=get(h1,'Xdata');
n=10;
Fmax=zeros(1,10);
I=zeros(1,10);
xmax=zeros(1,10);
a=length(x);
b=round(a/n);
c=1;
t=0;
for I=1:n
    [Fmax(1,I),I(1,I)]=max(y(c:c+b));
```

```
    c=c+b;
    t=t+I(1,I);
    xmax(1,I)=x(1,t);
    t=t+I(1,I);
end
```

B.3 Matlab Code for Finding Force Differences

Following software was prepared for the calculation of the magnitudes of force decreases at the instant of transition from loading to unloading in the cyclic loading tests described in Chapter 4.3.3. With the help of this software, force differences in all cycles were calculated and their averages were taken. This average value was then used in the study.

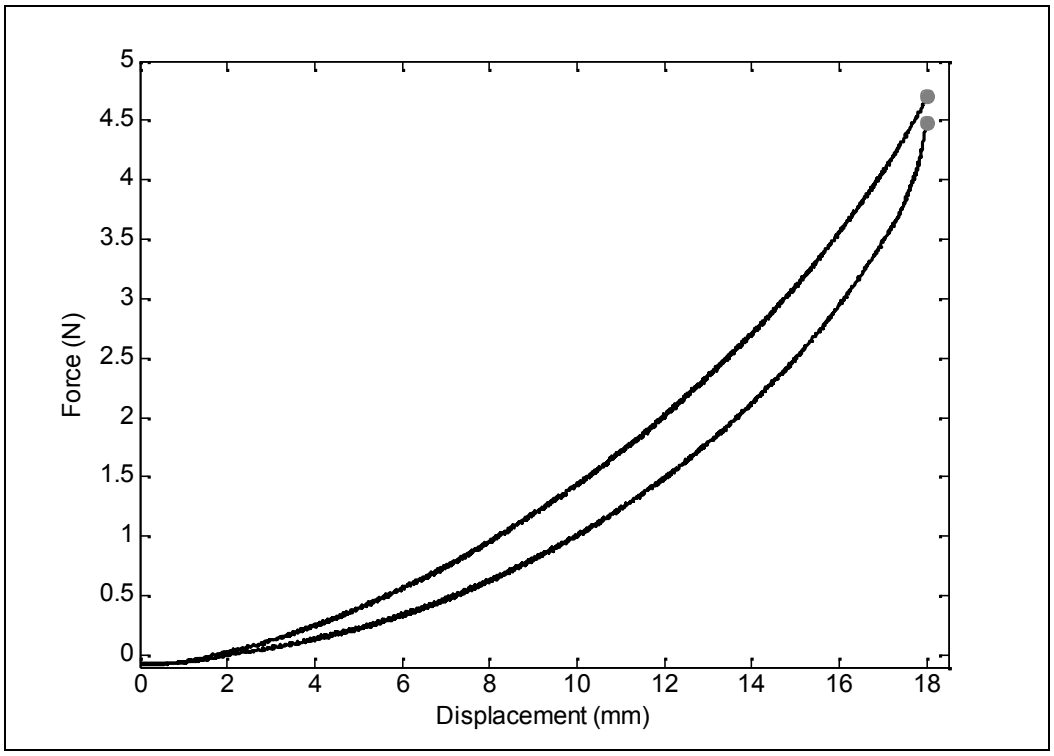

Figure B.2 Force decrease

```
h=findobj(gca,'Type','line');
y=get(h,'YData');
x=get(h,'XData');
L=length(x{1,1});
F=zeros(1,10);
a=0;
for i=1:10
    a=a+1;
    F(1,a)=y{i+10,1}(1,L)-y{i,1}(1,1);
end
Fark=fliplr(F);
M=mean(F);
```

B.4 Matlab Code for Calculating Pulse

Following software was prepared to inquire the amount of step developed in the motor with the distance taken by the indenter tip, as described in Chapter 3.3.2. This software basically shows a great similarity to the softwares controlling the indenter device, with the exception of some few additions. Basic codes facilitating the number of steps taken were marked in bold. With the help of the B-1 code, channel no.3 where the pulses are read are opened. B-2 code, that is the input range, gives data range which is read at the end of the measurement. B-3 code is used for taking the pulse data in the data matrix. Number of steps taken are calculated by the help of the B-4 cycle. In this cycle, when the pulse is lower than 2.5, number of steps taken increases by one and the total steps taken at the end of the cycle is calculated (See Chapter 3.3.2).

```
    global Zaman
    global mothiz
    global mothiz1
    global gerilim
    global Akatsayisi
    global Bkatsayisi
    global atilanadim
    if (mothiz<=0)
        gerilim=gerilim
    else
        gerilim=Akatsayisi*mothiz1-Bkatsayisi
    end
    set(handles.edit6, 'string', ' ')
    ao = analogoutput('nidaq',1);
    addchannel(ao,0:1);
    set(ao,'SampleRate',50)
```

```
set(ao,'TriggerType','Immediate');
putdata(ao,[0 0])
start (ao)
AI=AnalogInput('nidaq',1);
Chan0=AddChannel(AI,[0],'Force');
Chan1=AddChannel(AI,[1],'Hiz');
Chan2=AddChannel(AI,[2],'Yon');
Chan3=AddChannel(AI,[3],'Darbe'); .....(B-1)
Rate=100*20.50524934*10;
Samples=ceil(Rate*Zaman);
Samples
set(Chan0,'InputRange',[0 1])
set(Chan0,'SensorRange',[-0.29218 0.29218])
set(Chan0,'UnitsRange',[-25 25],'Units', 'N')
set(Chan1,'InputRange',[0 1])
set(Chan1,'SensorRange',[0 1])
set(Chan1,'UnitsRange',[0 9.7561],'Units', 'mm/s')
set(Chan2,'InputRange',[0 5])
set(Chan2,'SensorRange',[-11 1])
set(Chan2,'UnitsRange',[-1 1],'Units', 'none')
set(Chan3,'InputRange',[0 5]) .....(B-2)
set(AI,'SampleRate',Rate)
set(AI,'SamplesPerTrigger',Samples
AI.InputType = 'Differential';
putdata(ao,[gerilim 5.004])
start([ao,AI])
[data,time]=getdata(AI,Samples);
while strcmp(AI.Running,'On')
end
putdata(ao,[0 0])
start (ao)
figure
plot(time,data)
delete(ao)
clear ao
pulse=data(:,4); .....(B-3)
atilanadim=1;
for i=2 : Samples .....(B-4)
    if (pulse(i-1)>2.5)
        if (pulse(i)<2.5)
            atilanadim=atilanadim+1;
        end
    end
end
atilanadim
veri=[time data];
set(handles.edit6, 'string', num2str(atilanadim))
plot(time, data(:,1),time, data(:,4))
delete(AI)
clear AI
```

B.5 Filter

In order to filter the noisy test data, following software was prepared. Noisy data is filtered by using sgolayfilt which is a matlab function. This function applies the Savitzky-Golay FIR filter to the data to be cleaned. “y” value in the sgolayfilt function gives the data to be smoothened, 1 gives the degree of polynom and 201 gives the frame size.

```
h=findobj(gca,'Type','line');
y=get(h,'YData');
x=get(h,'XData');
smtlb = sgolayfilt(y,1,201);
figure
plot(x,smtlb)
```

B.6 Filter for Cyclic Loading

```
h=findobj(gca,'Type','line');
y=get(h,'YData');
x=get(h,'XData');
for i=1:20
y{i,:}=sgolayfilt(y{i,:},1,201);
end
```

B.7 Code for Determining the Contact Point of Indenter’s Tip with the Tissue

For the determination of the data starting from the contact point of indenter’s tip with the tissue in the cyclic loading tests, following software were prepared (See Chapter 3.7). st function is used for determining the contact point of each cycle and loading and unloading curves separately. st2 function, on the other hand, is used when a contact point of the total data (See Chapter 3.7). Explanation regarding the running of the softwares are given in the softwares themselves.

B.7.1 st Function

```
function out=st(c,c2,u)

%Required data are taken from the graph obtained at the end of
the experiment

h=findobj(gca,'Type','line');
y=get(h,'YData');
x=get(h,'XData');

%50 points with equal intervals are marked on the data

N1=length(y{11,1});
N=round(N1/50);
a=zeros(1,50);
for i=2:49
    a(1,i)=a(1,i-1)+N;
end
a(1,1)=1;
a(1,50)=N1;

%Values corresponding to these points are determined

for i=1:10
yileri{i,1}=0;
ygeri{i,1}=0;
end
for i=1:10
bileri{i,1}=zeros(1,50);
bgeri{i,1}=zeros(1,50);
end
f=0;
for j=10:-1:1
    f=f+1;
    yileri{f,1}=y{j+10,1};
    ygeri{f,1}=fliplr(y{j,1});
for i=1:50
    bileri{f,1}(1,i)=y{j+10,1}(1,a(1,i));
    bgeri{f,1}(1,i)=y{j,1}(1,a(1,i));
end
bgeri{f,1}=fliplr(bgeri{f,1});
end

%Comparison with the first value entered in the function, is made
by finding the successive differences (See Chapter 3.7). In case
the difference is bigger then the entered parameter, interval
sought for is determined.

kileri(1,10)=0;
kgeri(1,10)=0;
for i=1:10
cileri{i,1}=zeros(1,49);
cgeri{i,1}=zeros(1,49);
end
```

```
for j=1:10
for i=1:49
    cileri{j,1}(1,i)=bileri{j,1}(1,i+1)-bileri{j,1}(1,i);
    if cileri{j,1}(1,i)>=c
        kileri(1,j)=i;
        break, end
end
end

for j=1:10
for i=1:49
    cgeri{j,1}(1,i)=bgeri{j,1}(1,i+1)-bgeri{j,1}(1,i);
    if cgeri{j,1}(1,i)>=c
        kgeri(1,j)=i;
        break, end
end
end

%50 points are determined in the interval found and the above
process repeated. Thus, the contact point is determined more
precisely. Here comparison is made with the second parameter
entered in the function.

for i=1:10
a2ileri{i,1}=zeros(1,50);
a2ileri{i,1}(1,1)=a(1,kileri(1,i));
a2ileri{i,1}(1,50)=a(1,kileri(1,i)+1);
b2ileri{i,1}=zeros(1,50);
c2ileri{i,1}=zeros(1,49);
end

k2ileri=zeros(1,10);
for t=1:10

Nara=round((a(1,kileri(1,t)+1)-a(1,kileri(1,t)))/50);

    for i=2:49
        a2ileri{t,1}(1,i)=a2ileri{t,1}(1,i-1)+Nara;
    end
    for i=1:50
        b2ileri{t,1}(1,i)=yileri{t,1}(1,a2ileri{t,1}(1,i));
    end



    for i=1:49
    c2ileri{t,1}(1,i)=b2ileri{t,1}(1,i+1)-b2ileri{t,1}(1,i);

    if c2ileri{t,1}(1,i)>=c2
        k2ileri(1,t)=i;
        break, end
    end
end
```

```
%

for i=1:10
a2geri{i,1}=zeros(1,50);
a2geri{i,1}(1,1)=a(1,kgeri(1,i));
a2geri{i,1}(1,50)=a(1,kgeri(1,i)+1);
b2geri{i,1}=zeros(1,50);
c2geri{i,1}=zeros(1,49);
end

k2geri=zeros(1,10);
for t=1:10

Nara=round((a(1,kgeri(1,t)+1)-a(1,kgeri(1,t)))/50);

    for i=2:49
        a2geri{t,1}(1,i)=a2geri{t,1}(1,i-1)+Nara;
    end
    for i=1:50
        b2geri{t,1}(1,i)=ygeri{t,1}(1,a2geri{t,1}(1,i));
    end



    for i=1:49
    c2geri{t,1}(1,i)=b2geri{t,1}(1,i+1)-b2geri{t,1}(1,i);

    if c2geri{t,1}(1,i)>=c2
        k2geri(1,t)=i;
        break, end
    end
end

%with the determination of the contact point, graphs are drawn.
If the third parameter entered in the function is taken as 1, in
addition to the main graph, separate graph for each loading and
unloading curve is drawn.

if u==1
for j=1:10
    if k2ileri(1,j)==0
        k2ileri(1,j)=kileri(1,j);
    end
    ys=yileri{j,1}(a2ileri{j,1}(1,k2ileri(1,j)+1):a(1,50));
    figure
    plot(x{11,1}(a2ileri{j,1}(1,k2ileri(1,j)+1):a(1,50)), ys
,'r',...
        'LineWidth',2)
    hold on
    plot(x{11,1},yileri{j,1})
    title(['Number of Loading Cycle: ',num2str(j),'^{st} cycle'])
    xlabel('Displacement [mm]')
    ylabel('Force [N]')
end
```

```
%%%%

for j=1:10
    if k2geri(1,j)==0
        k2geri(1,j)=kgeri(1,j);
    end
    ys=ygeri{j,1}(a2geri{j,1}(1,k2geri(1,j)+1):a(1,50));
    figure
    plot(x{11,1}(a2geri{j,1}(1,k2geri(1,j)+1):a(1,50)), ys
,'r',...
        'LineWidth',2)
    hold on
    plot(x{11,1},ygeri{j,1})
    title(['Number of Unloading Cycle: ',num2str(j),'^{st}
cycle'])
    xlabel('Displacement [mm]')
    ylabel('Force [N]')
end
end

%If the third parameter as entered other than 1 a total graph is
drawn

figure
hold on
for j=1:10
    ysi=yileri{j,1}(a2ileri{j,1}(1,k2ileri+1):a(1,50));
    plot(x{11,1}(a2ileri{j,1}(1,k2ileri+1):a(1,50)), ysi)
ysg=ygeri{j,1}(a2geri{j,1}(1,k2geri+1):a(1,50));
  plot(x{11,1}(a2geri{j,1}(1,k2geri+1):a(1,50)), ysg,'g')
end
xlabel('Displacement [mm]')
ylabel('Force [N]')
```

B.7.2 St2 Function

```
function out=st2(c,c2,u)

%Required data are taken from the graph obtained at the end of
the experiment

h=findobj(gca,'Type','line');
y=get(h,'YData');
x=get(h,'XData');

%50 points with equal intervals are marked on the data

N1=length(y{11,1});
N=round(N1/50);
a=zeros(1,50);
for i=2:49
    a(1,i)=a(1,i-1)+N;
end
```

```
a(1,1)=1;
a(1,50)=N1;

%Values corresponding to these points are determined


for i=1:10
yileri{i,1}=0;
ygeri{i,1}=0;
end
for i=1:10
bileri{i,1}=zeros(1,50);
bgeri{i,1}=zeros(1,50);
end
f=0;
for j=10:-1:1
    f=f+1;
    yileri{f,1}=y{j+10,1};
    ygeri{f,1}=fliplr(y{j,1});
for i=1:50
    bileri{f,1}(1,i)=y{j+10,1}(1,a(1,i));
    bgeri{f,1}(1,i)=y{j,1}(1,a(1,i));
end
bgeri{f,1}=fliplr(bgeri{f,1});
end

%Comparison with the first value entered in the function, is made
by finding the successive differences (See Chapter 3.7). In case
the difference is bigger then the entered parameter, interval
sought for is determined.


kileri(1,10)=0;
kgeri(1,10)=0;
for i=1:10
cileri{i,1}=zeros(1,49);
cgeri{i,1}=zeros(1,49);
end



for j=1:10
for i=1:49
    cileri{j,1}(1,i)=bileri{j,1}(1,i+1)-bileri{j,1}(1,i);
    if cileri{j,1}(1,i)>=c
        kileri(1,j)=i;
        break, end
end
end

for j=1:10
for i=1:49
    cgeri{j,1}(1,i)=bgeri{j,1}(1,i+1)-bgeri{j,1}(1,i);
    if cgeri{j,1}(1,i)>=c
        kgeri(1,j)=i;
        break, end
```

```
end
end

%Average of these points determined for all cycles are taken
separately for the forward and backward movement. In case it is
different than zero and if it is smaller than the average found
for the forward movements, average found for the backward
movement is selected. In other case, the average of the forward
movement is selected.

ki=round(mean(kileri));
kg=round(mean(kgeri));

if ki>=kg & kg~=0;
    k=kg
else
    k=ki
end


%Same procedure is repeated by dividing the interval into three
portions

for i=1:10
a2ileri{i,1}=zeros(1,3);
a2ileri{i,1}(1,1)=a(1,k);
a2ileri{i,1}(1,3)=a(1,k+1);
b2ileri{i,1}=zeros(1,3);
c2ileri{i,1}=zeros(1,2);
end

k2ileri=zeros(1,10);
for t=1:10

Nara=round((a(1,k+1)-a(1,ki))/3);

    for i=2:2
        a2ileri{t,1}(1,i)=a2ileri{t,1}(1,i-1)+Nara;
    end
    for i=1:3
        b2ileri{t,1}(1,i)=yileri{t,1}(1,a2ileri{t,1}(1,i));
    end



    for i=1:2
    c2ileri{t,1}(1,i)=b2ileri{t,1}(1,i+1)-b2ileri{t,1}(1,i);

    if c2ileri{t,1}(1,i)>=c2
        k2ileri(1,t)=i;
        break, end
    end
end

%%%%
```

```
for i=1:10
a2geri{i,1}=zeros(1,3);
a2geri{i,1}(1,1)=a(1,k);
a2geri{i,1}(1,3)=a(1,k+1);
b2geri{i,1}=zeros(1,3);
c2geri{i,1}=zeros(1,2);
end

k2geri=zeros(1,10);
for t=1:10

Nara=round((a(1,k+1)-a(1,k))/3);

    for i=2:2
        a2geri{t,1}(1,i)=a2geri{t,1}(1,i-1)+Nara;
    end
    for i=1:3
        b2geri{t,1}(1,i)=ygeri{t,1}(1,a2geri{t,1}(1,i));
    end



    for i=1:2
    c2geri{t,1}(1,i)=b2geri{t,1}(1,i+1)-b2geri{t,1}(1,i);

    if c2geri{t,1}(1,i)>=c2
        k2geri(1,t)=i;
        break, end
    end
end

%Comparison for the forward and backward movement is done by
taking the average of the points found

ki2=round(mean(k2ileri));
kg2=round(mean(k2geri));

if ki2>=kg2;
    k2=ki2
else
    k2=kg2
end

%with the determination of the contact point, graphs are drawn.
If the third parameter entered in the function is taken as 1, in
addition to the main graph, separate graph for each loading and
unloading curve is drawn.

if u==1,
for j=1:10
    ys=yileri{j,1}(a2ileri{j,1}(1,k2+1):a(1,50));
    figure
    plot(x{11,1}(a2ileri{j,1}(1,k2+1):a(1,50)), ys ,'r',...
        'LineWidth',2)
```

```
    hold on
    plot(x{11,1},yileri{j,1})
    title(['Number of Loading Cycle: ',num2str(j),'^{st} cycle'])
    xlabel('Displacement [mm]')
    ylabel('Force [N]')
end
for j=1:10
    ys=ygeri{j,1}(a2geri{j,1}(1,k2+1):a(1,50));
    figure
    plot(x{11,1}(a2geri{j,1}(1,k2+1):a(1,50)), ys ,'r',...
        'LineWidth',2)
    hold on
    plot(x{11,1},ygeri{j,1})
    title(['Number of Unloading Cycle: ',num2str(j),'^{st}
cycle'])
    xlabel('Displacement [mm]')
    ylabel('Force [N]')
end
end

%If the third parameter as entered other than 1 a total graph is
drawn

figure
hold on
for j=1:10
ysi=yileri{j,1}(a2ileri{j,1}(1,k2+1):a(1,50));
xeksen=x{11,1}(a2ileri{j,1}(1,k2+1):a(1,50))-
x{11,1}(a2ileri{j,1}(1,k2+1));
    plot(xeksen, ysi)

ysg=ygeri{j,1}(a2geri{j,1}(1,k2+1):a(1,50));

  plot(xeksen, ysg,'g')
end
xlabel('Displacement [mm]')
ylabel('Force [N]')
```

B.8 Code for Decreasing Number of Experiment Data Points

Data obtained from the experiments consists of great many number of points. It is so much so that, some of the data contains millions of points. This results in the formation of huge files and causes the operations to take too long time. For this reason following software was prepared. By using this software, size of the file was decreased without changing the characteristic of the data obtained. Figure B.3 shows the reduction of data containing 565943 points to 1993 points by using this software. As seen from the graph, data points are superimposed. This process truly expedites any work carried on the data. Besides this, without

undertaking this process, it is nearly impossible to conduct any study on the data even in Excel. In the software, basic input defining the number of data points is the value 2000, written in bold. In case this value is entered smaller, lesser number of data point and if it is entered bigger, larger number of data point is obtained. Yet, value 2000, giving good results, was selected and insisted upon.

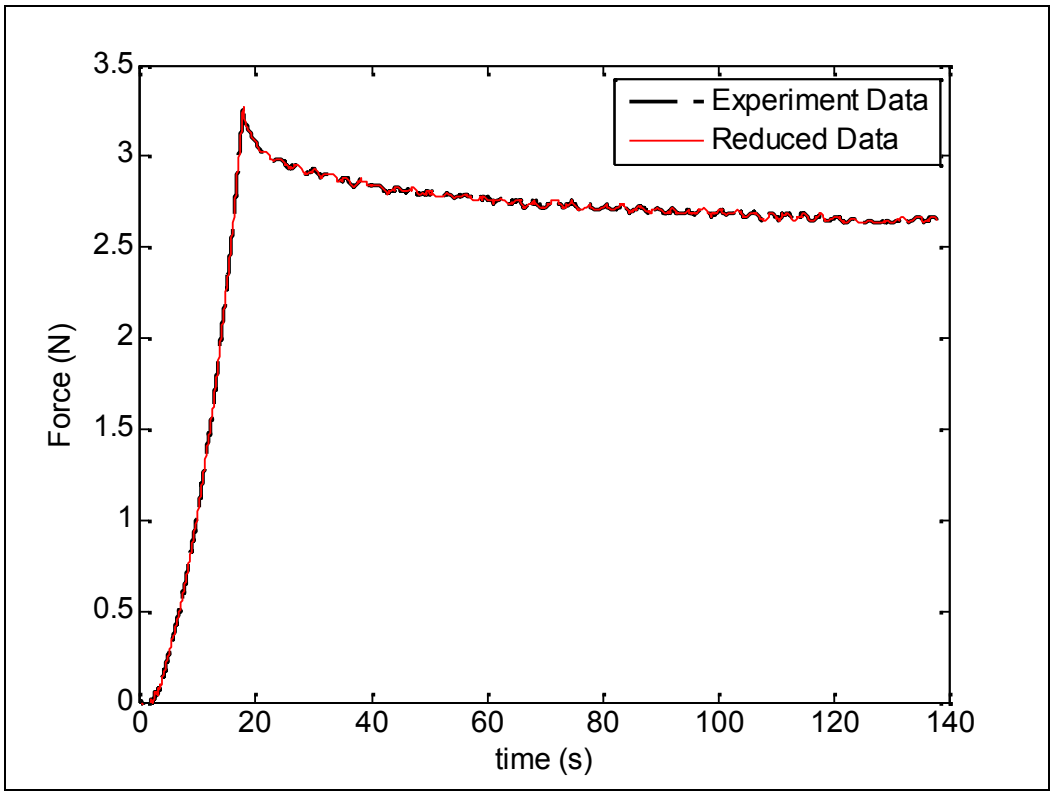

Figure B.3 Comparison of reduced data and experimental data.

```
h1=findobj(gca,'Type','line');
y1=get(h1,'YData');
x1=get(h1,'XData');
kat=round(length(x1)/2000)+1;
n=round(length(x1)/kat);
y=zeros(1,n);
k=1;
for i=1:n
y(1,i)=y1(1,k);
k=k+kat;
end
```

```
k1=1;
for i=1:n
x(1,i)=x1(1,k1);
k1=k1+kat;
end
figure
plot(x,y)
x2=x.';
y2=y.';
```

For the application of the same process to the results of the cyclic loading tests following software was prepared.

```
h1=findobj(gca,'Type','line');
y1=get(h1,'YData');
x1=get(h1,'XData');
kat=round(length(x1{1,1})/2000)+1;
n=round(length(x1{1,1})/kat);
y{20,1}=0;
for i=1:20
    y{i,1}=zeros(1,n);
end
for j=1:20
k=1;
for i=1:n
y{j,1}(1,i)=y1{j,1}(1,k);
k=k+kat;
end
end
x{20,1}=0;
for i=1:20
    x{i,1}=zeros(1,n);
end
for j=1:20
k1=1;
for i=1:n
x{j,1}(1,i)=x1{j,1}(1,k1);
k1=k1+kat;
end
end
figure
hold on
for i=1:20
plot(x{i,1},y{i,1})
end
for i=1:20
x2{1,i}=x{i,1}.';
y2{1,i}=y{i,1}.';
end
figure
hold on
for i=1:20
```

```
plot(x2{1,i},y2{1,i})
end
```

B.9 Calculation of Hysteresis

Hysteresis magnitudes observed at the end of the cyclic loading tests were used for carrying out the certain analysis in the study (See Chapter 4.3.2). Therefore, following software for the calculation of the hysteresis magnitudes was prepared. Hysteresis magnitude given by the area laying in between the loading and unloading curves obtained in the cyclic loading tests. In following software, these ares were calculated by using the trapezoidal rule (Chapra and Canale, 1998)

```
h1=findobj(gca,'Type','line');
y=get(h1,'YData');
x=get(h1,'XData');
for i=1:10
    y{i,1}=fliplr(y{i,1});
    x{i,1}=fliplr(x{i,1});
end
alani=zeros(1,10);
alang=zeros(1,10);
dileri=0;
dgeri=0;
Fark=zeros(1,10);
N=length(x{1,1})-1;
a=0;
for i=1:10
for j=1:N
dileri=(y{i+10,1}(1,j+1)+y{i+10,1}(1,j))*(x{i+10,1}(1,j+1)-
x{i+10,1}(1,j))/2;
dgeri=(y{i,1}(1,j+1)+y{i,1}(1,j))*(x{i,1}(1,j+1)-x{i,1}(1,j))/2;
alani(1,i)=alani(1,i)+dileri;
alang(1,i)=alang(1,i)+dgeri;
a=j;
if a==N
Fark(1,i)=alani(1,i)-alang(1,i);
end
end
end
Fark=fliplr(Fark);
c=(1:10);
figure
plot(c,Fark)
```

B.10 Calculation of R-Square Values

In order to determine the closeness of the curve to the experimental data if curve fitting had been carried out, or to inquire the capability of the equations used in Chapter 4.6.4 in modelling the existing experimental data, R-square values were being used. Again, for the comparison oriented studies, r-square values are needed. To this end, software given below was prepared.

```
h1=findobj(gca,'Type','line');
y=get(h1,'YData');
x=get(h1,'XData');
m=mean(y{2,1})
n=length(y{2,1});
st=0;
sr=0;
for i=1:n
    sti=(y{2,1}(1,i)-m)^2;
    st=st+sti;
    sri=(y{2,1}(1,i)-y{1,1}(1,i))^2;
    sr=sr+sri;
end
rsq=(st-sr)/st;
```

B.11 Code for the Correction of the Relaxation Data Containing Force Calibration Error

In some of the relaxation data, small errors arising from the force calibration efforts, took place (Figure B.4). For the correction of these errors, software below was prepared and though using it, better results were obtained (Figure B.5).

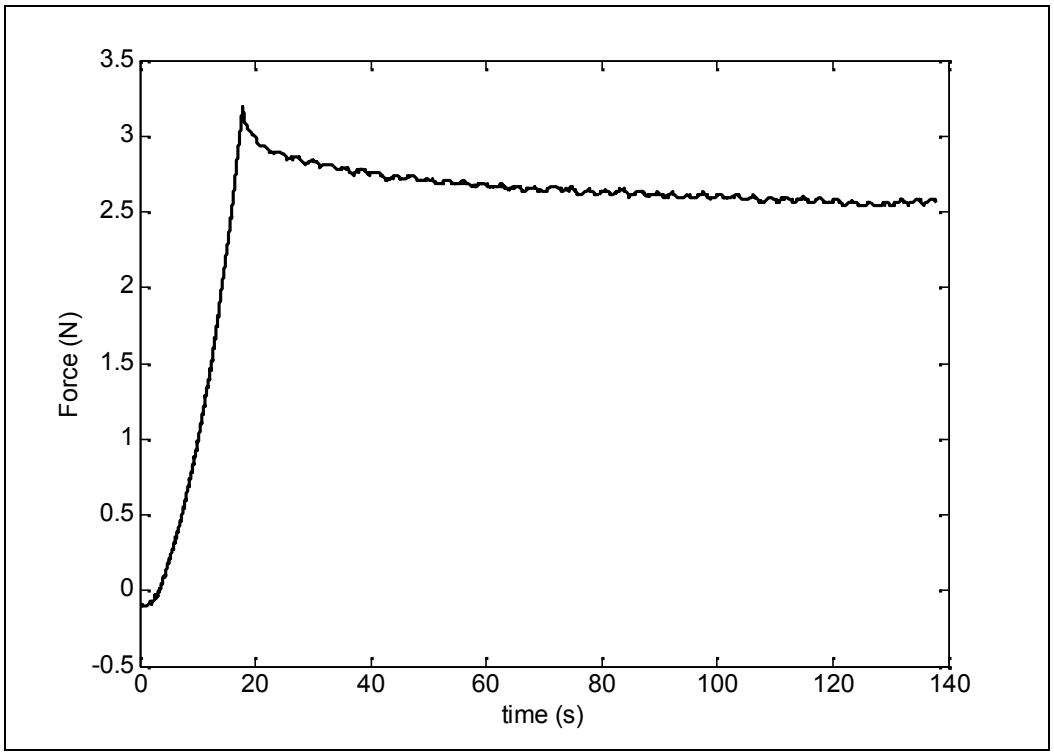

Figure B.4 Relaxation data containing force calibration error

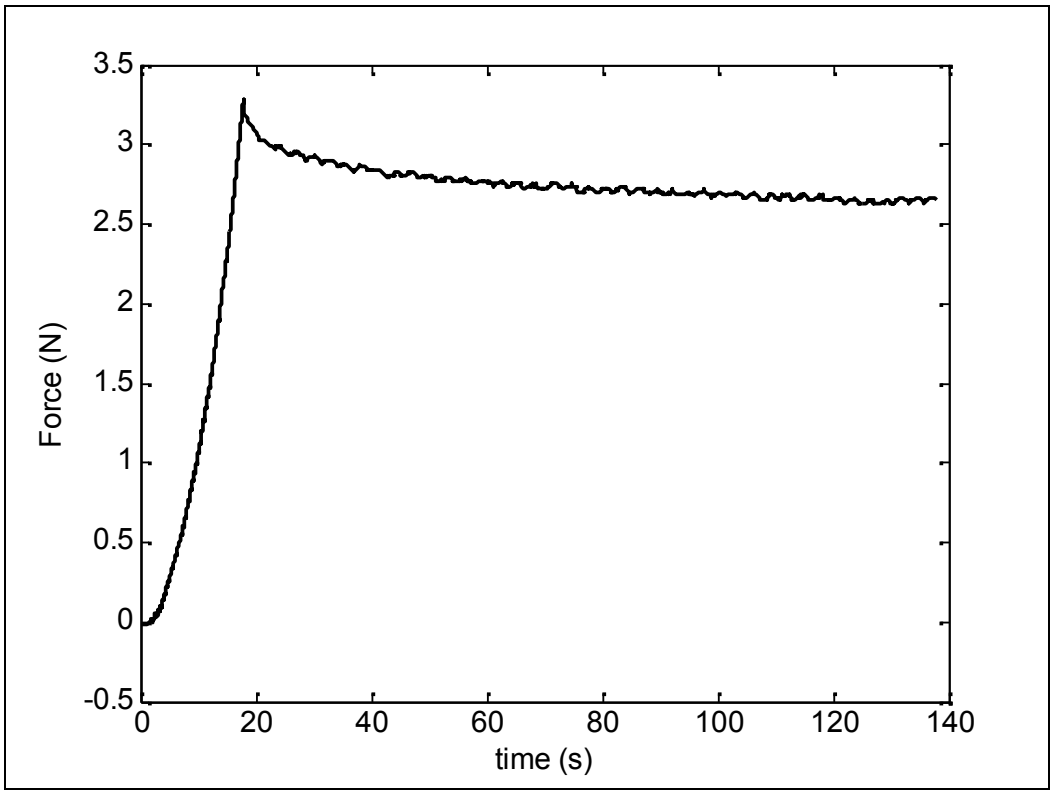

Figure B.5 Corrected relaxation data

```
h1=findobj(gca,'Type','line');
y1=get(h1,'YData');
x1=get(h1,'XData');
a=length (y1);
ab=abs(y1(1,1));
for i=1:a
    y1(1,i)=y1(1,i)+ab;
end
figure
plot(x1,y1)
```

APPENDIX C

VARIATION OF THE CONSTANTS OF THE EQUATION 4.2 WITH THE INCREASING MOTOR SPEED

As explained in the chapter 4.6.3.1 a general rule showing the constants changes with the increasing motor speed was not observed. It was observed that A and B coefficients decreased with increasing speed in Figure 4.38 and Figure 4.39. However, such an observation was not obtained in the following Figure C.1 and Figure C.2. For both constant it was obtained an increase for the value obtained at 8 mm/s motor speed. Consequently, it was not possible to say about motor speed affects on the tissue by using these constants.

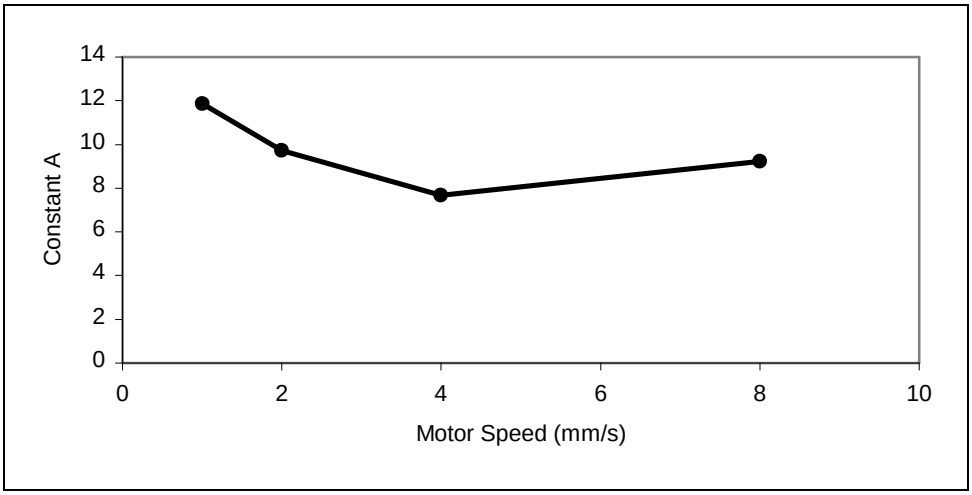

Figure C.1 Variation of A constant with motor speed

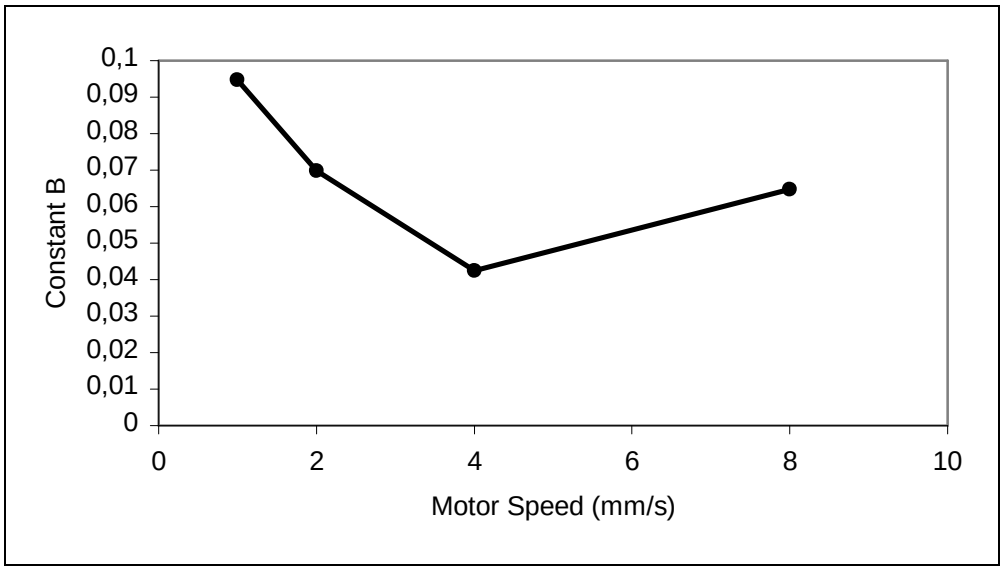

Figure C.2 Variation of B constant with motor speed

APPENDIX D

DOWNLOADING AND USE OF THE MATLAB CURVE FITTING SOFTWARES

Initially, software is downloaded to the personal computer from the relevant internet sites (Moisy, F., 2008, Rousseaou, J. M., 1999). For the downloading of the Ezyfit Toolbox, at first, the necessary file is drawn out of the zip file and is transferred into Toolbox folder under the Matlab folder. Later, Matlab program is started and is clicked to "Set Path" option in the File Menu. From the window opened, "add folder" is clicked and the Ezyfit file is selected, then, "save" is clicked and process is thus completed. Thus the Ezyfit Toolbox is loaded. For the uifit GUI, on the other hand, the downloaded exe file is started and in file where the software is prepared is opened. This file is then transferred to the work folder under the Matlab file and thus the process is completed.

D.1 Use of the Software

Use of the software is explained by the help of a simple example. Thus, it is anticipated that the software can be understood more easily. In this context, coefficients of the equation $y = 3x^3 + 5x^2 + 5$ will be determined by the help of the software. y values were determined for x values 1 to 10 and the a, b, c coefficients of the $y = ax^3 + bx^2 + c$ equation modeling these data were determined.

D.2 Use of the Uifit GUI

As a start, data desired to be modeled must be present in the Matlab workspace. The equation which is believed to simulate these data is written in the following form.

uifit(Data identified by workspace, ‘modelling equation’, [initial guesses for the coefficients])

Thus, the form which must be written for the case to be examined is,

uifit (x,y,’ $p(1)*x\text{^}3+p(2)*x\text{^}2+p(3)$’, [-1,1,1])..... (D.1)

where,

p(1), p(2) and p(3) are the constants to be found.

Initial guesses may be any value. Yet, in order to reach to the result in a fast way and to achieve convergence, it is better to select appropriate constants. Entering the command, uifit GUI window opens (Figure D.1).

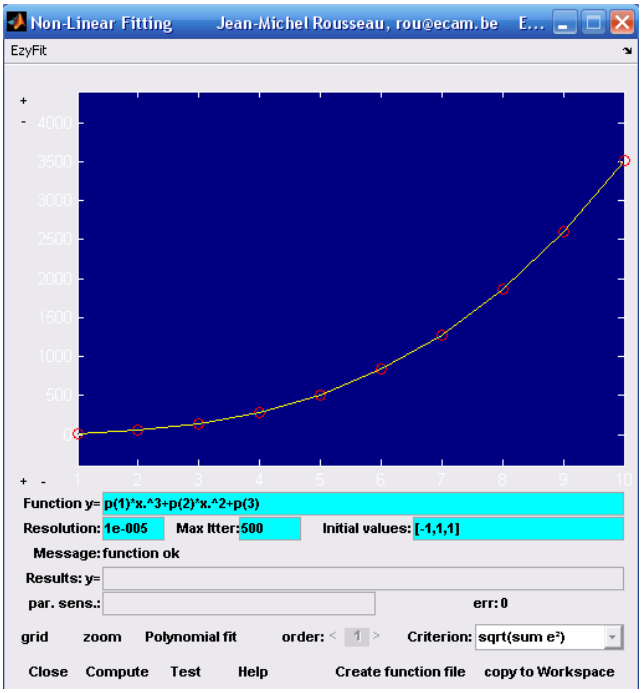

Figure D.1 uifit window is opened with entering the command D.1

From this window, appropriate resolution, maximum iteration values are entered and by pressing the compute button process is started. At the end of the process, parameters sought are determined (Figure D.2).

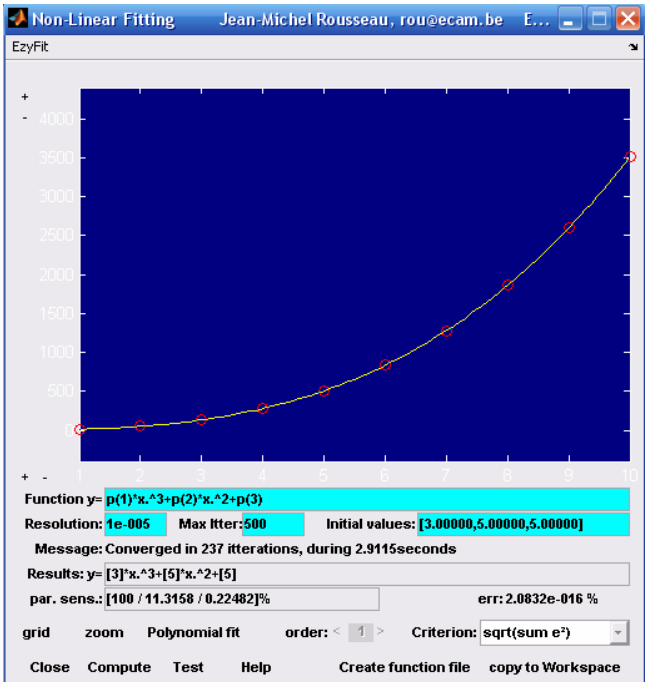

Figure D.2 The constants sought for, are determined with the completion of the process

D.3 Use of the Ezyfit Toolbox

For the solution to be reached, the graph pertaining to the data in concern must have been already drawn. Then, equation desired to simulate these data is entered in the following form,

showfit ('Equation; initial guesses for the constants')

For the case in concern, it must be as,

showfit ('$a * x.\text{^}3 + b * x.\text{^}2 + c$; a = -1; b = 1; c = 1') ..... (D.2)

Following the entering of the formula, curve fitting is completed and constants sought for are determined (Figure D.3).

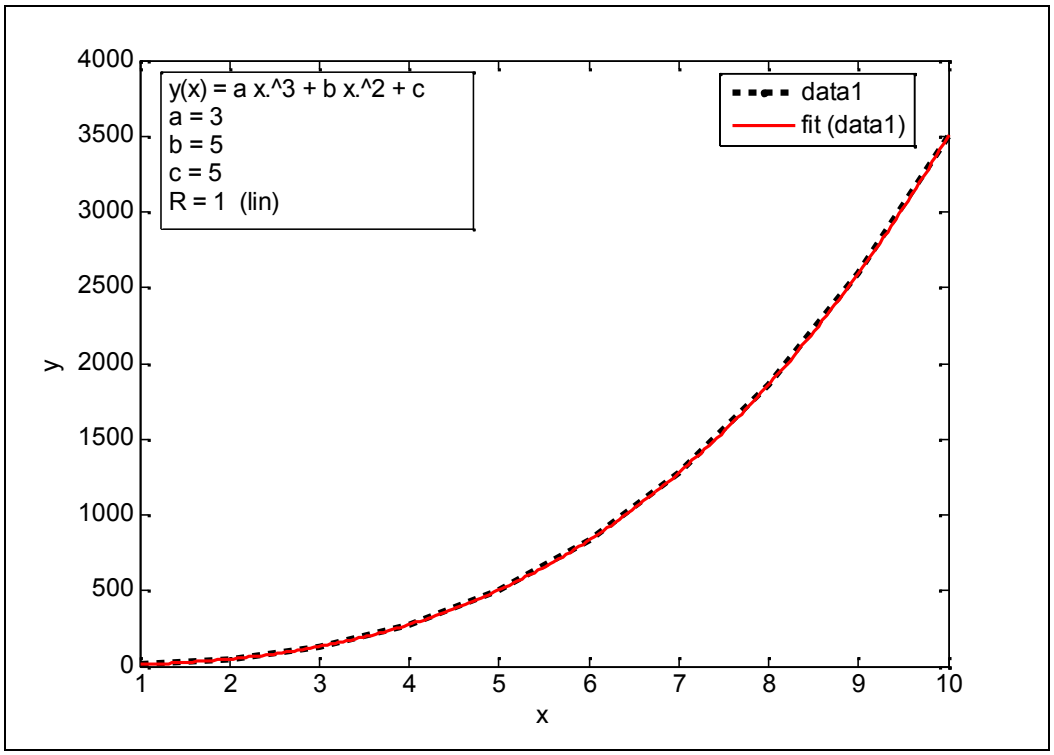

Figure D.3 Constants obtained with entering the command D.2

In case the appropriate results are not obtained, guesses are made in a more predictive way, and this process is repeated. By using the Eazyfit toolbox, utilizing any function, it is possible to find the relevant constants by curve fitting. Yet, the point which must be paid attention is that, the initial guesses made for the inquired constants of the related equation must be close to the correct values. In case diverging constants are selected, the curve fitting efforts may not give correct results. This is a phenomena which is observed more for the complicated equations and data than the simple equations. Additionally, Eazyfit posses an important advantage over uifit GUI. If the same parameter is repeated within the equation, uifit would not be able resolve the equation. In Eazyfit, on the other, such would not constitute a problem.

APPENDIX E

TEST RESULTS ABOUT SPEED DEPENDENCY IN THE CYCLIC LOADING TESTS

Below, test measurement results of two test groups, carried out in 2 days interval are laid down. Results were obtained by following the method described in Chapter 3.1.1.2, and 25 mm displacement was used in the tests. First of the graphs was obtained for regular and the second for random speed variations. As can be noted from the graphs, a consistent distribution attributable to motor speed did not take place. Yet, when the measurements at the same speeds were averaged, results presented in 3.1.1.2 were obtained

E.1 First Group Measurements

E.1.1 Regular Speed Increase

In Figure E.1, graph showing the variance of force when the motor speed was altered on a regular way, is seen. As can be noted clearly from Figure E.1, an organized trend in relation to the motor speed was not observed. For instance, in the transition from 1 mm/s speed to 2 mm/s speed, an increase in force was encountered and yet, in the transition from 8 mm/s to 4 mm/s a considerable fall in force was observed. In other words, it was not possible to declare that, the reactive force has increased with the increase in speed or that, it has fallen with the decreasing speed. This is a result brought by the in-vivo test, as discussed in Section 4.3.2.

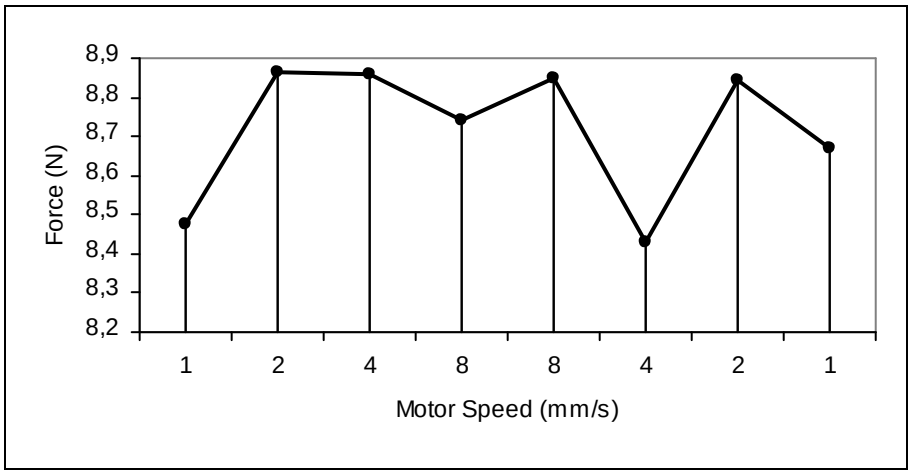

Figure E.1 Motor speed versus force graph for regular speed increase

E.1.2 Random Speed Increase

As in the case described in Figure E.1, for the random speeds also, a trend was not observed. That, in both speed increases or falls, force increase or decrease could have been encountered. In Figure E.2, in transition form 1 mm/s speed to 4 mm/s speed, a substantial increase attributed to muscle tone change was obtained.

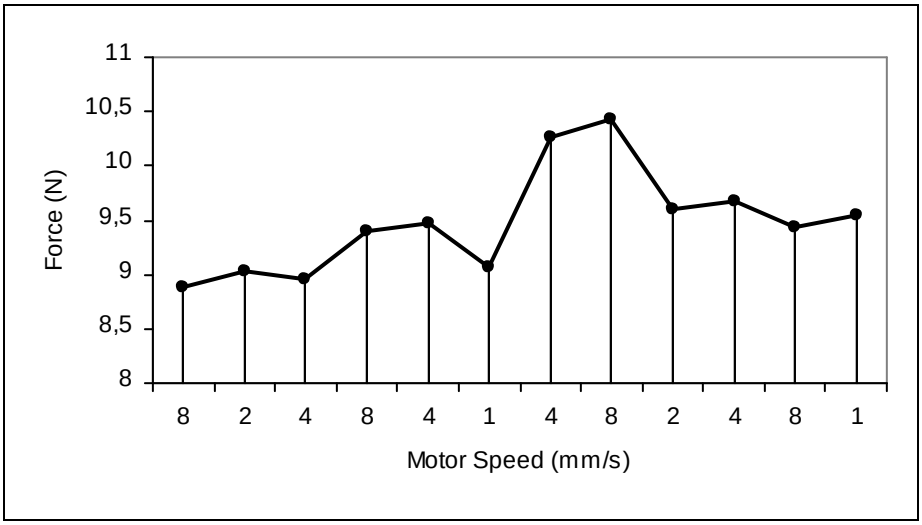

Figure E.2 Motor speed versus force graph for random speed increase

E.2 Second Group Measurements

In the second group measurements also, results similar to those of first group were obtained. No trend was observed, both in the regular speed changes (Figure E.3) and in the random speed changes (Figure E.4).

E.2.1 Regular Speed Increase

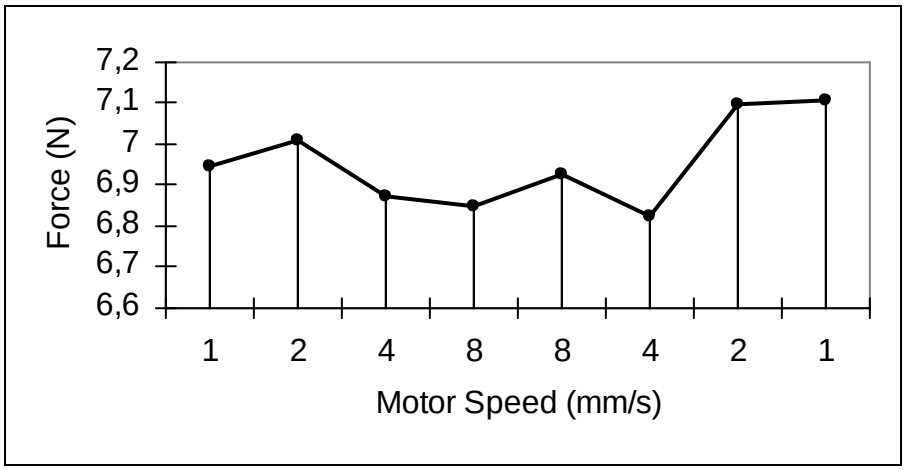

Figure E.3 Motor speed versus force graph for regular speed increase

E.2.2 Random Speed Increase

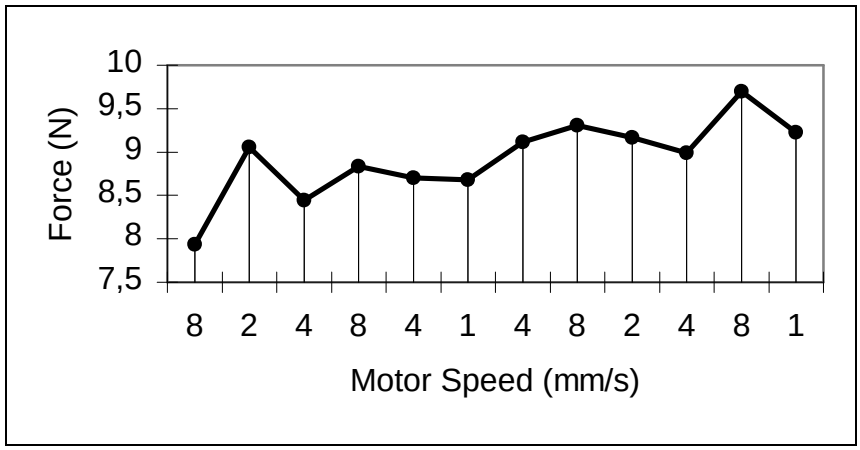

Figure E.4 Motor speed versus force graph for random speed increase

APPENDIX F

IMPROVEMENT MADE ON THE CREEP TEST PROTOCOL SOFTWARE

In the existing software, creep duration starts with the initial movement of the indenter tip. Yet, normally, this duration should start with reaching the target force. To eliminate this problem, following efforts were spent with regard to the software pertinent to the test protocole.

Portion of existing software, ensuring the achievement of target force and keeping it constant during a determined duration is given below.

```
while strcmp(AI.Running,'On')
    Veri1=getsample(AI);
    if(sayici==0)
      if(Veri1>Hedef)
        sayici=sayici+1; .....(a)
      end
    else
      Fark=Veri1-Hedef; .....(b)
      if (Fark>0)
        putvalue(dio,[0 0 0 0 0 0 0 0])..... (c)
      else
        putvalue(dio,[1 0 0 0 0 0 0 0])..... (d)
      end
      putdata(ao,[abs(Fark)*Kazanc 5])..... (e)
      start(ao)
    end
  end
```

Here, sayici (counter) is a number used for the commencement of the controlled movement of the indenter tip when the target force is achieved, and in the program its initial value is taken as zero. Hedef (target) is the number identifying the target force. This number is the number found by summing up the target force input derived by the user through interface and the value determined through calibration. Veri1 (data1) belongs to the force data gathered as indenter

edge starts to move. With the help of getsample function, instantaneous force data assignments are made.

Data collection system continues throughout the input time. This time is input by the user by using the interface. As mentioned before, time represents the summation of time elapsed to reach the target force and the duration of creep.

While-end cycle in the software ensures the assignment of each attained sample to the algorithm in this cycle. With getsample to force value up to that instant is assigned to Veri1. In the case that Veri1 is bigger than Hedef, target force is assumed and the sayici=1 value is achieved (code a). Therefore, next step, keeping the force value constant in a closed loop control, is proceeded. Here, force data is kept constant by the forward and backward movement of the indenter tip activated by the closed loop control cycle. Difference (Fark) is calculated by subtracting target (Hedef) force from data1 (Veri1) (code b). Difference (Fark) being greater than zero shows that the prevalent force is larger than the target force. In such case, indenter tip is moved backwards (code c). Difference being less than zero, on the other hand, indicates that the prevalent force is smaller than the target force and therefore the indenter tip is moved forward (code d). In code e, speed control in relation to the difference is carried out. Gain (Kazanc) is a value determined by the user and input through interface. It effects how fast the indenter tip should react to difference in actual and target force.

Incorporation of a code which starts the creep duration synchronously with the achievement of target force was, to solve the basic problem in the existing software.

To this end, arrangements shown below were formed.

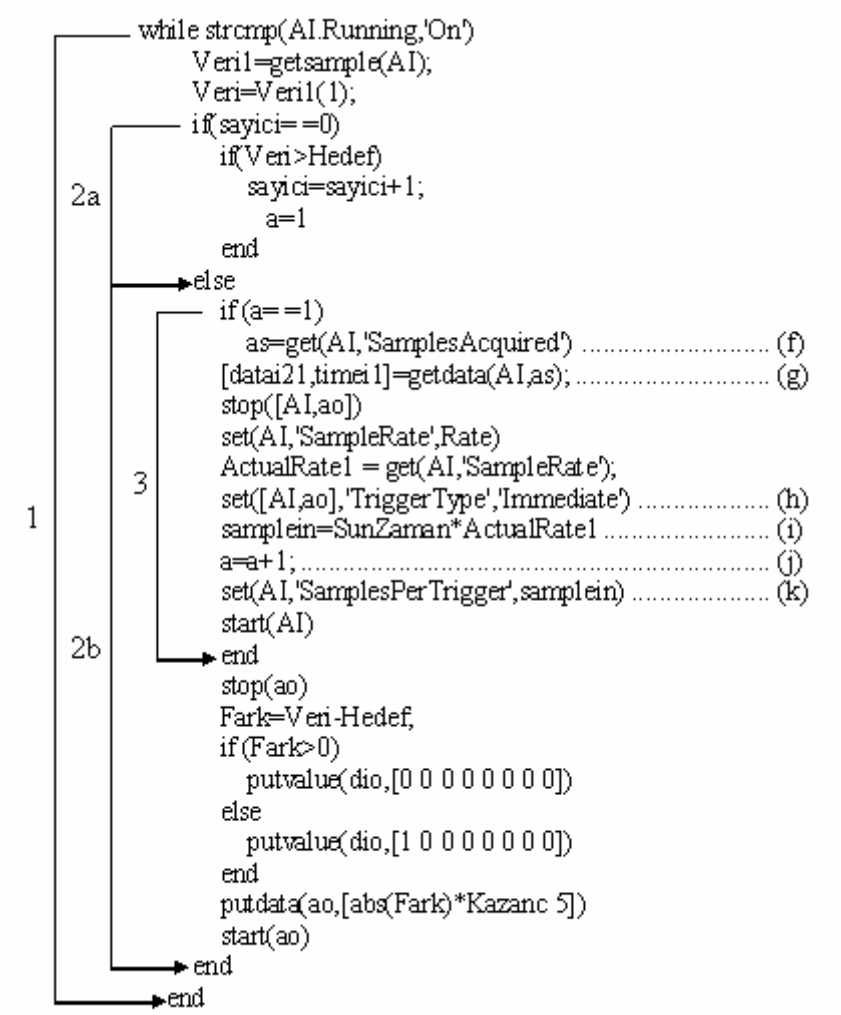

With the achievement of target force, force, speed, direction and pulse data collected up to that instant, were obtained by the help of the equation shown in (f) and were recorded by the help of the equation in (g). Later, AI and ao objects were stopped. While-end cycle Nr.1 in the software, ensures the assignment of each sample into this cycle. The 2a portion of the Nr.2 cycle ensures stopping of the indenter tip, and 2b portion ensures the forward backward movement of the tip at the target force.

In the start of this software, modifications explained in Section X are made. Pertinent to these modifications, trigger type of the analogue input and trigger type of the analogue output were adjusted as software and manual respectively. Yet, in order to keep the force constant, it was necessary to change the trigger

type. Trigger type (h) also, has been changed for both analogue input and analogue output as immediate. Creep time was attached to the codes in (i) and (k). Finally, analogue input object was run and Nr. 3 quest was left irrevocably (j).

Forward and backward movements achieved under control are as in the previous software.

Another alteration in the creep software was pertinent to the displacement. In the previous software this data is collected by using following code,

```
for i=2:Samples-1;
  dx(i)=(hizbilgi(i)/0.1686+31/300)*sign(yonbilgi(i)-2.5)/Rate; ..... (F.1)
  x(i)=x(i-1)+dx(i);
end
x(Samples)=x(Samples-1);
```

Here, Equation F.1 is used to calculate the instantaneous distance taken. Normally, hızbilgi(i) (speedinformation) data are obtained as voltage. Voltage values are translated into mm/s by the help of hizbilgi(i)/0.1686+31/300 process. Sign (yonbilgi[3](i) -2.5) gives the direction of the indenter tip and 1/Rate gives the time. These distances taken are added up by the Equation F.2,

```
x(i)=x(i-1)+dx(i);..... (F.2)
```

And the indenter displacement information is thus recorded. This process was used without any change, in the modified software.

Yet, due to the production of too many data much above the computer capacity in hand during the processing, caused “Out of Memory” error in Matlab.

This problem was solved by the help of two operations. Firstly, in order to create a field for x and dx in the computer, zero arrays with sample × 1 dimension were formed as follows.

```
x=zeros(Samples,1);
```

[3] yönbilgi means direction information

```
dx=zeros(Samples,1);
```

Secondly, existing operation was divided into 6 cycles. Thus, number of data in each cycle was decreased to one sixth of the main cycle and load on the computer's memory was relieved (). The codes are given below.

```
   D=floor(Samples/6);
   for i=2:D;
dx(i)=(hizbilgi(i)/0.145+31/300)*sign(yonbilgi(i)-2.5)/ActualRate1;
      x(i)=x(i-1)+dx(i);
   end
   for i=D+1:2*D;
dx(i)=(hizbilgi(i)/0.145+31/300)*sign(yonbilgi(i)-2.5)/ActualRate1;
      x(i)=x(i-1)+dx(i);
   end
   for i=2*D+1:3*D;
dx(i)=(hizbilgi(i)/0.145+31/300)*sign(yonbilgi(i)-2.5)/ActualRate1;
      x(i)=x(i-1)+dx(i);
   end
    for i=3*D+1:4*D;
dx(i)=(hizbilgi(i)/0.145+31/300)*sign(yonbilgi(i)-2.5)/ActualRate1;
      x(i)=x(i-1)+dx(i);
   end
    for i=4*D+1:5*D;
dx(i)=(hizbilgi(i)/0.145+31/300)*sign(yonbilgi(i)-2.5)/ActualRate1;
      x(i)=x(i-1)+dx(i);
   end
    for i=5*D+1:Samples-1;
dx(i)=(hizbilgi(i)/0.145+31/300)*sign(yonbilgi(i)-2.5)/ActualRate1;
      x(i)=x(i-1)+dx(i);
   end
    x(Samples)=x(Samples-1);
```

Another point observed here was that, keeping the number of cycles too many didn't help anything at all. With the idea that, the computer can now work without overload, number of cycles was increased to 10, yet, in such case, problems were encountered.

With these changes realized, indenter device was thus made ready to work for the creep test protocol.

APPENDIX G

CHANGES IN THE HYSTERESIS MAGNITUDES WITH SPEED

Graphs showing the variation of hysteresis magnitudes with speed are given below. Again for the sake of comparison, force speed graphs drawn by using the test data of the same tests are also presented. This way, variation of the hysteresis magnitude independently from the speed related force variation was much clearly observed. Results were found by using the cyclic loading tests with 25 mm displacement and consisting of 10 cycles. All tests were carried in one single day successively. First 8 measurements were made in regular speed changes the remaining 8 measurements were made by using random speed variations (See Chapter 4.3.2).

G.1 Force and Hysteresis Graphs Found by Using All Test Results

Graphs derived by using results of all tests conducted for the regular and random speeds, are given. In figure G.1 force versus speed and in Figure G.2 hysteresis versus speed graphs are presented. In both figures, an increase tendency depending on speed was observed. Yet, this increase is truly in small proportions for force magnitude. In Figure G.1, the difference between the smallest and biggest values is approximately 0.26 N.

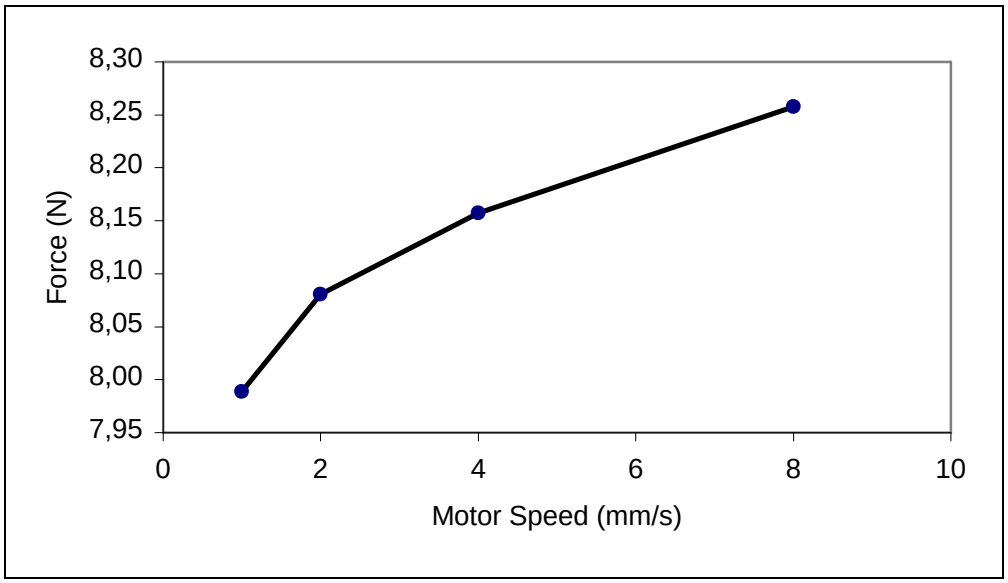

Figure G.1 Force–motor speed graph

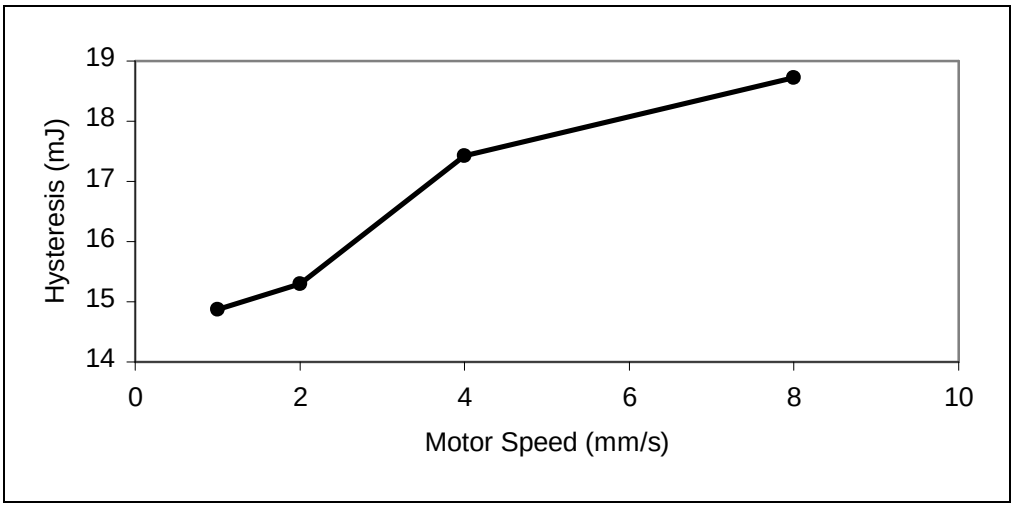

Figure G.2 Hysteresis - motor speed graph

Again for Figure G.1, it is beneficial to draw the attention to a certain point. In this figure, average of 4 measurements for 1 and 2 mm/s speeds and 6 measurements for 4 and 8 mm/s speeds are incorporated. This was originated from using the 4 mm/s and 8 mm/s speeds more, in the random speed determinations. Figure G.3 was obtained, on the other hand, by taking the

averages of the random and regular speeds separately, and then taking the average of these averages again. In this figure, it can be seen that, variation of force in relation to speed change is irregular.

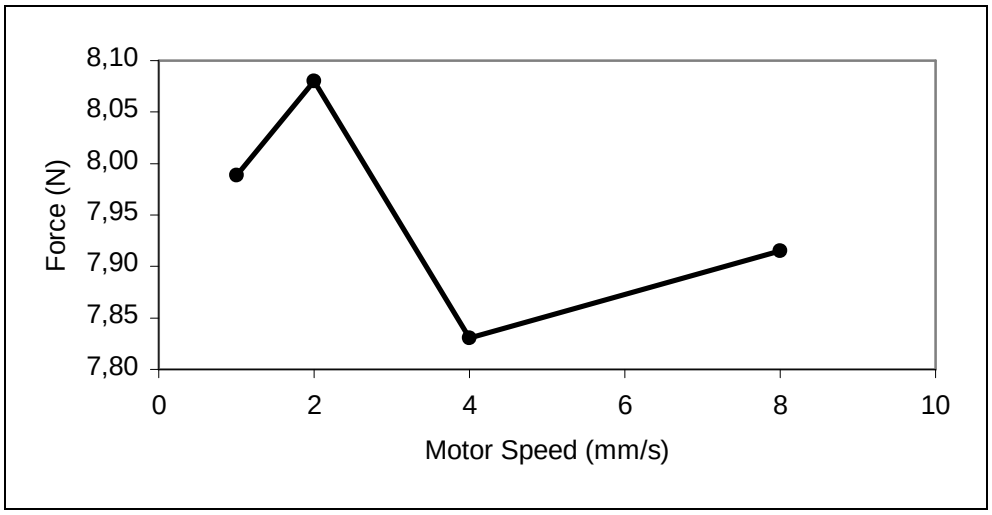

Figure G.3 Force–motor speed graph

G.2 Graphs Obtained by Using the Regular Speed Variations

In Figure G.4 force variations and in Figure G.5 hysteresis variation in relation to the speed are shown. Force variation has been irregular and falls and rises were encountered. In contrast to that, in relation to the speed, hysteresis magnitude has risen almost linearly.

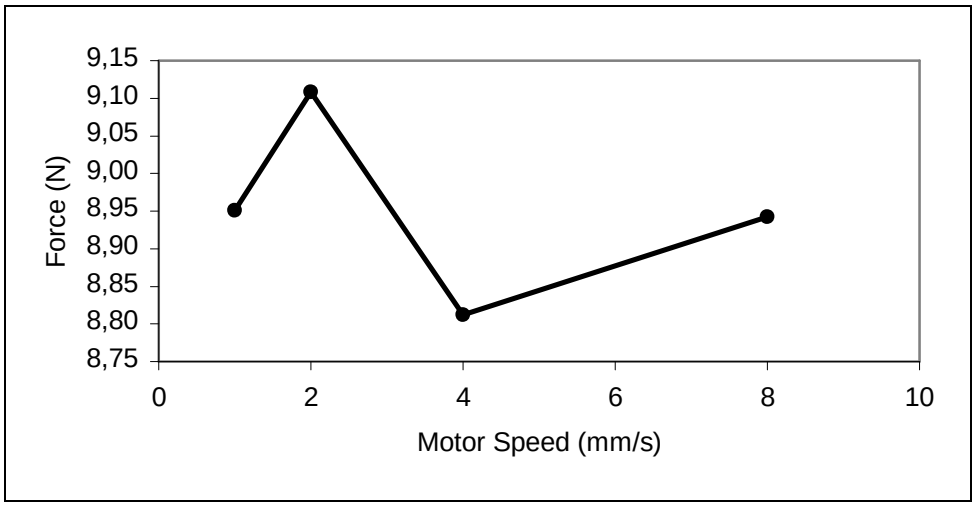

Figure G.4 Force–motor speed graph

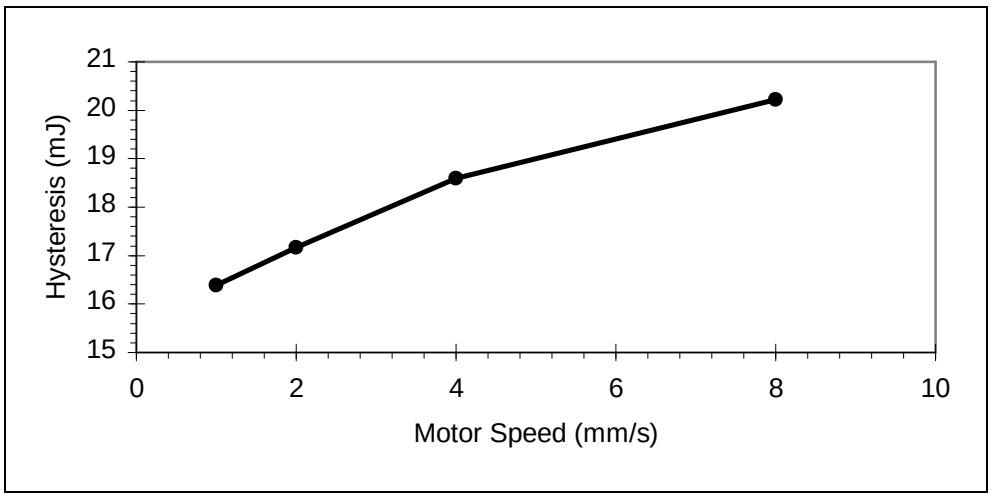

Figure G.5 Hysteresis - motor speed graph

G.3 Graphs for the Random Speed Variations

What was obtained for the random speeds were eventually parallel to those obtained for the regular speeds. Again, while the force magnitudes did not display any tendency in relation to speed (Figure G.6), hysteresis displayed an increase tendency with increase in speed (Figure G.7).

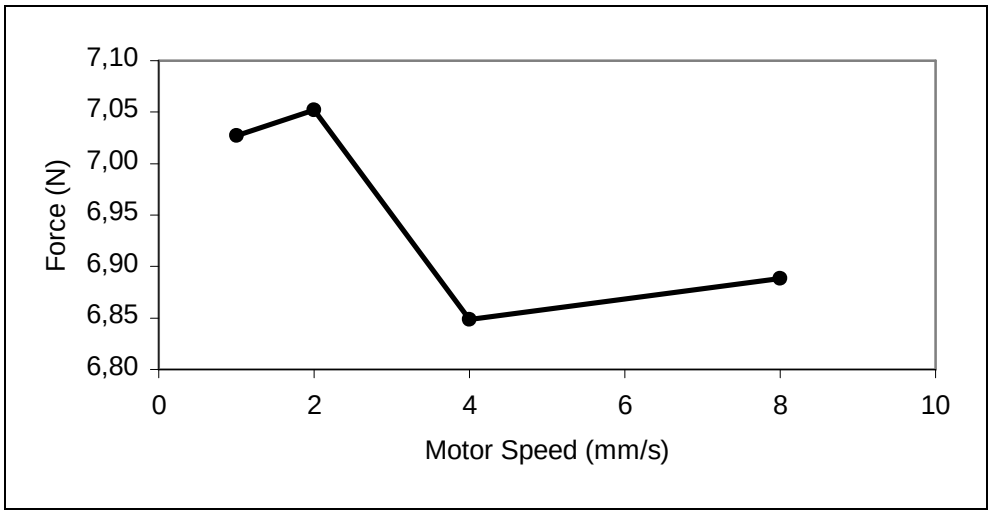

Figure G.6 Force–motor speed graph

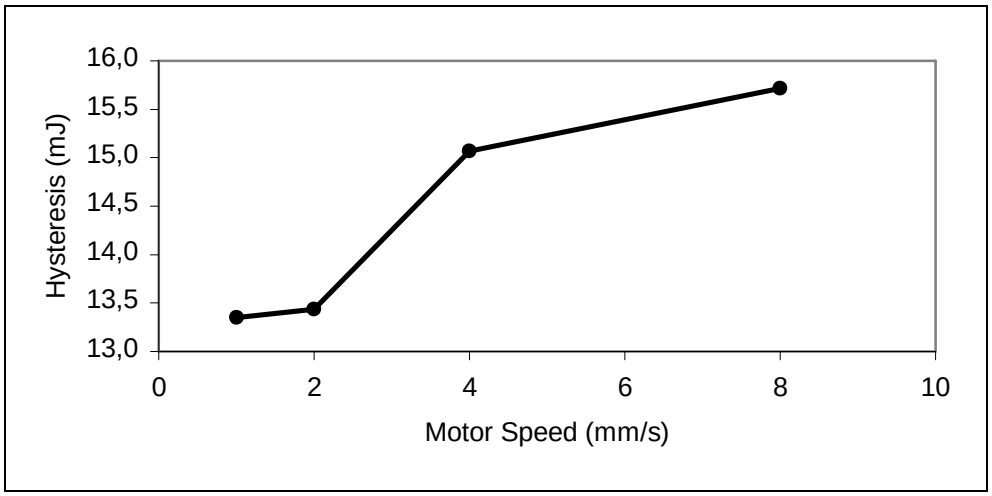

Figure G.7 Hysteresis - motor speed graph

APPENDIX H

EXAMINING THE RELAXATION DEPENDENT ANISOTROPY BEHAVIOR

In the Section 4.7.2.2.2, the results obtained from the Prony series coefficients were given. On the other hand, it was not possible to see a clear trend related to the anisotropy as seen in the force related anisotropy. When the force values obtained from the end of the relaxation time was considered, an increasing trend was observed between the angles 0º and 90º and a decreasing trend between the angles 90º and 180º. On the other hand, when the coefficients belonging to the Equation 4.11-c was considered, making such a conclusion was not possible. Although the coefficients vary with the increasing angle, a clear-cut changing could not have been observed. Consequently it was decided to made relaxation tests very carefully to see anisotropic behavior of the tissue. Following graphs shows this test results.

Figure H.1 Anisotropic response attributed to relaxation behavior.

In Figure H.1, the force values obtained from the end of the relaxation time and corresponding tip angles was given. Response force displayed by the tissue increased from 0º to 90º degrees and decreased from 90º to150º degrees. On the other hand, the response force took nearly same value at 180º with the 150º. This was an unexpected result when it was considered the other results. Consequently, this was most probably a result of the changes in the muscle tones.

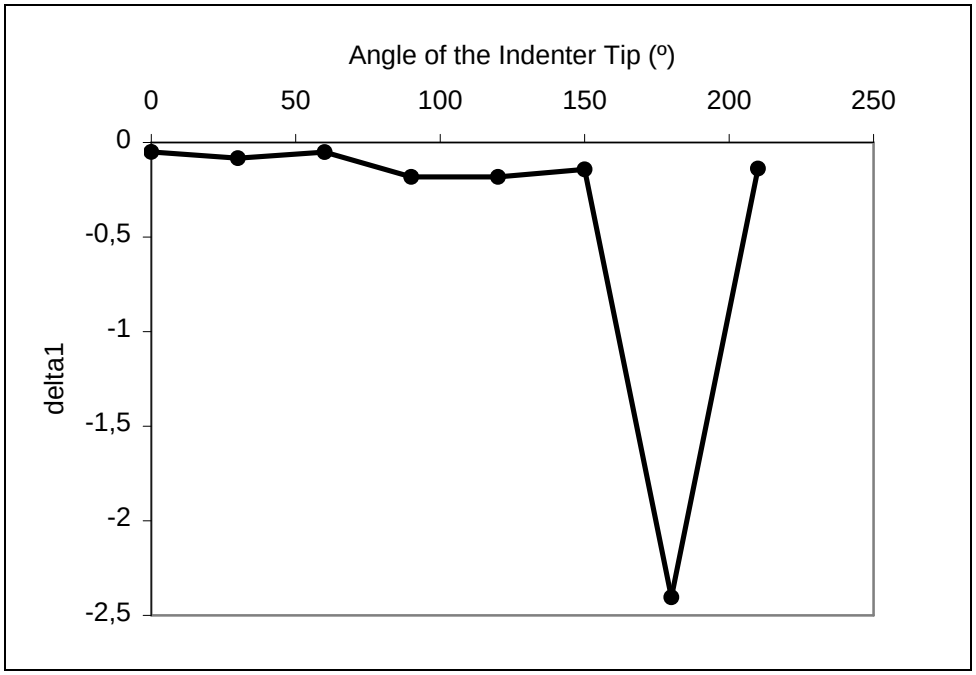

Figure H.2 Angle of the indenter tip versus δ_1 graph

As it can be seen from the Figure H.2, short term relaxation magnitude was showed great deviation at 180º from the general trend. Even without this value, it was still not possible to observe a proper trend.

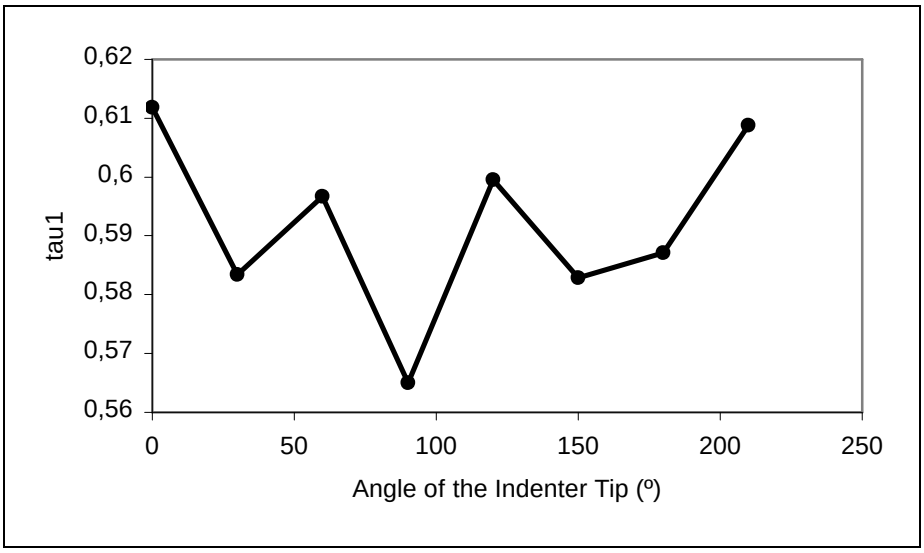

Figure H.3 Angle of the indenter tip versus τ_1 graph

For the short term relaxation time magnitudes, a periodic behavior was observed between the angles 0º and 180º. The force values with the related angles, 0º-180º, 30º-150º and 60º-120º took nearly the same values as it can be seen from the Figure H.3. On the other hand, it should have been expected decreasing in force magnitude at the angle 210º, the value was increased.

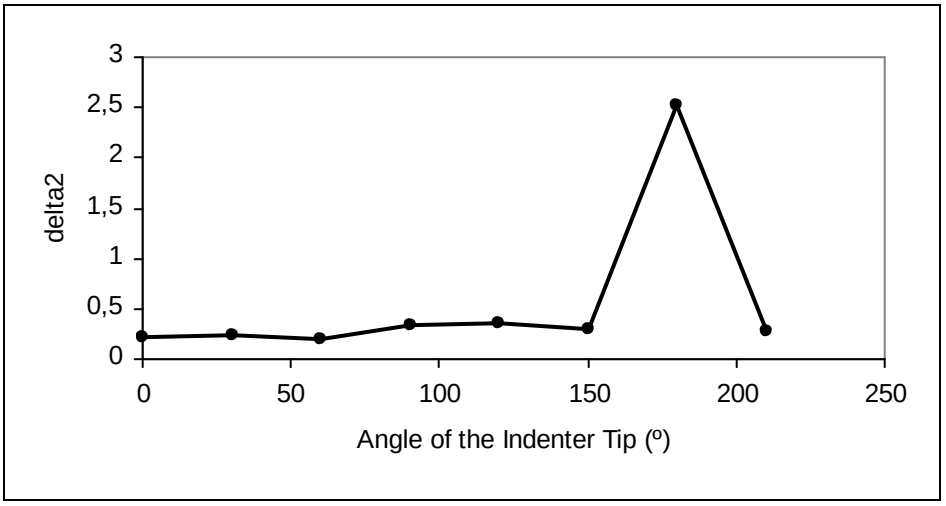

Figure H.4 Angle of the indenter tip versus δ_2 graph

The long term relaxation magnitude showed the same characteristic given in the Figure H.3.

Figure H.5 Angle of the indenter tip versus τ_2 graph

Although the values of the long term relaxation time constants was varied with increasing angle of the indenter tip, a clear-cut changing could not have been observed.

Table H.1 Coefficients for the relaxation tests

Angles of the Indenter Tip (º)	δ_1	τ_1 (s)	δ_2	τ_2 (s)	R-Square
0	-0,05033	0,61188	0,21018	33,281	0,93714
30	-0,08301	0,58345	0,23857	26,986	0,961361
60	-0,05113	0,59672	0,202	32,239	0,958069
90	-0,18208	0,56502	0,3317	18,798	0,948306
120	-0,182	0,59956	0,35156	21,524	0,970718
150	-0,14178	0,58284	0,28813	18,577	0,965188
180	-2,4041	0,58711	2,5166	6,1682	0,899406
210	-0,13772	0,60882	0,27572	18,488	0,944823

APPENDIX I

PUBLICATIONS

I.1 BIYOMUT 2007

İNDENTÖR DENEY CİHAZI İLE YUMUŞAK BİYOLOJİK DOKULARIN VİSKOELASTİK ÖZELLİKLERİNİN ARAŞTIRILMASI

Investigating Viscoelastic Properties of the Soft Biological Tissues via Indentor Test Device

Ali Tolga PETEKKAYA[1], Ergin TÖNÜK[1]
E-posta: e146945@metu.edu.tr, tonuk@metu.edu.tr

[1]Orta Doğu Teknik Üniversitesi, Makina Mühendisliği Bölümü, Ankara, Türkiye

Özetçe: **İndentör cihazları yumuşak biyolojik dokuların mekanik özellikleri araştırılırken sıkça kullanılan deney aletleridir. Özellikle yerinde (*in-vivo*) testi olanaklı kılmaları, bu cihazların önemini arttırmaktadır. Elimizde daha önce geliştirilmiş ve özellikle dizaltı ampütasyon cerrahisi geçirmiş bireylerin ampütasyon güdüğünde çalışılmak üzere tasarlanmış bir indentör cihazı mevcut olup, çalışmaya bu cihazın mevcut problemlerinin tespiti ve giderilmesiyle başlanmıştır. Problemlerin tespiti için, indentör hareketi 0.2-10 mm/s hız ve 0.1-5 mm deplasman aralıklarında 1/100 mm hassasiyetli mekanik komparatör aracılığıyla, kuvvet verilerinin doğruluğu da indentöre 2-50 N aralığında durağan yükleme yapılarak incelenmiştir. Bulunan problemler cihazı kontrol eden yazılımda değişiklikler yapılarak giderilmiştir. Mevcut problemlerin giderilmesiyle yumuşak doku üzerinde deneylere başlanmış ve viskoelastik modelleme için gerekli olan deney protokollerinden devirli yükleme ve gevşeme deneyleri yapılmıştır.**

Anahtar Sözcükler: İndentor deney cihazı, yumuşak biyolojik doku, devirli yükleme, gevşeme, viskoelastik

Abstract: **Indentor devices are test apparatus frequently used for identification of the properties of soft biological tissues. In particular, facilitating in-vivo testing makes these devices more important. A previously developed indentor device designed to work on residual limbs of the patients with trans tibial amputation, is in our hand and the study has been started to diagnose and solve the existing problems of this device. For the diagnosis of the problems, indentor movement has been tested at 0.2 to 10 mm/s indentation speed and 0.1 to 5 mm displacement intervals via a comparator of 1/100 mm sensitivity and accuracy of the force data is investigated by loading the indentor at 2 to 50 N loading range. After rectifying the identified problems by modifying the control software of the device, tests on soft tissues have been started for the cyclic loading and relaxation test procedures, essential for the viscoelastic modelling.**

Keywords: Indentor test device, soft biological tissue, cyclic loading, relaxation, viscoelastic

I. GİRİŞ

Canlı organizmaların önemli bir bölümünü oluşturan yumuşak dokular, diğer bilinen mühendislik malzemeleriyle karşılaştırıldıklarında daha karmaşık bir mekanik yanıt davranışı gösterirler. Bu sebeple, üzerinde birçok çalışma yapılan ve özellikleri araştırılan yumuşak dokuların mekanik davranışını modellemek üzere henüz genel kabul gören bir matematiksel malzeme modeli geliştirilememiştir. Ancak böyle bir modelin geliştirilmesiyle yumuşak doku davranışları daha iyi anlaşılıp sakatlanmalar, ilaç sanayi, cerrahi v.b. birçok alanda daha etkin bir şekilde kullanılabilecektir [1].

Yumuşak dokuların mekanik davranışının anlaşılması için uygulanması gereken ilk adım yapılacak sistematik deneylerdir. Deneyler temel olarak iki şekilde yapılır. Bunlardan biri, dokunun doğal ortamından kesilip çıkarılmasıyla, canlılığını yitirmiş olarak yapılan deneyler (*in vitro*) [2-3], diğeri de dokunun kendi fizyolojik ortamında canlı iken incelenmesidir (*in vivo*) [4]. Birinci tarzdaki deneylerde malzemeye ait bilgiler standart malzeme deneyleriyle (çekme deneyi gibi) elde edilebilmekte [2-3] ancak doku kendi fizyolojik ortamından çıkarıldığı ve belki de canlılığını yitirmiş olduğundan [1], verilerin canlı dokuyu temsildeki güvenirliliği sorgulanır bir hal almaktadır. İkinci yöntem olan dokunun bulunduğu ortamda incelenmesi ise beraberinde iki temel kısıtlamayı getirmektedir. Bunlardan birincisi ölçüm yapılabilecek alanların sınırlı olması ve genellikle dış organlarda deneylerin yapılabilmesidir. Bu özellikle insana ait dokuların incelenmesi esnasında çıkan bir problemdir. Hayvanlar için ise değişik sistemlerle iç organlar üzerinde de deneyler yapmak mümkün olmaktadır [5]. İkinci sınırlama da test yapılacak dokunun yada yüzeyin düzgün bir geometriye sahip olmamasıdır.

In vivo deneylerlere imkan sağlayan en uygun yöntem indentör cihazlarıyla yapılan deneylerdir [6,7]. Bu cihazlar 1900'lü yılların başından itibaren yumuşak dokuların özelliklerinin araştırılmasında kullanılmaktadır [8,9]. İndentör cihazlarıyla yapılan deneyler, indentör ucunun malzeme yüzeyinden içeri doru hareket etmesi ve bu esnada, zaman, kuvvet, yer değiştirme bilgilerinin kayıt edilmesiyle yapılır (Şekil 1.1).

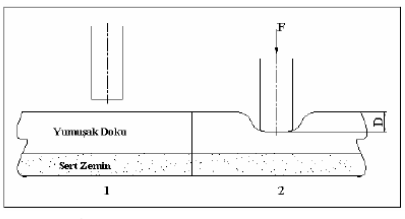

Şekil 1.1. İndentör cihazıyla dokuya yükleme yapılmadan önce(1) İndentör cihazıyla dokuya yükleme yapıldıktan sonra(2) Burada F kuvvet ve D indentörün dokuda aldığı mesafedir.

Uygulanan yönteme göre indentör ucunun geometrisi de hesaplamalara katılır [10]. Ayrıca indentör ucunun test edilen malzemeden daha sert olması gerekli olup, deney esnasında deformasyona uğramaması gereklidir.

İndentör cihazlarıyla devirli yükleme, gevşeme ve sünme deneyleri yapılabilir. Devirli yükleme sonucu elde edilen veriler, yumuşak dokuların doğrusal bir malzeme modeliyle temsilinde kullanılabildiği gibi [7,11], sanki doğrusal viskoelastik modellemelerde de kullanılabilir [1,12]. Devirli yükleme deneyi ile birlikte, sünme ve gevşeme deneyleri viskoelastik modellemelerde kullanılmaktadır [13].

II. MATERYALLER ve YÖNTEMLER

İndentör Deney Cihazı

Mevcut cihaz TÜBİTAK MİSAG-183 proje desteğiyle geliştirilmiş olup, devirli yükleme, gevşeme ve sünme test protokollerini uygulayabilir. Özellikle diz altı ampütasyon cerrahisi geçirmiş bireylerin ampütasyon güdüğünde çalışılmak üzere tasarlanmış cihaz küçük değişikliklerle yada değişiklik yapılmaksızın farklı dokularda da yerinde (*in vivo*) deneyler yapmak için kullanılabilir.

İndentör deney sistemi temel olarak üç bölümden oluşmaktadır. Bunlar, taşınabilir bilgisayar, denetim kutusu ve deney birimidir (Şekil 2.1).

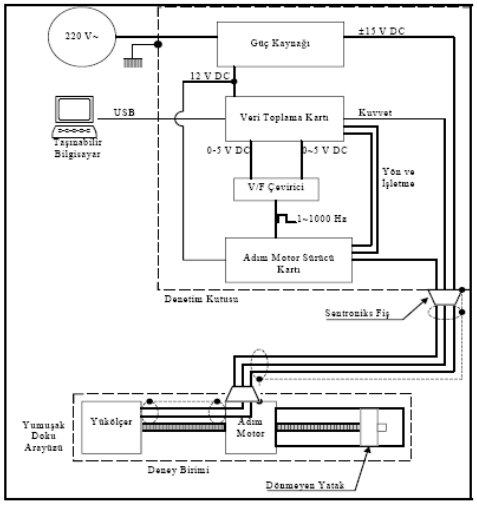

Şekil 2.1. İndentör deney sistemi blok şeması. Bilgisayarın USB girişinden yön ve motor hızı bilgilerini alan veri toplama kartı bu bilgileri motor sürücü kartına iletir. Motor hızını, 0-5 V arası değişken gerilim alabilen gerilim kanalı tayin eder. Kanallardan çıkan gerilimler V/F çevirici aracılığıyla uygun frekansa çevrilir ve adım motor sürücü kartına iletilir. Adım motor sürücü kartı işletme komutu ile birlikte istenen frekansta adım motorunu sürer. Bu sırada yük ölçerden toplanan veriler ilk olarak veri toplama kartına oradan da sayısallaştırılarak bilgisayara aktarılır.

Taşınabilir Bilgisayar

Pentium III 900 Mhz işlemcili, 30 GB hard disk kapasiteli, 256 MB hafızalı HP marka dizüstü bilgisayardır. Bilgisayarın sistemdeki görevi, indentör cihazının kontrolünün sağlanması, elde edilen verilerin toplanması ve işlenmesi olarak özetlenebilir. Bilgisayar bu işlevini Matlab® 6.1'de hazırlanan bir yazılım aracılığıyla yapar. Deney sisteminde dizüstü bilgisayar kullanılması, sistemin kolay taşınmasını ve klinik ortamlarda da kullanılabilmesini sağlamaktadır.

Denetim Kutusu

Denetim kutusunda, deney birimini kontrol eden ve deney biriminden gelen veriyi toplayan National Instruments NI 6020E veri toplama kartı, deney birimine ait adım motorunu veri toplama kartından gelen komuta göre süren sürücü motor kartı, hassas voltaj frekans çevirici, 12 ve 15 V DC' lik güç kaynakları mevcuttur. Voltaj-frekans çevirici veri toplama kartı ile motor sürücü kartı arasında yer alıp, veri toplama kartının iki kanalından gelen 0-5 V arasındaki gerilimleri 0.1-1000 Hz aralığında frekansa çevirir. Bu sayede adım motoru 0.0049-49 mm/s hız aralığında hareket edebilir. İki güç kaynağında 12 V DC olanı adım motorunu ve veri toplama kartını, 15 V DC simetrik güç kaynağı da yük ölçeri besler.

Deney Birimi

Temel olarak Haydon Switch Instrument 43000 serisi doğrusal hareketli bir adım motoru ve Entron ELW-D1-50N yük ölçerden oluşmaktadır. Yük ölçer indentör ucunun hemen alt kısmına yerleştirilmiş olup, 50 N' a kadar kuvvet ölçümü yapabilmektedir. Adım motoru her bir adımda 0.048768 mm hareket oluşturmaktadır. Dönmeyen yatak ile rotorun dönüşü sonucu ileri geri hareket yapan vidalı milin dönmesi engellenmekte ve yalnızca doğrusal hareket yapması sağlanmaktadır. Yük ölçerin ön kısmına değişik şekil ve çaplarda, değişebilen deney uçları takmak mümkündür.

Deney birimi ve denetim kutusu arasındaki iletişim iki ucunda sentroniks fiş bulunan ve elektromanyetik parazitten korunmuş bir kablo aracılığıyla yapılır. Veri toplama kartı ve bilgisayar arasındaki bağlantı da bilgisayarın USB girişi üzerinden sağlanır.

Deneyler Öncesi Yapılan İncelemeler

Güvenilir deneylerin yapılması, yapılan ölçümlerin hassas olmasıyla mümkündür. Bu sebeple mevcut indentör cihazında ayrıntılı incelemeler yapılmış ve incelemelerin sonuçlarına göre geliştirme işlemleri yapılmıştır. Bu incelemeler;

- İndentör hareketinin hassasiyetinin incelenmesi ve
- Kuvvet verisinin hassasiyetinin incelenmesi olarak sıralanabilir.

İndentör Hareketinin incelenmesi

İndentör hareketinin incelenmesi için Şekil 2.2'de görülen düzenek kurulmuştur. Bu sistem iki adet Mitutoyo marka manyetik ayak ve komparatörden oluşmaktadır. Komparatör aracılığıyla 1/100 mm hassasiyetinde yer değiştirme ölçümü yapmak mümkündür. Bu sistem ile 0.2 ile 10 mm/s arasında değişen hızlarda ve 0.1 ile 5 mm deplasman aralığında indentörün deplasman komutlarına uyabilme hassasiyetine bakılmıştır.

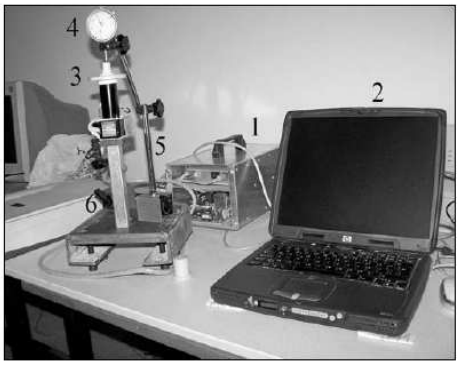

Şekil 2.2. İndentör deney cihazının hareketinin incelenmesi için kurulan düzenek. Resimde, Denetim kutusu(1) Dizüstü bilgisayar(2) Deney birimi(3) Komparatör(4) Manyetik ayak-1(5) Manyetik ayak-2(5) görülmektedir.

Ölçümler sonucunda indentörün 0.05 ile 4.42 mm aralığında değişen değerlerde daha fazla hareket ettiği gözlemlenmiştir. Hızın artmasıyla istenen deplasmandan sapma miktarı da artmıştır. Ölçümler sonucunda her hız için Şekil 2.2'de 8 mm/s için sunulan grafikteki sonuca benzer grafikler elde edilmiştir.

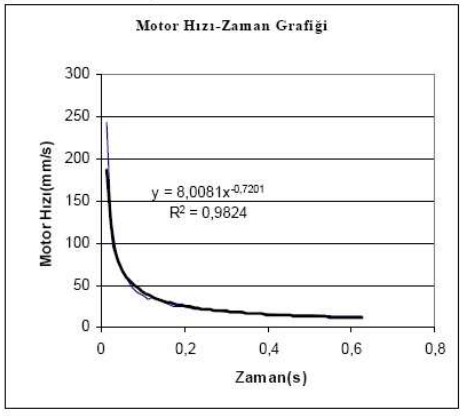

Şekil 2.2. 8 mm/s hız için elde edilen motor hızı-zaman grafiği ve grafik denklemi

Şekilden de görüleceği üzere indentör ucunun kat edeceği mesafe arttıkça, indentörün yavaşladığı sonucu ortaya çıkmıştır. Ancak yapılan ölçümlerde, indentörde böyle bir yavaşlamanın olduğu gözlemlenmemiştir. İndentörün zamana ve giriş motor hızına bağlı çıkış motor hızını veren denklem aşağıda verilmiştir.

$$m = e^{\left[\frac{1}{D-E\ln t}\ln\left(\frac{yt^F}{C}\right)\right]} \qquad (2.1)$$

Burada;

m = İndentör giriş hızı
t = Hareket zamanı
y = İndentörün deney sonuçlarıyla elde edilen teorik hızı
C = 1.423, D = 0.884, E = 0.188 ve F = 0.336 dır.

Formül mevcut yazılıma eklenmiş ve gerçekten de indentör ucu istenen deplasmanda gitmiş, ancak indentörün farklı hızlarda hareket ettiği gözlemlenmiştir.

Bu denemelerden sonra indentör hareketini kontrol eden yazılımın zaman tayini konusunda eksik olduğu anlaşılmıştır. Mevcut yazılımda yalnız kuvvet verisinin toplanmasına bağlı olarak zaman sınırlaması yoluna gidilmiştir. Ancak bunun indentörün hareketi için zaman sınırlaması yapmaya kafi gelmediği ve indentörün belli bir zaman daha hareket ettiği anlaşılmıştır. Bu problem, indentör hareketi içinde zamanı belirleyen bir algoritma eklenerek giderilmiştir. Geliştirme sonrasında yapılan ölçümlerde indentörün gerçekten istendiği miktarda hareket ettiği gözlenmiş ve 0 ile 0.5 mm aralığında küçük sapmalar tespit edilmiştir. Ancak bu sefer elde edilen verilerde indentör hareketi ile kuvvet verisinin eş zamanlı toplanmadığı tespit edilmiştir. Şekil 2.3'te de görüleceği üzere grafiğin sağındaki düz alan indentörün durduğu bölgeyi göstermekte ancak buna rağmen kuvvet verisi toplanmaya devam edilmektedir.

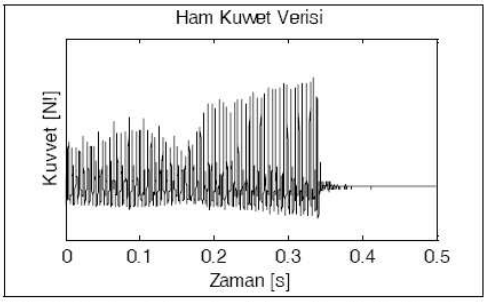

Şekil 2.3. 10 mm/s motor hızı ve 5 mm deplasman için elde edilen kuvvet-zaman grafiği

Dolayısıyla bu problemin gözlemi, kuvvet verisi toplanması ve indentör hareketinin eş zamanlılığının sağlanmasının gerekliliğini doğurmuştur. Mevcut yazılıma

eş zamanlılığı sağlayan kod eklenmiş ve yapılan ölçümlerde Şekil 2.4 teki gözlenen durum ortaya çıkmıştır.

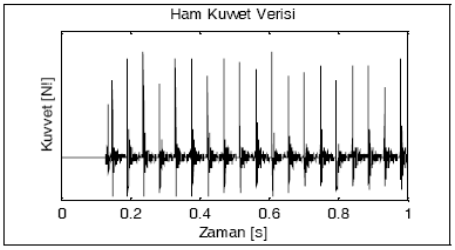

Şekil 2.3. Eş zamanlı olarak kuvvet verisi toplama ve indentör hareketini başlatma durumunda, 1 mm/s motor hızı ve 1 mm deplasman için elde edilen kuvvet-zaman grafiği

Kuvvet verisi bu sefer indentörün hareket etmesinden yaklaşık 0.1 s kadar önce toplanmaya başlanmıştır. Bu durumun daha iyi anlaşılması için mevcut yazılıma hareket zamanlarını tespit eden bir kod eklenmiş ve indentörü harekete geçiren sinyal ve kuvvet verisi toplanması arasında yaklaşık 10^{-5} saniyelik bir fark olduğu gözlenmiştir. Bu fark bir önceki durumda yaklaşık 10^{-1} s civarındaydı.

Motorun hareketinin başlama zamanının tespitiyle kuvvet verisini toplamaya başlatacak bir kodun eklenmesinin sorunu çözeceği düşünülmüştür. Adım motorunun her bir adımında motoru besleyen gerilim kanallarından birinin değeri 5 volttan 0 volta düşmektedir. Bu özellik kullanılarak kuvvet verisinin toplanmasına ilk gerilim düşmesinin tespitiyle başlatacak bir kod eklenmiştir. Bu son yapılan geliştirme sonucu indentör hareketi sırasında toplanan kuvvet verisi Şekil 2.4'te sunulmuştur.

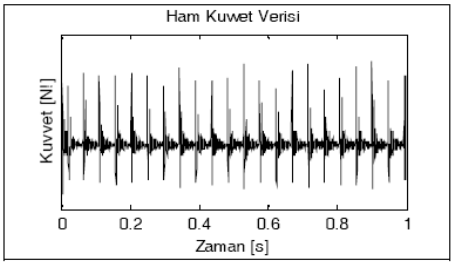

Şekil 2.4. İlk gerilim kuvvet verisi toplama ve indentör hareketini başlatma durumunda, 1 mm/s motor hızı ve 1 mm deplasman için elde edilen kuvvet-zaman grafiği

Mevcut problemler son değişiklikle birlikte giderilmiştir. Ancak yapılan değişiklik gerilim düşüş değerinin tespit edilebilmesi için örnek toplama hızının yüksek tutulmasını gerektirmekte, bu da düşük hızlarda elde edilen verilerde adım motorunun darbeleri nedeniyle yüksek gürültüye neden olmaktadır. Gürültünün, çalışmanın ilerleyen döneminde bir filtre yardımıyla giderilebileceği düşünülmektedir.

Kuvvet Verisinin Doğruluğunun İncelenmesi

Kuvvet verisinde olabilecek hataların tespiti için 2-50 N aralığında bir dizi durağan kalibrasyon ölçümleri yapılmıştır. Ölçümler sonucunda Şekil 2.5'teki grafik ve kalibrasyon denklemi elde edilmiştir.

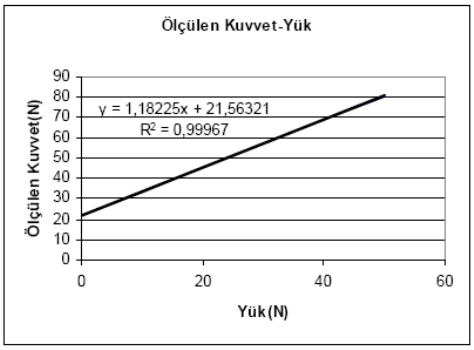

Şekil 2.5. Uygulanan yüke karşılık ölçülen kuvvet grafiği ve denklemi

Denkleme ait birinci katsayı kuvvet ölçerin üretici tarafından sağlanan kalibrasyon sabitinin bir miktar değiştiğinin göstergesidir, ikinci katsayı yük hücresinin yüksüzken de sıfırdan farklı bir gerilim (offset) vermesinden kaynaklanmaktadır. Birinci katsayının bire eşitlenip ikinci katsayının mevcut değerden çıkarılmasıyla kuvvet verisinin doğruluğunun sağlanabileceği açıktır.

Birinci katsayının bire indirilmesi için sensör aralığıyla arasında ters orantı kurulmuş ve sensör aralığının yeni değeri 0.34543 olarak tespit edilmiştir. Bu değer hesaplamadan önce üretici tarafından sağlanan 0.29218'dir. Yapılan düzeltme sonrasında ölçümler tekrarlanmış ve Şekil 2.6'daki grafik elde edilmiştir.

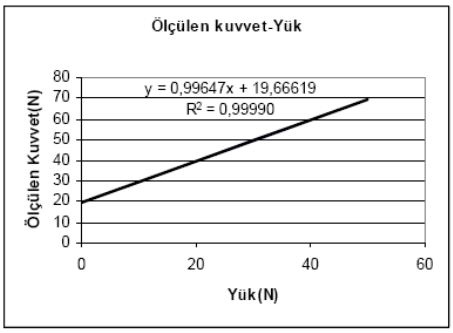

Şekil 2.5. Yük hücresi kalibrasyon denkleminin değiştirilmesi sonrasında elde edilen uygulanan yüke karşılık ölçülen kuvvet grafiği ve denklemi

Grafikten de görülebileceği gibi birinci katsayı 1'e çok yakın olarak bulunmuştur. İkinci katsayı da bir önceki değerinden daha düşük çıkmıştır. B katsayısının verilerden

çıkartılması için de ölçümlere başlanmadan önce indentör yüksüzken kuvvet verisi tespit edilmekte bu değer ölçümlerle elde edilen verilerden deney esnasında çıkarılmaktadır. Düzeltmelerden sonra yapılan ölçümlerde kuvvet verisinin -0.25 N ile +0.43 N arasında sapma yaptığı ve ortalama sapmanın 0.19 N olduğu gözlenmiştir.

III. SONUÇ

İndentör cihazında devirli yükleme ve gevşeme deney protokolleriyle ilgili ayrıntılı incelemeler sonucu geliştirmeler yapılmış, sünme protokolü için de geliştirme çalışmalarına başlanma aşamasına gelinmiştir. Çalışmanın bu aşamasında sistematik ölçümlere yeni başlanmış olup, yumuşak dokular hakkında ayrıntılı sonuçlar ileriki safhalarda görülebilecektir. Yapılan geliştirmelerden sonra indentörle yapılan deneme amaçlı ilk ölçümler Şekil 3.1'de görüldüğü gibi ön kol üzerinde yapılmış ve elde edilen sonuçlar aşağıda sunulmuştur.

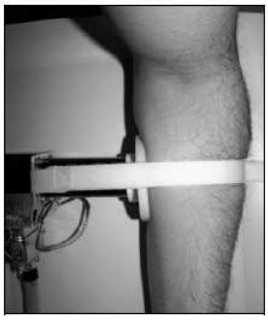

Şekil 3.1 Ölçümlerin yapıldığı bölge

Devirli Yükleme Deneyi

Devirli yükleme deneyi indentör ucunun belli bir hızda, istenen miktarda tekrarlı olarak ileri-geri hareket etmesiyle elde edilen ölçümlerdir. Şekil 3.2'de 5 mm/s hızda, devir sayısı 10 olan ve 20 mm deplasmanla yapılan bir devirli yükleme deneyine ait grafik görünmektedir.

Grafikte ilk 6 devirde kuvvetin maksimum değerinin giderek azaldığı ve beşinci devirden sonra hemen hemen sabit kaldığı görünmektedir. Bu durum deney yapılan bölgedeki doku sıvıların yükleme tekrarlandıkça yayılmasından ve dokunun "alışma etkisi" (preconditioning) göstermesinden kaynaklanmaktadır.

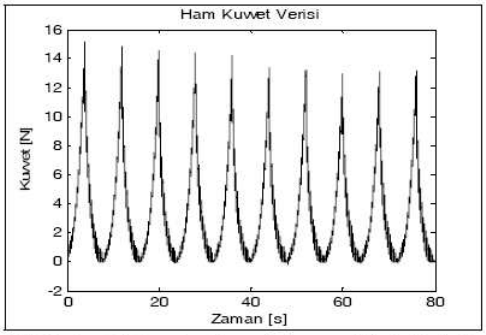

Şekil 3.2. 5 mm/s indentör hızı, 20 mm deplasman ve 10 devir için devirli yükleme deneyi

Gevşeme Deneyi

Gevşeme deneyi, indentör ucunun belli bir mesafeyi istenen hızda gitmesi ve o noktada belli bir zaman durmasıyla yapılan bir deneydir. Şekil 3.3'de 1 mm/s' lik hız, 10 mm deplasmanlı ve hareket tamamlandıktan sonra 120 saniye indentör ucunun bekletilmesi sonucu ortaya çıkan grafik görülmektedir. İndentörün hareketinin tamamlamasıyla birlikte uygulanan kuvvette belirgin bir düşüş görülmekte, ilerleyen zamanla birlikte kuvvetteki değişmenin azaldığı görülmektedir.

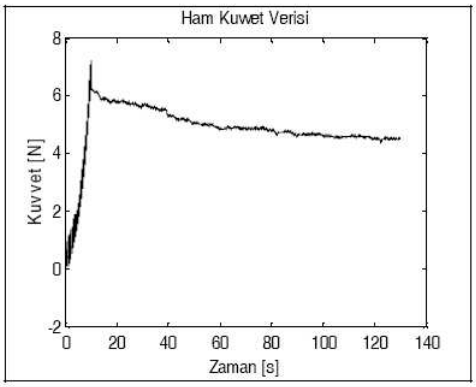

Şekil 3.3. 1 mm/s indentör hızı, 10 mm deplasman ve 120 saniye gevşeme süresi için gevşeme deneyi grafiği

Gevşeme deneyi yapılırken gözlenen diğer bir olay ise ölçümlerin harekete ve kas aktivitesindeki değişikliklere çok duyarlı olmasıdır. Şekil 3.4'de sunulan ve ön kolda yapılan deneyde, el belli bir süre hafif sıkılmadan kapatılmış ve sonrasında açılmıştır. Bu hareket grafiğe ani bir kuvvet yükselişi ve inişi olarak yansımıştır.

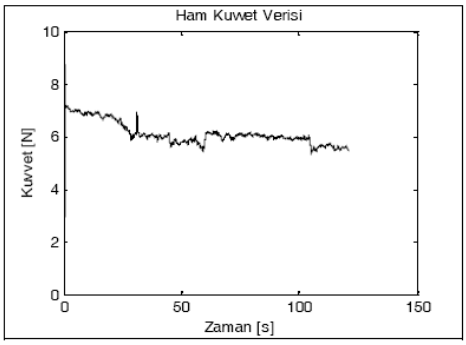

Şekil 3.4. 10 mm/s indentör hızı, 10 mm deplasman ve 120 saniye gevşeme süresi için gevşeme deneyi grafiği

IV. TARTIŞMA

Çalışma ile birlikte indentör cihazının çalışma ve ölçümüyle ilgili yetersizlikler belirlenmiş, sünme protokolü dışında diğer deney protokolleri için bu yetersizlikler düzeltilmiştir. Yapılan düzeltmeler, indentörün ileri-geri hareket deplasmanının doğruluğunun sağlanması ve yük hücresinin kalibrasyonu olarak özetlenebilir. Çalışma öncesi indentörün ileri ve geri hareketi için deplasmanın istenenden sapması 0.05 ile 4.42 mm aralığında iken, çalışma sonrasında bu aralık en fazla 0.5 mm'ye indirilmiştir. Devirli yükleme deneyinde oluşan ve geri hareketin ileri harekete oranla daha fazla oluşması problemi ve elde edilen verilerde devirler arası indentörün hareketsiz kaldığı zaman dilimleri de giderilmiştir.

Bu sayede güvenilir deneyler yapabilmenin önü açılmış ve yumuşak biyolojik dokular üzerinde deney verileri toplanmaya başlanmıştır. Çalışmanın bu aşamasında yoğun sistematik deneyler yapılacak ve yumuşak doku devirli yükleme davranışının yükleme hızına bağımlılığının araştırılması, yumuşak doku gevşeme ve sünme davranışlarının incelenmesi ve mekanik özelliklerin zamana bağlı değişimin araştırılması (gün içinde, günler içinde), gibi ayrıntılı araştırmalar yapılarak şimdikine oranla daha güvenilir ve kestirimci bir yumuşak doku mekanik modeli hazırlanması için kapsamlı bir veri bankası oluşturulacaktır.

Yumuşak doku mekanik özelliklerinin şimdikinden daha ayrıntılı bilinmesi, yumuşak dokuların çevre ile mekanik etkileşimlerinin (örneğin diyabetli bir ayağın ayakkabı ile, uzun süre yatmak zorunda kalan bireyin yumuşak dokularının yatak ile, protez ve ortezlerin ilgili organlarla v.b.) bilgisayarda daha ayrıntılı ve gerçekçi modellenmesine olanak sağlayacaktır. Bu modeller aracılığıyla yumuşak doku - çevre mekanik etkileşimi daha iyi anlaşılabilecek ve yumuşak dokuyla mekanik etkileşimde olan bileşenlerin mekanik tasarımlarına önemli katkı sağlayacağı umulmaktadır.

TEŞEKKÜR

Bu çalışmada kullanılan indentör sistemi TÜBİTAK'ın MİSAG-183 proje desteğiyle üretilmiştir. Yazarlardan Ali Tolga PETEKKAYA, TÜBİTAK yurtiçi yüksek lisans burs programından destek almaktadır.

KAYNAKLAR

[1] Fung, Y. C., "Structure and Stress-Strain Relationship of Soft Tissues", American Zoology, 1984, 24:13-22

[2] Soft Tissues: Biaxial, http://www.instron.com.tr/wa/applications/biomedical/biomaterial/soft_tissue2.aspx

[3] Waldman, S. D., Sacks, M. S., Lee, J. M., "Boundary Conditions During Biaxial Testing of Planar Connective Tissues", Journal Of Materials Science Letters, 2002, 21:1215-1221,

[4] Payne, P. A., "Measurement of Properties and Function of Skin", Clinical Physics and Physiological Measurement, 1991, 12(2):105-129

[5] Gefen, A., Margulies, S. S., "Are In Vivo and In Situ Brain Tissues Mechanically Similar?", Journal of Biomechanics, 2004, 37:1339–1352

[6] Vannah, W. M., Drvaric, D. M., Hastings, J. A., Stand, J. A., Harning, D. M., "A Method of Residual Limb Stiffness Distribution Measurement", Journal of Rehabilitation & Development, 1999, 36(1):1-7

[7] Zheng, Y., Mak, A. F., Lue, B., "Objective Assessment of Limb Tissue Elasticity: Development of A Manual Indentation Procedure", 1999, 36(2):71-85

[8] Kirk, E., Kvornig, S. A., "Quantitative Measurements of the Elastic Properties of the Skin and Subcutaneous Tissue in Young and Old Individuals", Journal of Gerontology, 1949, 4(4):273-284

[9] Sokoloff, L., "Elasticity of Aging Cartilage", Federation Proceedings, 1966, 25:1089-1095

[10] Giannakopoulos, A.E., "Elastic and Viscoelastic Indentation of Flat Surfaces by Pyramid Indentors", Journal of the Mechanics and Physics of Solids, 2006, 54:1305-1332

[11] Yu, W., Li., Y., Zheng, Y. P., Lim, N. Y., Lu, M. H., Fan, J., "Softness Measurements for Open-cell Foam Materials and Human Soft Tissue", Measurement Science and Technology, 2006, 17:1785-1791

[12] Fung, Y. C., "On Pseudo-elasticity of Living Tissues", Mechanics Today, 1980, 5: 487-504

[13] Tönük, E., Siver-Thorn, M. B., "Nonlinear Viscoelastic Material Property Estimation of Lower Extremity Residual Limb Tissues", ASME J. Biomech. Eng., 2004, 126:289-300

YUMUŞAK BİYOLOJİK DOKULARIN İNDENTÖR İLE DEVİRLİ YÜKLEME, GEVŞEME ve SÜNME YANITLARI

Cyclic Loading, Relaxation and Creep Response of Soft Biological Tissues with Indentor

Ali Tolga PETEKKAYA[1], Ergin TÖNÜK[1]
E-posta: e146945@metu.edu.tr, tonuk@metu.edu.tr

[1]Orta Doğu Teknik Üniversitesi, Makina Mühendisliği Bölümü, Ankara, Türkiye

Özetçe: **Yumuşak biyolojik dokular anizotropik, viskoelastik davranış gösteren canlı yapılardır. Devirli yüklemede alışma etkisi, yükleme ve ardından boşaltma yapıldığında histerisiz ayrıca gevşeme ve sünme özellikleri gösterirler. Bu çalışmada daha önce geliştirilmiş ve 0.2-12 mm/s hız aralığında hareket edebilen, 50 N 'a kadar yük uygulayabilen, hareketi 0.048768 mm hassasiyetli adım motoru ile sağlanan bir indentör deney cihazı yardımıyla yumuşak biyolojik dokuların devirli yükleme, gevşeme ve sünme yanıtları araştırılmıştır. Bu amaçla ön kol üzerinde, 15 mm silindirik indentör ucuyla deneyler yapılmıştır.**

Anahtar Sözcükler: Yumuşak biyolojik doku, mekanik yanıt, devirli yükleme, gevşeme, sünme, indentör deney cihazı

Abstract: **Soft biological tissues are live structures showing anisotropic and viscoelastic behaviors. Under cycling loading they show preconditioning effects, under loading and the consequent unloading they reflect hysteresis and they relax and creep. In this study, mechanical response of the soft biological tissues are studied with the help of a previously developed indentor test device capable of moving within 0.2-12 mm/s speed range and can apply 50 N load and whose movement is provided by a step motor with 0.048768 mm resolution. In this context, cyclic loading, relaxation and creep behaviors of the soft tissue are studied on the front arm. The experiments were performed with a 15 mm diameter cylindrical indentor tip.**

Keywords: Soft biological tissue, viscoelastic, cyclic loading, relaxation, creep, indentor test device

I. GİRİŞ

Yumuşak biyolojik dokular anizotropik, viskoelastik davranış gösteren canlı yapılardır [1,2,3]. Gerilim-gerinim davranışları doğrusal değildir [1,2,3]. Canlı olmaları sebebiyle mekanik özellikleri yaşlanma, hastalıklar, yaralanmalar vb. faktörlere bağlı olarak değişkenlik gösterir [4]. Yumuşak dokuların son derece karmaşık bir yapıya sahip olmaları ve mekanik özelliklerinin bahsedilen faktörlerle değişebilmesi sebebiyle henüz genel kabul gören bir yumuşak doku mekanik malzeme modeli geliştirilememiştir. Böyle bir malzeme modelinin geliştirilebilmesi ile yumuşak doku davranışları daha iyi anlaşılacak ve cerrahi simülasyon sistemlerinde [5,6], sakatlanma ve yaralanma mekaniğinin daha iyi anlaşılması, tedavileri planlaması, ilaç sanayi ve benzeri birçok alanda daha etkin bir şekilde kullanılabilecektir [2,7].

Yumuşak biyolojik dokular yapılan devirli yükleme deneylerinde alışma etkisi ve histerisiz gösterirler [3]. Sabit kuvvet uygulandığında sünme ve sabit deplasman uygulandığında gevşeme davranışı gösterirler [2]. Bu dokular bulundukları ortamla etkileşim içerisindedirler. Dolayısıyla bulundukları ortam mekanik özelliklerini etkilemektedir [7].

Yumuşak doku deneyleri temel olarak iki şekilde yapılır. Bunlardan birincisi dokunun doğal ortamından kesilip çıkarılmasıyla doku canlılığını yitirmiş iken yapılan deneylerdir (*in vitro*). Diğeri de dokunun kendi fizyolojik ortamında canlı iken incelenmesidir (*in vivo*). Birinci tarzdaki deneyler çekme deneyi gibi standart malzeme deney protokolleriyle yapılabilmektedir [8]. Ancak dokunun canlılığını yitirmesi ve çevre organlarla etkileşimi olmadığından, canlı organizmalarda yapılan deneyler sonucu elde edilen verilerden farklı sonuçlar elde edilmektedir [9]. Cansız dokularda oluşan gerilim canlı dokular için elde edilen gerilim değerlerinden daha düşük kalmaktadır [10]. İkinci yöntemde bu sorun giderilmekle birlikte, ölçüm yapılabilecek organların sınırlı olması ve ölçüm yapılan yüzeylerin düzgün bir geometriye sahip olmamaları problem teşkil etmektedir. Özellikle yapılan ölçümler dış organlar üzerinde yapılabilmekte, iç organlar için ise ancak değişik düzenekler yardımıyla hayvanlar üzerinde çalışılabilmektedir [11].

In vivo deneylere imkan sağlayan en uygun yöntem indentör cihazlarıyla yapılan deneylerdir [10,12]. İndentör cihazlarıyla yapılan deneyler, indentör ucunun malzeme yüzeyinden içeri doğru hareket etmesi ve bu esnada, zaman, kuvvet, yer değiştirme bilgilerinin kayıt edilmesiyle yapılır (Şekil 1.1).

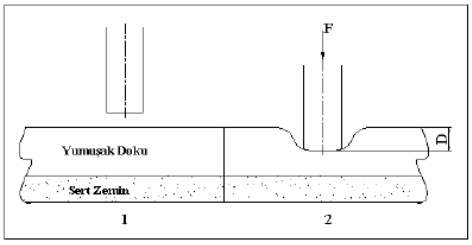

Şekil 1.1. İndentör cihazıyla dokuya yükleme yapılmadan önce(1) İndentör cihazıyla dokuya yükleme yapıldıktan sonra(2) Burada F kuvvet ve D indentörün dokuda aldığı mesafedir.

II. MATERYALLER ve YÖNTEMLER

İndentör Deney Cihazı

Deneylerin yapıldığı sistem dizüstü bilgisayar, denetim kutusu ve deney biriminden oluşmaktadır (Şekil 2.1). Deney birimi ölçümleri yapan indentör cihazı olup, Haydon Switch Instrument 43000 serisi doğrusal hareketli bir adım motoru ile 0.048768 mm çözünürlükte hareketi sağlanır. Kuvvet verileri indentörün ucunda bulunan, önüne değişik çap ve şekildeki indentör deney uçlarının takılabildiği Entran ELW-D1-50N yük ölçer tarafından alınmaktadır (Şekil 2.2). Yumuşak doku deneylerinde, doğruluğun sağlanması için indentör ucu kalınlığının deney yapılan yerdeki doku kalınlığının %25'ini geçmemesi tavsiye edilen bir durumdur [11]. Dolayısıyla farklı dokular için uygun indentör uçlarıyla çalışak önem teşkil eder.

Şekil 2.1. Denetim kutusu(1) Deney birimi(2) Dizüstü bilgisayar(3)

Dizüstü bilgisayar Matlab®6.1'de hazırlanan bir yazılım aracılığıyla indentör cihazının kontrolünü sağlar. Ayrıca deneylerde elde edilen veriler bilgisayarda toplanır ve işlenir.

Denetim kutusu NI 6020E veri toplama kartı, yüksek frekans çıkışı sağlayan voltaj-frekans çevirici, adım motorunu süren sürücü motor kartı, adım motorunu ve yük ölçeri besleyen güç kaynaklarından oluşmaktadır.

Deneyler öncesi deney cihazında iyileştirme çalışmaları yapılmıştır. Bu çalışmalar sonucunda deplasman verilerinde 0-0.5 mm aralığında ve kuvvet verilerinde ortalama olarak 0.19 N sapma olabilmektedir. Deney cihazı ve yapılan iyileştirmeler hakkında daha detaylı bilgilere "İndentör Deney Cihazı ile Yumuşak Biyolojik Dokuların Viskoelastik Özelliklerinin Araştırılması" çalışmasından ulaşılabilir.

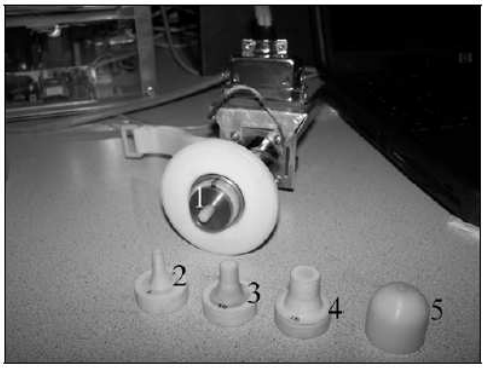

Şekil 2.2. Yük ölçer (1) Soldan sağa doğru 6, 10 ve 15 mm lik silindirik indentör uçları (2,3,4) Küresel indentör ucu (5)

III. SONUÇ

Çalışmada ön kol üzerinde devirli yükleme, gevşeme ve sünme deneyleri yapılmıştır (Şekil 3.1). Elde edilen verilerdeki gürültü filtre edilmiş ve sonuçlar aşağıda sunulmuştur. Veri toplama işlemi başlangıç aşamasında olup detaylı sonuçlar ileride görülebilecektir.

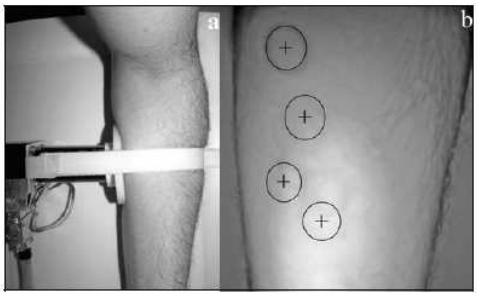

Şekil 3.1 İndentör cihazının bağlama pozisyonu(a) Ölçümlerin ağırlıklı olarak yapıldığı bölgeler(b)

Deney Verilerinin Filtre Edilmesi

İndentör cihazının kontrolünü sağlayan yazılımda kuvvet verilerinin toplanması ve indentör hareketinin eş zamanlılığının sağlanması için örnek toplama hızı yüksek tutulmuştur. Bu da özellikle düşük indentör hızlarında gürültülü verilerin toplanmasına neden olmuştur.

Gürültüden temizleme işlemi için Matlab®6.1'deki *sgolayfilt* fonksiyonu kullanılmıştır. Elde edilen sonuçlar Şekil 3.2 ve Şekil 3.3 de görülebilir.

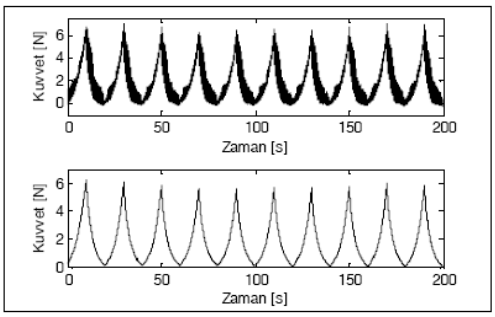

Şekil 3.2. Birinci grafikte 1 mm/s indentör hızı, 10 mm deplasman ve 10 devir için devirli yükleme deneyi sonucu görülmektedir. Birinci grafiğin altında yapılan filtre sonucu elde edilen grafik görülmektedir.

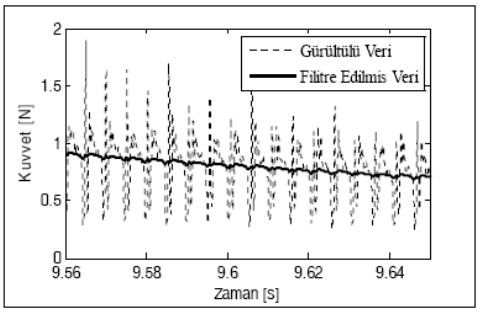

Şekil 3.3. 10 mm/s hızla yapılmış bir devirli yükleme deneyinin gürültülü ve filtreli hallerinin detayı

Devirli Yükleme Deneyi

Devirli yükleme deneyi indentör ucunun belli bir hızda, istenen miktarda, tekrarlı olarak ileri-geri hareket etmesiyle yapılır. Deneyler 1, 5 ve 10 mm/s hızlarda ve Şekil 3.1-b' de görülen noktalarda yapılmıştır. Devir sayısı 10,15 ve 20 olarak alınmıştır.

Yapılan çalışmada ilk dikkat çeken sonuç dokunun tekrarlı yükleme ile birlikte alışma etkisi göstermesidir. Şekil 3.3 de 1 mm/s indentör hızı ve 10 mm deplasman için yapılmış bir devirli yükleme deneyi görülmektedir.

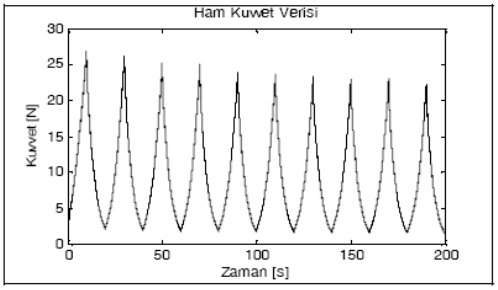

Şekil 3.3. 1mm/s indentör hızı, 10 mm deplasman ve 10 devir için devirli yükleme deneyi

Altıncı devire kadar dokunun tepki kuvveti giderek azalmakta, 6. devir sonrasında kararlı ve tekrar eden bir hal almaktadır. Aynı deneye ait kuvvet-yer değiştirme verisini gösteren grafikte (Şekil 3.4) ilk ve son iki devrin sonuçları görülmektedir. Grafikte artan devir sayısı ile birlikte oluşan alışma etkisi görülmekte ve son devirlerde hemen hemen tekrar eden yükleme boşalma durumu oluşmaktadır. Gözlenen bir diğer durum da histerisiz miktarının son devirlere doğru giderek azalmasıdır. Deneyde gözlenen en yüksek tepe kuvveti 27.39 N'la ilk devirde gözlenmiş en düşük tepe kuvveti de 22.52 N olarak son devirde gözlenmiştir.

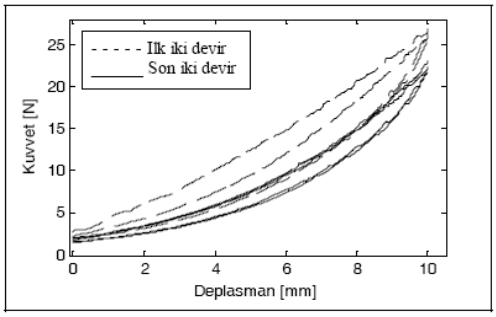

Şekil 3.4. 1mm/s indentör hızı, 10 mm deplasman ve 10 devir için devirli yükleme deneyi

Alışma etkisi bazı deneylerde çok net görülmesine rağmen, kimi ölçümlerde bu etkiye rastlanmamış, hatta kimi deneylerde kuvvet artışları gözlenmiştir (Şekil 3.5). Bu durumun kas hareketlerine yada indentör cihazının düzgün olarak bağlanmaması sebebiyle olabileceği düşünülmektedir ve nedenleri konusunda ayrıntılı araştırmalar yapılmaktadır. Kimi deneylerde ise daha önceki deneylerden kalan alışma etkisinin devam etmesinin neden olabileceği düşünülmektedir.

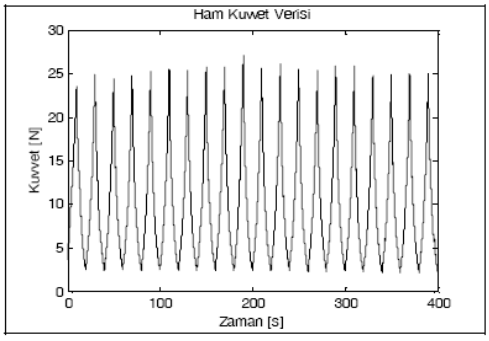

Şekil 3.5. 1mm/s indentör hızı, 10 mm deplasman ve 20 devir için devirli yükleme deneyi. Bu deneyde herhangibir alışma etkisi gözlenmeyip, maksimum kuvvet 27.12 N la 10. devirde ortaya çıkmıştır. Birinci devirde oluşan maksimum kuvvet 23.52 N dur.

Aynı deplasman ve farklı hızlarda yapılan deneylerde, en yüksek tepki kuvvetinin 1 mm/s hızda oluştuğu

görülmüştür. Şekil 3.6 da eş deplasmanlı ve 1, 2 ve 10 mm/s hızlarda gerçekleştirilmiş devirli yükleme deneyinin sonucu görülmektedir. 1 mm/s hızda elde edilen grafikte en yüksek kuvvet 6.2 N, 2 ve 10 mm/s hız değerleri için gözlenen en yüksek kuvvet yaklaşık 4.8 N'dur.

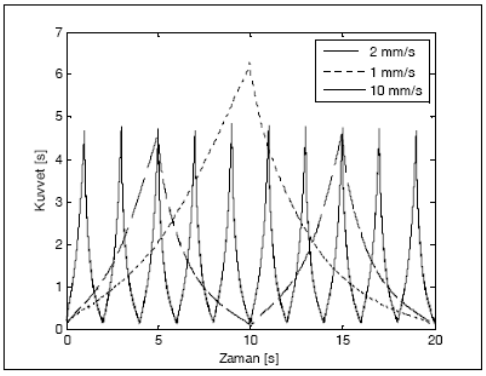

Şekil 3.6. 1, 2 ve 10 mm/s hızlarda devirli yükleme deneyi

1, 5 ve 10 mm/s hız değerleri ve 10 mm deplasman için diğer bir grup ölçümün sonuçları Şekil 3.7 de görülebilir. Bu ölçümlerde çok net bir şekilde hızın artmasıyla yumuşak doku tarafından uygulanan tepki kuvvetinin azaldığı görülmektedir.

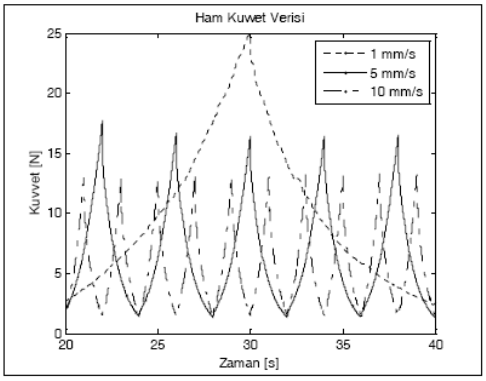

Şekil 3.7. 1, 5 ve 10 mm/s hızlarda devirli yükleme deneyi

Gevşeme Deneyi

Gevşeme deneyleri 10 ile 13 mm deplasman değerleri için, 120 ve 150 saniye boyunca yapılmıştır. İlk yükleme hızları 1 ve 10 mm/s'dir. Yapılan deneylerin tümünde gevşeme davranışı gözlenmiştir. Elde edilen sonuçların bir kısmı Şekil 3.8 de verilmiştir.

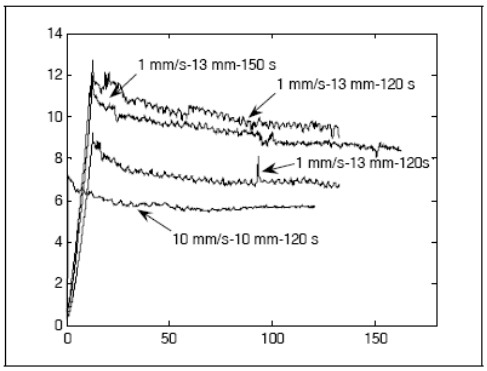

Şekil 3.8. Gevşeme deneyleri

Sünme Deneyi

Sünme deneyi iki temel parametreye bağlı olarak yapılır. Bunlar, dokuya uygulanacak sabit bir kuvvet ve bu kuvvetin ne kadar süre dokuya uygulanacağıdır. Deneyde, indentör ucu, istenen kuvvet değerine ulaşınca, bu değeri sabit tutacak şekilde kapalı devre kontrol çevirimi ile ileri veya geri hareket eder. Deney süresince kuvvet, yer değiştirme ve zaman verileri toplanır. Şekil 3.9'da hedef kuvvetin 15 N olduğu ve 1 mm/s hızla ilk yüklemenin yapıldığı bir sünme deneyine ait kuvvet zaman grafiği görülmektedir. Hedef kuvvete ulaşılmasından sonra 120 saniye süresince deneye devam edilmiştir.

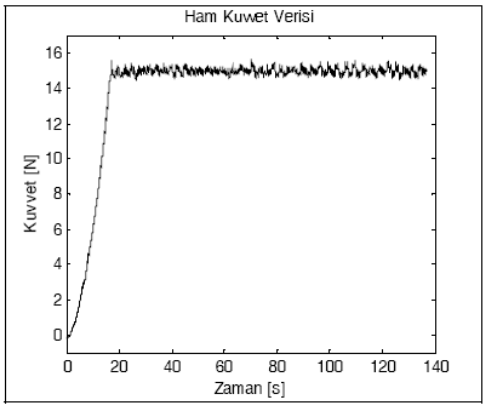

Şekil 3.9. 1 mm/s indentör hızı, 15 N hedef kuvvet ve 120 saniye sünme süresi için sünme deneyi

Şekil 3.10' de aynı sünme deneyine ait deplasman-zaman grafiği görülmektedir. Sünme bölgesinde deplasman zamanla artmaktadır. Deplasmanla zaman arasındaki bağıntıda grafik üzerinde sunulmuştur.

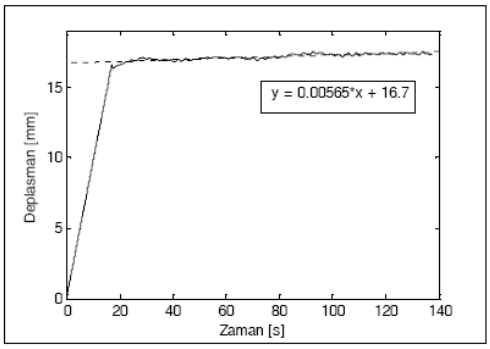

Şekil 3.10. 1 mm/s indentör hızı, 15 N hedef kuvvet ve 120 saniye sünme süresi için sünme deneyi. Grafikteki formülde y deplasmanı x zamanı temsil etmektedir.

Şekil 3.11 de 13 N hedef kuvvet için elde edilen deney sonuçlarından ikisi ve Şekil 3.12 de 15 N hedef kuvvet için elde edilen deney sonuçlarından iki tanesi görülmektedir.

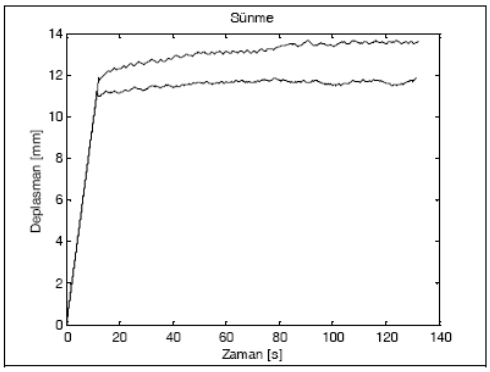

Şekil 3.10. 1 mm/s indentör hızı, 13 N hedef kuvvet ve 120 saniye sünme süresi için sünme deneyi sonuçları.

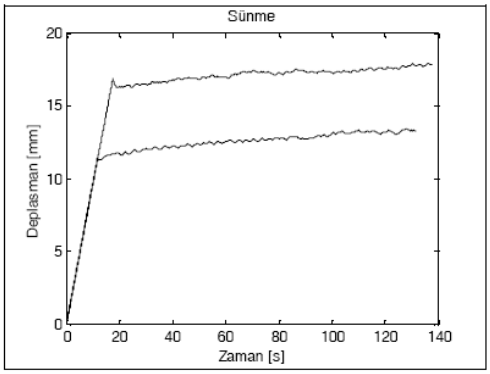

Şekil 3.10. 1 mm/s indentör hızı, 15 N hedef kuvvet ve 120 saniye sünme süresi için sünme deneyi sonuçları.

IV. TARTIŞMA

Çalışmada yumuşak biyolojik dokuların devirli yükleme, gevşeme ve sünme deneylerindeki mekanik yanıtları araştırılmıştır. Deneyler, hareketi adım motoru ile sağlanan, bilgisayar kontrollü indentör cihazı ile ön kolda yapılmıştır. Devirli yükleme deneyi için 1, 2, 5 ve 10 mm/s'lik hız değerlerinde 10-20 mm deplasman aralığında ölçümler yapılmıştır. Gevşeme deneylerinde 1 ve 10 mm/s hız değerlerinde, indentör ucu belirlenen deplasman değerine ulaşıncaya kadar ön yükleme yapılmış ve 120-150 s aralığında dokunun gevşeme süreci gözlenmiştir. Sünme deneylerinde, 13 ve 15 N luk kuvvet değerine ulaşıncaya kadar doku 1 mm/s hızla yüklenmiş ve 120 saniye boyunca sünme verileri toplanmıştır.

Devirli yükleme deneylerinde alışma etkisi, histerisiz davranışları gözlenmiş, eş deplasmanlar için, artan hızla birlikte dokunun uyguladığı tepki kuvvetinin azaldığı tespit edilmiştir. Gevşeme ve sünme deneylerinde beklenen davranışlar gözlenmekle birlikte, yeterli veri henüz elde edilemediğinden hız, zaman vb. parametrelere bağlı genel eğilimler tespit edilememiştir.

Çalışmanın bu aşamasında farklı denekler üzerinde, vücudun çeşitli bölgelerinde ve farklı hızlarda deneyler yapılmaya devam edilecektir. Verilerin yükleme hızına bağımlılığı ve deney verilerindeki zamana bağlı değişimler incelenecektir. Elde edilen veriler yardımıyla şimdikine oranla daha güvenilir ve kestirimci bir yumuşak doku mekanik modeli hazırlanması için kapsamlı bir veri bankası oluşturulacaktır.

Gelişmiş, kestirimci bir mekanik malzeme modeli, yumuşak dokuların bilgisayar ortamında daha iyi modellenmesine olanak tanıyacaktır. Böylece yumuşak dokular ile ilgili birçok süreç bilgisayar ortamında incelenebilip geliştirilebilecektir. Yine bazı ek çalışmalarla birlikte geliştirilecek cerrahi simülasyon sistemleri, cerrah eğitim süreçlerinde büyük yararlılıklar sağlayacaktır.

TEŞEKKÜR

Bu çalışmada kullanılan indentör sistemi TÜBİTAK'ın MİSAG-183 proje desteğiyle üretilmiştir. Birinci yazar Ali Tolga PETEKKAYA, TÜBİTAK yurtiçi yüksek lisans burs programı ile desteklenmektedir.

KAYNAKLAR

[1] Fung, Y. C., "On Pseudo-elasticity of Living Tissues," Mechanics Today, 1980, 5: 487-504
[2] Tönük, E., Siver-Thorn, M. B., "Nonlinear Viscoelastic Material Property Estimation of Lower Extremity Residual Limb Tissues," ASME J. Biomech. Eng., 2004, 126:289-300
[3] Giles J. M., Black A. E., Bischoff J. E., "Anomalous rate dependence of the preconditioned response of soft tissue during load controlled deformation," J Biomech., 2007, 40(4):777-785
[4] Kirk, E., Kvornig, S. A., "Quantitative Measurements of the Elastic Properties of the Skin and Subcutaneous Tissue in Young and Old Individuals," Journal of Gerontology, 1949, 4(4):273-284
[5] LapSim, The Laparoscopic Training Tool, http://www.surgical-science.com/

[6] Delingette, H., Pennec, X., Soler, L., Marescaux, J., and Ayache, N., "Computational Models for Image Guided, Robot-Assisted and Simulated Medical Interventions," Proceedings of the IEEE, 2006, 94(9):1678- 1688
[7] Fung, Y. C., "Structure and Stress-Strain Relationship of Soft Tissues," American Zoology, 1984, 24:13-22
[8] Soft Tissues: Biaxial, http://www.instron.com.tr/wa/applications/biomedical/biomaterial/soft_tissue2.aspx
[9] Ottensmeyer, M. P., Kerdok, Howe, A. E., R. D., Dawson, S. L., "The effects of testing environment on the viscoelastic properties of soft tissues," International Symposium on Medical Simulation, June 2004, 9–18.
[10] Brown, J. D., Rosen, J., Kim, Y. S., Chang, L., Sinanan, M., Hannaford B., "In-Vivo and In-Situ Compressive Properties of Porcine Abdominal Soft Tissues," Studies in Health Technology and Informatics - Medicine Meets Virtual Reality, 2003, 94:26-32
[11] Gefen, A., Margulies, S. S., "Are In Vivo and In Situ Brain Tissues Mechanically Similar?," Journal of Biomechanics, 2004, 37:1339–1352
[12] Vannah, W. M., Drvaric, D. M., Hastings, J. A., Stand, J. A., Harning, D. M., "A Method of Residual Limb Stiffness Distribution Measurement," Journal of Rehabilitation & Development, 1999, 36(1):1-7

İNDENTÖR DENEYLERİ İLE YUMUŞAK BİYOLOJİK DOKULARIN ANİZOTROPİK MEKANİK DAVRANIŞININ YERİNDE BELİRLENMESİ

In Vivo Identification of Soft Tissue Anisotropic Mechanical Response via Indenter Experiments

Ali Tolga PETEKKAYA[1], Ergin TÖNÜK[1,2]
e146945@metu.edu.tr, tonuk@metu.edu.tr

[1]Orta Doğu Teknik Üniversitesi, Makina Mühendisliği Bölümü, Ankara, Türkiye
[2]Orta Doğu Teknik Üniversitesi, Biyomedikal Mühendisliği Lisansüstü Programı, Ankara, Türkiye

Özetçe: ***Yumuşak biyolojik dokular yapıları itibariyle ve canlı olmaları sebebiyle oldukça karmaşık mekanik davranış sergilerler. Viskoelastik olmaları ve alışma etkisi göstermelerinin yanı sıra başka bir özellikleri de anizotropik olmalarıdır. Çalışmamızda yumuşak biyolojik dokuların anizotropik özelliklerinin araştırılması için indentör deneyleri yapılmış ve bu deneyler için büyük eksenleri 8 mm, 16 mm ve 24 mm küçük eksenleri 2 mm, 4 mm ve 6 mm olan üç adet elipsoid uç üretilmiştir. Bu uçlar kullanılarak ön kol üzerinde, 8 mm/s hızda, çeşitli noktalarda 10°'lik ve 30°'lik aralıklarla deneyler yapılmış ve sonuçları sunulmuştur.***

Anahtar Sözcükler: Anizotropi, yumuşak biyolojik doku, indentör deneyleri, elipsoid uç

Abstract: ***Soft biological tissues display substantially complex mechanical behaviors due to their structures and for being alive. Besides being viscoelastic and their capability to show preconditioning effect, another important feature is being anisotropic. In our study, indenter tests were conducted to investigate the anisotropic behaviors of soft biological tissues and three ellipsoid tips with 8 mm, 16 mm and 24 mm major axis and 2 mm, 4 mm and 6 mm minor axis were produced. By using these tips and by applying 10° and 30° increments at 8 mm/s indentation speed, at various points on the forearm soft tissue experiments were carried out and the results were presented.***

Keywords: Anisotropy, soft biological tissue, indentor tests, elipsoid tip

I. GİRİŞ

Mühendislikte uzun yıllardır başarıyla kullanılan ve deney gereksinimini önemli ölçüde azaltan inceleme yöntemlerinin biyomekanikte istenen düzeyde başarılı olmamasının en önemli nedenlerinden birisi, mühendislik malzemelerinin önemli bir bölümüyle ilgili mekanik yanıtların ayrıntılı olarak bilinmesi, buna karşılık biyolojik malzemelerde, özellikle de yumuşak dokuda mekanik yanıtın bu ayrıntıda bilinmemesidir. Gerek ayrıntılı mekanik incelemeler gerekse andırımlar için yumuşak doku mekanik yanıtının bilinmesi kaçınılmazdır.

Yumuşak biyolojik dokuların mekanik yanıtları doğrusal ve/veya elastik değildir. Devirli yükleme ve boşalma deneylerinde yükleme ve boşalma eğrileri aynı yolu takip etmediği gibi doğrusallıktan sapma da göz ardı edilemeyecek kadar belirgindir (Şekil 1.1). Yükleme ve boşalma eğrileri arasında histerisiz olarak adlandırılan ve bir devirde kaybedilen mekanik enerjiyi gösteren bir alan oluşur. Sabit gerinme altında gevşeme (Şekil 1.2), sabit gerilme altında ise sünme davranışı gösterirler (Şekil 1.3).

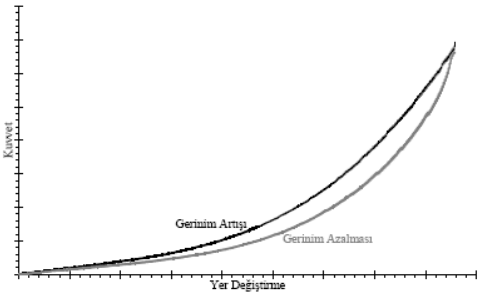

Şekil 1.1. Yumuşak dokularda histerisiz eğrisi

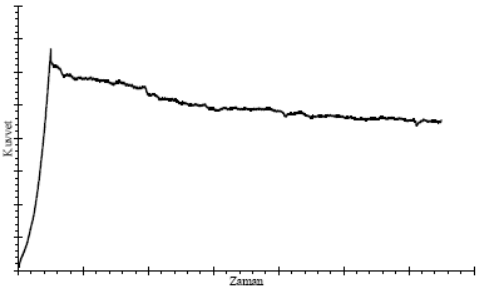

Şekil 1.2. Yumuşak dokunun sabit yer değiştirme altında gevşeme yanıtı

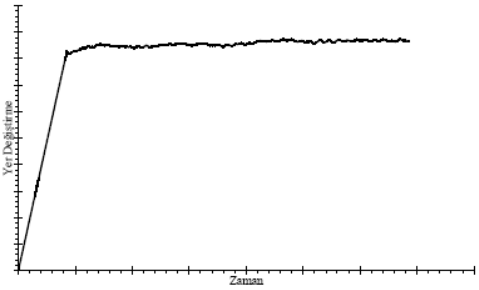

Şekil 1.3. Yumuşak dokunun sabit yük altında sünme yanıtı

Tüm bu davranışlara ek olarak, devirli yükleme altında alışma (Mullins) etkisi gösterir (Şekil 1.4). İlk birkaç devirde doku daha direngen görünürken izleyen devirlerde tekrar edilebilir ve daha az direngen yanıt gösterir.

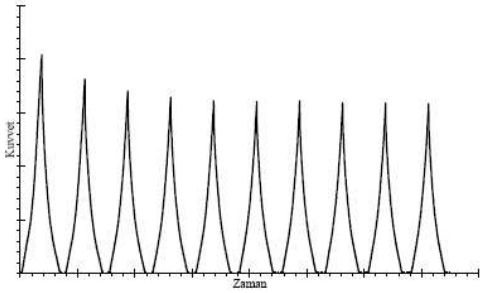

Şekil 1.4. Yumuşak dokuda alışma (Mullins) etkisi

Yumuşak doku mekanik yanıtının yöne bağlı olduğu (anizotropik davranış gösterdiği) bilinmektedir [1].

Yumuşak biyolojik doku mekanik yanıtının belirlenmesi için değişik yöntemler önerilmiştir [2]. Bu yöntemlerden indentör deneyleri yumuşak dokunun yanıtının canlılar üzerinde ve yerinde belirlenmesine izin verdiği için bu çalışmada tercih edilmiştir.

II. MATERYALLER ve YÖNTEMLER

Yumuşak doku deney sistemi dört bölümden oluşmaktadır. Bunlar indentör cihazı, denetim kutusu, dizüstü bilgisayar ve indentör cihazı sabitleme aparatıdır (Şekil 2.1). İndentör cihazı aracılığıyla doku mekanik olarak yüklenir ve dokunun uyguladığı tepki kuvveti ölçülür. İndentör ucunun hareketi Haydon Switch Instrument 43000 serisi 0.048768 mm çözünürlüklü adım motoru ile sağlanır. Tepki kuvveti indentör ucunun altında bulunan Entran ELW-D1 50 N'luk yük hücresi yardımıyla ölçülür. Sistemin denetimini sağlayan donanım denetim kutusu içerisinde yer almaktadır. Bu donanım NI-6020E PCI veri toplama kartı, adım motorunu süren sürücü kartı ve veri toplama kartından gelen hız bilgisini motor sürücü kartına aktaran voltaj-frekans çevirici ile güç kaynaklarıdır [3].

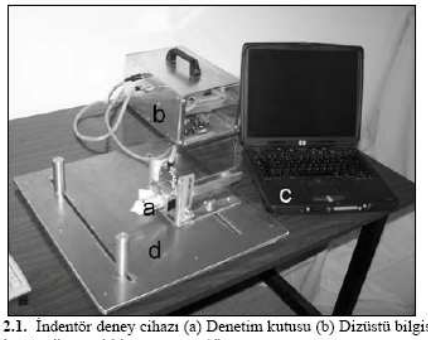

Şekil 2.1. İndentör deney cihazı (a) Denetim kutusu (b) Dizüstü bilgisayar (c) İndentör cihazı sabitleme aparatı (d)

Dizüstü bilgisayarda bulunan ve Matlab® 6.1 programı kullanılarak hazırlanan arayüz yazılımı aracılığıyla farklı deney protokollerinin uygulanması ve elde edilen verilerin depolanıp işlenmesi sağlanır. Mevcut sistemin yer değiştirme hassasiyeti ±0.1 mm aralığında gerçekleşirken, tepki kuvveti ölçüm hassasiyeti ±0.2 N'dur.

İndentör Cihazı Sabitleme Aparatı

İndentör cihazının dokuya bağlanma şekli elde edilen veriler üzerinde etkilidir. Daha önce kullanılan kemer yardımıyla indentör cihazının dokuya bağlanmasında aşağıda belirtilen sorunlarla karşılaşılmıştır.

- Kemeri sıkma miktarına bağlı olarak ölçü yapılan noktadaki doku kalınlığı ve doku üzerindeki ilk gerilmeler değişmektedir. Bu da tekrar edilen deneylerde elde edilen sonuçların değişmesine yol açtığı gibi deneyin bilgisayarda yapılacak andırımının da gerçek durumu yansıtmamasına neden olmaktadır.
- Aynı noktada tekrar deney yapmak güç olmaktadır. İndentör cihazı deney sırasında kayabilmekte, sökülüp bağlamalarda ölçüm yapılan noktayı tam olarak bulmak güç olmaktadır.

Bu nedenle yeni bir bağlama sisteminin geliştirilmesine karar verilmiştir. Geliştirilen sistem aşağıda sıralanan parametrelere göre tasarlanmıştır.

- Bağlama sonucu ölçüm yapılacak bölge herhangi bir şekilde dış etkiye maruz kalmamalıdır.
- Ölçüm yapılacak bölgedeki doku kalınlığı bağlama ile birlikte değişmemelidir.
- İndentör cihazı farklı pozisyon ve açılarda sabitlenebilmeli ve bu sayede doku üzerinde değişik noktalarda ölçüm yapılabilmelidir.
- Anizotropi araştırmasında eliptik indentör ucunun konumu değiştirilirken deney noktası kaybedilmemelidir. Bu durum farklı indentör uçların kullanılması durumunda da gereklidir.
- Kullanımı ve taşınması kolay olmalıdır.

Tüm bu özellikler dikkate alınarak Şekil 2.2'de görülen sistem tasarlanmıştır. Şimdilik deneyler önkol üzerinde yapıldığından tasarım özellikle önkolun bağlanması göz önüne alınarak yapılmıştır. Sistem tabla, kol dayanakları ve indentör cihazı konumlandırıcı olmak üzere üç temel elemandan oluşmaktadır.

Tabla diğer tüm elemanların üzerinde sabitlendiği ve iki adet kılavuz yolun bulunduğu elemandır. Yollardan birinde kol dayanakları diğerinde ise indentör cihazı konumlandırıcısı (İCK) sağa sola doğru hareket ettirilip uygun yerlerde sabitlenebilirler (Şekil 2.3-A).

Kol dayanakları biri bileği diğeri dirseği desteklemek üzere kullanılan elemanlardır. Bu dayanaklar indentör ucunun dokuya etkisi sonucu kolun hareket etmesine engel olurlar.

İCK ile indentör cihazının ölçüm için uygun olan noktada sabitlenmesi sağlanır. Dikey yollarda cihazın, aşağı-yukarı ve açısal (Şekil 2.3-B), tablaya ait yollarda ise ileri-geri, yanal yönlerde doğrusal ve açısal konumlandırması yapılır.

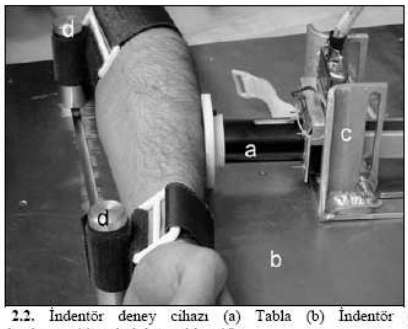

Şekil 2.2. İndentör deney cihazı (a) Tabla (b) İndentör cihazı konumlandırıcısı (c) ve kol dayanakları (d)

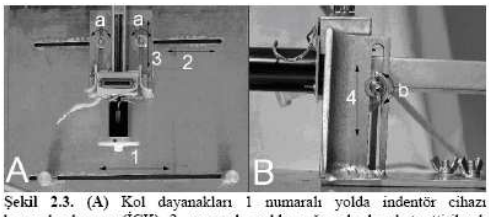

Şekil 2.3. **(A)** Kol dayanakları 1 numaralı yolda indentör cihazı konumlandırıcısı (İCK) 2 numaralı yolda sağa-sola hareket ettirilerek uygun noktalarda sabitlenebilirler. İCK' na ait 3 numaralı yolda indentör cihazının ileri-geri yönlerde sabitlenmesi sağlanır. a noktalarında İCK açısal olarak konumlandırılabilir. **(B)** İndentör cihazının yüksekliği 4 numaralı yol kullanılarak ayarlanır. b noktasından cihaz açısal olarak sabitlenebilir.

Elipsoid uçlar

Yumuşak biyolojik dokuların anizotropik özellikleri küresel veya silindirik (eksenel simetrik) uçlarla belirlenemez. Bu amaçla eksenel simetrisi bozulmuş, Bischoff [1] tarafından teorik incelemesi yapılmış elipsoid uçlar kullanılmıştır. Elipsoid uçlarla aynı noktada, 10°'lik açılarla deneyler yapılarak dokunun yüzey düzlemindeki anizotropisi belirlenmiştir.

Elipsoid deney uçları uzun ve kısa eksen uzunlukları olmak üzere iki temel ölçüye sahiptir (Şekil 2.4).

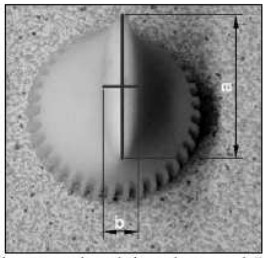

Şekil 2.4. Şekilde a uzun eksen b kısa eksen uzunluğunu vermektedir. Uçlar bu ölçülere göre tasarlanıp üretilmektedir.

Deneyler için farklı ölçülere sahip üç adet elipsoid uç üretilmiştir (Şekil 2.5). Doku kalınlığının düşük olduğu yerlerde küçük ölçülü uçlar, yüksek olduğu yerlerde büyük ölçülü uçlar kullanmak gerekmektedir. Yüksek doku kalınlığını olduğu noktalarda daha büyük yükler ve yer değiştirme miktarlarıyla çalışılabilmekte, buralarda küçük ölçülü elipsoid ucun kullanılması dokuya zarar verebilmektedir. Ayrıca doku kalınlığından bağımsız olarak, dokuya küçük yerdeğiştirme miktarları uygulanırken, küçük ölçülü uçlarla çalışmak daha uygundur.

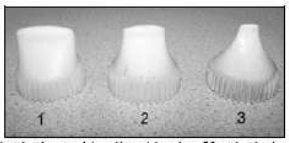

Şekil 2.5. Farklı ölçülere sahip elipsoid uçlar. Uç ölçüleri; a = 24 mm, b = 6 mm (1) a = 16 mm, b = 4 mm (2) a = 8 mm, b = 2 mm (3)

İndentör cihazına eklenmiş hizalayıcı eleman yardımıyla elipsoid uçlar istenen açılarda yerleştirilebilmektedir (Şekil 2.6).

Şekil 2.6. Hizalayıcı uç ve yollar yardımıyla 10° lik aralıklarla ölçümler yapılabilmektedir.

III. SONUÇ

Ön kol üzerinde eliptik indentör uçlarıyla yapılan devirli yükleme deneylerinde dokunun anizotropik davranışı gözlenebilmiştir. Bu deneylerde eliptik ucun konumu 10°'lik aralıklarla 0° ile 170° arasında değiştirilmiştir (Şekil 3.1).

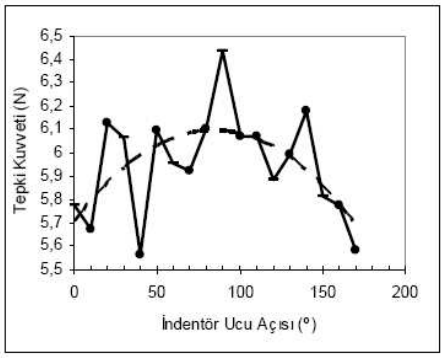

Şekil 3.1. 24 mm'lik yer değiştirme ve 8 mm/s hız altında ön kol üzerinde gerçekleştirilen ölçüm sonucu. Deneyde büyük ekseni 16 mm olan uç kullanılmıştır. Ölçümlerde düzenli bir dağılım gözlenmemekle birlikte, verilere ait kesikli çizgi ile gösterilen eğilim grafiği ve 30 derecelik artırımlara karşı gelen noktaların oluşturduğu eğri (bu noktalar grafikte noktalı çizgi olarak işaretlenmiştir) genel eğilim olarak diğer ölçüm sonuçları ile tutarlılık göstermektedir.

Ancak bu ilk deneylerde deneğin konumunu uzun süre koruyamayarak kas tonusunun değişmesi olasılığı olduğundan diğer ölçümler 30°'lik aralıklarla 0° ile 150° arasında yapılmıştır. Ayrıca kontrol amaçlı 180° (0°) ve bazı deneylerde 210° (30°) de ölçümler yapılmış ve ilk yapılan 0° ve 30°' lik ölçümlerle karşılaştırılmıştır. Deneylerde kontrol verileri ile ana ölçümlerin birbirine yakın çıkması o ölçümlerin güvenilir olduğunu göstermektedir. Ancak kontrol ölçümü ile ana ölçümdeki büyük farklılaşma, deney noktasında sapma ya da kas tonusunda değişme olduğunun bir işareti olmaktadır.

Daha önceki deneylerin büyük çoğunluğunda alışma etkisinin ilk beş devir içinde oluştuğu gözlenmişti. Bu nedenle, çalışmada on devirden oluşan devirli yükleme deneyleri yapılmıştır ve ardışık ölçümler arasında dokunun doğal durumuna gelmesi için uzun süre beklenmemiş, bu nedenle ölçümlerin birçoğunda alışma etkisine rastlanmamıştır. Deney sonuçları değerlendirilirken her devire ait en büyük yer değiştirmeye karşılık gelen kuvvetler belirlenmiş, en büyük ve en küçük uç iki değer çıkarılıp diğer kuvvetlerin ortalaması alınmıştır. Sonuç olarak tüm açılar için bu ortalama kuvvetler hesaplanmış yumuşak doku tepki kuvvetinin eliptik indentör ucu açısına göre grafikleri çizilmiştir (Şekil 3.2).

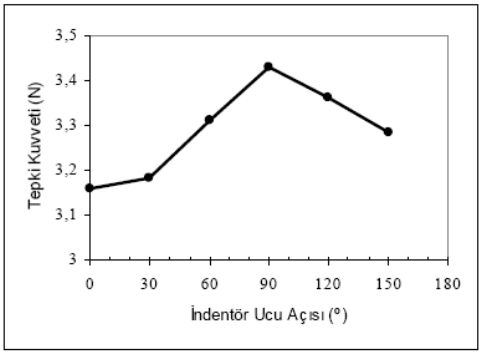

Şekil 3.2. 18 mm lik yer değiştirme ve 8 mm/s hız altında ön kol üzerinde gerçekleştirilen ölçüm sonucu. Deneyde büyük ekseni 8 mm olan uç kullanılmıştır.

Sonuçlarını vermiş olduğumuz bu iki ölçüm önkol üzerinde farklı noktalarda gerçekleştirilmiştir.

IV. TARTIŞMA

Bugüne kadar yapılan çalışmalarda yumuşak dokuların elastik olmayan özellikleri, sünme ve gevşeme davranışları ile alışma etkisi incelenmişti [4]. Bu çalışmada ise yumuşak dokunun yüzey düzlemi içerisindeki anizotropik özelliklerinin araştırılması için eliptik uçlarla ve değişik açılarda yumuşak doku deneyleri yapılmış, ilk sonuçları sunulmuştur.

Aynı nokta için yapılan deneylerde elipsoid uçun değişen açısıyla birlikte dokunun cevabının da değiştiği gözlenmiştir. Deneylerde iki farklı artırım açısı kullanılmış olup bunlar 10° ve 30°'dir.

10° artırım kullanılarak yapılan ölçümlerde ardışık açılara karşılık gelen düzensiz değişimler olabilmektedir. Ancak aynı ölçümde 30° lik artırımlara karşılık gelen noktalara bakıldığında diğer ölçümlerle tutarlılık gözlenmekte ve benzer eğilimler yakalanmaktadır. Dolayısıyla, bu gözlem, ara değerlerin kas tonusu farklılaşmasından ziyade, dokunun gerçek cevabı olması ihtimalini arttırmaktadır.

Bunun dışında 30° artırım kullanılarak, farklı uçlar yardımıyla, değişik noktalarda ölçümler yapılmıştır. Bu ölçümlerde dokunun cevabı karakteristik olarak genelde aynı olmuştur.

Çalışmamızda farklı ölçümler yapılmaya devam edilecek ve 10° için gözlemlediğimiz bu durumun doğruluğu araştırılacaktır. Keza ölçüm sonuçlarının doğrulanması doku davranışını daha iyi anlamak açısından küçük açı değişimleriyle çalışmanın önemini arttıracaktır.

Elde edilen deneysel veriler, evrik sonlu elemanlar yöntemi ve anizotropik, alışma (Mullins) etkisi, gevşeme ve sünmeyi modelleyebilecek bir malzeme modeli kullanılarak [5] yumuşak doku mekanik özelliklerinin belirlenmesinde kullanılacak, belirlenen mekanik özelliklerle yumuşak dokunun çevre ile mekanik etkileşiminin gerçekçi andırımları yapılabilecektir.

TEŞEKKÜR

Çalışmada kullanılan indentör deney cihazı TÜBİTAK MİSAG-183 projesi dahilinde geliştirilmiştir. Yazarlardan Ali Tolga PETEKKAYA, TÜBİTAK yurtiçi yüksek lisans burs programından destek almıştır. Elipsoidal indentör uçları ve indentör cihazı sabitleme aparatı Emir BİRANT'ın (Birant Makina) destek ve yardımlarıyla üretilmiştir.

KAYNAKLAR

[1] Bischoff, J, E, Static Indentation of Anisotropic Biomaterials Using Axially Asymmetric Indenters—a Computational Study, Journal of Biomechanical Engineering, 126(4), 498-505, 2004

[2] Payne, P. A., "Measurement of Properties and Function of Skin", Clinical Physics and Physiological Measurement, 1991, 12(2):105-129

[3] Petekkaya, A, T, Tönük, E., İndentör Deney Cihazı İle Yumuşak Biyolojik Dokuların Viskoelastik Özelliklerinin Araştırılması, 12. Biyomedikal Mühendisliği Ulusal Toplantısı, İstanbul, 106-111, 2007.

[4] Petekkaya, A, T, Tönük, E., Yumuşak Biyolojik Dokuların İndentör İle Devirli Yükleme, Gevşeme Ve Sünme Yanıtları, 12. Biyomedikal Mühendisliği Ulusal Toplantısı, İstanbul, 86-91, 2007.

[5] Üsü, K, Tönük, E., Yumuşak Dokuların Mekanik Davranışının Geliştirilmiş Sanki-doğrusal Visko-Elastik Model ile Andırımı, Biyomut 2008, 13. Biyomedikal Mühendisliği Ulusal Toplantısı, Ankara, 29-31 Mayıs 2008.

I.3 Soft Tissue Mechanical Models Section of the Book Named as Ortapedi Biyomekaniği

3.3.2 Yumuşak Doku Mekanik Modelleri

Ali Tolga PETEKKAYA
ODTÜ Makina Mühendisliği Bölümü

Kerem ÜSÜ
ODTÜ Makina Mühendisliği Bölümü

Ergin TÖNÜK
ODTÜ Makina Mühendisliği Bölümü
ODTÜ Biyomedikal Mühendisliği Lisansüstü Programı

3.3.2.1 Giriş

İskelet sisteminin üzeri bir yumuşak doku tabakasıyla kaplı olduğu için insan bedeninin dış dünya ile olan mekanik etkileşimi hemen her zaman yumuşak dokular aracılığıyla olmaktadır. Öte yandan insan bedenini oluşturan dokulardan, kemik dışında kalan hemen tüm dokular yumuşak doku olarak adlandırılmaktadır. Yumuşak dokuların çeşitli kuvvetler altında nasıl bir mekanik davranış göstereceğinin önceden kestirilebilmesi veya mekanik davranışın bilgisayarda andırımının (simülasyonunun) yapılabilmesi için yumuşak doku mekanik davranışının ayrıntılı olarak bilinmesi ve bu davranışı temsil edecek bünye denklemleri ile bu denklemlere ait katsayıların belirlenmesi gerekir. Protez kovanı ile amputasyon güdüğü arasındaki mekanik etkileşimi bilgisayarda modelleyebilmek amacıyla güdük üzerindeki yumuşak dokuların modellenmesi [1-9], yemek borusunun modellenmesi [10], eklem kıkırdağının modellenmesi [11], bağlar ve kirişlerin modellenmesi [12], yumuşak doku mekanik davranışının bilinmesinin gerekliliğini gösteren bazı örneklerdir. Bu bölümün amacı, okurlarda yumuşak doku mekanik davranışının modellenmesi ve bu davranışın belirlenmesi ile ilgili yaygın olarak kullanılan yöntemler hakkında bir farkındalık yaratmak ve araştırmacılara ilgili kaynaklara yönetmektir.

Mekanik açıdan, mühendislik malzemeleri ile karşılaştırıldığında, yumuşak dokuların davranışları daha karmaşıktır. Bu karmaşıklığın nedenleri arasında dokunun iki fazlı (katı ve sıvı) [13] veya kimi yazarlara göre daha fazla fazlı (katı ve iyonik çözeltiler gibi) [14] olmasının yanı sıra kollajen, elastin gibi farklı ve karmaşık yapıtaşlarından oluşmuş olmasının [15, 16] da etkisi vardır. Yaşayan ve koşullara göre kendini

uyarlayan biyolojik dokuların mekanik özelliklerinin de gerek çevreyle mekanik etkileşim sonucu, gerekse diğer etmenler nedeniyle zaman içinde değişmesi kaçınılmazdır. Öte yandan, biyolojik malzemelerin mekanik özelliklerinin çeşitli sınıflamalar kullanılarak çizelgeler halinde sunulmaya çalışılması da mühendislik malzemeleri kadar kesin ve güvenilir sonuçlar vermemiştir. Özellikle yumuşak dokularda, kullanılacak bünye denklemi konusunda araştırmacılar arasında genel kabul gören bir yaklaşım henüz yoktur. Araştırmacıların önemli bir bölümü, dokuların mekanik özelliklerinin kişiden kişiye önemli değişiklikler gösterdiğini ve gerçeğe yakın modelleme yapılabilmesi için geometrik (anatomik) özelliklerle birlikte kişiye özgü olarak belirlenmesi gerektiğini öne sürmüştür [7-9]. Yine yumuşak doku mekanik özellikleri üzerinde deneğin yaşının [17-20] ve sağlık durumunun [21-24] önemli etkisi olduğu şeklinde görüşler de vardır.

Biyolojik dokuların yumuşak ve sert doku olarak ayrılması, mekanik davranışlar açısından da olanaklıdır. Kemik gibi sert dokular katı cisimler mekaniği kuramında "küçük gerinme" kuramına büyük ölçüde uydukları için gerek bünye denklemlerinin ve bu denklemlere ait katsayıların elde edilmesi, gerekse bilgisayar andırımları yumuşak dokulara göre daha kolaydır. Ancak unutulmamalıdır ki görece kolay bu yaklaşımda sert dokular çoğunlukla tek bir malzemeden oluşmuş sürekli bir ortam olarak modellenmektedir ve bu yaklaşımla ilgili kısıtlamaların dikkate alınması önemlidir. Öte taraftan, yumuşak doku olarak adlandırılan, kemik dışında kalan dokularda gerinmeler nadiren "küçük gerinme" kuramı ile modellenebilecek büyüklükte olur. Çoğu durumda, daha genel, karmaşık ve doğrusal olmayan "büyük gerinme" kuramının kullanılması gerekli olur. Ayrıca, doğrusal elastik malzeme modelleri (Hooke bünye denklemleri) de yumuşak dokuların mekanik davranışını modellemede çoğu zaman yetersiz kalır. Yine yumuşak dokularda, genellikle mühendislik malzemelerinde yok sayılabilecek düzeyde görülen alışma etkisi (*preconditioning, Mullin's effect*, malzemenin ilk birkaç

yüklemede daha direngen davranması, sonraki yüklemelerde direngenliğinin azalarak tekrar edilebilir bir gerilme-gerinim özelliğine kavuşması, Şekil 3.3.2.1), yükün artma ve azalma yönlerinde görülen iki farklı direngenlik (ve bir yükleme-yük azaltma çeviriminde yok sayılamayacak düzeyde mekanik enerji kaybı, Şekil 3.3.2.2), sabit yer değiştirme (veya gerinme) altında tepki kuvvetinin (gerilmenin) azalması yani gevşeme (Şekil 3.3.2.3), sabit kuvvet (veya gerilme) altında yer değiştirmenin (veya gerinmenin) artması yani sünme (Şekil 3.3.2.4) etkilerinin görüldüğü birçok çalışmada belirtilmiştir [15].

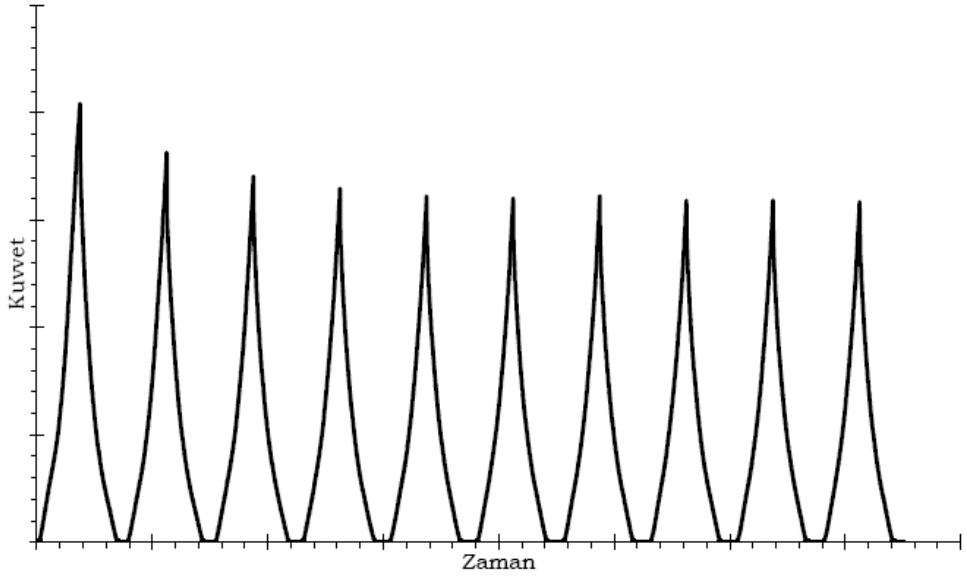

Şekil 3.3.2.1 Yumuşak dokunun peşpeşe yapılan yüklemelerde gösterdiği alışma etkisi

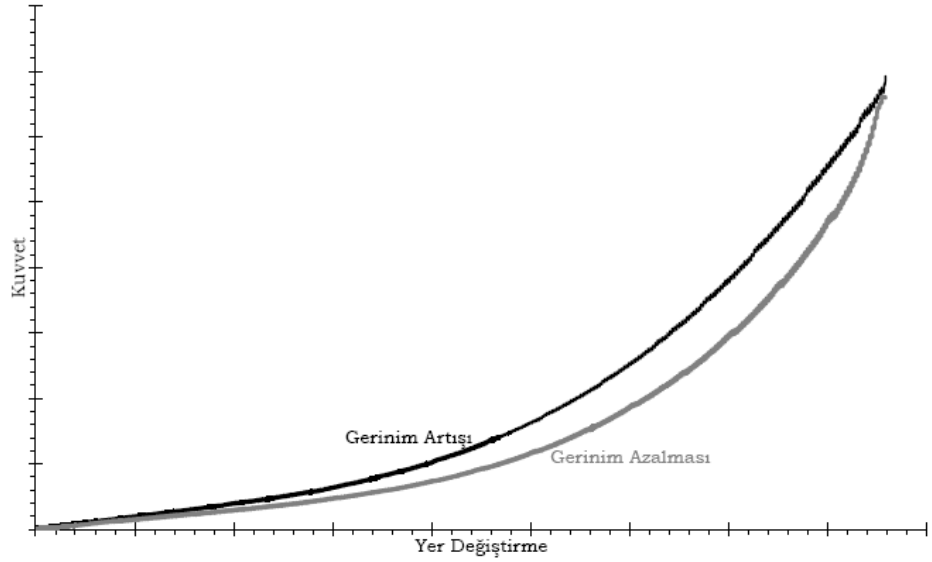

Şekil 3.3.2.2 Yumuşak dokunun gerinmenin artması ve azalması yönündeki davranışı

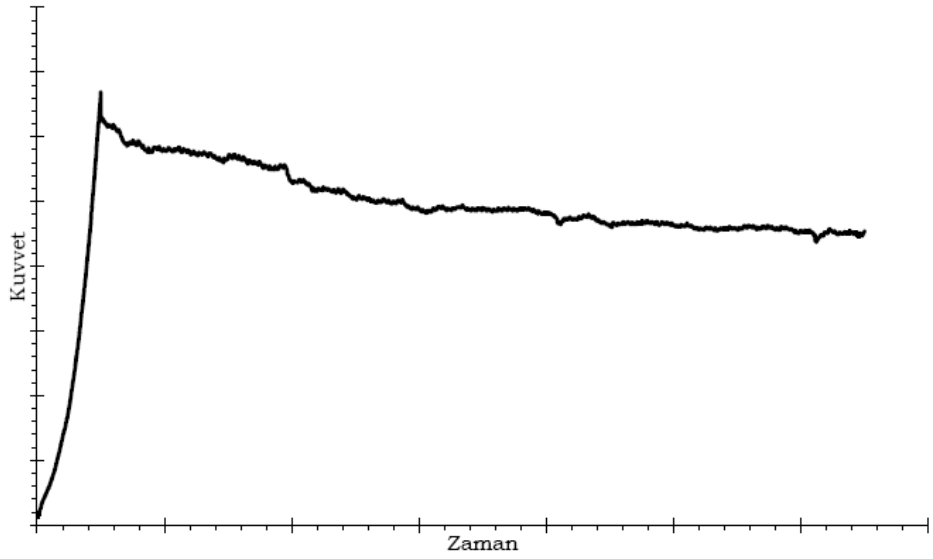

Şekil 3.3.2.3 Yumuşak dokunun sabit gerinmede gevşeme davranışı

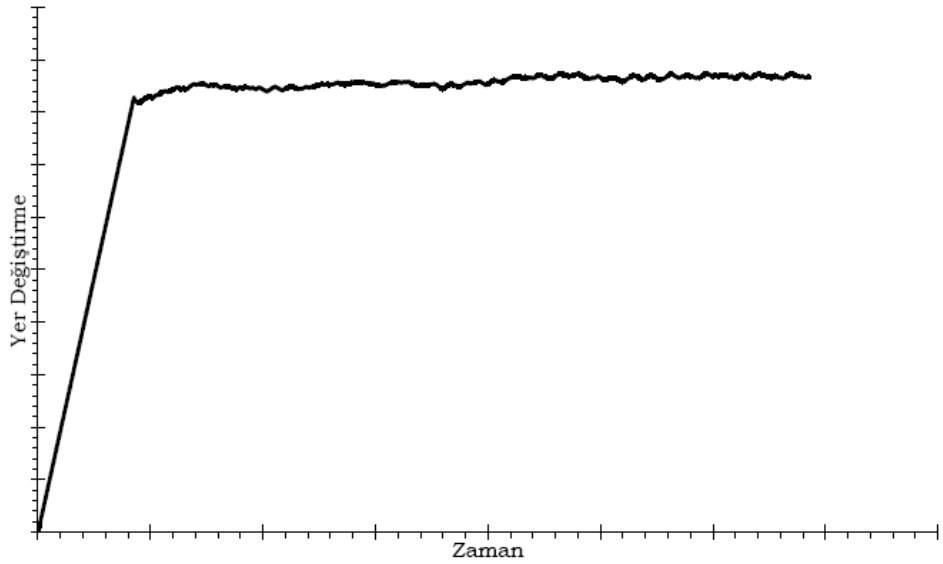

Şekil 3.3.2.4 Yumuşak dokunun sabit gerilmede sünme davranışı

3.3.1.2 Yumuşak Doku Deneyleri

Tüm malzemelerde olduğu gibi yumuşak dokuların mekanik davranışının belirlenmesi ve bünye denklemlerinin oluşturulması için kullanılan yöntem deneyseldir. Yumuşak doku mekanik davranışını belirlemek için değişik deney yöntemleri vardır. Her bir yöntemin kendisine özgü üstünlükleri ve zayıflıkları bulunmaktadır. Bu üstünlük ve zayıflıklardan çalışma için önemli olanları değerlendirilerek en uygun deney yöntemine karar verilmelidir. Bu deneylerden elde edilen mekanik yanıtlar arasında farklar olduğu karşılaştırmalı çalışmalar yapan çeşitli yazarlar tarafından rapor edilmiştir [25-27].

3.3.2.2.1 Eks-Vivo (Laboratuvar) Deneyleri

Deney yapılacak doku yerinden çıkartılır ve laboratuvar ortamında, yaşam koşullarının benzetildiği bir ortamda, doku cansız bir durumda iken deney yapılır [27]. Deneyler laboratuvar ortamında yapıldığı için hem deney örneğinin geometrisi gerçeğe yakın olarak belirlenebilir, hem

de deneyden daha iyi veriler elde edilebilir. Ancak doku kendi fizyolojik ortamından çıkartıldığı ve canlılığını yitirdiği için hem mekanik özelliklerinde bazı değişiklikler olabildiği gibi, doku fizyolojik mekanik gerilmeden arındırılmış olduğu için elde edilen mekanik yanıt dokunun kendi fizyolojik ortamındakinden farklı olabilir [28]. Buna karşın dokunun yaşam koşullarının benzetilmesi deney verilerinin ölü koşullarla karşılaştırıldığında daha iyi olmasını sağlamaktadır.

3.3.2.2.2 İn-Vitro (Laboratuvar) Deneyleri

İn-vitro deneyler de eks-vivo deneylerde olduğu gibi doku bulunduğu ortamdan çıkarılarak cansız bir durumda iken yapılır. Ancak dokunun yaşam koşulları benzetilmeye çalışılmaz. İn-vitro deneylerde özellikle yumuşak dokuların canlılığını yitirmesinden dolayı mekanik malzeme özelliklerinin önemli ölçüde değiştiği kanısı yaygındır [27].

3.3.2.2.3 İn-Situ (Cansız Denek Üzerinde) Deneyler

İn-situ deneylerde yumuşak doku yerinde incelenir. Ancak organ canlı değildir. İn-situ deneyler taze dondurulmuş veya fikse edilmiş kadavralarda da yapılabilir [26]. Her durumda, incelenen doku canlılığını yitirmiş olacağı için mekanik özelliklerinin değiştiği düşünülmektedir. Öte taraftan, çoğunlukla deney örneğinin düzgün bir geometriye sahip olması sağlanamaz ve sınır koşulları tam olarak belirlenemez.

3.3.2.2.4 İn-Vivo (Canlı Denek Üzerinde) Deneyler

İn-vivo deneyler, doku denek üzerinde kendi fizyolojik koşullarındayken ve denek canlıyken yapılır. Girişimsel ve girişimsel olmayan iki yöntem vardır. İn-vivo deneylerin üstün yönü, üzerinde deney yapılacak doku ile çevre dokuların mekanik etkileşimlerinin deney sırasında da var olması ve dokunun canlı olması yoluyla, dokunun gerçek davranışına en yakın yanıtı vermesidir. Ancak, deneğin canlı olması nedeniyle etik kurallara uygun, deneğe zarar vermeyecek biçimde

yapılmasına özen gösterilmelidir. Öte yandan, deney örneğinde düzgün bir geometri sağlamak olanaklı olmadığı gibi, deney bölgesindeki sınır koşullarını da gerçeğe yakın olarak belirleyebilmek her zaman olası değildir.

3.3.2.2.4.1 Girişimsel İn Vivo Deneyler

Girişimsel yöntemde dokuya kuvvet uygulanarak bu kuvvet sonucu dokuda oluşan yer değiştirme zaman bilgisiyle birlikte kaydedilir [29].

3.3.2.2.4.2 Girişimsel Olmayan İn Vivo Deneyler

Girişimsel olmayan yöntemde dışarıdan dokuya bir yer değiştirme uygulanır ve doku içinde oluşan yer değiştirmeler tıbbi görüntüleme yöntemleriyle (manyetik rezonansla görüntüleme [22], ultrasonografi v.b.) ölçülür ve buradan da doku üzerinde oluşan gerinmeler hesaplanır [30].

3.3.2.2.5 Yumuşak Doku Mekanik Malzeme Deney Sistemleri

Yumuşak doku deneyleri standart malzeme deney sistemleri üzerinde yapılabileceği gibi, yumuşak doku deneyleri yapmak için özel olarak tasarlanmış sistemler de vardır. Bu bölümde her iki tip sistemden de kısaca söz edilecektir.

3.3.2.2.5.1 Tek Eksenli Çekme Deneyleri

Tek eksenli çekme deneyleri için uygun kapasitedeki bir çekme cihazı ile dokunun cihaza bağlanmasına uygun çeneler veya dokunun dikilebileceği uygun bir aparat yeterlidir. Genellikle kesit alanı dikdörtgen olan, düzgün geometrideki deney örnekleri hazırlanır. Zaman zaman cihazın çene yer değiştirmesi dokudaki uzama olarak kabul edilir, zaman zaman da doku üzerinde alınan iki referans noktasının yer değiştirmesi ölçülerek dokudaki uzama ve gerinme buradan hesaplanır.

Tek eksenli çekme deneyleri yumuşak doku mekanik özelliklerinin belirlenmesinde kullanılsa da [31,32], Fung [15] tarafından yumuşak doku mekanik özelliklerini belirlemek için yeterli olmadığı belirtilmiştir.

3.3.2.2.5.2 Çift Eksenli Çekme Deneyleri

Çift eksenli çekme deneylerinde genellikle bu iş için özel olarak tasarlanmış bir deney sistemi aracılığıyla deney örneği birbirine dik iki eksende birden çekilir [33]. Her iki eksende de dokuya uygulanan kuvvet ve hareket eden çenelerin yer değiştirmesi ölçülür. Dokuda oluşan gerinmelerin hesaplanması için genellikle doku üzerine yüksüzken çizilen referans noktalarının hareketi izlenir. Buradan yer değiştirmeler ve gerinmeler hesaplanır. Çift eksenli deneylerde sınır koşullarını kontrol etmek tek eksenli deneylerden daha zordur.

3.3.2.2.5.3 Emme Kabı Deneyleri

Çekme deneyleri için deney örneğinin organizmadan izole edilmesinin zorunluluğu nedeniyle deneylerin yerinde yapılabilmesi amacıyla geliştirilmiş bir yöntemdir. Temel olarak üzerinde deney yapılacak doku üzerine geometrisi bilinen bir kap yerleştirilip kabın içindeki hava boşaltılır ve dokuda oluşan şekil değiştirme ölçülür. Alexander [34] ve diğer araştırmacılar tarafından kullanılan yöntem dokunun mekanik özellikleri hakkında fikir verse de önemli kısıtlamaları vardır.

3.3.2.2.5.4 Germe Deneyleri

Germe deneyleri de çekme deneyleri gibi yapılır. Ancak germe deneylerindeki fark, dokunun çekme cihazının çenelerine bağlanması yerine doku boyutlarından daha büyük plakalara yapıştırılmasıdır. Germe deneylerinde kuvvet doku kalınlığının normaline dik yönde uygulanır. İn vitro yapılabildiği gibi [35] in vivo da [36] yapılabilmektedir.

Tek eksenli olduğu için dokunun mekanik özellikleri hakkında kapsamlı bilgi vermediği düşünülmektedir [15].

3.3.2.2.5.5 Basma Deneyleri

Basma deneyleri de germe deneylerine benzer biçimde ancak çenelere ait yüzeylerin dokuyu sıkıştırmasıyla yapılır. Basma deneylerinde doku serbest bırakılabilir ve basmanın etkisiyle yanal yönlerde genleşir (*unconfined test*) veya yanal yüzlerin genleşmesi kısıtlanabilir (*confined test*) [37]. Bu durumda doku sıvısının deney bölgesini terk edebilmesi için çenelerden birisi geçirgen yapılır.

3.3.2.2.5.6 İndentör Deneyleri

Yumuşak doku deneylerinde yaygın olarak kullanılan yöntemlerden birisidir. Tercih edilen geometrideki indentör ucu ile yumuşak doku bastırılırken ucun yer değiştirmesi ve dokunun uca uyguladığı tepki kuvveti zamanla birlikte kaydedilir. Böylece in vivo yumuşak doku deneyleri de yapılabilir. Değişik indentör ucu geometrileri ile yumuşak dokunun serbest yüzeyi üzerinde bulunan anizotropinin de belirlenebileceği kuramsal olarak gösterilmiştir [38]. Ancak, bu deneylerle yumuşak dokuda bulunan tüm anizotropinin belirlenebilmesi olası değildir.

3.3.2.2.6 Yumuşak Doku Mekanik Malzeme Modelleri

3.3.2.2.6.1 Bünye Denklemleri

Bünye denklemleri, ilgilenilen malzemenin gerilme-gerinme (veya çoğu zaman gerilme-gerinme-zaman) ilişkisini genel bir üç boyutlu gerilme altında veren denklemdir. Herhangi bir yapısal analiz yapılmadan önce, yapıyı oluşturan tüm malzemelerin bünye denklemlerinin bilinmesi zorunludur. Çevremizdeki çok farklı malzemeler için çok farklı bünye denklemleri bulunmaktadır. Uzun yıllardan beri kullanılagelen mühendislik malzemeleri için mekanik davranışlarını oldukça geniş

koşullarda büyük bir hassasiyetle modelleyebilecek bünye denklemleri oluşturulmuş olmakla birlikte biyolojik malzemeler için genel kabul görmüş bünye denklemleri daha azdır. Bunun iki nedeninden birisi biyolojik dokularda deney yapmanın güçlüğü, diğeri ise yumuşak dokuların gösterdiği karmaşık mekanik yanıtın bir denklem ile ifade edilmesidir [39].

Çevremizdeki çok değişik malzemelerin önemli bir bölümünü üç ideal malzeme modeli (veya bunların bir bileşimi) ile belirli bir hassasiyette modelleyebiliriz. Bu üç ideal malzeme modeli ağdalı olmayan akışkan, doğrusal (Newton) ağdalı akışkan ve doğrusal elastik (Hooke) katı modelleridir. Ancak biyolojik dokuların önemli bir bölümü, fizyolojik koşullar altında, bu ideal modeller veya bunların bir bileşimi kullanılarak istenen hassasiyette modellenemez [15].

Bünye denklemleri malzemenin fiziksel yapısıyla ilgili olduğu için belirli bir koordinat takımına bağlı değildir ve deneylerle belirlenir. Esnemez katı cisim biyomekaniği dışında, biyomekaniğin her alanında bünye denklemlerinin belirlenmesine gereksinim duyulur. Bünye denklemlerinin bilinmediği durumlarda biyomekanik niceliksel olamaz ancak niteliksel olabilir. Biyolojik yapılar için bünye denklemlerinin belirlenebilmesi için öncelikle yeterli miktarda verinin sistematik olarak toplanması gereklidir. Aksi durumda yapılan mekanik analizler ve biyomekanik kestirimler dokunun gerçek davranışını istenen hassasiyette modelleyemeyecektir [28].

3.3.2.2.6.2 Yalancı Elastik Malzeme Modelleri

Yumuşak doku davranışı, çok küçük gerinmeler dışında doğrusal olmaktan uzaktır. Deney sırasında gerinmenin artışı sırasında izlenen kuvvet-yer değiştirme (veya gerilme-gerinme) eğrisi ile gerinmenin azalması yönünde izlenen kuvvet-yer değiştirme (veya gerilme-gerinme) eğrisi birbirinden belirli biçimde farklıdır (Şekil 3.3.2.2). Eğrinin şeklinin belirli frekans bantlarında belirgin biçimde değişmediği gösterilmiştir

[28]. Bu nedenle basit bir yaklaşımla, gerinmenin artması yönünde bir elastik malzeme katsayısı seti, azalması yönünde başka bir elastik malzeme katsayısı seti kullanılmaktadır. Dokunun gerçek davranışı elastik olarak modellenemeyeceği için bu modele yalancı-elastik (*pseudo-elastic*) denmiştir. Ancak yalancı-elastik malzeme modelleri zamana bağımlı davranışı gözardı ettiği için kullanım alanı sınırlıdır [40]. Yumuşak dokunun artan gerinimle birlikte artan direngenliği (veya teğet elastik modülü) başlangıçta yumaklanmış olarak duran kollajen ve elastin moleküllerinin artan gerinim ile açılmaları ve gerilmeleri ile ilintili olduğu düşünülmektedir [40].

Yumuşak dokunun doğrusal olmayan davranışını modellemek için yaygın olarak kullanılan yöntemlerden birisi de gerinme enerjisi (yoğunluğu) fonksiyonudur. Gerinme enerjisi fonksiyonu kullanılarak büyük gerinmeler için Kirchoff gerilmeleri Green gerinmeleri cinsinden şu şekilde ifade edilebilir:

$$S_{ij} = \frac{\partial(\rho_0 W)}{\partial E_{ij}}$$

Burada ρ_0 malzemenin ilk durumda (şekil değiştirmemiş durumda) kütle yoğunluğudur. Burada kullanılan gerinme enerjisi fonksiyonu termodinamik olarak anlamlı bir fonksiyon değildir, çünkü yumuşak dokunun alışma etkisi dışında işlemin gerinmenin artma veya azalma yönünde olmasına bağlı olarak katsayıları değişmektedir. Bununla beraber, bir yalancı-gerinme enerjisi fonksiyonunun varlığı problemin matematik olarak tanımlanmasını büyük ölçüde kolaylaştırmaktadır. Burada sözü edilen fonksiyonların bazı dokular için 1.5 bazıları içinse 2'ye kadar çıkabilen uzama oranları (son, şekil değiştirmiş uzunluğun ilk uzunluğa oranı) için gerçek doku ile uyumlu sonuç vermeleri beklenmektedir [39]. Literatürde özellikle yumuşak doku modellemek için, veya başka amaçlarla geliştirilmiş ama yumuşak dokuyu da başarıyla modelleyebilecek, değişik gerinme enerjisi fonksiyonları vardır.

Bu fonksiyonların hemen tümü görüngüsel (*phenomenological*) olup dokuda görülen gerinmenin artışı ile direngenlikte meydana gelen artmanın mekanik nedenlerini modellememektedir.

Vaishnav [41] tarafından kullanılan gerinme enerjisi fonksiyonu damarlar gibi silindirik yapılar içindir, silindirik koordinat sisteminde ifade edilmiştir ve bir polinom biçimindedir:

$$\rho_0 W = A E_{\theta\theta}^{\ 2} + B E_{\theta\theta} E_{zz} + C E_{zz}^{\ 2} + D E_{\theta\theta}^{\ 3} + E E_{\theta\theta}^{\ 2} E_{zz} + F E_{\theta\theta} E_{zz}^{\ 2} + G E_{zz}^{\ 3}$$

Burada A, B, C, D, E, F ve G malzeme sabitleri olup deneysel verinin fonksiyon tarafından kestirilen davranışa uyumunu sağlayacak biçimde belirlenir.

Fung [42] tarafından önerilen fonksiyon ise üstel biçimdedir:

$$\rho_0 W = \frac{C}{2} \exp[a_1 E_{\theta\theta}^{\ 2} + a_2 E_{zz}^{\ 2} + 2 a_4 E_{\theta\theta} E_{zz}]$$

Burada a_1, a_2, a_4 ve C malzeme sabitleridir.

Cilt için Tong [39] tarafından önerilen fonksiyon ise

$$\rho_0 W = f(\alpha, E) + C \exp\left[F(a, E)\right]$$

$$f(\alpha, E) = \alpha_1 E_{11}^{\ 2} + \alpha_2 E_{22}^{\ 2} + 2\alpha_4 E_{11} E_{22} + \alpha_3 (E_{12} + E_{21})^2$$

$$F(a, E) = a_1 E_{11}^{\ 2} + a_2 E_{22}^{\ 2} + 2a_4 E_{11} E_{22} + a_3 (E_{12} + E_{21})^2$$

biçimindedir. Burada C, α_1, α_2, α_3, α_4, a_1, a_2, a_3 ve a_4 malzeme sabitleri, x_1 ve x_2 cildi oluşturan düzlem üzerindeki birbirine dik iki koordinat eksenidir.

Tong [39] daha yüksek mertebeden terimler içermesi için denklemin aşağıdaki biçimini de denemiştir:

$$F(a, E) = a_1 E_{11}^{\ 2} + a_2 E_{22}^{\ 2} + 2a_4 E_{11} E_{22} + a_3 (E_{12} + E_{21})^2 + \gamma_1 E_{11}^{\ 3} + \gamma_2 E_{22}^{\ 3} + \gamma_4 E_{11}^{\ 2} E_{22} + \gamma_5 E_{11} E_{22}^{\ 2}$$

burada γ_1, γ_2, γ_3 ve γ_4 ek malzeme sabitleridir.

Akciğer özekdokusu için Hoppin [43] tarafından önerilen fonksiyon ise aşağıda sunulmuştur:

$$\rho_0 W = \sum_{i=1}^{4} a_i \left(\lambda_1^{2i} + \lambda_2^{2i} + \lambda_3^{2i}\right) + \sum_{i=1}^{2} b_i \left(\lambda_1^{2i}\lambda_2^{2i} + \lambda_2^{2i}\lambda_3^{2i} + \lambda_1^{2i}\lambda_3^{2i}\right)$$
$$+ c_1 \lambda_1^2 \lambda_2^2 \lambda_3^2 + \sum_{i=2}^{3} c_i \left(\lambda_1^{2i}\lambda_2^2 + \lambda_2^{2i}\lambda_3^2 + \lambda_3^{2i}\lambda_1^2 + \lambda_1^2\lambda_2^{2i} + \lambda_2^2\lambda_3^{2i} + \lambda_3^2\lambda_1^{2i}\right)$$

Burada a_i, b_i ve c_i malzeme sabitleridir ve fonksiyon genel bir üç boyutlu gerilme durumu için geçerlidir. Ancak bu biçimin en büyük kısıtlaması malzemenin eşyönlü (izotropik) olduğu varsayımıdır. Bu varsayımı kaldırmak için önerilen biçim ise

$$\rho_0 W = C \exp\left(a_1 E_{11}^2 + a_2 E_{22}^2 + 2a_4 E_{11} E_{22}\right) + \text{permütasyon ile simetrik terimler}$$

Mezenter ve kaslar için önerilen gerinme enerjisi fonksiyonu ise [42, 44] şöyledir:

$$\rho_0 W = \frac{dT}{dE}\alpha T + \beta$$

Burada T birim alandaki çekme kuvveti, E gerinme, α ve β ise malzeme sabitleridir. Bu denklem gerilmesiz duruma çok yakın durumlar için iyi sonuç vermese de diğer tüm gerilmelerde istenen hassasiyette kestirim yapabilmektedir.

Alt ekstremite yumuşak dokularının modellenebilmesi için Mooney [45] tarafından önerilen ve daha sonra değişik araştırmacılar tarafından terim sayısı arttırılarak daha çok kauçuk ve polimerik malzemelerin modellenmesinde yararlanılan malzeme modeli kullanılmıştır. Bu model

$$W = \sum_{i+j=1}^{N} C_{ij} \left(I_1 - 3\right)^i \left(I_2 - 3\right)^j$$

biçiminde ifade edilir. Burada I_1 ve I_2 Green-Lagrange büyük gerinme tensörünün ilk iki değişmezi (*invariant*), C_{ij} ise malzeme sabitleridir. N sayısının aldığı değere bağlı olarak malzeme modeli isimlendirilir. Bu biçimdeki bir model Tönük [7] tarafından kullanılmış olan James-Green-Simpson modelinin eksenel simetrik ve sıkıştırılamaz malzemelere uygulanmış tipidir

$$W = C_I \left(I - 3\right) + C_J \left(I - 3\right)^2 + C_K \left(I - 3\right)^3$$

Burada I sıkıştırılamaz malzeme için eksenel simetrik Green-Lagrange gerinme tensörünün tek bağımsız değişmezidir.

Fung [42] tarafından önerilen fonksiyon

$$W = \frac{1}{2}\alpha_{ijkl}E_{ij}E_{kl} + \beta_0\beta_{mnpq}E_{mn}E_{pq}\exp\left(v_{ij}E_{ij} + \frac{1}{2}\gamma_{ijkl}E_{ij}E_{kl} + \ldots\right)$$

biçimindedir. Burada α_{ijkl}, β_{mnpq}, β_0, γ_{ijkl} ve v_{ij} malzeme sabitleridir.

3.3.2.2.6.3 Viskoelastik Malzeme Modelleri

Viskoelastik malzemeler katılarla ağdalı sıvıların özelliklerini bir arada gösteren malzemelerdir. Bu malzemeler, katı ve sıvı özelliklerinin baskınlığına göre katıya daha yakın veya sıvıya daha yakın davranabilirler. Viskoelastik malzemelerin tipik özellikleri, histerezis (malzemenin gerinmesi ve ardından ilk durumuna döndürülmesi sonucu belirgin biçimde mekanik enerji kaybı, gerinme artarken direngenliği daha yüksek azalırken düşük olması, Şekil 3.3.2.2'deki gibi), gevşeme (sabit gerinmede gerilmenin azalması, Şekil 3.3.2.3), sünme (sabit gerilmede gerinmenin artması, Şekil 3.3.2.4) ve gerinme hızına bağlı davranıştır.

En temel iki tip viskoelastik malzeme modeli Maxwell ve Voigt modelleri olup tek boyutlu mekanik model olarak Şekil 3.3.2.5'deki gibi gösterilebilir. Burada yay, elastik davranışı; amortisör ise ağdalı davranışı temsil etmektedir. Maxwell modeli viskoelastik akışkanları modellemekte uygundur. Voigt modelinin tepkisi gerçek viskoelastik katılarla uyuşmadığı için en basit viskoelastik katı modeli için üç elemanlı (bazen Kelvin modeli olarak anılır) model (Şekil 3.3.2.6) önerilmiştir [46-52].

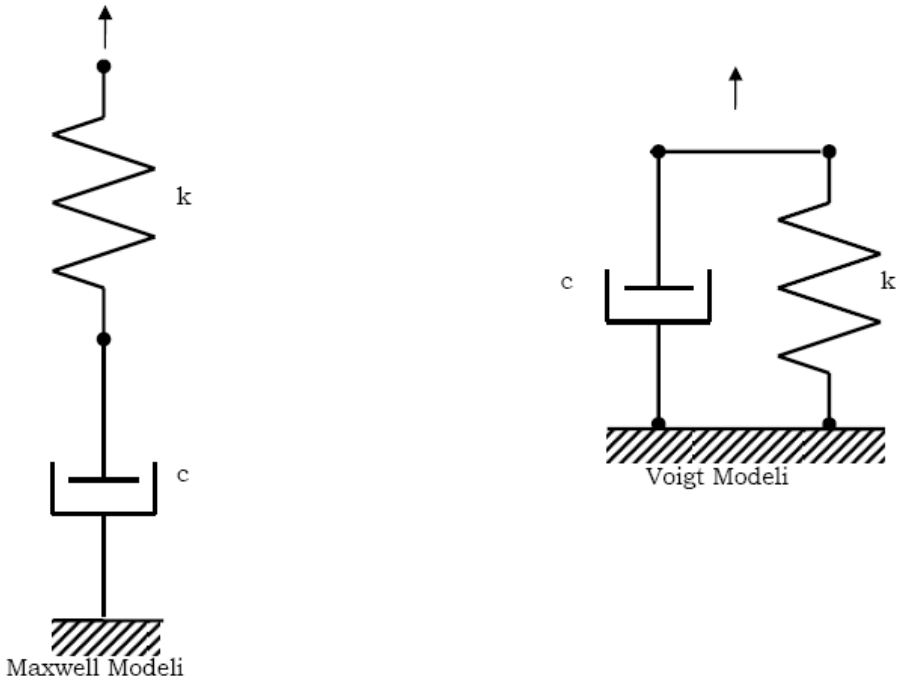

Şekil 3.3.2.5 Temel viskoelastik malzeme modellerinin tek boyutlu mekanik modelleri

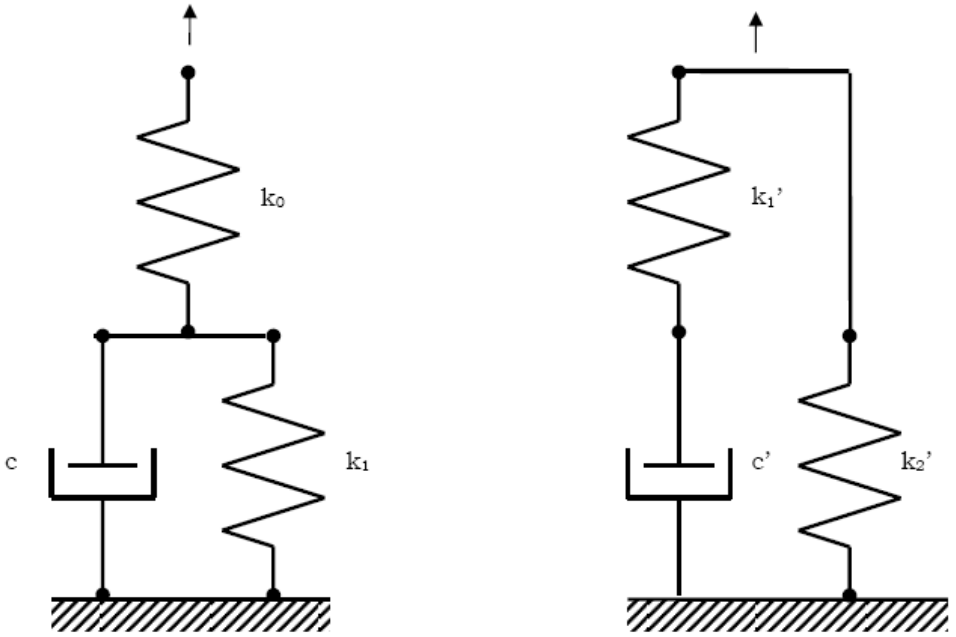

Şekil 3.3.2.6 Üç elemanlı (Kelvin) viskoelastik malzeme modelinin iki farklı gösterimi

Üç elemanlı modelde gerçek viskoelastik katılarda görülen anlık elastik yanıt görülebilmektedir. Bu modellerde gevşeme ve sünme davranışı tek bir üstel ifade ile temsil edilmektedir ve çoğu gerçek viskoelastik katının davranışı bu temsile uymamaktadır. Örneğin dizaltı amputasyon güdükleri üzerinde indentör ile yapılan deneylerden elde edilen yumuşak doku verisinde kısa ve uzun süreli iki sünme davranışı için üç elemanlı model yerine Şekil 3.3.2.7 de gösterilen beş elemanlı bir model kullanılmıştır [8].

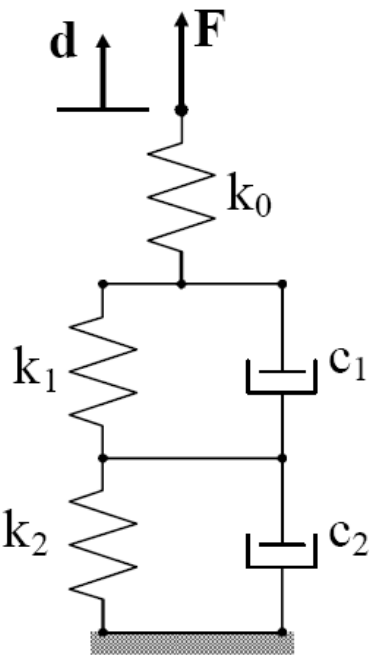

$$W(t) = W_0\left[1-\delta_1\left(1-e^{\left(\frac{-t}{\tau_1}\right)}\right)-\delta_2\left(1-e^{\left(\frac{-t}{\tau_2}\right)}\right)\right]$$

Şekil 3.3.2.7 Beş elemanlı viskoelastik katı modeli ve bünye denklemi

Bu modelde doğrusal olmayan davranış için bir gerinme enerjisi fonksiyonu (W_0) kullanılmıştır. Modelde iki gevşeme oranı (δ_1 ve δ_2) ile iki

gevşeme zaman sabiti (τ_1 ve τ_2) kullanılmıştır. Bu tür modeller gerçek davranışı modellemek üzere Prony serisi olarak genellenebilir:

$$W(t) = W_0\left[1 - \sum_{i=1}^{n} \delta_i \left(1 - e^{\left(\frac{-t}{\tau_i}\right)}\right)\right]$$

Bu tür modellerde iki temel kısıt, doku davranışının viskoelastik olduğu varsayımı ve elde edilen bünye denklemlerinin cebirsel değil diferansiyel olmasıdır. Yapılan deneylerde, viskoelastik malzeme varsayımının dar bir hız aralığında (veya frekansta) iyi sonuç verse de aralığın genişlemesi ile model hassasiyetinin düştüğü gösterilmiştir [15]. Öte yandan, malzemenin bünye denkleminin cebirsel yerine diferansiyel olması, elastik malzemeye göre daha karmaşık bir bünye denkleminin çözülmesi gereği, sistem denklemlerini daha da karmaşık hale getirecektir.

Schwartz [53] tarafından önerilen doğrusal elastik tensör-kütle yönteminde elde edilen tensör denklemleri gerçek zamanlı çözümlemeye izin verecek denli hızlı çözülebilmektedir.

Sanjeevi [54] ise oluşan gerilmeyi elastik ve ağdalı etkilerden olmak üzere ayrı ayrı incelemiştir.

DeHoff [55] ise Haut ve Little denklemlerini kullanarak kollajenin viskoelastik davranışını kestirmiştir.

Fung [15] tarafından önerilen ve yumuşak doku modellemesi konusunda çok bilinen bir standart model olan yalancı-doğrusal viskoelastik teori (*quasi-linear viscoelastic theory*) doğrusal olmayan, zaman ve yükleme geçmişine bağlı yumuşak doku mekanik davranışını modellemek üzere pek çok araştırmacı tarafından başarı ile kullanılmıştır. Bu kurama göre gerilim ile gerinim arasındaki ilişki şu şekilde genel bir formül ile gösterilebilir:

$$\sigma(t) = G(t) * \sigma^e(\varepsilon)$$

Burada $\sigma(t)$ gerilimin zamana bağlı değişimini, $G(t)$ indirgenmiş gevşeme fonksiyonunu ve $\sigma^e(\varepsilon)$ anlık elastik gerilim tepkisi

fonksiyonunu ifade eder. Farklı $G(t)$ ve $\sigma^e(\varepsilon)$ fonksiyonları kullanılarak farklı modellerin elde edilebilmesiyle birlikte literatürde en fazla kullanılanları şu şekildedir;

$$G(t) = \frac{1 + C\left[E_1(t/\tau_2) - E_1(t/\tau_1)\right]}{1 + C\,\ln(\tau_2/\tau_1)}$$

$$\sigma^{(e)}(\varepsilon) = A\left(e^{B\varepsilon} - 1\right)$$

Buradaki indirgenmiş gevşeme fonksiyonu içerisinde üç parametre bulunmaktadır. Bunlardan τ_1 ile τ_2 sırasıyla kısa ve uzun dönem gevşeme davranışlarını kontrol ederken, C parametresi de gevşemenin genliğini belirlemektedir. İfade içerisindeki E_1 birinci üstel integral fonksiyonudur ve şu şekilde tanımlanır:

$$\mathrm{E_1(y)} = \int_{\mathrm{y}}^{\infty} \frac{\mathrm{e^{-z}}}{\mathrm{z}}\,\mathrm{dz}$$

Anlık elastik gerilim tepkisi fonksiyonunu içerisindeki iki parametre *(A, B)* ile birlikte toplam beş parametreli bir model oluşmaktadır.

Bu denklemler kullanılarak elde edilen model ise şu şekildedir;

$$\sigma(t) = \int_{\tau=0}^{t} G(t-\tau)\,\frac{\partial \sigma^{(e)}(\varepsilon)}{\partial \varepsilon}\,\frac{\partial \varepsilon}{\partial \tau}\,d\tau$$

Yumuşak doku mekanik yanıtını modellemede kullanılan bir başka yöntem ise Bailey Norton yasası ve Prony serisi yaklaşımıdır:

$$\sigma = \int_0^t \mathrm{E_R(t,\varepsilon)}\,\frac{\mathrm{d\varepsilon}}{\mathrm{dt}}\,\mathrm{dt}$$

$$\mathrm{E_R(t)} = \mathrm{k_0} + \sum_{\mathrm{i=1}}^{\ell} \mathrm{k_i e^{-t/\tau_i}}$$

$$\mathrm{E_R(t,\varepsilon)} = \mathrm{k_0\varepsilon} + \sum_{\mathrm{i=1}}^{\ell} \mathrm{k_i e^{-t/\tau_i}}$$

Burada $E_R(t)$ doğrusal, $E_R(t,\varepsilon)$ ise doğrusal olmayan gevşeme fonksiyonlarıdır.

$$\dot{\varepsilon} = \dot{\varepsilon}_{cr} + \dot{\varepsilon}_{el}$$

ifadesi ise Bailey Norton yasasıdır.

3.3.2.2.6.4 Gözenekli-Elastik Malzeme Modelleri

Gözenekli-elastik (*poroelastik*) malzeme modelleri, gözenekli bir elastik katı ortam içerisinde sıvı akışını modelleyen yaklaşımdır ve biyomekanikte zaman zaman yumuşak doku ve özellikle de eklem kıkırdaklarının modellenmesi için kullanılır. Katı üzerinde oluşan gerinmeler nedeniyle sıvı üzerinde oluşan basınç farkları sonucunda sıvı akışı olmaktadır [56]. Yumuşak dokunun iki fazlı modellenmesine yönelik Zhu [57] tarafından hazırlanan çalışmada modelleme ile ilgili ayrıntılar verilmiştir. Ün [58, 59] tarafından yumuşak doku mekanik davranışının modellenmesinde sonlu elemanlar andırımı kullanılmıştır. Ancak gerek modeldeki karmaşıklık gerekse model katsayılarının elde edilmesine yönelik zorluklar nedeniyle bugüne kadar yaygın kullanım alanı bulamamıştır.

3.3.2.2.7 Yumuşak Doku Malzeme Sabitlerinin Belirlenmesi (Yumuşak Doku Mekanik Karakterizasyonu)

Bünye denklemlerindeki malzeme sabitlerinin belirlenebilmesi, ancak ilgili malzemeler üzerinde ayrıntılı deneyler yapmakla olasıdır. Yapılan deneylerin cinsine göre, eğer kontrollü ortamda ve basit bir geometrili deney örneği kullanılıyorsa cebirsel denklemlerle dokunun gerilme-gerinme-zaman özellikleri (bünye denklemi katsayıları) elde edilebilir. Ancak geometri karmaşıksa (örneğin indentör deneylerinde olduğu gibi indentör ucunun dokuyla dokunması, büyük yer değiştirmeler gibi) evrik yöntemlere (genellikle evrik sonlu elemanlar yöntemi) başvurulur.

3.3.2.2.7.1 Analitik Yaklaşımlar

Deney yapılan geometrinin basit olduğu veya basit geometrilerle modellenebildiği (genellikle yarı-sonsuz ortam) ve bununla beraber malzemenin bünye denkleminin de görece basit olduğu (genellikle

doğrusal elastik veya doğrusal viskoelastik malzeme) ve tüm bunlara ek olarak gerinmelerin ve yer değiştirmelerin küçük olduğu çok kısıtlı sayıdaki yumuşak doku deneyleri için mekanik davranış, içerisinde malzeme sabitinin de bulunduğu tek bir analitik denklem ile ifade edilebilmektedir. Bu durumda, analitik denklemden malzeme sabiti çözülerek deney sonucuna bağlı olarak sayısal değer kolaylıkla elde edilebilir [60, 61]. Ancak analitik yaklaşımlar, içerdikleri çok fazla kısıtlama nedeniyle çoğunlukla istenenlere yanıt verememektedir.

3.3.2.2.7.2 Evrik Sonlu Elemanlar Modeli

Evrik sonlu elemanlar modelinde, deney yapılan bölge ve yakın çevresinin sonlu elemanlar modeli hazırlanır. Gerekli sınır koşulları, deney sırasında uygulanan yükler, dokunun uyması beklenen bünye denklemi modele girilir. Ancak bünye denklemi ile ilgili katsayılar bilinmediği için başlangıç değerleri seçilir. Rastgele seçilen bu değerlerle sonlu elemanlar andırımı çalıştırılır, malzeme sabitleri rastgele seçilmiş dokunun tepkisi elde edilir. Üzerinde deney yapılmış gerçek dokunun malzeme sabitleri, rastgele seçilen malzeme sabitlerinden farklı olacağı için, bilgisayar anırımından elde edilen tepki de gerçek dokudan elde edilenden farklı olacaktır. Aradaki farkı kapatmak üzere bilgisayar andırımındaki malzeme sabitleri değiştirilerek andırım yeniden çalıştırılır. Andırımdan elde edilen tepki, gerçek dokudan deneysel olarak elde edilen tepkiye istenen ölçüde yaklaştığında, andırımda kullanılan malzeme sabitlerinin de gerçek yumuşak dokunun malzeme sabitlerine istenen ölçüde yaklaştığı varsayılır ve böylece yumuşak doku mekanik malzeme sabitleri istenen hassasiyetle kestirilebilir.

Evrik sonlu elemanlar yönteminin kullanımı sırasında dikkat edilmesi gereken noktalar şunlardır:

- Yumuşak dokunun uyması beklenen bünye denkleminin önceden bilindiği varsayılır. Eğer kullanılacak bünye denklemi üzerinde deney

yapılan dokunun mekanik davranışını modellemede yetersiz kalırsa evrik sonlu elemanlar yönteminden bünye denkleminin değiştirilmesine yönelik bir bilgi edinilmez.

- Genellikle deney koşullarında yumuşak dokuda büyük gerinmeler, büyük yer değiştirmeler, başka bir cisme dokunma ve doğrusal olmayan bünye denklemleri gibi problemin yüksek derecede doğrusallıktan sapmasına neden olan kaynaklar vardır. Bu durumda, elde edilecek malzeme sabitleri kestiriminin tek (kapalı, dışbükey bir komşuluk içerisinde) olduğuna dikkat edilmelidir.

Evrik yöntemlerle yumuşak doku mekanik özelliklerinin belirlenmesine ilişkin daha ayrıntılı bilgiler için Flynn [62] ve Tönük'ün [9] çalışmalarına başvurulabilir.

Kaynaklar

1. Zhang, M., Lord, M., Turner-Smith, A. R., Roberts, V. C., 1995, "Development of a Nonlinear Finite Element Modeling of the Below-Knee Prosthetic Socket Interface", Med. Eng. Phys, v. 17, pp. 559-566.
2. Zhang, M., Mak, A. F. T., 1996, "Finite Element Analysis of the Load Transfer betwen an Above-knee residual limb and its prosthetic socket-Roles of Interface Friction and Distal-end Boundary Conditions", IEEE Trans. Rehab. Eng. V. 4, pp. 337-346.
3. Zhang, M, Mak, A. F. T., Roberrts, V. C., 1998, Finite Element Modeling of a Residual Lower Limb in a Prosthetic Socket": A Survey of Development in the First Decade", Med. Eng Phy, v. 20, pp. 360-373.
4. Zachariah, S. G., Sanders, J. E., 1996, "Interface Mechanics in Lower-Limb External Prosthetics: A Review of Finite Element Methods", IEEE, Trans. Rehab. Eng, v. 4, pp 288-302.
5. Vannah, W. M., Childress, D. S., 1996, "Indentor Tests and Finite Element Modeling of Bulk Muscular Tissue in vivo", J. Rehabil. Res. Dev., v. 33, pp. 239-252.
6. Commean, P. K., Smith, K. E., Vannier, M. W., Szabo, B. A., Actis, R. L. 1997, "Finite Element Modeling and Experimental Verification of Lower Extremity Shape Change Under Load", J. Biomech, v. 30, pp. 531-536.
7. Tönük, E., Silver-Thorn, M. B., 2003, Nonlinear Elastic Material Property Estimation of Lower Extremity Residual Limb Tissues, IEEE Transactions on Neural Systems and Rehabilitation Engineering, vol. 11, pp. 43-53.
8. Tönük, E., Silver-Thorn, M. B., 2003, "Nonlinear Elastic Material Property Estimation of Lower Extremity Residual Limb Tissues". IEEE, Transactions on Rehabilitation Engineering Vol 11, No 1, pp. 43-53.

9. Tönük, E., 2004b, Evrik Sonlu Elemanlar Yöntemi ile Malzeme Özelliklerinin Kestirilmesi ve Biyomekanik Uygulamaları, MSC.Software Kullanıcılar Konferansı, sf. 25-32, 3-4 Haziran 2004, İstanbul.
10. Yang W., Fung, T. C., Chian, K. S., Chong, C. K., 2006, Investigations of the viscoelasticity of esophageal tissue using incremental stress-relaxation test and cyclic extension test, Journal of Mechnaics In Medicine and Biology, v. 6 pp. 261-272.
11. Lu, X. L., Mow V. C., 2008, Biomechanics of articular cartilage and determination of material properties, Medicine and Science in Sports and Exercise, v. 40, pp 193-199.
12. Hurschler, C., Loitz-Ramage, B., Vanderby, R. Jr, 1997, A structurally based stress-stretch relationship for tendon and ligament, Journal of Biomechanical Engineering, v. 119, pp. 392-399.
13. Suh J.K., DiSilvestro M.R., 1999, "Biphasic poroviscoelastic behavior of hydrated biological soft tissue", Journal of Applied Mechanics, ASME, v. 66, pp. 528-535.
14. Lu X.L., Miller C., Chen F.H., Guo X.E., Mow V.C., 2007, "The generalized triphasic correspondence principle for simultaneous determination of the mechanical properties and proteoglycan content of articular cartilage by indentation", Journal of Biomechanics, v. 40, pp. 2434-2441.
15. Fung, Y. C., 1993, Biomechanics, mechanical Properties of Living Tissues, Second Ed. Springer-Verlag.
16. Humphrey, J. D., 2002, Cardiovascular Solid Mechanics, Cells, Tissues, Organs, Springer.
17. Bönniger, M., 1905, "Die elastische Spannung der Haut und deren Beziehung zum Oedem," Ztschr. F. Exper. Path. U. Therapie, Vol. 1, pp. 163-183.

18. Kirk, E., Kvorning, S. A., 1949, "Quantitative Measurements of the Elastic Properties of the Skin and Subcutaneous Tissue in Young and Old Individuals," J. Gerontol., Vol. 4, pp. 273-284.
19. Sokolof, L., 1966, "Elasticity of aging cartilage," Fed. Proc., Vol.25, N.3, pp. 1089-1095.
20. Zheng Y. P., Mak A. F. T., Lue B. K., 1999, "Objective assessment of limb tissue elasticity: development of a manual indentation procedure," J Rehabil Res Dev, Vol.36, N.2, pp. 71-85
21. Lawrence, A.J., Rossman, P.J., Mahowald, J.L., Manduca, A., Hartmann, L.C., Ehman, R.L., 1999, "Palpating Breast Cancer by Magnetic Resonance Elastography," Proceedings of the 7th Annual Meeting of ISMRM, Philadelphia, pp. 215.
22. Manduca, A., Oliphant, T.E., Dresner, M.A., Mahowald, J.L., Kruse, S.A., Amromin, E., Felmlee, J.P., Greenleaf, J.F., Ehman, R.L., 2001, "Magnetic resonance elastography: Non-invasive mapping of tissue elasticity," Medical Image Analysis, Vol.5, pp. 237–254.
23. Gefen, A., Megido-Ravid, M., Azariah, M., Itzchak, Y., Arcan, M., 2001, "Integration of Plantar Soft Tissue Stiffness Meausurements in Routine MRI of the Diabetic Foot," Clinical Biomechanics, Vol.16, pp.921-925
24. Geyer, M. J., Brienz, D. M., Chib, V., Wang, J., 2004, "Quantifying Fibrosis in Venous Disease: Mechanical Properties of Lipodermatosclerotic and Healthy Tissue", Adv Skin Wound Care, Vol.17, pp. 131-142
25. Brown, J.D., Rosen, J., Kim, Y. S., Chang, L. C., Sinanan, M. N., Hannaford, B., 2003, "In-Vivo and In-Situ Compressive Properties of Porcine Abdominal Soft Tissues," in Proc. Medicine Meets Virtual Reality, v.94, pp.26-32.
26. Gefen, A., Margulies, S. S., 2003, "Are in vivo and in situ brain tissues mechanically similar?," J. Biomechanics, Vol.37, pp. 1339-1352

27. Ottensmeyer, M. P., Kerdok, A. E., Howe, R. D., Dawson, S. L., 2004, "The Effects of Testing Environment on the Viscoelastic Properties of Soft Tissues," International Symposium on Medical Simulation, pp. 9-18.
28. Fung, Y. C., 1984, "Structure and Stress-Strain Relationship of Soft Tissues," Amer. Zool., Vol.24, pp.13-22.
29. Klaesner J. W, Hastings M. K., Zou D., Lewis C., Mueller M. J.,2002, Plantar tissue stiffness in patients with diabetes mellitus and peripheral neuropathy. Archives of Physical Medicine and Rehabilitation, Vol. 83(12), pp.1796-1801.
30. Ottensmeyer, M. P., 2002, In Vivo Measurement of Solid Organ Tissue Mechanical Properties, Studies in Health Technology and Informatics, Vol.85, pp.328-333.
31. Tanaka, E., Tanaka, M., Aoyamaa, J., Watanabe, M., Hattori, Y., Asai, D., Iwabea, T., Sasaki, A., Sugiyama, M., Tane, K., 2002, "Viscoelastic properties and residual strain in a tensile creep test on bovine temporomandibular articular discs," Archives of Oral Biology, Vol.47, pp.139–146.
32. Prete, Z. D., Antoniucci, S., Hoffman, A. H. ,Grigg, P., 2004, "Viscoelastic properties of skin in Mov-13 and Tsk mice," J. Biomechanics, Vol.37, pp. 1491-1497.
33. Planar-Biaxial Soft Tissue Test System, Instron, 2004, http://www.instron.com.tr/wa/library/streamfile.aspx?doc=527 27. Mart. 2008 tarihinde alınmıştır.
34. Alexander, H., Cook, T. H., 1977, Accounting for natural tension in the mechanical resting of human skin, The Journal of Investigative Dermotology, Vol.69, pp.310-314.
35. Miller, K., Chinzei, K., 2002, "Mechanical properties of brain tissue in tension," ," J. Biomechanics, Vol.35, pp. 483-490.

36. Payne, P. A., 1991, "Measurement of Properties and Function of Skin", Clinical Physics and Physiological Measurement, Vol:12(2), pp.105-129.
37. DiSilvestro, M. R., Suh, J. F., 2001, A cross-validation of the biphasic poroviscoelastic model of articular cartilage in unconfined compression, indentation, and confined compression, J. Biomechanics, Vol.34, pp. 519-525.
38. Bischoff, J. E., 2006, Reduced parameter formulation for incorporating fiber level viscoelasticity into tissue level biomechanical models, Annals of Biomedical Engineering, v. 34, pp. 1164-1172.
39. Tong, P. and Fung, Y. C.,1976, The Stress-Strain Relationship for the Skin, J. Biomechanics, vol. 9, pp. 649-657.
40. Fung, Y. C., 1980, On Pseudo-elasticity of Living Tissues, Mechanics Today J., vol. 5, pp. 487-504.
41. Vaishnav, R. N., Young, J. T., Janicki, J. S. and Patel, D. J., 1972, Nonlinear Anisotropic Elastic Poperties of the Canine Aorta, Biophysical J., vol. 12, pp. 1008-1027.
42. Fung, Y. C., 1973, Biorheology of Soft Tissues, Biorheology J., vol. 10, pp. 139-155.
43. Hoppin, F. G., Lee, G. C., Dawson, S. V., 1975, Properties of Lung Parenchyma in Distortion, J. Applied Physiology, vol. 39, pp. 742-751.
44. Fung, Y. C., 1967, Elasticity of Soft Tissues in Simple Elongation, Am. J. Physiology, vol. 213, pp. 1532-1544.
45. Mooney, M., 1940, A Theory of Large Elastic Deformation, Journal of Applied Physics, vol. 11, pp. 582-592.
46. Bland, D. R., 1960, The Theory of Linear Viscoelasticity, Pergamon Press.
47. Bergen, J. T. (ed), 1960, Viscoelasticity, Phenomenological Aspects, Academic Press.

48. Flügge, W, 1967, Viscoelasticity, Blaisdell Publishing Company.
49. Ferry, J. D., 1970 Viscoelastic Properties of Polymers, John Wiley & Sons.
50. Lockett, F. J., 1972, Nonlinear Viscoelastic Solids, Academic Press.
51. Christensen, R. M., 1982, Theory of Viscoelasticity, An Itroduction, Second Edition, Academic Press.
52. Lakes, R. S., 1998, Viscoelastic Solids, CRC Press.
53. Schwartz, J. M., Denninger, M., Rancourt, D., Moisan, C., Laurendeau, D., 2005, Modeling Liver Tissue Properties Using a NonLinear Viscoelastic Model for Surgery Simulation, Medical Image Analysis, vol. 9, pp. 103-112.
54. Sanjeevi, R., 1982, A Viscoelastic Model for the Mechanical Properties of Biological Materials, J. Biomechanics, vol. 15, pp. 107-109.
55. Dehoff, P. H., 1978, On the Nonlinear Viscoelastic Behavior of Soft Biological Tissues, J. Biomechanics, vol. 11, pp. 35-40.
56. Cowin, S. C., 2004, Anisotropic Poroelasticity: Fabric Tensor Formulation, Mechanics of Materials, vol. 36, pp. 665-677.
57. Zhu, C. ,J., http://www.orl.columbia.edu/nyohrl_new/hmpage/tutorial, 21. Haziran. 2001 tarihinde alınmıştır.
58. Ün K., Spilker R. L. , 2006a, A penetration-based finite element method for hyperelastic 3D biphasic tissues in contact: Part 1 - Derivation of contact boundary conditions, Journal of Biomechanical Engineering, v. 124, pp. 124-130.
59. Ün K., Spilker R. L. , 2006b, A penetration-based finite element method for hyperelastic 3D biphasic tissues in contact. Part II: Finite element simulations, Journal of Biomechanical Engineering, v. 124, pp. 934-942.
60. Hayes, W. C., Keer, L. M., Herrmann, G., Mockros, L. F., 1970, A Mathematical Analysis for Indentation Tests of Articular Cartilage, Journal of Biomechanics, v. 5, pp. 541-551.

61. Argobast, K.B., Thibault, K. L., Pinheiro, B. S., Winey, K. I., Margulies, S. S., 1997, A high-frequency shear device for testing soft biological tissues, Journal of Biomechanics, v. 30, pp. 757-759.

62. Flynn, D. M., Peura, G. D., Grigg, P., Hoffman, A. H., 1998, A finite element based method to determine the properties of planar soft tissue, Journal of Biomedical Engineering, v. 120, pp. 202-210.